TRIBOLOGICAL EVALUATION OF UNLUBRICATED AND MARGINALLY LUBRICATED BEARING MATERIALS

Sarma Volety

PhD Thesis

TRIBOLOGICAL EVALUATION OF UNLUBRICATED AND MARGINALLY LUBRICATED BEARING MATERIALS

BY

BANGARESWARA SARMA VOLETY

B.Tech., M.Sc.

A thesis submitted in partial fulfilment for the requirements of the degree of

DOCTOR OF PHILOSOPHY

at the University of Central Lancashire in collaboration with

Goodrich Aero Engine Controls

October 2010

DECLARATION

I declare that while registered with the University of Central Lancashire for the degree of the Doctor of Philosophy, I have not been a registered candidate or enrolled student for another award with the institute or with any other academic or professional institution during the research programme. No portion of this work referred to in this thesis has been submitted in support of any application for another degree or qualification of any other University or Institution of learning.

Signed ... ……..

V. B. Sarma

ABSTRACT

This thesis presents friction and wear rate measurements of the copper based bearing materials used in thrust bearing of aircraft fuel pumps. Highly detailed friction and wear data was collected from 20% and 30% lead in bronze (leaded bronze) substrates and 10% indium in lead (lead/indium) coated leaded bronze substrates in unlubricated and marginally lubricated conditions. Measurements were made under a wide range of load and speed using a thrust washer test apparatus and pin on disc test equipment.

During the running-in period in unlubricated test conditions, the substrate friction and wear rate was found to depend on the percentage of lead content and its microstructure. High friction and wear rates were observed for lead/indium coatings due to the high contribution of ploughing and transfer of coating to the counterface surface. The coefficient of friction for lead/indium coatings appeared to depend on their thickness. During steady state conditions, the friction coefficient of both substrates and coatings remained constant and thin coatings had lower friction than uncoated and thick coated substrate materials. In marginally lubricated test conditions, the fluid film limited metal to metal contact for a limited time interval and the friction coefficient observed was low. When the fluid was removed from the contact due to the evaporation or flow, the situation became dry test and the test results were similar to those described above.

By making appropriate assumptions, the frictional heating model of Ashby was applied to lead/indium coated surfaces in dry test conditions to attempt to identify the melting of lead/indium (if any). Both flash and bulk temperature was evaluated for pin on disc and thrust washer tests and this suggested that melting of lead/indium happened during the running-in period, but not during steady state operation. Scanning electron microscope observations of worn surfaces revealed evidence of melting of lead/indium. A loose black powder was found outside the wear track from lead/indium coated test specimens under high load and high speed conditions in unlubricated and marginally lubricated tests. EDAX analysis showed that the black powder in the form of wear debris generated from lead/indium coating and contained about 10% oxygen suggesting that the lead oxide was present in various forms. A black smeared layer on the uncoated leaded

bronze substrates was also identified in marginally lubricated test conditions and EDAX showed the black layer was lead and copper, with less than 10% oxygen suggesting that lead oxide and cuprous oxide were present. The tribological performance on small number of lead-free materials such as Graphit-ic and Chromium Graphit-ic coatings was also investigated for comparison with lead/indium coatings.

Acknowledgements

I would like to express my deep gratitude to Prof. Ian Sherrington and Prof. Derek Arnell for given me this opportunity and supported me throughout this project. Without their support and invaluable suggestions, I cannot finish this thesis. I am deeply grateful to Goodrich Aero Engine Controls for their financial support throughout my PhD.

I am thankful to Nathalie Renevier for her guidance and demonstration of laboratory equipments. I also acknowledge the principal technicians and department staff for their technical and administrative support.

My special thanks go to all my colleagues from CM222 who created a friendly and supportive environment in the office throughout my research work. I have many memorable with them throughout my thesis.

At last not, but not least; I would like to express my deepest thanks with all my heart to all members of my family who supported me in every aspect of my life. My special hearty wishes go to my wife for her support in every aspect of my life and making me happier. My parent's contribution throughout my life is unforgettable and invaluable. I must thank God for given me outstanding parents and to them I am dedicating this thesis work. God bless you Mom and Dad.

Nomenclature

Symbol	Designation	Units
μ	Coefficient of friction	[-]
μ_a	Coefficient of adhesive friction	[-]
A	Contact area	[mm^2]
a	Contact radius	[mm]
A_1	Area of the sphere	[mm^2]
A_1, A_2, A_3, A_4	Area of groove at four different areas	[mm^2]
A_{avg}	Average area	[mm^2]
A_n	Nominal contact area	[mm^2]
A_p	Area of the ploughing	[mm^2]
a_r	Contact radius for the real area of contact	[m]
A_r	Real area of contact	[mm^2]
A_w	Area of the annulus of washer	[mm^2]
C	Specific heat capacity	[J/kg]
C_1, C_2	Constants for a given indenter size	[-]
D	Ball diameter	[mm]
D	Diameter of wear track	[mm]
d	Indentation diameter	[mm]
d	Ploughing depth	[mm]
D_1, D_2	Inside and outside diameters of washer	[mm]
*E**	Effective modulus of elasticity	[GPa]
E_1, E_2	Young's modulus of body 1, body 2	[GPa]
f	Friction force	[N]
F_1, F_2	Friction force, Load cell force	[N]
h	Height of washer	[mm]
h	Scar height	[mm]
HK	Knoop hardness	[kgf/mm^2]
H_s	Dimensionless number	[-]
HV	Vickers hardness number	[kgf/mm^2]

k or SPWR	Specific wear rate	[mm³/N.m]
K	Archard's wear coefficient	[-]
K_1, K_2	Thermal conductivities of surface materials	[W/mK]
k_{abr}	Abrasive wear coefficient	[-]
l	Long diagonal length	[mm]
L	Surface length	[mm]
l_1 and l_2	Physical lengths of washer and disc	[mm]
l_{1b}, l_{2b}	Equivalent linear heat diffusion distances – bulk heating	[mm]
l_{1f}, l_{2f}	Equivalent linear heat diffusion distances – flash heating	[mm]
LV	Load x Velocity	[Nm/s]
P	Pressure	[MPa]
P_F	Final pressure	[N/mm²]
P_I	Initial pressure	[N/mm²]
P_{max}	Maximum pressure	[MPa]
P_{mean}	Mean contact pressure	[MPa]
PV	Pressure x Velocity	[N/mm^2.m/s]
q'	Heat input at real area of contact	[W/m²]
q	Heat generated at nominal contact area	[W/m²]
Q	Heat generated	[Watt]
R^*	Effective radius of curvature	[mm]
R_1, R_2	Radius of curvature of body 1, body 2	[mm]
R_a	Surface roughness	[µm]
R_{a1}, R_{a2}, R_{a3}	Measured roughness at different areas	[µm]
r_t	Track radius	[mm]
S	Shear strength	[N/mm^2]
t	Heat injection time	[sec]
T_0	Temperature of the remote sink	[º C]
T_1, T_2	Transition loads	[N]
T_b	Nominal or bulk temperature	[º C]
T'_b	Sink temperature	[º C]
T_f	Flash temperature	[º C]
V	Sliding velocity	[m/s]
V	Volumes lost	[mm³]

V_w	Volume of wear	[mm^3]
W	Normal load	[N]
X or L	Sliding distance	[m]
x, y	Co-ordinates	[-]
α	Thermal diffusivity	[m^2/s]
δ	Deflection	[µm]
η	Absolute viscosity	[Ns/m^2]
θ	Attack angle	[degrees]
v_1, v_2	Poisson's ratio	[-]
ρ	Density of material	[kg/m^3]
σ_y	Yield stress	[N]

Abbreviations

AT	After Test
BHN	Brinell hardness number
BL	Boundary lubrication
BOD	Ball on disc
BT	Before Test
COF	Coefficient of friction or Friction coefficient
EDAX	Energy Dispersion X-ray Spectroscopy
EHL	Elasto hydrodynamic lubrication
HDL	Hydrodynamic lubrication
LV	Load x Velocity
Mat	Material
ML	Mixed lubrication
Pb/bronze	Leaded bronze
Pb/In	Lead/Indium
POD	Pin on disc
PV	Pressure x Velocity
PVD	Physical Vapour Deposition
R	Running-in
RPM	Revolutions per minute
SD	Standard deviation
SEM	Scanning Electron Microscope
SPWR	Specific wear rate
SYS	System
Thick	Thickness
TWT	Thrust washer test
UNC	Uncoated
Vol	Volume loss
WLI	White Light Interferometer
Wt %	Weight percentage

List of Figures

Page

Figure 1.1 Gear pump thrust bearing in fuel pumps 2
Figure 1.2 Thrust faces of journal bearing and gear shaft in fuel pump 3
Figure 1.3 Summary of test procedures on test specimens 5
Figure 1.4 Lay out of the thesis 6
Figure 2.1 Schematic of rotating shaft supported by journal bearing and thrust bearing 8
Figure 2.2 Tribo system 17
Figure 2.3 Schematic illustration of sliding friction 17
Figure 2.4 Schematic of hard sphere sliding on softer material 20
Figure 2.5 Adhesive wear mechanisms 24
Figure 2.6 Wear mechanism maps for unlubricated steel sliding in air at room temperature in pin on disc configuration 24
Figure 2.7 Wear transition of plain carbon steel sliding against tool steel in pin on disc test 25
Figure 2.8 The PV relationships for dry bearings 28
Figure 2.9 Schematic of abrasive wear 30
Figure 2.10 Types of lubrication 41
Figure 2.11 Stribeck curve 41
Figure 3.1 Tribological test process 44
Figure 3.2 Conventional Pin on disc test apparatus 45
Figure 3.3 Pin end geometry in the POD test apparatus 45
Figure 3.4 Conventional Thrust washer test apparatus 48
Figure 3.5 Schematic of a stylus profilometer 51
Figure 3.6 General surface profile 52
Figure 3.7 Wear loss in a tribo contact 55
Figure 3.8 Talysurf profile of a wear track on test sample 56
Figure 3.9 Volume of sphere 57
Figure 3.10 Nominal point contact of ball on disc 58
Figure 3.12 Frictional heating calculations 62
Figure 4.1 Schematic of thrust washer test apparatus 1 70
Figure 4.2 Real Thrust washer test apparatus 1 70

Figure 4.3 Views of various elements in thrust washer tester 71
Figure 4.4 V-block and loading arm 72
Figure 4.5 Fenner speed ranger controller 72
Figure 4.6 Flow chart of TWT 74
Figure 4.7 Calibration of transducer 75
Figure 4.8 Schematic of forces acting on washer-disc contact 75
Figure 4.9 Specifications of steel washer 76
Figure 4.10 Instrument amplitude output 78
Figure 4.11 An Examples of a Coefficient of friction against time graph 79
Figure 4.12 Example of a coefficient of friction vs. time graph showing various characteristics of friction 80
Figure 4.13 Typical examples of coefficient of friction against time graphs from TWT apparatus 1 82
Figure 4.14 Wear track on a test specimen 83
Figure 4.15 Measured wear areas from Talysurf profilometer 85
Figure 4.16 Modifications on TWT apparatus 1 89
Figure 4.17 Thrust washer test apparatus 2 90
Figure 4.16 Steel washer (counterface) 92
Figure 4.17 Pin on disc test apparatus 94
Figure 4.18 Example of running-in and steady state period of a coated surface 99
Figure 5.1 Mean COF against contact pressure in uncoated leaded bronze substrates in dry test conditions 104
Figure 5.2 SPWR against contact pressure in uncoated leaded bronze substrates in dry test conditions 105
Figure 5.3 Mean COF and mean SPWR against PV of uncoated leaded bronze substrates in dry test conditions 106
Figure 5.4 Mean COF against contact pressure in uncoated leaded bronze substrates in marginally lubricated test conditions 107
Figure 5.5 SPWR against contact pressure in uncoated leaded bronze substrates in marginally lubricated test conditions 108
Figure 5.6 Mean COF and mean SPWR against PV of uncoated leaded bronze substrates in marginally lubricated test conditions 108
Figure 5.7 Mean COF against contact pressure of 1 μm lead/indium coated substrates in dry test conditions 110

Figure 5.8 System SPWR against contact pressure of 1 µm lead/indium coated substrates in dry test conditions 111
Figure 5.9 Mean COF and system SPWR against PV of 1 µm lead/indium coated substrates in dry test conditions 111
Figure 5.10 Mean COF against contact pressure of 1 µm lead/indium coated substrates in marginally lubricated test conditions 113
Figure 5.11 System SPWR against contact pressure of 1 µm lead/indium coated substrates in marginally lubricated test conditions 114
Figure 5.12 Mean COF and system SPWR against PV of 1 µm lead/indium coated substrates in marginally lubricated test conditions 115
Figure 5.13 Mean COF against contact pressure of 5 µm lead/indium coated substrates in dry test conditions 116
Figure 5.14 System SPWR against contact pressure of 5 µm lead/indium coated substrates in dry test conditions 116
Figure 5.15 Mean COF and mean SPWR against PV of 5 µm lead/indium coated substrates in dry test conditions 117
Figure 5.16 Mean COF against contact pressure of 5 µm lead/indium coated substrates in marginally lubricated test conditions at 0.26 m/s 118
Figure 5.17 System SPWR against contact pressure of 5 µm lead/indium coated leaded bronze substrates in marginally lubricated test conditions 119
Figure 5.18 Mean COF and system SPWR against contact pressure of 5 µm lead/indium coated substrates in marginally lubricated test conditions 119
Figure 5.19 Mean COF and mean system SPWR against coating thickness from TWT apparatus 1 in dry test conditions 121
Figure 5.20 Mean COF and mean system SPWR against coating thickness of TWT apparatus 1 in marginally lubricated test conditions 122
Figure 5.21 Mean COF and SPWR against load in uncoated leaded bronze substrates at 0.47 m/s 124
Figure 5.22 Mean COF and SPWR against load for uncoated leaded bronze substrates in dry test conditions at 0.24 m/s 125
Figure 5.23 Mean COF and SPWR against load for uncoated leaded bronze substrates in marginally lubricated test conditions at 0.26 m/s 127
Figure 5.24 Mean COF and SPWR against load for uncoated leaded bronze substrates in marginally lubricated test conditions 128

Figure 5.25 Ploughing COF and running-in time against load in 1 μm lead/indium coated substrates in dry test conditions at 0.47 m/s 129
Figure 5.26 Ploughing COF and SPWR (R) against load in 1 μm lead/indium coated substrates in dry test conditions at 0.47 m/s 130
Figure 5.27 Steady state COF and system SPWR against load in 1 μm lead/indium coated substrates in dry test conditions at 0.47 m/s 130
Figure 5.28 Ploughing COF and running-in time against load of 1 μm coated substrates in dry test conditions at 0.24 m/s 131
Figure 5.29 Ploughing COF and SPWR (R) against load of 1 μm coated substrates in dry test conditions at 0.24 m/s 132
Figure 5.30 Steady state COF and system SPWR of 1 μm coated substrates in dry test conditions at 0.24 m/s 132
Figure 5.31 Ploughing COF and running-in time against load of 1 μm coated substrates in marginally lubricated test conditions at 0.26 m/s 134
Figure 5.32 Ploughing COF and SPWR (R) against load of 1 μm coated substrates in marginally lubricated test conditions at 0.26 m/s 135
Figure 5.33 Steady state COF and system SPWR of 1 μm coated substrates in marginally lubricated test conditions at 0.26 m/s 135
Figure 5.34 Ploughing COF and running-in time against load of 1 μm coated substrates in marginally lubricated test conditions at 0.13 m/s 136
Figure 5.35 Ploughing COF and SPWR (R) against load of 1 μm coated substrates in marginally lubricated test conditions at 0.13 m/s 136
Figure 5.36 Steady state COF and system SPWR of 1 μm coated substrates in marginally lubricated test conditions at 0.13 m/s 137
Figure 5.37 Ploughing COF and running-in time against load of 5 μm coated substrates in dry test conditions at 0.47 m/s 139
Figure 5.38 Ploughing COF and SPWR (R) against load of 5 μm coated substrates in dry test conditions at 0.47 m/s 139
Figure 5.39 Steady state COF and system SPWR of 5 μm coated substrates in dry test conditions at 0.47 m/s 140
Figure 5.40 Ploughing COF and running-in time against load of 5 μm coated substrates in dry test conditions at 0.24 m/s 141
Figure 5.41 Ploughing COF and SPWR(R) against load of 5 μm coated substrates in dry test conditions at 0.24 m/s 141

Figure 5.42 Steady state COF and system SPWR of 5 μm coated substrates in dry test conditions at 0.24 m/s 141
Figure 5.43 Ploughing COF and running-in time against load of 5 μm coated substrates in marginally lubricated test conditions at 0.26 m/s 143
Figure 5.44 Ploughing COF and SPWR(R) against load of 5 μm coated substrates in marginally lubricated test conditions at 0.26 m/s 143
Figure 5.45 Steady state COF and system SPWR of 5 μm coated substrates in marginally lubricated test conditions at 0.24 m/s 145
Figure 5.46 Ploughing COF and running-in time against load of 5 μm coated substrates in marginally lubricated test conditions at 0.13 m/s 145
Figure 5.47 Ploughing COF and SPWR(R) against load of 5 μm coated substrates in marginally lubricated test conditions at 0.13 m/s 145
Figure 5.48 Steady state COF and system SPWR of 5 μm coated substrates in marginally lubricated test conditions at 0.13 m/s 146
Figure 5.49 Comparing of test results against coating thicknesses 148
Figure 5.50 Examples of friction-time graph in TWT apparatus 149
Figure 5.51 Examples of friction-time graph in POD apparatus 150
Figure 5.52 Flash temperatures against PV in TWT apparatus 152
Figure 5.53 Bulk temperatures against PV in TWT apparatus 152
Figure 5.54 Flash temperatures at various stages of coefficient of friction 153
Figure 5.55 Flash temperatures against LV in POD test apparatus at 0.47 m/s 157
Figure 5.56 Bulk temperatures against LV in POD test apparatus at 0.47 m/s 157
Figure 5.57 Flash temperatures against LV in POD test apparatus at 0.24 m/s 158
Figure 5.58 Bulk temperatures against LV in POD test apparatus at 0.24 m/s 158
Figure 5.59 Flash temperatures at different sliding velocities in POD apparatus 158
Figure 5.60 Mean COF and SPWR against PV of Toughmet substrates 163
Figure 5.61 An example of COF against time in Toughmet substrates 164
Figure 5.62 Worn Toughmet specimens after test 165
Figure 5.63 Mean COF against PV of Graphit-ic based coatings 167
Figure 5.64 SPWR against PV of Graphit-ic based coatings 167
Figure 5.65 Wear debris on AT 110-16D at P: 0.17 N/mm^2 and speed: 250 rpm test 169
Figure 5.66 Comparing mean COF and SPWR against load for Graphit-ic coating in dry test conditions 170

Figure 5.67 Ball and test specimen after 6 N load, 250 rpm 171
Figure 5.68 Comparing Toughmet substrates with leaded bronze substrates from TWT apparatus in dry test conditions 171
Figure 5.69 Comparing 10% lead/indium coated leaded bronze substrates with lead free coatings from TWT apparatus in dry test conditions 172
Figure 5.70 Comparison of 10% lead/indium coated leaded bronze substrates and Graphitic coated Toughmet substrates from POD apparatus in dry test conditions 172
Figure 5.71 Comparison of trends of test results among the test apparatus in dry test conditions 173
Figure 5.72 Comparison of trends of test results among the test apparatus in marginally lubricated test conditions 174
Figure 6.1 EDAX analysis and elemental composition of the black layer produced in marginally lubricated 20% leaded bronze substrate 180
Figure 6.2 EDAX analysis and elemental composition of worn areas of lead/indium coated leaded bronze substrates 182
Figure 6.3 5 µm lead/indium coated leaded bronze substrate 185
Figure 6.4 Worn-unworn areas on test disc in TWT apparatus 1 188
Figure 6.5 Microstructure of leaded bronze showing dark areas of lead distribution 189
Figure 6.6 Equilibrium diagram of 10% lead/indium 190
Figure 6.7 EDAX analysis on worn test specimens 194
Figure 6.8 Thin black layer from lead/indium smeared on leaded bronze substrates 197
Figure 6.9 Decrease in running-in time with increase in load 200
Figure 6.10 Influence of sliding velocity on ploughing COF at different track radii in dry test condition 201
Figure 6.11 Material transfer from leaded bronze substrates to the steel ball surface in dry test conditions 202
Figure 6.12 Material transfer from leaded bronze substrates to the steel ball surface in marginally lubricated test conditions 202
Figure 6.13 Various effects from leaded bronze substrates and lead/indium coatings 203
Figure 6.14 Smeared thin black layer (dark areas) from lead/indium coatings 204
Figure 6.15 Wear depths of test materials after running-in period: Load 2 N 205

Figure 6.16 Evidence of melting of lead/indium 211
Figure 6.17 SEM/EADX observations on Toughmet CX-105 212

List of Tables

Page

Table 2.1 Typical coefficient of friction values of unlubricated metals and alloys sliding on themselves or on mild steel at room temperature in air 21
Table 4.1 Voltage readings from transducer amplifier 75
Table 4.2 Nominal chemical composition of test materials 77
Table 4.3 Nominal chemical compositions (by wt %) of counterface materials 77
Table 4.4 Mechanical and thermal properties of test materials 77
Table 4.5 Roughness data of test materials measured from Talysurf profilometer 78
Table 4.6 Example COF calculations on a 1 μm lead/indium coated 30% leaded bronze substrate 78
Table 4.7 Example SPWR calculations on 30% leaded bronze substrate by gravimetric method 84
Table 4.8 Example SPWR calculations on 10% Pb/indium using Talysurf profilometer 85
Table 4.9 Combination of speeds and loads for marginally lubricated test conditions 87
Table 4.10 Combination of speeds and loads for unlubricated test conditions 87
Table 4.11 Steel washer dimensions for TWT 2 92
Table 4.12 Test conditions for Toughmet substrates 92
Table 4.13 Test conditions for candidate coatings 93
Table 4.14 Test conditions for lead based material in dry test conditions 96
Table 4.15 Test conditions for lead based materials in marginally lubricated test conditions 96
Table 4.16 Test conditions for Graphit-ic coatings on POD apparatus 97
Table 4.17 Number of rotations and total test time in POD at different velocities 98
Table 4.18 An example calculations of COF and SPWR during running-in and steady state for lead/indium coated 20% leaded bronze substrates 99
Table 5.1 Mean COF and SPWR results of uncoated leaded bronze substrates in dry test conditions 104
Table 5.2 Mean COF and mean SPWR of uncoated leaded bronze substrates at different sliding velocities in dry test conditions 105

Table 5.3 Mean COF and mean SPWR of uncoated leaded bronze substrates at different PV values in dry test conditions 106
Table 5.4 Mean COF and SPWR of uncoated leaded bronze substrates in marginally lubricated test conditions 107
Table 5.5 Mean COF and mean SPWR and their standard deviation of uncoated leaded bronze substrates at different sliding velocities in dry test conditions 108
Table 5.6 Mean COF and mean SPWR of uncoated leaded bronze substrates at different PV values in marginally lubricated test conditions 109
Table 5.7 COF and SPWR of 1 µm lead/indium coated leaded bronze substrates in dry test conditions at a sliding velocity of 0.12 m/s 110
Table 5.8 Mean COF of 1 µm lead/indium coated substrates as a function of PV in dry test conditions 112
Table 5.9 System SPWR of 1 µm lead/indium coated substrates as a function of PV in dry test conditions 112
Table 5.10 Mean COF and SPWR of 1 µm lead/indium coated substrates in marginally lubricated test conditions at a constant sliding velocity of 2.93 m/s 113
Table 5.11 Mean COF of 1 µm lead/indium coated substrates at increase in PV in marginally lubricated test conditions 114
Table 5.12 System SPWR of 1 µm lead/indium coated substrates at increase in PV in marginally lubricated test conditions 114
Table 5.13 Test results of 5 µm lead/indium coated substrates in dry test conditions at a sliding velocity of 0.12 m/s 115
Table 5.14 Mean COF of 5 µm lead/indium coated substrates in dry test conditions at different PV values 117
Table 5.15 System SPWR of 5 µm lead/indium coated substrates in dry test condition at different PV values 117
Table 5.16 Mean COF and SPWR of 5 µm lead/indium coated leaded bronze substrates in marginally lubricated test conditions 118
Table 5.17 Mean COF of 5 µm lead/indium coated substrates at different PV in marginally lubricated test conditions 120
Table 5.18 System SPWR of 5 µm lead/indium coated substrates at different PV in marginally lubricated test conditions 120

Table 5.19 Comparing COF and SPWR against coating thickness in dry and marginally lubricated test conditions 121
Table 5.20 Mean COF and SPWR of uncoated 20% leaded bronze and 30% leaded bronze substrates in dry test conditions 123
Table 5.21 Mean COF and SPWR results of uncoated substrates in dry test conditions 125
Table 5.22 Mean COF and mean SPWR of uncoated leaded bronze substrates in dry test conditions 126
Table 5.23 Mean COF and SPWR results of uncoated substrates in marginally lubricated test conditions at 0.26 m/s 126
Table 5.24 Mean COF and SPWR results of uncoated substrates in marginally lubricated test conditions at 0.13 m/s 127
Table 5.25 Mean COF and mean SPWR of uncoated leaded bronze substrates in marginally lubricated test conditions 128
Table 5.26 COF and SPWR of 1 μm lead/indium coated substrates in dry test conditions at 0.47 m/s 129
Table 5.27 COF and SPWR of 1 μm lead/indium coated substrates in dry test conditions at 0.24 m/s 131
Table 5.28 Mean ploughing COF and mean SPWR of 1 μm lead/indium coated substrates at different sliding velocities in dry test conditions 133
Table 5.29 Steady state COF and system SPWR of 1 μm lead/indium coated substrates at different sliding velocities in dry test conditions 133
Table 5.30 COF and SPWR of 1 μm lead/indium coated substrates in marginally lubricated test conditions at 0.26 m/s 134
Table 5.31 COF and SPWR of 1 μm lead/indium coated substrates in marginally lubricated test conditions at 0.13 m/s 136
Table 5.32 Mean Ploughing COF and mean SPWR (R) period of 1 μm coated leaded bronze substrates in marginally lubricated test conditions 137
Table 5.33 Mean steady state COF and SPWR of system for 1 μm coated leaded bronze substrates in marginally lubricated test conditions 138
Table 5.34 COF and SPWR of 5 μm lead/indium coated substrates in dry test conditions at 0.47 m/s 138
Table 5.35 COF and SPWR of 5 μm lead/indium coated substrates in dry test conditions at 0.24 m/s 140

Table 5.36 Ploughing COF and SPWR (R) for 5 μm lead/indium coated substrates in dry test conditions 142
Table 5.37 Steady state COF and system SPWR of 5 μm lead/indium coated substrates in dry test conditions 142
Table 5.38 COF and SPWR of 5 μm lead/indium coated substrates in marginally lubricated test conditions at 0.26 m/s 143
Table 5.39 COF and SPWR of 5 μm lead/indium coated substrates in marginally lubricated test conditions at 0.13 m/s 144
Table 5.40 Mean COF and mean SPWR of 5 μm lead/indium coated substrates in marginally lubricated test conditions 146
Table 5.41 Mean COF and mean SPWR of 5 μm lead/indium coated substrates in marginally lubricated test conditions 146
Table 5.42 Comparing COF and SPWR against coating thickness in dry and marginal lubrication conditions 147
Table 5.43 Contact conditions used in TWT apparatus and POD apparatus for comparing test materials 148
Table 5.44 Temperature measurements from TWT apparatus in dry test conditions at a sliding velocity of 0.12 m/s 151
Table 5.45 Temperature measurements from lead/indium coated leaded bronze substrates in dry test conditions in POD test apparatus at a sliding velocity of 0.47 m/s 156
Table 5.46 Temperature measurements from lead/indium coated leaded bronze substrates in dry test conditions in POD test apparatus at a constant sliding velocity of 0.24 m/s 156
Table 5.47 Mean COF and SPWR of Toughmet CX-105 and AT-110 in dry test condition at 0.17 m/s 162
Table 5.48 Mean COF and SPWR at change in PV of Toughmet substrates 163
Table 5.49 Thrust washer results of Graphit-ic and Chromium Graphit-ic coatings 166
Table 5.50 POD test results of Graphit-ic coatings in dry test conditions 169

Contents

Declaration *ii*
Abstract *iii*
Acknowledgements *v*
Nomenclature *vi*
Abbreviations *ix*
List of Figures *x*
List of Tables *xvii*

Chapter 1 Introduction 1

1.0 Introduction: The Purpose of Research 2
1.1 Method 4
1.2 Measurements 4
1.3 Layout of Thesis 6

Chapter 2 Materials for Sliding Bearings and Their Tribological Characteristics 7

2.0 Bearings 8
2.1 Requirements of Sliding Bearings 9
2.2 Bearing Materials 11
2.2.1 Metallic Bearings and Their properties 12
2.3 Coatings 13
2.3.1 Soft Metal Coatings and Their Properties 14
2.4 Introduction to Tribo-Systems 16
2.5 Friction 17
2.5.1 Mechanism of Sliding Friction 18
2.5.2 Friction of Materials 21
2.5.3 Effect of Operating Conditions 22
2.6 Wear 23
2.6.1 Adhesive Wear 23
2.6.2 Wear Volume Calculation 26
2.6.3 The PV Factor 26
2.6.4 Abrasive Wear 30

2.6.5 Wear of Metals and Alloys 31
2.7 Tribological Mechanisms in Coated Surfaces 38
2.7.1 Hardness of the Coating in Relation to the Substrate Hardness 38
2.7.2 Thickness of the Coating 39
2.7.3 Effect of Ploughing and Deformation 39
2.8 Lubrication 40
2.8.1 Fluid Film Lubrication 40
Summary 42

Chapter 3 Friction and Wear Measurement Techniques 43
3.0 Tribological Test Geometries 44
3.1 Pin on Disc and Thrust Washer Test Apparatus: General 45
3.1.1 Pin on disc Test Apparatus 45
3.1.2 Thrust Washer Test Apparatus 47
3.2 Methods to Measure the Tribological Characteristics of Coatings 49
3.2.1 Surface Texture 50
3.2.2 Hardness 53
3.2.3 Adhesion Tests 54
3.3 Wear Rate 55
3.3.1 Specific Wear Rate 56
3.4 Contact Pressure Calculations 57
3.4.1 Hertzian Formula for Non-Conforming Elastic Bodies 59
3.4.2 Plastic Deformation: Non-Hertzian Contact 60
3.5 Frictional Heating Calculations 61
3.5.1 Ashby's Method 61
3.5.2 Effect of Surface Films 66
Summary 67

Chapter 4 Detailed Descriptions of Test Apparatus Used 68
4.0 Introduction 69
4.1 Thrust washer test Apparatus 1 69
4.2 Experimental Details 73
4.2.1 Test Procedure 73

4.2.2 Flow Chart Thrust Washer Test 73
4.2.3 Calibration of Input and Output Devices 74
4.3 Materials 76
4.3.1 Steel Washer (counterface) 76
4.3.2 Test Materials (substrates) 76
4.4 Examples of Friction and Wear Measurements 78
4.4.1 Coefficient of Friction (COF) 78
4.4.2 An Example of Various Characteristics of Friction against Time graph 79
4.4.3 Explaining Mean Coefficient of Friction 81
4.4.4 Specific Wear Rate (SPWR) 83
4.4.3 Correlations of Results 86
4.5 Problems with Thrust Washer Test Machine 1 88
4.5.1 Modifications 88
4.6 Thrust Washer Test Apparatus 2 89
4.6.1 Materials and Test Conditions 91
4.6.2 Advantages of New Thrust washer 93
4.7 Pin on Disc Test Apparatus 93
4.7.1 Test Materials and Test Conditions 95
4.7.2 Coefficient of Friction and Specific Wear Rate Measurements 98
Summary 100

Chapter 5 Experimental Results 101
5.0 Overview 102
5.1 Thrust washer Test Results 102
5.1.1 Uncoated Leaded Bronze Substrates 103
5.1.2 1 µm Lead/Indium Coated Leaded Bronze Substrates 109
5.1.3 5 µm Lead/Indium Coated Leaded Bronze Substrates 115
5.1.4 Comparing test results as a function of coating thickness 120
5.2 Pin on disc test results 122
5.2.1 Uncoated Leaded Bronze Substrates 123
5.2.2 1 µm Lead/Indium Coated Leaded Bronze Substrates 128
5.2.3 5 µm Lead/Indium Coated Leaded Bronze Substrates 138

5.2.4 Comparing Test Results As a Function of Coating Thickness 147
5.2.5 Examples of Coefficient of Friction Against Time Graph 148
5.3 Frictional Heating Calculations 151
5.3.1 Thrust Washer Test Apparatus 151
5.3.2 Pin on Disc Test Apparatus 155
5.4 Toughmet Substrates and Graphit-ic Coatings 161
5.4.1 Toughmet Substrates 161
5.4.2 Graphit-ic Coatings and Cr-Graphit-ic Coatings 165
5.5 Comparison of Toughment with Leaded Bronze and Graphitic with Lead/Indium 171
5.6 Comparison of TWT Apparatus and POD Test Apparatus 173
Summary 174

Chapter 6 Observations and Discussion 176
6.0 Overview of the Project 177
6.1 Thrust washer Test Results 177
6.1.1 Uncoated Leaded Bronze Substrates 178
6.1.2 1 µm Lead/Indium Coated Leaded Bronze Substrates 181
6.1.3 5 µm Lead/Indium Coated Leaded Bronze Substrates 184
6.1.4 Comparison of COF and SPWR According to Coating Thickness 186
6.1.5 Various Observations and Influences of Test Parameters On Friction and Wear Behaviour of Test Materials 186
6.1.6 Ranking of Materials from TWT Apparatus 190
6.2 POD Test Results of Leaded Bronze Substrates and Lead/Indium Coatings 191
6.2.1 Uncoated Leaded Bronze Substrates 192
6.2.2 1 µm Lead/Indium Coated Leaded Bronze Substrates 193
6.2.3 5 µm Lead/Indium Coated Leaded Bronze Substrates 196
6.2.4 Comparing COF and SPWR according to Coating Thickness in POD Apparatus 198
6.2.5 Various Observations and Influences of Test Parameters on Friction and Wear Behaviour of Test Materials 199

6.2.6 Ranking of test materials from POD Apparatus 206
6.3 Comparison of TWT Apparatus and POD Apparatus 206
6.4 Frictional Heating Calculations from Ashby's Method 207
6.4.1 Thrust Washer Test Apparatus (Flat on Flat Contact) 207
6.4.2 Pin on disc Test Apparatus (Ball on Flat Contact) 209
6.5 Toughmet Substrates, Graphit-ic and Cr-Graphit-ic Coatings 211
6.5.1 Toughmet Substrates 212
6.5.2 Graphit-ic and Cr-Graphit-ic Coatings 213
6.6 Comparison of Toughmet and Leaded Bronze Substrates 214
6.7 Comparison of Graphit-ic and Lead/Indium Coatings 215
6.8 Conclusions from All Test Materials 215

Chapter 7 Conclusions and Further Recommendations 218
7.0 Final Conclusions 219
7.1 Further Recommendations 220
7.1.1 New Materials and Surface Engineering 220
7.1.2 Experimental Investigations 221
7.1.3 Wear Mechanism Analysis 222
7.1.4 Data Analysis 222

References 224

Appendix
Presentations and Publications 234

CHAPTER 1

INTRODUCTION

1.0 Introduction – The Purpose of Research

Bearing materials are designed to have low friction, high wear resistance, high load carrying capacity and self lubricating properties even in near vacuum and hot corrosive conditions. Bearing materials for this study are principally copper based alloys (i.e. bronze based) which are used as journal bearings and thrust bearings in fuel pumps for an aircraft gas turbine engine. The fuel pump associated with this project is a high pressure gear pump. The gear pump is one of the leading designs for medium to large engine civil aircraft. A section of the high pressure stage is shown in figure 1.1, the gear shaft rotates in-between two journal bearings whose end faces act as thrust bearings as shown in figure 1.2. In this arrangement some of the pressurised fuel is fed back through grooves on to the thrust face of the bearings to encourage hydrodynamic lubrication at the contact between the flat side of the journal bearing and the flat side of the gear face (i.e. the thrust face of the gear pump). This interface is the main subject for tribological study in this project.

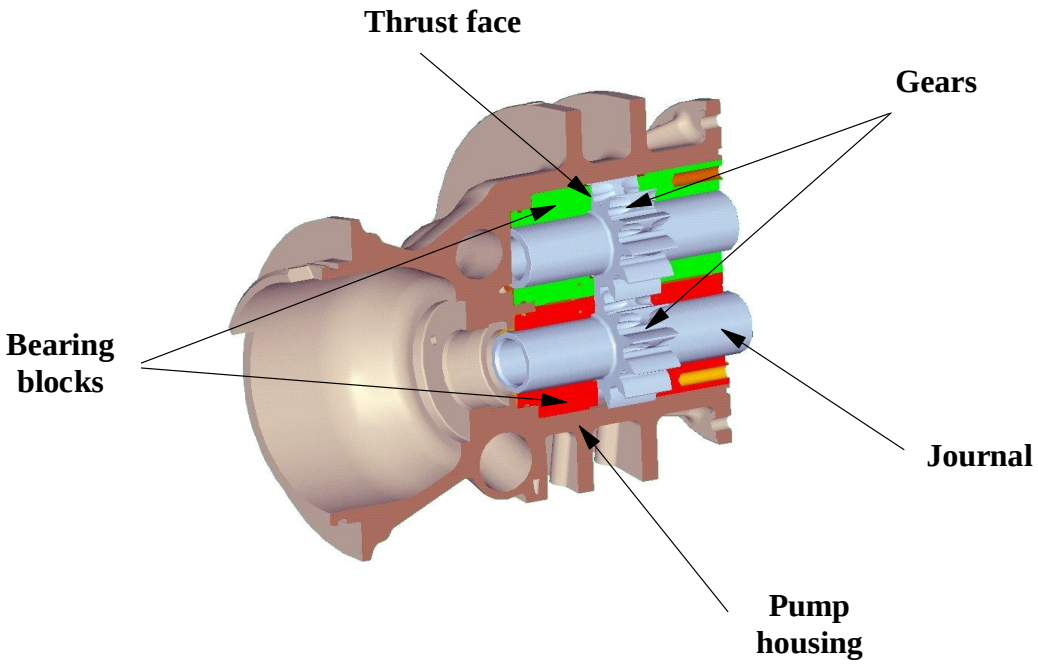

Figure 1.1 Gear pump thrust bearing in fuel pumps. (Adapted from Goodrich Aero Engine Controls (2009)).

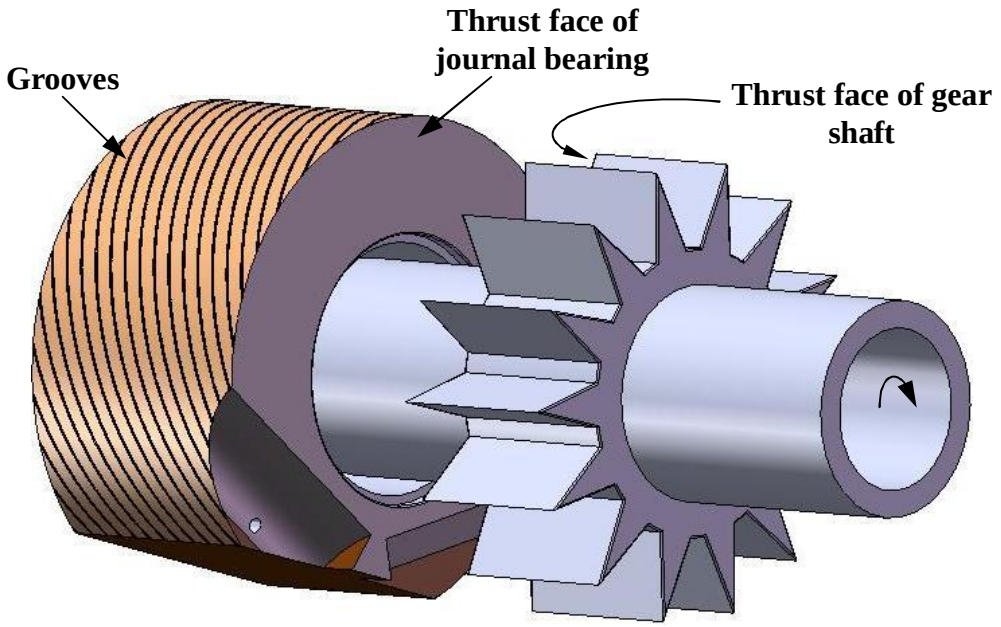

Figure 1.2 Thrust faces of journal bearing and gear shaft in fuel pump (After Goodrich Aero Engine Controls (2009)).

In the gear pump, lubrication of journal bearings and gear shafts is achieved by the leakage flow through the journal bearings. Hydrodynamic pressure is generated when the gears are running against the slightly concave journal faces. One of the main concerns identified in relation to the fuel pump is the breakdown of the fluid film between the thrust faces of journal bearings and gear shaft when there is a break in the supply of fuel either during start-up or fuel supply failure. In these conditions the design of the contacting materials is very important to avoid fuel pump damage and to accommodate a period of “emergency running”. The main intention of this project was to measure and understand the friction and wear properties of a range of bearing materials supplied by Goodrich Aero Engine Controls (2009) using suitable tribological test methods to replicate these contact situations in the fuel pump. The second issue of concern is that although lead is a tribologically helpful material, it is environmentally harmful. Consequently, a second reason for conducting the project was to benchmark the materials carefully used in the pump to allow comparison with reduced lead, or even lead free materials at a future date. The third aim was to determine whether different test

regimes (conventional tests or accelerated tests) could be used reliably to obtain friction and wear data about bearing materials.

1.1 Method

This project involved measuring friction and wear characteristics of thrust bearing materials namely 20% leaded bronze, 30% leaded bronze substrates and both these substrates coated with 1 µm and 5 µm thick 10% lead/indium alloys sliding against a high chromium steel counterface material as used on gear shafts in fuel pumps. In addition to these materials, a few candidate lead-free coatings, such as Graphit-ic coatings, were investigated to assess their tribological properties and potential to replace traditional lead-based materials in the future. In order to understand and identify the tribological properties of these materials, the real contact situation was replicated in a smaller scale using a suitable test apparatus, a thrust washer tester (TWT). To conduct accelerated friction and wear tests on the same materials, a conventional pin on disc (POD) test apparatus has been used to conduct high contact pressure tests. The project has also sought to understand the contact theoretically by predicting the frictional heating between the contacting faces to identify possible melting phases of 10% lead-indium coating (if any).

To summarise, the main objectives were to:

- Measure the friction and wear of 20% leaded bronze, 30% leaded bronze substrates and both these substrates coated with 1µm and 5 µm 10% lead/indium in unlubricated as well as marginally lubricated conditions.
- Measure friction and wear of candidate lead free coatings in unlubricated conditions.
- Make theoretical predictions of frictional heating (flash temperature and bulk temperature).
- Compare the rankings of test materials from thrust washer test apparatus and pin on disc test apparatus

1.2 Measurements

To investigate coefficient of friction (COF) and wear rate of the test materials mentioned before, two types of test apparatus, namely thrust washer test apparatus

and pin on disc test apparatus, were chosen. All the test specimens used in this project were supplied by Goodrich Aero Engine Controls (GAEC, 2009), who manufacture aircraft fuel systems. The thrust washer test apparatus simulates the in-service thrust bearing contact conditions and the pin on disc test apparatus was used for accelerated tests in which high contact pressures are applied to a small area. The operating conditions of the gear pump were simulated on thrust washer test apparatus by maintaining the product of pressure and velocity (PV). This product was plotted against COF and specific wear rate (SPWR) to try to understand the tribological effects. In pin on disc test apparatus, product of load and velocity (LV) was used when comparing the friction and wear results of all test materials. The frictional heating calculations on the substrate/counterface contacts were analysed theoretically in both types of test apparatus to identify temperatures for phase transformation on the coating material (if any). Candidate coatings such as "Graphit-ic", supplied by Teer coatings (2009), which has good wear resistant properties, was tested for friction and wear properties in the same way as the test specimens to establish its potential as a replacement coating for 10% lead/indium. A summary of the total test process is shown in Figure 1.3

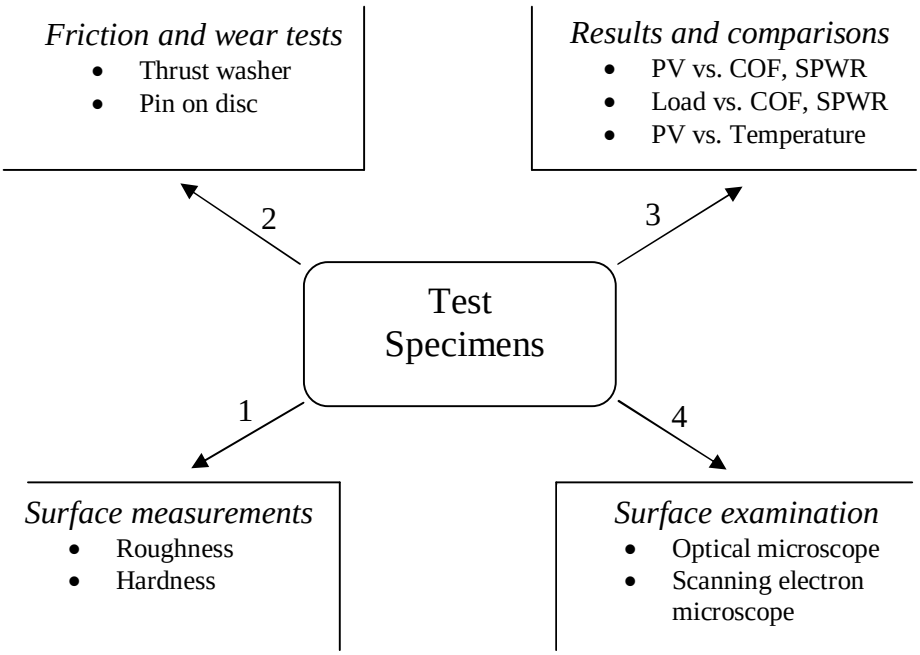

Figure 1.3 Summary of testing procedures on test specimens.

1.3 Layout of the Thesis

This thesis has been divided mainly into seven chapters. The "Introduction" chapter, details the problems identified in the fuel pumps and the main objectives of this thesis work. The next two chapters; materials for sliding bearings and their tribological characteristics and, friction and wear measurement techniques, present a literature survey and fundamentals of friction and wear in coated surfaces, influence of various parameters on friction and wear, and various methods to measure friction and wear of surfaces. Chapter 4 gives details of the tribological test machines used in this project, mechanical and thermal properties of test specimens supplied by GAEC (2009). Chapter 5 shows the calculated results obtained from friction and wear measurements for the different types of test apparatus, with comparison graphs. Chapter 6 discusses all the results, including the graphs shown in the previous chapters and describes various observations obtained from the test samples using optical microscope/white light interferometer. Chapter 7 gives the conclusions drawn from all test results and further recommendations on test materials for the gear pump thrust bearings. The complete layout of the thesis is shown in figure 1.4

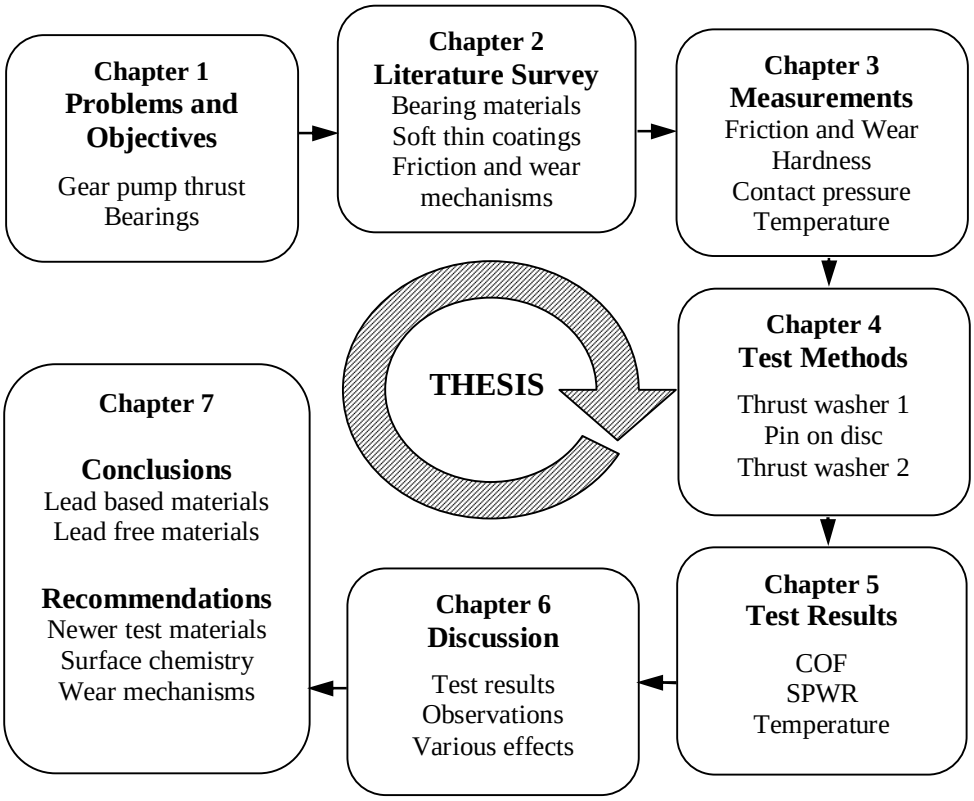

Figure 1.4 Layout of the thesis.

CHAPTER 2

MATERIALS FOR SLIDING BEARINGS AND THEIR TRIBOLOGICAL CHARACTERISTICS

2.0 Introduction - Bearings

Bearings are machine elements which provide support and constrained motion relative to a driving mechanism. They transmit the load from a moving member to a stationary member and prevent motion in the direction of the applied load (Neale, 1996; Bhushan, 1999). Bearings can be generally classified according to: a) the direction of force acting on them: (radial bearings and thrust bearings); b) the frictional mechanism that is operative: (sliding contact bearings and rolling contact bearings). In radial bearings, the load acts perpendicular to the axis of rotation whereas in thrust bearing, the load acts along the axis of rotation.

In sliding contact bearings, the load is transmitted between moving parts by sliding contact. Two common types of sliding contact bearings are journal bearings and thrust bearings. A journal bearing supports and constrains rotational motion when it is subject to radial loading whereas a thrust bearing constrains axial motion, often while permitting rotation. A schematic of rotating shaft supported by journal bearing and thrust bearing is shown in figure 2.1.

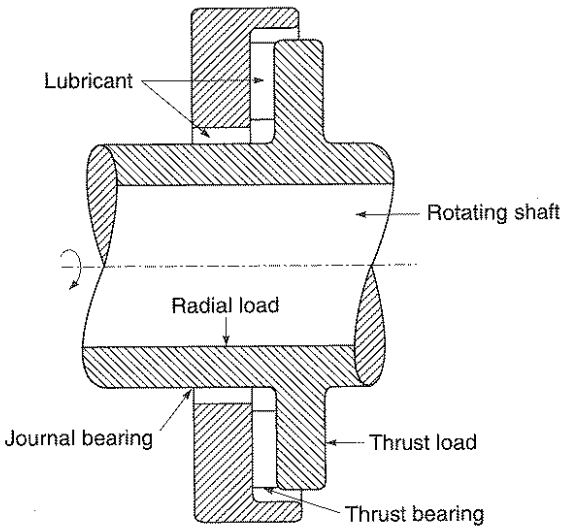

Figure 2.1 Schematic of rotating shaft supported by journal bearing and thrust bearing (Adapted from Bhushan (1999)).

This project was specifically concerned with investigating tribological behaviour and potential improvements of a particular type of sliding bearing, which is currently in use in aircraft fuel pumps; therefore, rolling contact bearings are not discussed here. Section 2.1 discusses the requirements of sliding contact bearings;

Section 2.2 reviews the bearing materials in current use; Section 2.3 discusses the use of soft metal coatings in sliding bearings; Sections 2.4 to 2.7 review the tribological characteristics of bearing materials and soft metal coatings which are particularly pertinent to this project. Sections 2.8 summarize details of the lubrication regimes.

2.1 Requirements of Sliding Bearings

The choice of materials for sliding contact bearings for a particular application depends on: the type of bearing (journal, thrust etc), the type of lubricant used and, finally the operating and environmental conditions used. Since no such bearing material exists that can satisfy all the requirements needed for a good bearing, prior selection must be made on the basis of important characteristics required for the application. In general, the bearing materials are selected depending on various important requirements described by many authors (Barwell, 1979; Neale, 1996; Holmberg and Matthews, 1994; Arnell, et. al., 1991) summarized below.

2.1.1 Compatibility

Even when a lubricating film normally prevents direct contact between the shaft and the bearing surfaces, there are times during operation metal-to-metal contact takes place. Due to the rubbing operation of the shaft and bearing, high localised temperatures can occur and adhesion between the hot contact spots can result in damage to one or both materials. Therefore, the selection of a compatible material pair is very important to resist welding action and minimise the wear mechanisms (Hamrock, 1994).

2.1.2 Conformability

Conformability is an important characteristic required for a bearing material. It allows bearing to conform to mis-alignments between the shaft and the bearing due to the inaccuracy in manufacturing or installation of parts. During sliding contact between the bearing surfaces, mis-alignments and non-flatness of surfaces can lead to high friction and wear. Bearing materials with a low modulus of elasticity are readily conformable and can reduce friction, wear losses and premature failure (Hamrock, 1994).

2.1.3 Embeddability

During the sliding operation of bearings, debris produced at the sliding interface or dirt from the lubricant can result in high friction and abrasive damage of one or both surfaces. Therefore, the bearing material must be soft enough to allow any abrasive particles that may enter the bearing surface to become embedded (i.e. pressed into the bearing surface) to reduce the abrasive friction and wear losses (Rabinowicz, 1995; Zeren, 2007).

2.1.4 Fatigue Strength

In many tribological situations, for example in crankshaft bearings, there are frequent variations in both the normal load and the friction forces acting at the bearing surface. These load variations can cause fatigue cycling. Bearings must therefore have adequate fatigue strength to minimise fatigue failures at the bearing surface (Fuller, 1984).

2.1.5 Compressive Strength

Compressive strength is the ability of a material to support loads without collapsing or rupturing. Compressive strength in bearings is normally enhanced by supporting the relatively soft bearing material on a harder steel backing (Fuller, 1984).

2.1.6 Thermal Conductivity

Thermal conductivity is the ability to dissipate heat due to frictional effects from the contact surfaces. The thermal conductivity of the bearing material should be high enough to ensure satisfactory dissipation of the heat generated by friction if hydrodynamic lubrication condition cannot be maintained (Williams, 2005).

2.1.7 Wear Resistance

The bearing material should be wear resistant to withstand higher contact loads and higher temperature environments so that wear losses can be minimised (Bhushan, 2001).

2.1.8 Corrosion Resistance

Corrosion resistance is the ability to protect the surface from corrosion by acids formed in lubricating oils, chemical environment, or the effects of oxidation. Copper-lead, cadmium and silver alloys are especially vulnerable to attack (Landown and Price, 1996).

Out of the above bearing material requirements, compatibility, conformability, thermal conductivity and wear resistance are particularly applicable and important to the test materials investigated in this thesis work.

Compatibility of the substrate-counterface system was a property of the materials designed and supplied by GAEC (2009), whereas conformability and embedability are only applicable to leaded bronzes, and not to the lead/indium coatings, since their small coating thickness does not provide the ability to align or embed wear particles during operation. Fatigue strength, compressive strength and corrosion resistance requirements have not much influence on the test materials used for this work.

2.2 Bearing Materials

Materials for bearings are classified as metals and non-metals. Metals include various types of soft metals such as babbits, copper-based materials, aluminium based materials, cast iron, silver and porous metals. Non-metals include wood, carbon-graphite, plastics (such as PTFE, polyamide, nylon, acetal, polyethylene etc), elastomers, ceramics, cermets etc. The bearing materials can be selected depending on the contact geometry, operational and environmental conditions (Ludema, 1996). The majority of plain bearing materials are metal based because of their favourable characteristic features such as embeddability and conformability, discussed earlier. These materials are generally considered as “classical” bearing materials because of their excellent friction and wear resistance characteristics, long life time and low cost. Some of the copper bearing materials such as leaded bronze act as solid lubricant in the absence of a lubricating film, and self align according to the change in operating conditions (Prasad, et. al., 1996; Zeren, et. al., 2007). Since this project was mainly based on soft metal coatings of lead/indium alloy and bulk materials of leaded bronze, non-metallic bearings are not discussed here.

2.2.1 Metallic Bearings and Their Properties

The most commonly used metal-based bearings are classified as:

(a) Babbitts
(b) Copper alloys
(c) Aluminium alloys
(d) Porous metal bearings

Out of these, copper alloys are of the main interest to this project. Therefore, the other metallic bearing type materials are not fully described here (Complete descriptions of these metal based bearings are given elsewhere (ESDU, 1988; Anonymous, 1990; Bhushan, 2001)).

(a) Babbitt's

Tin and lead based alloys are commonly known as Babbitt's or white metals and are the best known bearing materials because of their wide range of tribological applications. Babbitt's have the ability to embed dirt and have excellent compatibility properties under boundary lubricated conditions (Zeren, 2007). These alloys are generally used as thin coatings over automotive engine bearings.

(b) Copper Alloys

The copper alloys are generally categorized into copper-lead, leaded bronze, tin-bronze and aluminium bronze alloys. Copper alloys exhibit a range of physical properties such as hardness and strength, and shows high thermal conductivity (CDA, 2010). Due to their higher lead content and better compatibility properties copper-lead and leaded-bronzes are the best bearing alloys (Bhushan and Gupta, 1997; Ahsan, et. al., 2003). Copper-lead bearings usually contain 25% to 45% lead and often small amounts of other elements. They are widely used where loads are higher than those can be carried by babbitts. The conformability of copper-lead is lower than that of white metals (Fuller, 1984). Bronze bearings are one of the most common types of bearings used in dry and liquid lubricated bearing systems designed for low to medium loads. Leaded tin bronzes are widely used for plain bearings and for other tribological applications. They contain a large quantity lead usually from 20% to 30% mainly added to provide solid lubrication during sliding through smearing of the lead over the mating surfaces (Prasad,

2004). Increase in lead content provides additional embeddability and solid lubricating properties, but reduces strength. Tin bronzes are harder than leaded bronzes and small amounts of lead content in tin bronzes provide some scoring resistance (Bhushan, 1999).

(c) Aluminium Alloys

The typical alloying elements in Aluminium alloys are copper, zinc, magnesium, silicon and manganese. Aluminium alloys have excellent corrosion resistance, good thermal conductivity and are available at low cost. But the embeddability and galling resistance of aluminium alloys are lower than that of lead based alloys. For better compatibility with steel, high tin content is added to aluminium alloys (Glaeser, 1992). The most commonly used Aluminium bearing material is SAE 750, which has 6.5% tin to improve compatibility (Anonymous, 1990).

(d) Porous Metal Bearings

These bearings are made of powdered metals (generally contains 90% Cu and 10% Sn) and are used as a replacement to plain metal bearings when there is a lack of space or inaccessibility for lubrication occurs. The deep pores can be filled with lubricating oil so that the bearing does not require further lubrication during the application (Glaeser, 1992). These types of bearings are commonly rated on the basis of PV (product of bearing pressure and velocity). Typical applications are pedal bearings, water-pump bearings etc.

2.3 Coatings

The main function of a coating on a bearing surface is to control friction and minimise wear (and sometimes corrosion) so that the lifetime of the bearing increases. The coating separates the bearing surface and the counterface material so that direct metal to metal contact will not take place and friction and wear losses are minimised. Liquid lubricants can be used instead of coatings but their applications are limited by the operating temperature and environmental conditions. In severe wear conditions liquid lubricants may not function properly due to improper supply, evaporation and chemical breakdown due to high temperatures. In bearings running at low speeds and at high contact loads in dry conditions, there is direct contact between the between the shaft and bush which can be minimised by surface coatings. Applying a coating to the substrate allows wear mechanisms such as adhesion, abrasion, fatigue, etc to be controlled.

Coatings can be classified into soft coatings and hard coatings. These materials have different resistance to friction, wear, thickness, load carrying capacity, temperature and contact geometry (Bhushan, 2001).

Soft coatings are used as solid lubricants (Holmberg and Matthews, 1994). Solid lubricants protect surfaces from severe damage and reduce friction to a significant extent during relative motion. The thickness of soft coatings varies from a fraction of a micrometre to a maximum of 50 μm. These coatings have good wear resistant properties and are commonly used in aerospace industries especially in applications such as bearing systems operating in high load and high speed conditions. Examples of soft coatings include layered solid coatings (MoS_2, graphite), polymers and soft metals (Ag, Au, Pb, In and Sn).

Hard coatings can have very good wear resistance properties and are extensively used in highly loaded and/or high temperature conditions. The thicknesses used for hard coatings are typically several micrometres to several millimetres (Holmberg and Matthews, 1994; Stachowiak and Batchelor, 2005). They generally have higher hardness than their substrates. Some hard coatings can withstand temperatures above 1000 ºC. Some of the examples of hard coatings are metals (such as nickel, chromium, and molybdenum), oxides, carbides and nitrides.

Since much of the attention in this project is based on soft metal coatings, hard coatings are not discussed further here.

2.3.1 Soft Metal Coatings and Their Properties

Soft metal coatings including lead, silver, gold and indium provide the low shear conditions needed for sliding applications. Bowden and Tabor (1964) studied various soft metal coatings sliding against metal surfaces and found that coatings in the thickness range from 0.1 to 10 μm can show a coefficient of friction lower than 0.1 but have limited wear life. The thickness, surface roughness and oxidation of the coatings are important parameters in applications with thin films (Holmberg and Matthews, 1994). The surface roughness of the substrate is an important factor especially when the thickness of the soft coating is of the same order of magnitude as the substrate roughness; it is less important for thick

coatings (Sherbiney and Halling, 1977; Jahanmir, et. al., 2003). Some important tribological characteristics of lead and indium are described below.

Lead

Lead is a soft material which has lubricating properties when in a harder matrix or on a harder substrate. It is commonly used in babbitt metal and lead bronze bearings. Lead has good antifriction properties and, to get the benefit of these properties, a minimum of 15% lead is considered to be required in bronze bearings (Bowden and Tabor, 1950; Anonymous, 1990). The surface of lead oxidizes readily and when oxidised, it appeared in black colour (Anonymous, 1990). Due to incorporation of this oxide, lead can become harder and more brittle each time it melts. This is one reason why bearings made incorporating lead are not subjected to repeating melting. For better score resistance and anti seizure properties, lead-indium is used as a coating. The advantage of lead over other solid lubricant films such as the easy formation of leadoxide (PbO), a good solid lubricant within the lead film (Clauss, 1972).

The coefficient of friction of lead sliding against itself is very high in the range of 1 to 2 (Arnell and Soliman, 1978). When sliding against steel, the coefficient of friction is about 0.9. A low coefficient of friction of about 0.3 has been observed when a steel ball slides against a 30 μm lead film deposited on a copper substrate (Bowden and Tabor, 1950). This was due to the low shear properties of lead. The optimum film thickness value is not the same for different substrate materials, such as steel, and the optimum film thickness is influenced by the hardness of the metal substrate. A low coefficient of friction of 0.1 was observed by Bowden and Tabor (1950) when an optimum film thickness of 0.2 to 1 μm was deposited on a steel ball sliding on a steel surface. It was shown that surface roughness plays an important role, the higher the roughness of substrate, the higher the coefficient of friction when a thin film of lead was deposited on a steel ball sliding against a steel substrate. This arises due to increased penetration of the coating and increased steel/steel contact with rougher surfaces. In vacuum, an optimum film thickness of lead coatings in the range of 0.2 to 1 μm has been observed by Arnell and Soliman (1978) to give a minimum coefficient of friction at a surface roughness of 0.5 μm. Overall, it can be concluded that the coefficient of friction increases with very thin films, thick films and also with rough substrates. At high

loads in air and at increased temperature up to 300 ºC in vacuum, a low coefficient of friction and decrease in film life time was observed by Bowden and Tabor (1950). It is suggested that the reason for this could be increased load and temperature cause melting of the coating at the contact resulting in low shear strength, but increased wear rate.

Indium

Indium is a soft silver white metallic material that oxidises relatively slowly (Anonymous, 1990; Holmberg and Matthews, 1994). The addition of indium increases the hardness and tensile strength of copper, silver and lead alloys. It also increases the corrosion resistance when used in lead alloys. A low coefficient of friction of 0.08 has been observed for an optimal thickness range of 0.1 to 1 µm in air by Arnell and Soliman (1978) and in vacuum by Bowden and Tabor (1950). The coefficient of friction has been found to decrease with increasing load when an indium coated steel ball slides on a steel surface (Sherbiney and Halling, 1977).

2.4 Introduction to Tribo-Systems

The formal definition of tribology is the "science and technology of interacting surfaces in relative motion and of related subjects and practices" (Bhushan, 1999), it involves the study of friction, wear and lubrication. Whenever two bodies interact and slide against each other, there are various tribological losses, principally energy consumption due to friction and material loss due to wear. The more expensive tribological loss is usually wear, which can lead to the failure of a component. Industries dealing with mechanical components generally aim at minimising friction and wear losses to protect the lifetime of the component and minimise frictional energy consumption.

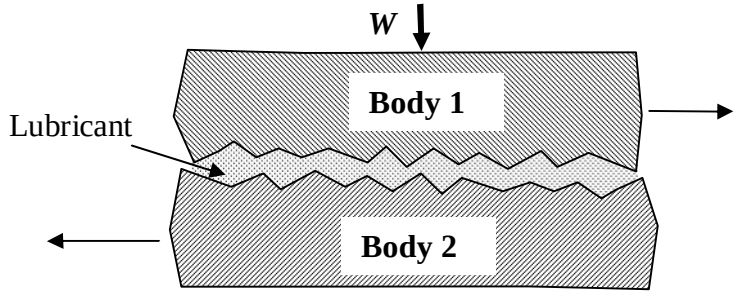

Figure 2.2 Tribo system.

A basic tribo-system is shown in figure 2.2 which shows two interacting bodies - body 1 and body 2 - separated by a lubricant or thin film under particular environmental conditions.

The tribological behaviour of the tribo system is influenced by various factors such as:

- The test materials and their microstructure
- The operational conditions, such as load, sliding speed, contact geometry
- The mechanical properties of the components of the system
- Thermal effects (temperature).

2.5 Friction

When two solid bodies slide against each other, friction occurs. Friction is the resistance to sliding or rolling of one body in contact with another. The tribological response when two bodies are sliding or rolling against each other will determine their life time (Landown and Price, 1996). Several factors that can influence the friction between two solid bodies sliding against each other are the operating conditions such as loads, speeds, temperature and, contact conditions such as contact geometry and other environmental conditions.

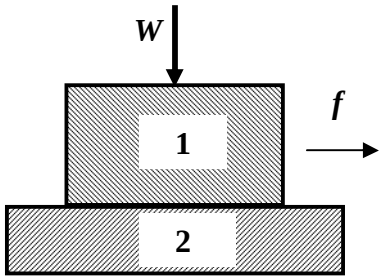

Figure 2.3 Schematic illustration of sliding friction.

When two solid bodies 1 and 2 as shown in figure 2.3 are loaded together and a tangential force (*f*) is applied, then the tangential force required to initiate the motion is called the static friction force and the force required to maintain this relative motion is called the kinetic friction force. In general the static friction force is higher than or equal to the kinetic friction force.

The two basic laws of friction generally referred as Amontons (1699) laws, are described below.

The first law of friction states that the frictional force is proportional to the normal load. The friction coefficient (μ) is the constant ratio between the frictional force (*f)* and normal load (*W*) as shown in figure 2.3

$$\mu = \frac{f}{W} \tag{2.1}$$

The observed coefficients of dry friction typically vary from 0.05 to > 10. The higher friction values have been observed with soft, clean metals sliding against themselves in vacuum (Bhushan, 2001).

The Second law of friction states that friction force is independent of the apparent area of contact between the contacting bodies. It should be emphasized that coefficient of friction is strictly constant only for a given set of sliding materials under a given set of operating conditions such as temperature, normal pressure, humidity and sliding velocity.

2.5.1 Mechanism of Sliding Friction

Adhesion Theory of Friction

A mechanism of sliding friction, known as the adhesion theory of friction, was first put forward by Bowden and Tabor (1950). They postulated that when two nominally flat surfaces are held together by the application of a normal force, the contact only takes place at the tips of the higher asperities, the load being supported by the deformation of contacting asperities. The sum of the areas of all the contact spots constitutes the real area of contact (A_r) and, for most material under normal loading, the real are of contact is much smaller than the apparent area of contact (A_p). Even at modest loads, the pressures at these very small localised contacts are so high that severe plastic deformation will occur and welded junctions will be formed (Hutchings, 1992). When these two surfaces slide relative to each other, rupture takes place at the weakest regions of the contact and, after shearing of the existing contacts, new contacts are formed. The friction force for the system will depend on the shear strength (*S*) of the materials (Bowden and Tabor, 1950). For dry contact systems, the friction force (f_a) is defined by Bowden and Tabor (1950) as,

$$f_a = A_r S \tag{2.2}$$

The coefficient of adhesive friction (μ_a) for components in dry contact is then the ratio between the average shear strength of the contact junctions and the mean contact pressure at the contacts (P_{mean})

$$\mu_a = \frac{A_r S}{W} = \frac{S}{P_{mean}} \tag{2.3}$$

If shear occurs in one of the sliding bodies, the shear strength of the relevant body should be used. For plastic contacts, the adhesive coefficient of friction is defined by Bhushan (2001) as.

$$\mu_a = \frac{\tau_a}{H} \tag{2.4}$$

Where, τ_a is the shear stress and H is the hardness of the softer of the contacting materials. μ_a is independent of the surface roughness in plastic contacts such as a copper sliding against copper (Rabinowicz, 1995).

Deformation and Ploughing Theories of Friction

During the sliding of two contacting surfaces against each other, two types of interactions commonly occur: localised plastic deformation of asperities and ploughing. Plastic deformation happens due to the interlocking of asperities at the microscopic level and ploughing is due to scoring of the softer surface by the harder material at the macroscopic scale. These mechanisms are resulting in material displacement or fracture. Ploughing of either or both surfaces can also be caused by wear particles trapped between the contacting surfaces. Ploughing increases friction force and creates wear particles which causes further increase of friction and wear (Suh, 1981). In metals the dominant wear mechanism of energy dissipation is plastic deformation (Rigney, 1981).

The expressions for the ploughing component of friction when a spherical asperity of radius R is in sliding contact with a softer body, as shown in figure 2.4, is described by Moore (1972). The expression for the ploughing contact area is summarized as,

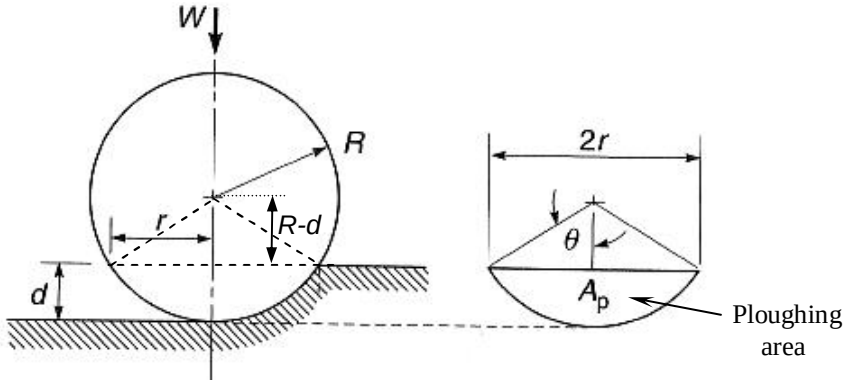

Figure 2.4 Schematic of hard sphere sliding on softer material (Adapted from Moore (1972)).

From the figure 2.4,

$$A_1 = \frac{1}{2}\pi r^2 \tag{2.5}$$

$$A_p = \frac{1}{2}R^2\left(2\theta - sin2\theta\right) \tag{2.6}$$

A_1 is the load support area (i.e. horizontal projection of asperity contact), A_p is the ploughing area of the component, θ is the attack angle, r is the half radius of the contact and d is the ploughing depth.

Using Pythagorean Theorem, $r^2 + \left(R-d\right)^2 = R^2 \Rightarrow r = \sqrt{2Rd - d^2}$ (2.7)

But $$sin\theta = \theta - \frac{\theta^3}{3!} + \cdots$$

For small values of θ, $$A_p \approx \frac{2}{3}R^2\,\theta^3$$

But $$sin\theta = \frac{r}{R} \approx \theta \qquad for\ small\ \theta$$

Therefore, $$A_p \approx \frac{2}{3}\frac{r^3}{R} \tag{2.8}$$

The ploughing coefficient of friction, μ_p is given as:

$$\mu_p = \frac{A_p}{A_1} = \frac{4}{3\pi}\frac{r}{R} \tag{2.9}$$

Similar expressions for other asperity shapes are described by Suh (1986).

2.5.2 Friction of Materials

As discussed before, the coefficient of friction depends on the type of contact, mating material, surface preparation and operating conditions. Some typical values of friction between metals have been identified from many experimental investigations and the coefficients of friction obtained for various combinations of metals and alloys given by Bhushan and Gupta (1997) are summarized in table 2.1 below.

Table 2.1 Typical coefficient of friction values of unlubricated metals and alloys sliding on themselves or on mild steel at room temperature in air. (Bhushan and Gupta (1997)).

Material	Coefficient of friction	
	Self mated	On mild steel
Soft metals In, Pb, Sn	0.8 - 2	0.5 - 0.8
Metals Al, Co, Cr, Fe, Mg, Mo, Ni, Ti, W, Zn, Zr	0.5 - 1.5	0.4 - 1.5
Alloys Leaded bronze (Cu, Sn, Pb) Grey cast iron Mild steel	 - 0.8 - 1.0 0.7 - 0.9	 0.2 - 0.4 0.3 - 0.5 -

Clean metal and alloy surfaces exhibit high adhesion which results in a high coefficient of friction and high wear rates (Bowden and Tabor, 1964). During sliding, strong metallic bonds are formed across the interface and significant metal transfer from one body to another takes place. The coefficient of friction can be reduced by introducing oxide films on the interface which separate the two metallic surfaces and act as a low shear strength film. But at high contact loads, the oxide film breaks down and coefficient of friction increases. This kind of transition is commonly observed in metals.

For soft ductile metals such as lead, indium and tin, the contact area is large even at low loads which can result in a high coefficient of friction. Lead based white babbitts, brass and bronze exhibit low friction. All these metals form films of low

shear strength which are responsible for the low coefficient of friction. In lead based alloys, a thin transferred film of lead is formed during sliding against steel and exhibit an intrinsically low coefficient of friction (Roberts, 1990).

2.5.3 Effect of Operating Conditions

The coefficient of friction for metals and alloys depend on the operating conditions such as sliding velocity, pressure, temperature, relative humidity (Suh, 1986; Hutchings, 1992). The coefficient of friction of metallic pairs can increase with an increase in load if the increase in load breaks the oxide film. High sliding velocities and high contact pressure result in surface frictional heating. For metals with low melting points, high sliding velocity can result in the formation of a thin molten layer at asperity contacts, which reduces its shear strength so that friction drops to a low value determined by viscous forces in the liquid layer (Bowden and Tabor, 1964).

At high temperatures, formation of oxide layers can result in low friction but interfacial softening may result in high ploughing in softer materials (Teruji Nojiri, et. al., 1971; Rabinowicz, 1995). Coefficient of friction generally decreases with an increase in velocity. Increase in contact temperature can result in softening of the metal due to metal phase transformation, and this can cause mechanical properties to be improved or degraded. An example of this kind is cobalt sliding against stainless steel (Rabinowicz, 1995).

Bowden and Tabor (1950) have investigated the friction and wear of various bearing materials. They have concluded that all good bearing materials have a common soft, low melting constituent in which actual shearing takes place during sliding. With copper-lead alloys, the shearing takes place in lead film. With white metals, the shearing takes place in the soft lead-base or tin-base matrix that has become smeared over the surface. This action will reduce the seizure since high local temperature developed under severe conditions of running will readily cause local softening or melting of the low-melting constituent at the region of the momentary contact. They have also concluded that hard particles in the duplex structure of babbits contribute very little to the load carrying capacity of the material. For white metal alloys, the basic frictional properties are determined

essentially by the softer matrix itself and the hard particles have little influence (Davis and Eyre, 1991).

2.6 Wear

Wear is defined as the progressive loss of material from the operating surface of one body sliding or rolling over another body (Bhushan, 1999). Wear starts to be observed at the micro level when the asperity tips of two surfaces interact and break down under the application of load and interfacial sliding. The factors affecting the wear are load, speed, temperature, material properties, surface texture, lubrication, environment etc. Wear can occur by either mechanical or chemical means and is generally accelerated by frictional heating (temperature). Various wear mechanisms indicated below have a common feature of removing material from the sliding surface (Rigney, 1988).

- Adhesive wear
- Abrasive wear
- Fatigue wear
- Erosive wear
- Corrosive wear
- Fretting wear
- Thermal wear

Out of these wear mechanisms, adhesive and abrasive wear are the dominant wear mechanisms encountered in most sliding contact conditions and only these wear mechanisms are described in this chapter. Detailed descriptions of other wear mechanisms are given by Bhushan (2001) and Hutchings (1992).

2.6.1 Adhesive Wear

Adhesive wear results from the transfer of material from one body to another during relative sliding motion. This happens when the asperities of the surfaces at the real area of contact collide with each other and form adhesive bonds, known as junctions, due to the application of a very high local pressure. The junctions must be broken when the surfaces slide against each other otherwise friction and wear increases (Hutchings, 1992). If the bonds break at the original interface, no wear occurs, but, if the break occurs in one of the materials, a small particle of that material is transferred to the opposing surface. The theory of adhesive wear assumes that a subsequent contact will cause the transferred particle to be removed so that it forms a loose wear particle (Landown and Price, 1996). As the sliding continues, this cyclic process is repeated, as shown in figure 2.5.

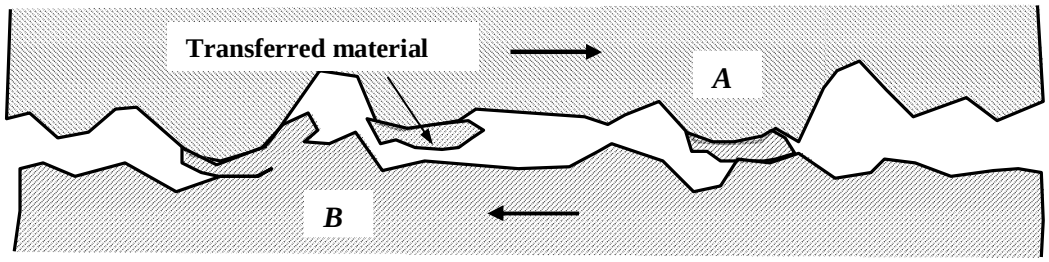

Figure 2.5 Adhesive wear mechanisms (arrows indicate direction of sliding).

Adhesive wear can be divided into mild wear and severe wear mechanisms. In mild wear an oxide film separates the two surfaces and protects them against the formation of strong metal-metal junctions. As the sliding velocity or load increases, the oxide film on contacting surfaces cannot form quickly enough to prevent direct metal-metal contact and severe wear takes place. Various types of severe wear include welding, galling, scoring, scuffing etc. The transition between mild wear and severe wear are commonly observed in many metals due to change in operating conditions such as normal load, sliding speed and even with sliding time or sliding distance (Hutchings, 1992).

Transition from Mild Wear to Severe Wear

The transitions from mild wear to severe wear have been explained by Lim and Ashby (1987) for an unlubricated steel sliding on a carbon steel in air at room temperature in pin on disc contact. The wear transition for this particular contact mechanism can be illustrated by wear mechanism maps.

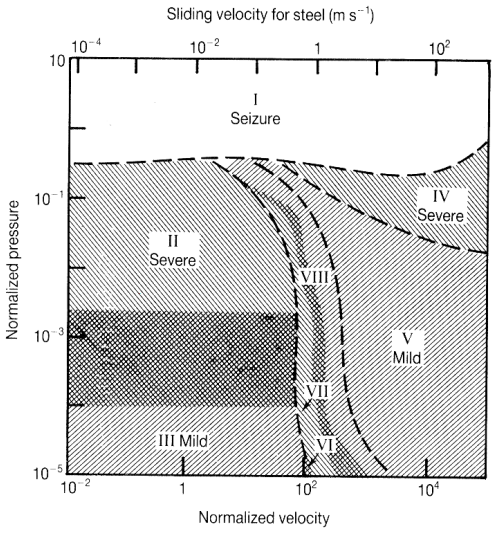

Figure 2.6 Wear mechanism maps for unlubricated steel sliding in air at room temperature in pin on disc configuration (Adapted Lim and Ashby (1987)).

In general, these represent the wear behaviour of most metals in air. These are plotted on axes of normalized pressure, i.e. nominal pressure divided by the surface hardness, and normalized sliding velocity, i.e. sliding velocity divided by velocity of heat flow. In the map shown in figure 2.6, various regions correspond to the different wear regimes with boundaries of sliding velocities and contact pressures beyond which oxidative wear occurs. There are several mechanisms which change their wear behaviour depending on the operating conditions. The transitions in wear mechanism occur if normal loads and/or sliding velocities are changed.

As an example, figure 2.7 shows a mild-severe-mild transition in steel against steel rubbing contact as the effect of increasing load. It can be seen that there are two transitions; one from mild wear to severe wear at transition load T_1 and a second from severe to mild wear at transition load T_2. These are explained by the different rates of change in the number of asperity collisions and the rate of oxidation as the load is increased. The rate of asperity collisions and the interfacial temperature increase approximately linearly with load, but the rate of oxidation increases exponentially with the interfacial temperature

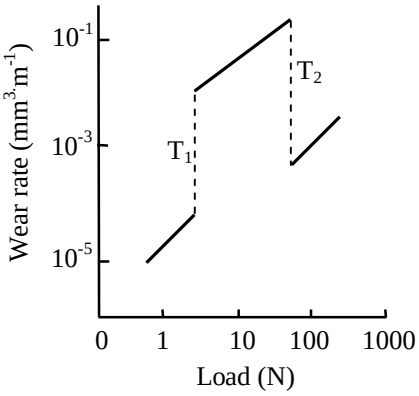

Figure 2.7 Wear transition of plain carbon steel sliding against tool steel in pin on disc test (after Hutchings (1992)).

Before transition load T_1, the rate of oxidation is sufficiently high for the asperities to re-oxidise between collisions, so that the wear rate is low, the surfaces are smooth, and the wear debris is fine oxide. Between loads T_1 and T_2, the rate of oxidation is not sufficiently high to re-oxidise the asperities between the increasingly frequent collisions, so that wear rate increases by two orders of

magnitude, the wear debris consists of large metallic particles and the rubbing surfaces are rough.

Above T_2, because the rate of oxidation increases exponentially with temperature, and the temperature increases with load, the rate of oxidation is again sufficiently high to cause the asperities to re-oxidise between collisions, so that the wear rate falls and the debris is again fine oxide particles.

2.6.2 Wear Volume Calculation

Archard (1953) developed a simple model of adhesive wear, showing that the volume of material being worn away is proportional to the applied load *W* and sliding distance *X*, and inversely proportional to the hardness *H*, of the worn surface.

Therefore the volume of wear (V_w) is given by

$$V_w = \frac{\mathrm{K}WX}{H} \tag{2.10}$$

Where, K is the adhesive wear coefficient (also known as Archard's wear coefficient) and is dependent on the properties of the materials in contact. The value of K ranges between 10^{-7} and 10^{-2} in metals (Archard and Hirst, 1956).

Archard's Wear Rules

Archard (1953) suggested two simple rules which state that, wear rate is independent of apparent area of contact and is directly proportional to the applied load. He also indicated that wear rate (i.e. volume or mass of material removed per unit sliding distance or per unit time) is independent of sliding distance and independent of velocity (this assumption does not hold for all material combinations). Methods to calculate wear rate were described in chapter 3.

2.6.3 The PV Factor

The PV factor in a bearing system is the product of nominal bearing operating pressure (P) and sliding velocity (V) and is commonly used as a criterion to relate power loss, surface temperature and wear rate (Suh, 1986). It is a measure of the energy input rate to the sliding interface (Arnell, et. al., 1991). The wear rate of some materials, such as polymers is often proportional to PV. The maximum

permissible value of a PV for a material is known as the PV limit. The PV limit for a given application or a tribo-system depends, among other factors, on whether it is dry or lubricated. The PV factor is used in the selection of polymeric sliding bearing materials in flat on flat contact situations.

Basic Explanation of PV

The theoretical derivation of the relationship between wear rate and PV starts from the reasonable assumption that the rate of wear will be proportional to rate of energy dissipated at the sliding interface (Arnell, et. al., 1991). This can be explained in the following way for a flat bearing surface subjected to a normal load W and a frictional force f moving with a velocity V against its substrate.

The rate of energy dissipation q, is obtained as:

$$q = fV \tag{2.11}$$

But frictional force f is the product of friction coefficient μ, and normal load W. Therefore,

$$f = \mu W \tag{2.12}$$

Equating 2.11 and 2.12 gives,

$$q = \mu WV \tag{2.13}$$

Equation 2.13 gives the rate of energy dissipation over an area A. Therefore, the energy dissipated per unit area Q is q/A

$$Q = \frac{q}{A} = \frac{\mu WV}{A} = \mu PV \tag{2.14}$$

Where P is the apparent pressure applied on the bearing. From the initial assumption, the volume of wear rate V_w is proportional to the rate of energy dissipation as,

$$V_w = kWV \tag{2.15}$$

Where k is the constant of proportionality and is called the specific wear rate (SPWR) which is the volume of wear per unit normal load per unit sliding distance. The depth wear rate or the rate of linear wear normal to the sliding distance is the ratio of volume of wear to contact area A, so that

$$\frac{V_w}{A} = Q = \frac{kWV}{A} = kPV \tag{2.16}$$

Equation 2.15 suggests that for any material there is a limiting PV factor above which the material would fall very rapidly owing to melting or thermal decomposition and is knows as the PV limit of the material. The PV factors or PV curves which are supplied by bearing manufacturers refer to unlubricated sliding against counterfaces of specific material having specific surface finish.

It cannot be assumed that SPWR increases with increase in PV, as SPWR is the volume of material lost per unit load per unit distance of sliding. The effect of increasing speed is to increase the distance slid in unit time, so wear per unit time will increase with velocity, but SPWR will generally not, unless there is an effect of flash or bulk temperature. The Archard equation is consistent with the above derivation of SPWR since Archard also calculated wear in terms of distance of sliding. However, if speed increases, the sliding distance per unit time increases so volume of wear per unit time will increase.

The relationship between P and V for dry bearings is plotted for log P against log V by Lancaster (1973) as shown in figure 2.8

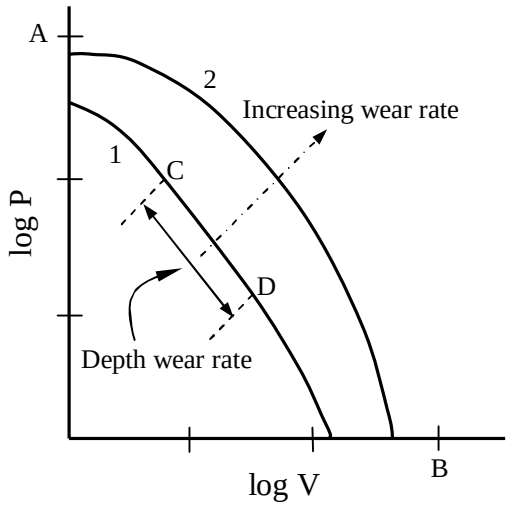

Figure 2.8 The PV relationships for dry bearings (Lancaster, 1973).

In figure 2.8, the point A represents the limiting load carrying capacity of the bearing and point B represents the velocity limit where the surface temperature becomes excessive. Curve 1 represents the criterion for choosing a load at a chosen velocity to give a specific wear rate under continued sliding. Curve 2 represents the same criterion, but at limiting PV conditions because of the thermal softening or yielding of the material at high contact stresses.

A literature survey on the tribological characteristics of various combination of bearing materials and soft metallic coatings revealed that the majority of authors presented friction and wear data against applied load or sliding distance rather than PV, especially with non-conformal contact geometries such ball on disc, ball on ball, cylinder on disk etc (See for example An, et. al., 2004; Zeren, et. al., 2007; Zhang, et. al., 2007; Guermazi, et. al., 2009). This can be explained by examining Archard's wear equation which indicates that the volume loss of material increases with load, but does not refer to sliding speed (rather, it refers to the sliding distance). This suggests that the sliding velocity has no influence on the wear rate of the material. However, as the speed increases, the energy input per unit time increases, and this can lead to transitions in wear rate, as in the mild-severe transition, which are a result of the increased temperature. Therefore, when comparing different materials, friction and wear data have often been presented against load, while keeping the sliding speed constant or against the sliding distance while keeping the load constant.

Also, with non-conformal test geometries, the contact pressure changes gradually as the tip of the ball wears due to sliding on the disk leading to the formation of flat zone and a continuous change in test conditions the wear rate obtained would be non-uniform (Ravikiran and Lim, 1999). This is not the case with conformal contact geometries such as thrust washer test apparatus and flat pin on disc apparatus where friction and wear data are presented against pressure or sliding speed (See for example: Jackson and Green, 2001; Balic and Blanchet, 2005; Carignan and Rabinowicz, 1980). In the case of conformal contacts such as flat pin on disc, thrust washer test etc, the nominal pressure at the sliding interface remains the same giving uniform wear rates. As indicated earlier, it is common to represent PV against wear rate especially for bearing materials with flat on flat contact conditions (see for example, Ravikiran and Lim, 1999; Jackson and Green, 2001; Hu Zhongliang, et. al., 2008), since PV describes the energy input that results in melting or marked softening of the material, which can have major influences on the outcome of friction and wear measurements. Therefore, in this project, PV was used as the main criterion when presenting friction and wear rates in the thrust washer test apparatus. For the pin on disc test apparatus, the load against friction coefficient and wear rate was presented.

2.6.4 Abrasive Wear

When two surfaces with different hardness slide against each other, the asperities of a rough hard surface can plough or cut the softer surface (Hutchings, 1992). This phenomenon is schematically shown in figure 2.9. Therefore, abrasive wear is the wear due to cutting or ploughing action of:

- a hard, rough surface sliding against a softer surface (two body abrasion, figure 2.9 (a))
- hard particles trapped between the two sliding surfaces (three body abrasion, figure 2.9 (b))

In the case of ductile materials with high fracture toughness, which includes many metals and alloys, the hard asperities result in the plastic flow of the softer materials. In most abrasive wear mechanisms, scratching of the softer surface is commonly observed and a series of wear grooves is observed parallel to the direction of sliding (Glaeser, 1992)

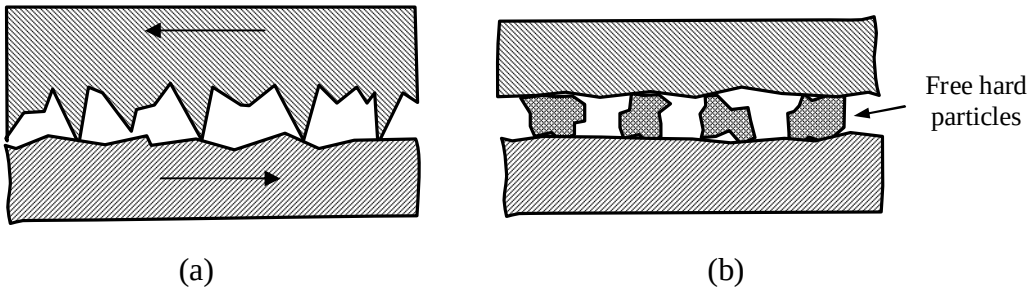

Figure 2.9 Schematic of abrasive wear (a) Two body abrasion (b) Three body abrasion (arrow indicates direction of sliding).

Material loss from a surface by plastic deformation during abrasion can occur by several deformation modes such as ploughing, wedge formation and cutting action (Hokkirigawa and Kato, 1988). In ploughing, material is displaced from a groove to the sides without removal of material, but after repeated sliding on the surface the material removal occurs by a fatigue mechanism (Suh, 1986). In soft metals such as indium and lead, the amount of wear debris produced is small and deformed materials are displaced along the sides of the grooves. In the wedge formation process, an abrasive wear tip ploughs a groove and develops a wedge at its front. The derivation for the abrasive wear of plastic contact for a hard conical

asperity in sliding contact with a softer surface in abrasive wear give by Suh (1986) as:

$$V_w = \frac{k_{abr} WX}{H} \tag{2.17}$$

Where, k_{abr} is the abrasive wear coefficient.

The above equation is based on the Archard's wear equation for adhesive wear described in equation 2.10. Typically k_{abr} ranges from 10^{-6} to 10^{-1}

There is significant experimental evidence from Goddard and William (1962) which suggests that two body abrasion is inversely proportional to the hardness of the softer material and proportional to the normal load and sliding distance for many pure metals. Hardness is an important factor for abrasive wear resistance. According to Rabonowicz, et. al., (1961), during three body abrasion with alumina particles, the wear resistance of metals is proportional to the hardness of the work piece. Brittle materials can produce large particles resulting in high wear rates. The volume of wear generally increases linearly with increase in applied load.

2.6.5 Wear of Metals and Alloys

As discussed earlier, clean metal contacts in air exhibit high adhesion, which leads to high friction and wear rates. The wear rate can be much higher if the clean contacting surfaces are sliding in vacuum (Arnell and Soliman, 1978). The slightest contamination mitigates contact or forms chemical films which reduce adhesion resulting in reduction of friction and wear (Buckley, 1981). For soft metals such as lead, indium and tin, the contact area is large even at low loads resulting in higher wear rates. Metallurgical compatibility determines the wear rate of a given metal pair (Archard, 1953). Lead-based white metals, brass and bronze exhibit relatively low friction and wear in dry and lubricated test conditions (Prasad, 2004). Wear rates of alloys are generally lower than those of pure metals. Several wear mechanisms discussed earlier change according to the change in operating conditions such as load and speed. The transitions in wear rates occur as a function of sliding time or distance. Increase in normal load lead to mechanical damage due to high surface stresses. Increase in load and speed

results increase in interface temperature. At high load and speed combinations, there may be localized melting near the surface (Holmberg and Matthews, 1994).

Literature Survey on Leaded Bronze and Soft Metal Coatings

The tribological characteristics of various copper based bearing materials such as leaded bronze, tin bronze, aluminium bronze etc have been investigated by many authors and researchers. Due to their excellent antifriction and wear resistant characteristics even at high operating conditions, such kinds of materials are extensively used for various bearing applications. In this section, the details of some important publications discussing leaded bronzes and soft metal coatings of lead based alloys are summarized. Since this project deals with copper based bearing materials and lead/indium based soft metal coatings, much of the attention was paid to publications discussing these materials.

Kayaba (1962) investigated the friction and wear characteristics of tin based white metals and aluminium based alloys sliding against mild steel using a flat on flat test configuration in dry test conditions. Because these bearing materials are soft and show higher wear rates (as indicated by Bowden and Tabor (1950)) in unlubricated test conditions, lower contact pressures and sliding velocities were employed. In this investigation, the amount of wear per unit sliding distance was measured gravimetrically for a fixed sliding distance. The author identified that the dry wear of comparatively soft bearing materials which had both soft and hard phases was directly proportional to the applied load. Both of these materials showed increase in wear rate with load. The dry wear of the aluminium-base alloys was rather less than that of tin-base white metal due to the surface melting even at the smaller loads. The friction coefficient was almost constant regardless of increase in load and speed for the tin-base white metal (0.4-0.45), but for the aluminium-base alloys, which readily adhere to mild steel, the coefficient of friction (0.38 to 0.6) was greatly influenced by the load though the minimum value for these alloys was smaller than that for the tin-base white metals. Under lubricated conditions the coefficient of friction was almost constant regardless of speed for all alloys below a certain load.

Ahsan, et. al., (2003) studied the tribological characteristics of two different types

of leaded tin bronzes. One alloy was referred by them as “good bearing” which had 18% lead content while the other, referred as “failed bearing” had 5.8% lead content. The good bearing lasted for seven years while the failed bearing lasted for seven days for the same industrial application and under the same operating conditions. A pin on disk test apparatus was used to assess the dry friction and wear characteristics of both of these materials. A constant normal load and constant linear speed were applied to a pin made of gray cast iron sliding against these materials. They found that the good bearing material showed a substantially higher wear resistance than the failed bearing due a stable lead layer formation on the worn surface. This layer also helped in keeping the iron debris from the counterface and forms patches of iron-rich transfer layer. They believed that the lead and iron transfer layers acted as protective layers, reducing the friction coefficient and wear damage. No such stable transfer layers of lead and or iron formed on the failed bearing containing the smaller amount of lead. Therefore, the higher lead content of the good bearing compared with lower lead of the failed bearing helped to establish a protective transfer layer on the worn surface. The steady state friction coefficients were found to be 0.24 and 0.19 for the failed and good bearings, respectively. The wear rate of the failed sample was several times higher than that of the good sample. The higher lead content of the good bearing was believed to lead to the formation of a more or less continuous tribo layer on the bronze surface. This soft layer acted as a protective layer and helped to reduce friction coefficient as well as wear damage. The soft lead layer was also expected to have the ability to embed wear debris. The formation of a lead layer on the worn surface of leaded alloy in which lead exists in the free state and its added effects in reducing wear damage have been reported previously by several investigators (for example: Tabor, 1945; Mohan, et. al., 1990; Montgomery, 1970; Fein, 1969).

The sliding wear behaviour of leaded-tin alloys and aluminium bronzes over a wide range of applied pressures and speeds was studied by **Prasad (2004)** using a pin on disc test machine. The sliding speeds used in his study were 0.42 and 4.60 m/s. In the experiment the pressure was increased in steps until specimen seizure was identified. The wear rate was plotted as a function of applied pressure at the varying sliding speeds. He observed an increased wear rate with pressure and

increasing the sliding speed led to substantially increased wear rate of aluminium bronzes while this trend reversed in the case of leaded-tin bronzes. Improved wear performance of the leaded-tin bronzes with increasing sliding speed was understood to be due to the effective smearing of lead leading to lubrication. Deteriorating wear behaviour of the aluminium bronze with change in speed or pressure was observed and this could be due to the severe wear conditions leading to specimen seizure. Material removal mechanisms comprised mainly of crack assisted "chipping" in the case of the leaded-tin bronzes at 0.42 m/s. The wear mechanism changed to wear induced plastic deformation of the subsurface regions followed by the effective formation of heavily deformed transfer layers and a lubricating film of lead at higher speed (4.60 m/s)

The dry sliding wear behaviour of copper-lead alloys was studied as a function of lead content by **Molian, et. al., (1991)** using a pin on disk test apparatus. They have identified increased specific wear rate with increases in lead content up to 40 wt% after which a drop in wear rate was observed. Their study of wear mechanisms showed that oxidative wear had been the primary dominant material removal mechanism at low contact pressures whereas plastic deformation and adhesion were the rate-controlling mechanisms at high contact pressures. The dry wear was presented in terms of the weight loss of the pin as a function of sliding distance. With the exception of hardness values, the results confirmed the trends predicted by Archard's wear equation. They identified increased wear volume with either an increase in sliding distance or an increase in load. High wear, with the exception of pure copper, was observed in Cu-Pb alloys for the test conditions used. The observed wear rates were plotted as a function of pressure and lead content. A reduction in the coefficient of friction occurred with increase in lead content. This was attributed to the contribution from the size and volume fraction of lead distributed in the matrix. They also observed that pure copper exhibited a low wear rate and was relatively unaffected by the load. The wear resistance of the alloys was significantly affected by the addition of lead. They identified that the maximum specific wear rates are recorded at the lower loads and are constant at high loads. Most of the transfer film in the high-lead-containing alloys possessed a dark greyish colour, which indicated subsequent oxidation because of the high flash temperature at the sliding interface. Oxidative wear appears to be a

major wear mechanism for pure copper and Cu-Pb alloys at low contact pressures.

Montgomery (1970) investigated the tribological behaviour of some commercial leaded tin bronze alloys for seals and bearings in reciprocating machinery applications. A block on ring test apparatus was used to assess the friction and wear behaviour of these alloys at light loads. Both stationary bronze blocks and moving bronze rings were mated with hard surfaces using a friction and wear testing machine. The tribological behaviour of a bearing bronze was influenced by the operating conditions, as pointed out by Fein (1969) in a complex manner by a combination of run duration, load, temperature, lubricant, atmosphere and the specific mating materials. Where the bronze specimen was a moving ring sliding on a stationary hard block, there was a general trend toward lower wear rates with increasing hardness, but hardness was not a completely reliable guide to wear resistance. Where the bronze specimen was a stationary block sliding on a hard steel ring, there was no apparent effect of hardness; the lowest wear rate was obtained with the softest bronze. With bronze blocks, equivalent wear rates were obtained with both 10% and 20% Pb containing alloys although the higher lead content resulted in a somewhat lower coefficient of friction. Alloys with a more coarse lead distribution showed the lower wear rates reported by previous workers when tested as stationary bronze blocks but showed exactly the opposite effect when tested as moving bronze rings. This reversal of the effect of lead distribution may well be a consequence of the increased hardness of specimens with fine distributions.

Ruggeri, et. al., (1980) studied the tribological behaviour of a thin film of cadmium sliding on carbon steel in dry test conditions using pin on ring conformal contact geometry. The pin was made of fully annealed carbon steel and the rings were successively coated by electroplating with nickel, copper and cadmium films to obtain good adhesion to the hard substrate and to minimize diffusion into the hard mating surface. Different sliding velocities and contact loads were implemented to get a wider range of test conditions. Cadmium coatings showed good friction and wear properties under severe operating conditions where they act as a good solid lubricant. Under mild operating conditions they have shown high friction and under intermediate conditions high

wear. The absence of cadmium on rubbing surfaces resulted in significantly worse tribological behaviour as shown by the results for nickel and copper coatings tested under the same conditions. Even a trace of cadmium was found to act as a good solid lubricant. At low temperature, the melting point of the cadmium was not reached and the frictional behaviour was poor. A high temperature causes softening of the coating and thus smoother sliding. The temperature of the white layer whose hardness permitted a low friction coefficient to be achieved was also dependent on the temperature, as was the transition from severe to mild wear.

Gerkema (1985) studied the tribological characteristics of lead thin film coatings in high vacuum between 20 °C and 300 °C using a steel ball on disc test apparatus at different contact loads. Experimental results were given for pure lead coatings, lead films containing a small amount of silver, copper, platinum or molybdenum. Pin on disc experiments indicated that lead coatings on steel, sputtered as well as electrodeposited, had sliding distances comparable with those reported for ion-plated lead films. A thin copper layer at the lead-steel interface, or a small addition of copper or platinum to the lead coating, significantly increased the sliding distance with low friction and wear. The addition of molybdenum to lead also extended the sliding distance but high friction and wear rates were observed.

Bekir (2009) investigated the tribological and mechanical properties of copper, aluminium and tin-lead based alloys for journal bearing applications using a radial journal bearing wear test apparatus with non-conformal contact. These test materials were slid against a steel shaft under lubricated test conditions at 20 N load and 0.78 m/s sliding velocity. The highest friction coefficient and bearing temperature occurred in Cu-Sn and Cu-Zn bearings, whereas the lowest friction coefficient and bearing weight loss occurred in Zn-Al, AlCuMg and SnPbCuSb bearings. The highest bearing wear rate occurred in CuSn10 and CuZn30 bearings, and the lowest bearing wear rate occurred in ZnAl bearing. The mechanical properties of CuSn10, CuZn30 and AlCuMg2 bearing materials were better than those of ZnAl, and SnPbCuSb bearing materials. The lowest coefficient of friction and wear loss was recorded for lead containing bearing material with lead content less than 3%.

Jahanmir, et. al., (1976) studied the sliding wear resistance of soft metallic coatings such as Cd, Ag, Au and Ni deposited on steel substrate. The results indicated that the tribological behaviour of soft coatings is consistent with the delamination theory of wear, especially the critical nature of the plating thickness. The author identified a reduction in wear rate of three orders of magnitude when the coating material is softer than the substrate and thinner than a critical thickness. The optimum plate thickness was found to be of the order of 0.1μm for cadmium, silver, gold or nickel plated on various types of steel. Cadmium, silver and nickel reduce wear only in non-oxidizing environments, whereas gold reduces wear both in air and in inert atmospheres. The roughness of the substrate surface prior to plating and the nature of the coating/substrate bond had significant effects on the life of these coatings. For major wear reduction the coating material must be softer than the substrate material. They concluded that high wear resistance is possible with an optimum thickness of soft coating. The surface roughness of the substrate and the coating/substrate bond strength were two important factors for the wear resistance of soft metallic coatings.

The sliding wear behaviour of a leaded tin bearing bronze was investigated by **Prasad, et. al., (1996)** over a range of applied pressures and sliding speeds with respect to the influence of lead on the wear response. Significantly high wear rates were found at the minimum sliding speed due to extensive micro-cracking and subsurface deformation. Higher sliding speeds led to increased frictional heating made the alloy matrix viscoplastic and a stable transfer layer formed on the specimen surface reducing the direct metal contact. They identified the formation of a lead film on the wear surface under these conditions which was mainly responsible for the improved wear behaviour of the alloy at higher speeds. Material removal mechanisms involved delamination of the undeformed subsurface region causing chipping off at the minimum sliding speed. The material removal was a combination of adhesion, micro cracking and three body abrasive wear.

Ugur, et. al., (2007) studied the tribological characteristics of tin bronzes and tin-based lead bronzes using a specifically designed sliding wear tester with non-conformal contact in dry test conditions. The coefficient of friction and wear rates

were calculated at different contact loads. They observed increased coefficients of friction and wear rate with increase in load. They also identified that tin-based lead bronzes had a slightly higher coefficient of friction (0.73) than tin bronzes (0.69) and reduction in embeddability occurred with decrease in the amount of lead in bronze. This suggested that the highest-lead content bronze has the necessary strength and load carrying capacity for the particular application.

2.7 Tribological Mechanisms in Coated Surfaces

The main parameters controlling the tribological properties of coated surfaces are the coating to substrate hardness relationship, thickness of the coating, surface roughness of the coating and substrate, and the size and hardness of any debris present at the contact (Bowden and Tabor, 1950). These parameters have a big influence on the friction at the contact. Holmberg (1991b) schematically described the various characteristics of a tribological contact when a hard spherical body slides on a coated flat surface and their influences on the outcome of the friction and wear mechanisms. In this section only the macro mechanical friction and wear shown by soft coatings, which are the ones relevant to this project, are briefly summarized. For the remaining combination of contacts the reader should refer to Holmberg (1991b).

2.7.1 Hardness of the Coating in Relation to the Substrate Hardness

The tribological behaviour of a coated surface is influenced by the hardness of the coating and its relationship to the substrate hardness. The effect of the substrate hardness depends on the thickness of the coating, as the coating thickness increases, the properties of the substrate become less influential (Arnell, 1990). Bowden and Tabor (1950) explained that a soft thin coating on a harder substrate reduces both contact area and shear strength so that the coefficient of friction observed would be low. On the other hand, a hard coating on soft substrate will reduce the wear by preventing the ploughing effect (Holmberg, et. al., 1993), but if a low shear strength microfilm is not presented on the coating then the coefficient of friction will be higher as the hard coating supports the load whereas the shear takes place in the microfilm. An example of this kind of response was observed with a thin low shear strength MoS_2 film on a hard Boron Nitride coating (Kuwano, 1990).

2.7.2 Thickness of the Coating

When a hard slider moves on a hard flat substrate coated with a thin soft coating, the effect of ploughing is low. Here the coefficient of friction is determined by the shear strength of the film and the contact area between the slider and coating, which depends, in turn, on the deformation of the substrate. An example of this kind was shown by Roberts (1990) where, with a steel ball sliding on a smooth steel plate coated with thin MoS_2, the coefficient of friction was low (0.02). If a thick coating is present on the hard substrate, the effect of ploughing is higher and coefficient of friction increases. So the coefficient of friction is a function of film thickness (Ravindran, et. al., 1980). The thickness of film should be less than 1 micrometre to give low friction coefficient values (Sherbiney and Halling, 1977).

2.7.3 Effect of Ploughing and Deformation

When a hard slider moves on a harder flat surface with a soft thick coating, the coefficient of friction is higher than with a thin coating, due to the ploughing explained by Sherbiney and Halling (1977) for lead films. The increase in coefficient of friction with sliding time or distance is due to the elastic or plastic deformation of the film and increase in contact area between the slider and coating in which shear takes place. Due to the high thickness of the coating, the load carrying capacity of the surface decreases. On the other hand if a hard smooth slider moves on a soft smooth substrate deposited with a hard thin coating, then the coefficient of friction is higher due to the increase in shear strength and deformation of the substrate (Suh, 1986). If a thick hard coating is placed on the softer substrate, instead of thin hard coating, the deformation of the substrate is lower and the thick coating carries part of the load. Ploughing of the coating is prevented by its hardness and contact area between the slider and coating is decreased due to decreases in deflection.

The other effects such as roughness of the substrate in relation to the thickness of the coating, roughness of the counterface, loose debris particles presented on the surface during the sliding process etc., make a major contribution in the outcome of the friction and wear mechanism and are discussed by Holmberg and Matthews (1994).

2.8 Lubrication

In order to reduce high friction and wear rates between dry surfaces sliding against each other, a lubricant is often introduced between them. The main purpose of a lubricant is to minimise friction and wear losses between the contacting surfaces in relative motion. In the adhesive wear mechanisms, the lubricant will reduce the adhesive bonding between the asperities at the real area of contact and in the abrasive wear mechanism, lubricants will partially protect the softer surface against severe scratching by the harder material with which it is in contact (Bhushan and Gupta, 1997).

There are two types of lubrication; fluid film lubrication and solid lubrication. Fluid film lubricants include liquid and gaseous lubricants whereas solid lubricants include additives in greases and thin or thick coatings deposited on surfaces.

2.8.1 Fluid Film Lubrication

In this type of lubrication, a lubricating film is introduced intentionally to separate the two surfaces in contact during relative motion to reduce friction and wear losses (Hamrock, 1994). There are several different lubrication regimes, including hydrostatic, hydrodynamic and elasto-hydrodynamic lubrication. However, this project aimed to investigate the behaviour of sliding bearing materials unlubricated and under conditions of minimal lubrication with kerosene. The regime of unlubricated sliding has been covered in the previous sections, so the following discussion is confined to the regimes of boundary lubrication and mixed lubrication.

Boundary Lubrication (BL)

In this lubrication regime, the contacting surfaces are very close to each other and considerable asperity interaction takes place. The two surfaces are protected by a thin boundary lubricant molecular film in the order of 1-3nm thick (figure 2.10 (d)) which helps in reducing the coefficient of friction, which varies between 0.03 and 0.2 (Holmberg, 1992a). The important physical properties of the boundary films are melting point, shear strength and hardness.

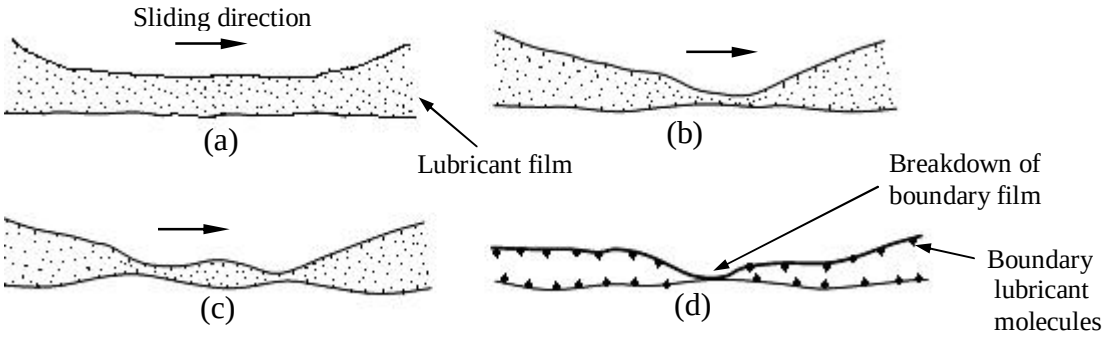

Figure 2.10 Types of lubrication (a) Hydrodynamic (b) Elasto-hydrodynamic (c) Mixed (d) Boundary lubrication (After Holmberg (1994)).

Mixed Lubrication (ML)

This lubrication regime is a mixture of boundary lubrication and hydrodynamic regimes. Even though the contacting surfaces are separated by a thin film (0.025-2.5μm) of lubricant, asperity contact takes place at some areas (figure 2.10 (c)). Due to the asperity contacts at these areas, adhesion can take place. The total contact load is partly carried by the asperity contact and partly by the hydrodynamic action. The coefficient of friction ranges from 0.01 to 1 (Godfrey, 1968).

The **Stribeck** curve (figure 2.11) plays an important role in identifying the different regimes of lubrication such as boundary, mixed, and hydrodynamic lubrication (Anonymous, 1992). It gives the relationship between coefficient of friction (μ) and a dimensionless number *Hs*.

$$H_S = \eta V / W \tag{2.18}$$

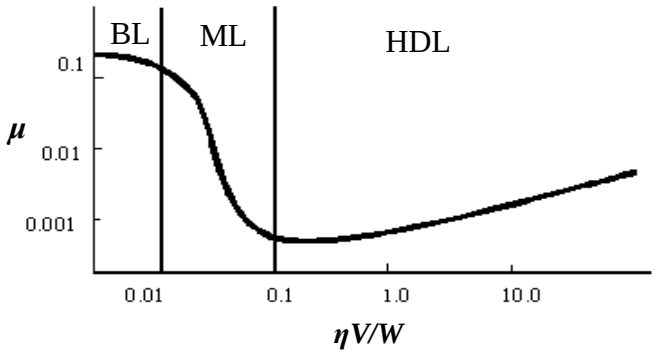

Figure 2.11 Stribeck curve (After Anonymous (1992)).

Where η is the absolute viscosity (N.s/m²), V is sliding speed, (m/s) and W is the load, (N). Higher *Hs* numbers indicate relatively thick lubricant film and no asperity contact, so that coefficient of friction is low, whereas lower *Hs* numbers indicate thin film lubrication with significant asperity contact and higher coefficient of friction.

Summary

Chapter 2 has reviewed materials for sliding contact bearings and their tribological characteristics. Much of the attention was has been given to copper based bulk materials and soft metal coatings which are used as solid lubricants for sliding contact bearings. Typical friction coefficient values for bulk materials and alloy metal coatings gathered from various investigators were tabulated. Various friction and wear mechanisms were described and tribological characteristics of leaded bronzes and soft metal coatings gathered from various authors summarized. Different lubrication regimes including the importance of the Stribeck curve were summarised. In the following chapter, equations to calculate friction and wear rates are described. Various techniques to measure surface characteristics of a given material and frictional heating calculations are also described.

CHAPTER 3

FRICTION AND WEAR MEASUREMENT TECHNIQUES

3.0 Tribological Test Geometries

The friction and wear characteristics of a test material in contact with a counterface material are generally measured using a suitable test method that, ideally, should replicate the real contact situation. There are various tribological test methods available and each test method has its own identity and limitations. The main issue concerning the laboratory testing is whether the selected test method can simulate the contacting conditions and wear mechanisms prevailing in the real applications. In order to manage this, the real contact conditions, such as contact geometry, contact pressure, temperature etc., have to be identified. Depending on the type of contact geometry, loading conditions and type of wear mechanism (i.e. adhesive, abrasive, erosive etc), the test method differs. Since this project work mainly dealt with thrust washer and pin on disc test apparatus, a brief description of these conventionally used test methods is given in this chapter. A complete demonstration of the specific test apparatus used is discussed in chapter 4. Figure 3.1 illustrates the general tribological testing process which starts with examining the test sample for surface texture in the "as received" state. Friction and wear tests are then conducted followed by a thorough investigation of the tested surface to investigate the wear characteristics.

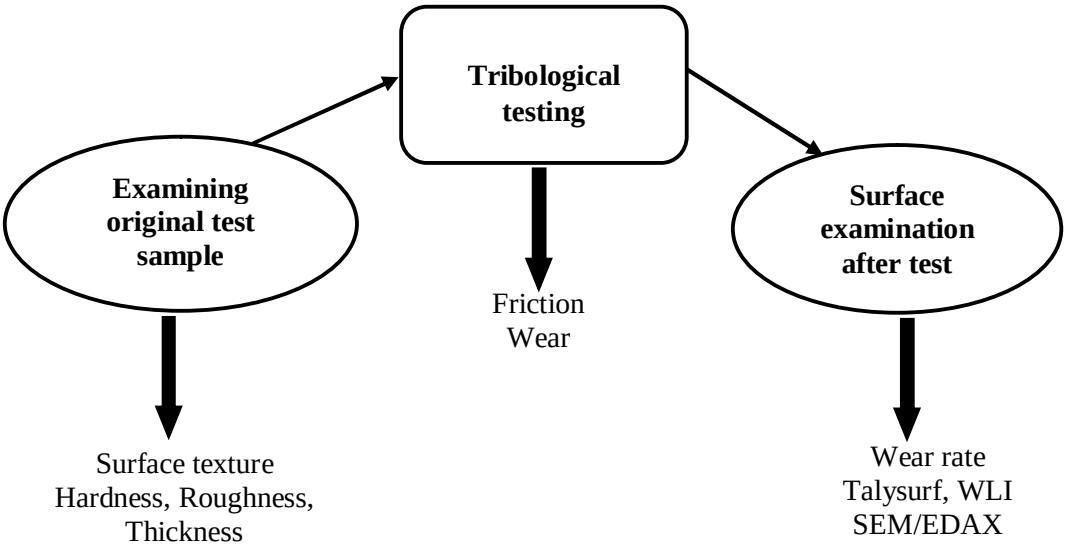

Figure 3.1 Tribological test process.

3.1 Pin on Disc and Thrust Washer Test Apparatus: General

3.1.1 Pin on Disc Test Apparatus

A conventional pin on disc test, ASTM G99-95 (Anonymous, 2002) uses a flat on flat test configuration as shown in figure 3.2, where a steel pin is loaded and slides against a rotating disc shaped test specimen under a set of desired test conditions. A fixed load is applied vertically on the steel pin and the sliding speed is fixed or changed depending on the duration of the test. The friction coefficient, as a function of time is continuously monitored using the load and force transducers. In addition to the flat on flat geometry, the POD method can be used with a range of loads and speeds, various pin diameters, various pin end shapes (figure 3.3) such as cylindrical, truncated cone and domed, and several track radii on a single disc. This test method can determine the sliding wear rate and coefficient of friction of a coated or uncoated surface. The specific wear rate is calculated by measuring the volume loss on the test specimen using the methods described later in this chapter.

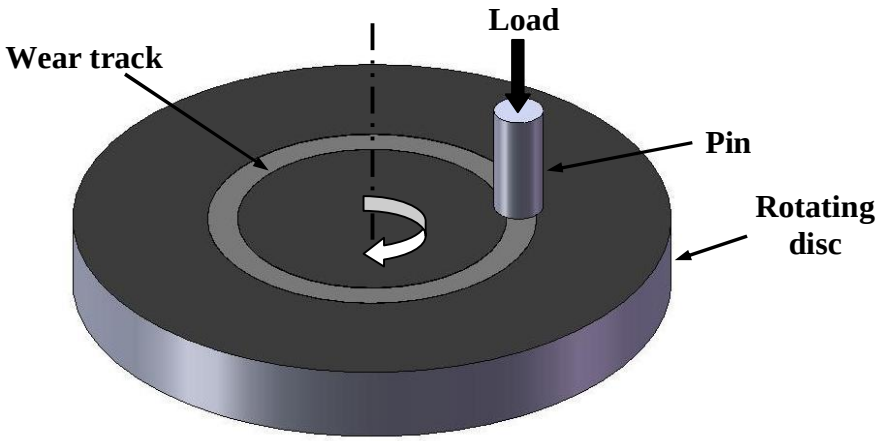

Figure 3.2 Conventional Pin on disc test apparatus.

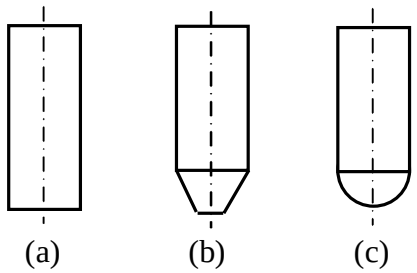

Figure 3.3 Pin end geometry in the POD test apparatus (a) Flat end (b) Truncated (c) Domed.

Three different pin type geometries can be used in a pin on disc test apparatus as shown in figure 3.3. Each type of pin has its advantages and disadvantages. The choice of selecting the type of pin depends on the requirement of the contact geometry and loading conditions (George Plint, 2006).

The cylindrical flat end pin (figure 3.3 (a)) is the most commonly used in pin on disc apparatus. The contact area on the flat ended pin remains essentially unchanged with wear. However, if the pin is not exactly normal (90º) to the disc surface, the pin will make contact on one edge and the resulting misalignment will yield extremely high contact pressures. This misalignment damages the coating with severe scratching especially on thin coated surfaces. Also, it is difficult to measure wear by volume loss as the whole pin face wears, leaving no reference surface against which to determine geometrical changes.

The truncated cone end pin (figure 3.3 (b)) facilitates the measurement of wear by volume, as the diameter of the contact area is a function of the wear that has occurred. As more material is removed, the pin face recedes along the cone and the contact area increases which means that the contact pressure decreases with wear. As with the simple cylindrical pin, the truncated cone is susceptible to misalignment problems.

The domed pin (figure 3.3 (c)) is most commonly used for high contact pressure applications. This domed pin overcomes the misalignment problems occurring with the flat end pin and truncated pin. It is also amenable to wear measurement by volume change, a flat circular contact area developing and growing as wear progresses. In this project, a steel ball was used instead of flat end pin to overcome the misalignment problems and also to facilitate high contact pressures. Since this project is investigating thin films, it would be difficult to run (align) in a flat ended pin against a “dummy” surface to form a flat-on-flat contact against the test specimen.

Advantages of POD Test Apparatus

1) The pin on disc method is an accelerated test. Since, in each sliding rotation, the pin (counterface) is in contact with the same disc (substrate)

surface, the friction and wear performance of the coated and uncoated surfaces can be identified in the test.

2) Since the radius of the contact area between the pin and disc is very small (usually in the order of μm^2) high contact pressures can be applied at modest loads.
3) Several pin geometries can be used depending on the requirements of contact and operating conditions
4) Several tests can be conducted on the same specimen at different track radii so that repeated friction and wear results can be achieved.
5) The test apparatus can be used in dry and lubricated test conditions

Disadvantages of POD Test Apparatus

1) With the ball on flat configuration, the contact area and pressure change continuously as the ball and counterface wear. Due to this phenomenon, the contact pressure changes the test conditions.
2) Vibration problems due to the uneven surface roughness of the disc surface can give unreliable friction data and uneven wear loss especially in dry test conditions.
3) Both ball and disc wear individually or at the same time depending on the type of test materials and their physical properties so that wear rate measurements made by the wear transducer are a combination of the wear depths of the two surfaces.
4) The use of a ball on soft substrates gives high initial Hertz contact pressures resulting in work hardening and deformation of the softer component.
5) Temperature measurements are very difficult to model due to the discontinuous contact of ball on disc from time to time.
6) The pin on disc used in this project is limited to constant load and constant speed only: The contact load and sliding speed cannot be changed during the test.

3.1.2 Thrust Washer Test Apparatus

The thrust washer test (TWT) is a conventional ASTM D3702 (Anonymous, 2007) standard test method used to evaluate the performance of materials in

rubbing contact under a set of desired test conditions. The typical test apparatus, as shown in figure 3.4, is mainly used to identify the coefficient of friction and wear rate in a rubbing contact between a test specimen and a steel washer. In general, the test method involves a rotating test specimen loaded against a stationary steel washer under a prescribed set of test conditions. The coefficient of friction and wear rate are calculated, respectively, from measurements of the friction torque and loss of material in the rubbed region of the test specimen. A complete description of the thrust washer test apparatus used in this thesis work is given in chapter 4.

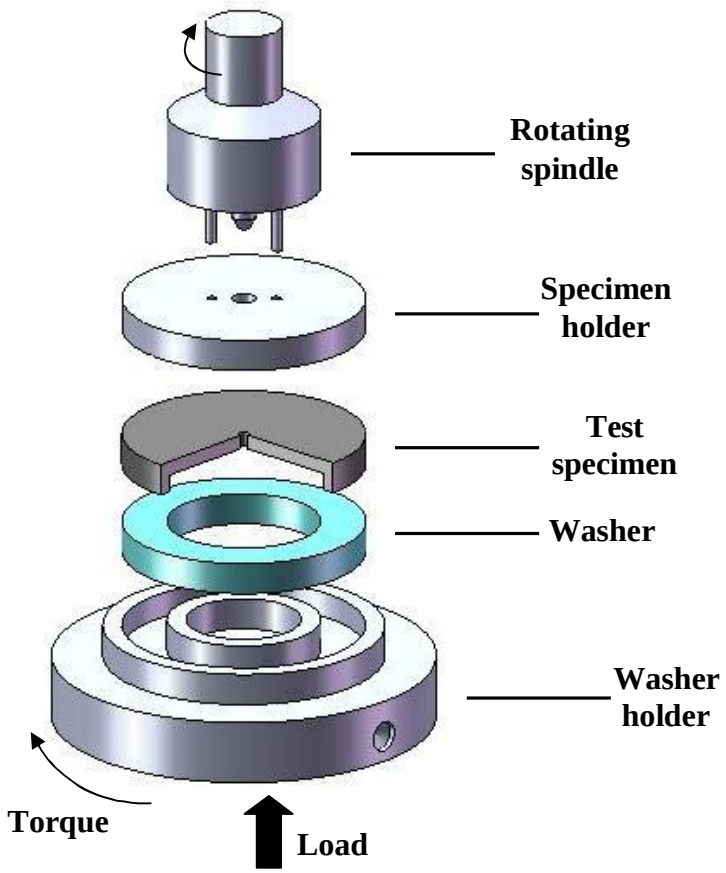

Figure 3.4 Conventional Thrust washer test apparatus (After Anonymous (2007)).

Advantages of TWT Apparatus

1) The main advantage of TWT is the high contact area between washer and test specimen, which can replicate the contact conditions in any conformal contact situation.

2) There is a continuous conformal contact between the counterface and substrate and, if the specimen runs evenly, the wear rate and frictional heating are uniform over the specimen surface.
3) High sliding speeds and high contact loads can be achieved although the contact pressure is low compared with that in the pin on disc test.
4) The sliding speed can be changed without interrupting the test process.

Disadvantages of TWT

1) Because of the high contact area between the substrate and counterface, high contact pressures cannot be achieved so that high PV factors are not possible.
2) An uneven substrate surface gives a non-uniform wear rate over the specimen surface.
3) Misalignments in installation of washer on disc at the start of the test results in immediate edge effects and severe scratching of the substrate material by the edges of the washer.
4) If the washer material is harder than the disc material, then the frictional behaviour is characterized by the circumferential edge effects.
5) The use of a washer type counterface can result in 3 body abrasive wear since the loose wear debris produced during the operation cannot slip out from the contact interface due to conformal contact.
6) The test processing time is usually longer than that of the POD test.

3.2 Methods to Measure the Tribological Characteristics of Coatings

Due to the difficulty in understanding the tribological contact mechanisms, it is not possible to predict, from first principles, the friction and wear rate for a particular contact situation. However, there is a variety of tribological test methods by which the tribological properties such as friction and wear of coatings can be evaluated and some of them have been discussed earlier. Each tribological test method has its own contact geometry, limitations, test parameters and environmental conditions, and it is very difficult to compare various test methods

for a particular coating material as test parameters are not always published and are not common to all test materials. There are certain standard test methods for evaluating the tribological characteristics of coating materials. The general properties of a coating are surface roughness, hardness, thickness, physical - chemical properties, friction, wear etc. The tribological performance of coatings and materials is strongly influenced by the most important factors that influence the outcome of friction and wear tests; these are the surface roughness, hardness, thickness and environmental factors (Holmberg and Matthews, 1994).

3.2.1 Surface Texture

Surface texture is generally categorised into three components: roughness, waviness, and form (Anonymous, 1992). Surface roughness is one of the most important parameters that influence the friction and wear properties of a coated surface (Holmberg and Matthews, 1994; Sedlacek et. al., 2009). Roughness of a surface means arrangement of peaks and valleys of wavelengths with varying amplitudes and spacings in molecular dimensions. The waviness is the surface irregularities of the longer wavelengths and is formed due to the vibrations when machining, heat treatment etc. Surface form is the general shape of the surface, neglecting roughness and waviness, which is caused principally by errors in the machine tool guide way, and deformations due to stress patterns in the component.

Roughness can be measured by two groups of instruments: contact methods and non-contact methods.

(a) Contact Methods

In contact type methods, a component of the measuring device is in contact with the surface to be measured. An example of this kind of device is a stylus profilometer.

Stylus Profilometer

In this method a stylus moves over a surface to be measured. A driving unit (gear box) drives the stylus, an electronic amplifier records the signal obtained from the vertical displacement of the stylus and sends it to a data logger which stores the measured signals. The stylus is mechanically coupled to a linear variable

differential transducer (Bhushan, 1999). In general the stylus is made of diamond and has a very small radius tip. One limitation of this test method is the shape of the stylus. For very delicate surfaces, the stylus may damage the surface when measuring for roughness. This technique is especially useful for coarser surfaces.

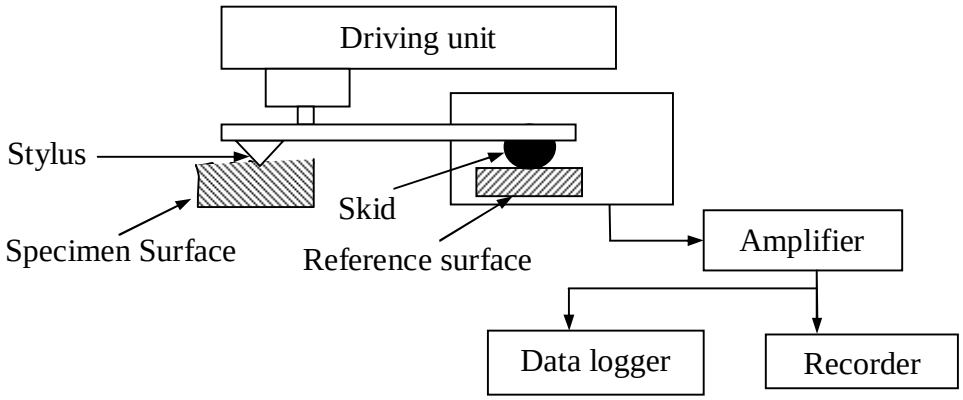

Figure 3.5 Schematic of a stylus profilometer (Bhushan, 1999).

Quantifying Surface Roughness

In general, surface roughness is quantified as average surface roughness (R_a) which is the arithmetic mean deviation of the surface heights from the mean line through the profile (Hutchings, 1992). The distinction between roughness and form error is arbitrary although it clearly involves the horizontal scale of irregularities. By various methods, form error and waviness may be subtracted from the surface profile recorded by a profilometer so that the graph depicts only the roughness values. A simple mechanical method commonly used in stylus profilometry is to arrange for measuring head of the instrument to be supported in a small skid which rides on the surface just behind or in front of the stylus as shown in figure 3.5. The profilometer then records the displacement of stylus relative to the skid. This enables the average local level of the surface to be used as a datum, and surface disturbances of wavelength longer than the size of skid are not recorded. Another alternative approach is to filter the displacement signal during or after recording so that components corresponding to long wavelength surface displacements (form error or waviness) are removed. Electronic filtering methods may also be used to remove the roughness signal and detect only the form error or waviness. If filters are removed, the distinction between roughness and form error may be quantified by quoting the filter cut off wavelength. This

cut-off filter is used to specify the range of spatial wavelengths (or the spatial frequencies) in the waviness and roughness data. A roughness number without specifying the cut-off filter used in the roughness calculation has no significance. In modern profiling instruments, this is a digital filter in the analysis software incorporating a Gaussian Filter. On most profilometers, the cut of length is set as 1/6 of the traversing length and is limited to values such as 0.08, 0.25, 0.8, 2.5 and 8 mm (White house, 1997).

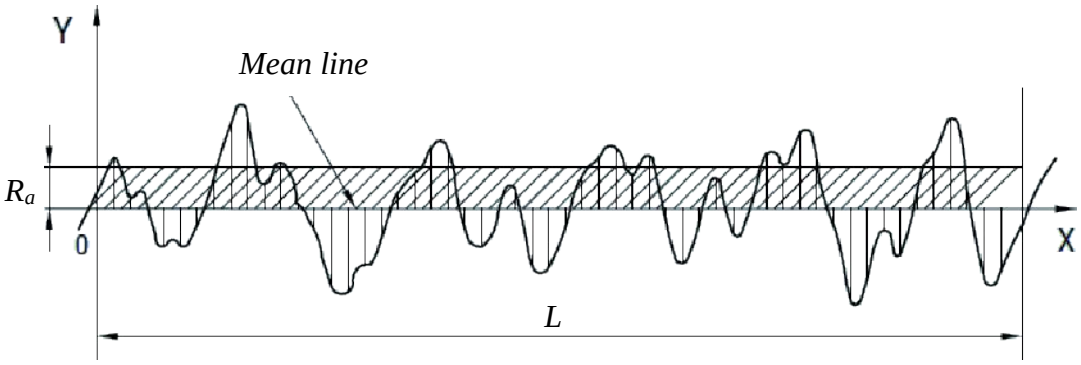

Figure 3.6 General surface profile (Hutchings, 1992).

From the figure 3.6, the average roughness 'R_a' is defined by

$$R_a = \int_0^L \frac{1}{L} |y(x)\, dx| \qquad (3.1)$$

Where 'y' is the height of the surface above the mean line at a distance 'x' from the origin and, L is the overall length of the profile under examination.

(b) Non-Contacting Methods

An optical profiler is a non-contacting type interferometer which records surface topography without damaging or distorting the surface. The surface measurement is based on a two-beam optical interference between beams reflected from the surface under examination and from an almost perfectly plane reference surface. This creates fringes which are recorded digitally by an array of photodiodes linked to a microprocessor. Accurate displacements known from the reference surface under microprocessor control cause changes in the fringe pattern from which the distribution of surface heights over the specimen can be measured. For examination of very fine surface features especially on compliant surfaces, this test method has a clear advantage over a stylus profilometer.

An example of the most commonly used non-contacting type interferometer is a white light interferometer (WLI). A WLI gives 3-D height data about a surface. This data can be used to characterise initial specimen topography as well as the loss of material due to wear.

3.2.2 Hardness

The hardness of a surface is resistance to plastic deformation by indentation (Bhushan, 2001). Hardness also relates its resistance to scratching, abrasion and cutting action. When comparing similar films for their plasticity behaviour, a hardness test is very useful without any special specimen preparations. In general the hardness measurements are categorized into three types: 1) Static indentation hardness 2) Dynamic hardness 3) Scratch hardness.

Of the above three types, the static indentation hardness tests are the more commonly used.

Static Indentation Hardness Test

In this test method a ball or a diamond cone or pyramid type of indenter is loaded against the surface of material to be tested. Then the hardness of the surface is measured by taking the ratio of load applied and some measurement of the permanent indentation. These tests are mostly applicable to relatively hard materials (Bhushan, 2001). Static indentation hardness tests are divided into macro hardness tests such as Brinell hardness tests and Rockwell hardness tests, and micro hardness tests such as the Vickers hardness test and the Knoop hardness test. Macro hardness tests are preferred to assess the bulk hardness of metals.

In the Brinell hardness test, the hardness number is obtained by dividing the normal load by the curved surface area of the indentation.

$$\text{Brinell hardness number (BHN)} = \frac{2W}{\pi D\,(D - \sqrt{D^2 - d^2})} \qquad (3.2)$$

Where W is the applied load, D is the ball diameter and d is the indentation diameter.

In the Rockwell hardness test, the hardness number is determined by measuring the penetration depth under a major load compared to initial penetration depth made by a minor load (Bhushan, 2001)

$$\text{Rockwell hardness number, } R = C_1 - C_2\,\Delta t \tag{3.3}$$

Where C_1, C_2 are constants for a given indenter size, shape and hardness scale and Δt is the penetration depth in millimetres between the major and minor loads.

Micro hardness tests are used on brittle materials, thin materials and coatings. The two principal types of micro hardness tests; Vickers and Knoop hardness tests use highly polished diamond pyramidal indenters. Very small loads from 1 to 25g are used for both tests.

$$\text{Vickers hardness, } HV = \frac{1.8544\,W}{d^2} \tag{3.4}$$

Where W is the imposed load in kg and d is the mean diagonal value in mm.

$$\text{Knoop hardness, } HK = \frac{14.229\,W}{l^2} \tag{3.5}$$

Where, l is the long diagonal, mm. The advantage of the Knoop hardness test over the Vickers hardness test is that a longer diagonal is obtained for a given depth of indentation.

3.2.3 Adhesion Tests

The adhesion of a coating is the strength of bond between a substrate and a coating. This is an important coating property that will influence the functionality of the coating surface. Adhesion assessments are done by various test methods such as scratch and indentation tests and laser techniques.

Scratch and Indentation Test

This is the most common and commercially available contact type test method where an indenter is pulled across the coating surface under increasing normal load until detachment occurs. The load corresponding to failure gives the adhesion strength often referred as the critical load. This is the most common method to study the adhesion of metal films on glass and of thin hard coatings on hard

substrates (Anonymous, 2000). Using this test method, a quick and convenient adhesion measurement can be made.

Various features of commercially available scratch tester are,

- The scratch tester has the ability to characterize the film - substrate system and to quantify parameters such as friction force, adhesive strength and scratch resistance.
- Real time display of normal load, friction force and coefficient of friction during scratch operation.
- Real time display of acoustic emission and penetration depth (to measure the depth wear rate).
- Facilitates various scratch modes such as constant, incremental and progressive loading, single pass or multi-pass scratching to perform more tests on a single test specimen modes.

3.3 Wear Rate

The definition of wear is given in chapter 2. When two interacting surfaces, as shown in figure 3.7, slide against each other, the removal of material from either of the surfaces due to various tribological conditions is called “wear”. The wear is evaluated by the amount of material lost and the state of the worn surface. The degree of wear is quantified by the wear rate, specific wear rate or wear coefficient. Wear rate is the wear volume per unit sliding distance. Specific wear rate is the volume of the material lost per unit sliding distance per unit normal load and wear coefficient is the product of specific wear rate and hardness of the worn material. In this project, the surface wear was characterised by calculating the specific wear rate of the material.

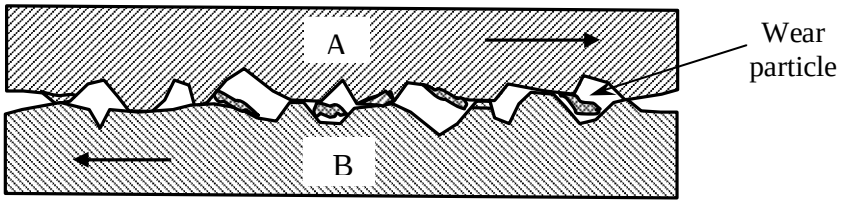

Figure 3.7 Wear loss in a tribo contact (Van Beek, 2004). (Arrows indicate the direction of sliding motion).

3.3.1 Specific Wear Rate (SPWR)

Specific wear rate is very useful when comparing similar materials for their wear resistance (Arnell, et. al., 1991). It is given by:

$$SPWR = \frac{Volume\ lost}{Load * Sliding\ distance} = \frac{V}{W * L}\ \ in\ \ (mm^3/N.m) \tag{3.6}$$

$$Volume\ of\ \ material\ \ lost = Area\ of\ the\ groove * Circumeference$$
$$i.e\ V = A * 2\pi r\ \ \ in\ \ (mm^3) \tag{3.7}$$

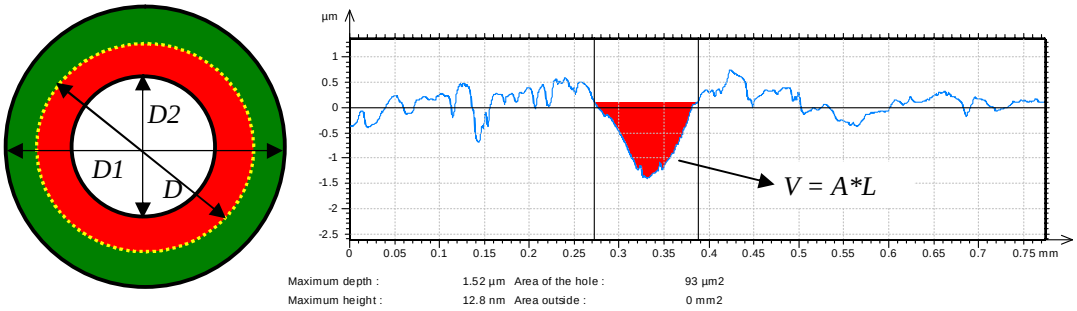

(a) (b)

Figure 3.8 Talysurf profile of a wear track on test sample (a) wear track (b) wear profile from Talysurf profilometer.

The area of the groove (red region in figure 3.8 (b)) is measured from Talysurf profilometer and '*r*' is the mean radius of the wear track. The Talysurf profilometer measures the worn area by sliding the probe across the wear track and provides a wear profile as shown in figure 3.8 (b). The red region in the profile indicates the area of the material lost at one particular region of the wear track. By taking successive wear profile measurements along the wear track circumference and averaging them, the average area of the material lost is obtained. The shape of the groove cannot be predicted as semicircular or rectangular due to the fact that material lost is not perfectly uniform throughout. This non-uniformity is associated with the flatness of the surface and mis-alignments in the specimen to substrate contact. The above equations apply to both substrate and counterface materials.

In figure 3.8 (a), the mean diameter of wear track, $D = \frac{(D_1 + D_2)}{2}$

Where, D_1 is outer diameter of the washer (mm) and D_2 is inner diameter of the washer (mm).

The Case of Spherical Counterface Material (Circular or Elliptical Groove)

According to Vaan Beek (2004), the SPWR of circular or elliptical scar can be calculated from figure 3.9 as,

$$Volume\ of\ scar = \frac{\pi h^2}{3}(3R - h) \tag{3.8}$$

Where, '*h*' is the height of the scar and is given as,

$$h = R - (R^2 - r^2)^{1/2} \tag{3.9}$$

Where, *R* - radius of the ball (mm); *r* - is the half width of the scar (mm)

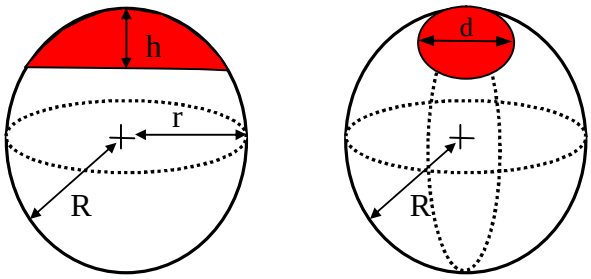

(a) (b)

Figure 3.9 Volume of sphere (a) Scar height (b) Scar diameter. (Van Beek, 2004).

From equations 3.6 to 3.8,

$$SPWR = \frac{Volume\ lost}{Load * Sliding\ distance} = \frac{\left(\pi h^2 / 3\right)(3R - h)}{WL} = \frac{\pi h^2 (3R - h)}{3WL}$$

$$SPWR = \frac{\pi h^2 (3R - h)}{3WL} \tag{3.10}$$

Where, $h = R - (R^2 - r^2)^{1/2}$

For a circular or elliptical scar on the ball (figure 3.9 (b)), the SPWR is calculated by measuring the area of the scar, i.e. circular scar area, $A = \pi r^2$ or an elliptical scar area, $A = d*h$.

3.4 Contact Pressure Calculations

It is well know that whenever two solid surfaces loaded against each other, the initial contact occurs only at few asperity contact spots in the real area of contact (Bowden and Tabor, 1950). With increases in normal load, the asperity contacts

increase further and deform either plastically or elastically depending on the loading conditions and material properties. At the tips of the asperity contacts, where the actual contact occurs, there may be some local elastic deformation that takes place also. The contact pressure at the asperity tips in the real area of contact is so high that micro-welding can take place and influence the friction and wear properties of the contacting surfaces (Hutchings, 1992). If the interacting surfaces are completely smooth, then real area of contact and apparent area of contact would be equal and the contact pressure would be just the ratio between normal load and apparent contact area. But in reality, all surfaces are rough on some scale and contact occurs only at the tips of the higher surface asperities, so contact pressure at the real area of contact is much higher than if only the apparent area of contact was considered.

In this project, two different types of test apparatus were used; each had different contact geometry, the contact pressure calculations for each of them were different. The contact pressure in TWT apparatus was measured simply by the ratio between the actual load applied and the apparent contact area between the substrate and counterface contact. It was assumed that the contact pressure is uniformly distributed between counterface and substrate due to the flat on flat contact situation. However, in the case of POD test apparatus, the contact pressure was not uniform. So the initial contact pressure was calculated by the Hertzian model of non-conformal contact, in the case of bulk materials, and final contact pressure was obtained from the measured contact area.

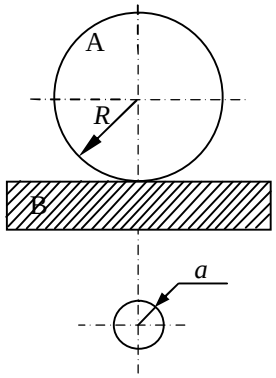

Figure 3.10 Nominal point contact of ball on disc.

In the case of thin coated surfaces, due to their plastic deformation (i.e. the initial contact pressure exceeded the hardness of lead/indium), the initial and final contact area were calculated from the measured contact area from the actual contact radius assuming that the contact area would be circular (figure 3.10).

The real area of contact, for plastically deforming asperities A_r is given by:

$$A_r = \frac{Load}{Hardness} = \frac{W}{H}$$

The apparent area of the contact, $A_p = \pi.r^2$

Where *r* is the measured contact dimension, mm (assuming circular contact area).

3.4.1 Hertzian Formula for Non-Conforming Elastic Bodies

The first analysis of deformation and pressure at the surfaces of two curved solids in elastic contact was discussed by Hertz (1896) and these contacts are referred to as Hertzian contacts. The contact stresses acting in the non-conformal contacting surface, as in pin on disc contact, are determined using the Hertz equations. The assumptions of Hertzian contact are,

- Surfaces are continuous, smooth and non-conforming
- The deformation is purely elastic for bulk materials
- The stress distribution below the surface is not affected by the finite dimensions of the contacting bodies
- The surfaces are assumed frictionless so that only a normal pressure is transmitted

For a circular contact area (figure 3.10), formulae for the contact radius *a* and deflections δ are described by Bhushan and Gupta (1999) as:

$$\delta = \left(\frac{9W^2}{16R^*E^{*2}}\right)^{1/3}, \quad a = \left(\frac{3WR^*}{4E^*}\right)^{1/3} \tag{3.12}$$

Where,

$$\frac{1}{E^*} \equiv \frac{1-\nu_1^2}{E_1} + \frac{1-\nu_2^2}{E_2}$$

$$\frac{1}{R^*} \equiv \frac{1}{R_1} + \frac{1}{R_2}$$

'E'* is the composite Young's modulus; E_1, E_2 and ν_1, ν_2 are the Young's modulus and Poisson's ratio for bodies 'A' and 'B' respectively.

The pressure distribution is hemispherical with a maximum pressure at the centre of contact (i.e. when $r = 0$), so,

$$P = P_{\max}\left(1-(r/a)^2\right)^{1/2} \tag{3.13}$$

The maximum contact pressure $P_{\max}$ is 1.5 times the mean contact pressure P_{mean} given as,

$$P_{\max} = \frac{3}{2}P_{mean} = \frac{3}{2}\left(\frac{W}{\pi a^2}\right) = \left(\frac{6WE^{*2}}{\pi^3 R^{*2}}\right)^{1/3} \tag{3.14}$$

3.4.2 Plastic Deformation: Non-Hertzian Contact

According to Hertzian theory, when a normal load is applied between two contacting solid bodies, they initially deform elastically, but when the normal load increases, one of the bodies with lower hardness starts to deform plastically at some distance below the surface. On increasing the normal load, the plastic zone grows until the entire material surrounding the contact has plastically deformed. The deformation has developed from elastic to elastic-plastic followed by fully plastic. Plastic deformation is initiated in one of the solid bodies and as the plastic deformation proceeds, the mean contact pressure increases, and if the mean contact pressure exceeds 1.1 times the yield stress (σ_y) of the other mating solid body, it too begins to deform plastically (Hutchings, 1992). Consequently one or both solid bodies can be permanently deformed. The test conditions for plastic and fully plastic deformations are described by Johnson (1985) are summarized below.

Onset of plastic deformation $P_{mean} = 1.1\ \sigma_y$

Limit of fully plastic deformation (metals) $P_{mean} = H = 3\ \sigma_y$

Where, H is the harness of the materials (GPa)

The assumptions used in calculating the contact pressure between a hard sphere and a thin metallic coated disc are,

- the sphere is assumed to be rigid
- the deformation in the thin coated surface is fully plastic
- The measured hardness of a soft thin coating on a hard substrate is very close to the hardness of the substrate, because, with a thin soft coating on a hard substrate, the contact area is defined by the hardness of the substrate (Arnell, et al., 1991)

3.5 Frictional Heating Calculations

When two solid bodies slide against each other friction occurs. At the regions of real area of contact, the frictional work is transformed to internal heat energy which causes the temperature of the sliding bodies to increase (Archard, 1958/59) This can result in high, short-term local temperature rises known as flash temperatures at the contact points and, as the heat diffuses into the material, the overall bulk temperature rises. These increases in temperature can influence the tribological behavior and failure of sliding components. High flash temperatures can result in local changes in structure and properties of sliding materials, oxidation of the surface and the possibility of melting of the contacting solids. The increase in surface temperatures can affect the friction and wear mechanisms depending on the type of material and contact conditions used. To understand failure of tribological components, flash temperatures at the actual contacting bodies need to be predicted. Flash temperature theory was originally formulated by Blok (1937) and further developed by Archard (1953) and Jaeger (1942). Their theories give a set of formulae for flash temperature calculations using various contact geometries and velocity ranges. According to Archard (1953) and Jaeger (1942) theory, the flash temperature is the temperature rise above the temperature of the solids entering the contact which is called the bulk temperature. So the maximum local contact temperature is the sum of bulk temperature and flash temperature.

Calculations of contact temperature rises in the two contact geometries used in this project – flat on flat and ball on disc – have been fully described by Ashby (1990, 1991) and the methods are summarized below.

3.5.1 Ashby's Method

The frictional heating in both thrust washer and ball on disc equipment was analysed using Ashby's methods which introduces the concept of an "effective heat dissipation length". This analysis was able to model contact geometry in a more effective manner than Archard's method and was more amenable to computer based analysis. This analysis is adopted to allow a theoretical comparison of the thermal conditions of the pin on disc and thrust washer tests.

Ashby described the frictional heating equations for both flat on flat (thrust washer) and ball on flat (pin on disc) contacts by considering the bulk substrate materials only. But in this thesis work, Ashby's method was applied by taking some assumptions to the lead/indium coated substrate in dry test conditions. The assumptions were:

- The hardness of the lead/indium coating was similar to the hardness of the substrate.
- Thermal properties of the coating such as conductivity, diffusivity, specific heat capacity etc were only considered when predicting the flash and bulk temperatures on lead/indium coated leded bronze substrates and thermal properties of the substrates were neglected.

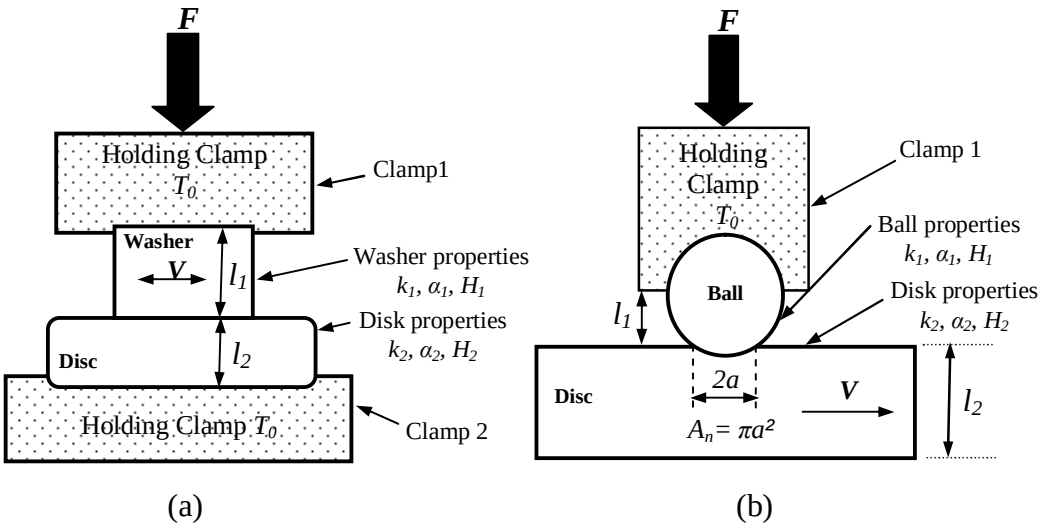

(a) (b)

Figure 3.12 Frictional heating calculations (b) Thrust washer contact (a) Ball on disc contact (After Ashby, et. al., (1990, 1991)).

Figure 3.12 shows two contact geometries, (a) thrust washer contact (b) pin on disc contact, where the counterface materials such as washer in thrust washer contact and ball in pin on disc contact were clamped to a holder at temperature T_0 and loaded against a rotating disc. The properties of the holding clamp and counterface materials are indicated in the figure 3.12. The bulk temperature T_b is the total surface temperature measured over the nominal contact area A_n and the flash temperature T_f is measured at the asperity contacts in the real area of contact A_r.

(a) Bulk Temperature Equations

When two solid bodies are loaded against each other under a normal force F and sliding at a relative velocity V with a coefficient of friction μ, the rate of heat generation q at a nominal area of contact A_n is,

$$q = \frac{\mu FV}{A_n} \tag{3.15}$$

It is assumed that the heat flow is linearly conducted from the contacting surfaces. This assumption also applies to a fast moving heat source repeatedly sliding over the same path.

The Flat on Flat Contact (Thrust Washer Contact)

The bulk surface temperature T_b is given by:

$$\frac{\mu FV}{A_n} = \frac{K_1}{l_{1b}}(T_b - T_0) + \frac{K_2}{l_{2b}}(T_b - T_0) \tag{3.16}$$

Where K_1 and K_2 are the thermal conductivities of the two contacting materials. The terms l_{1b} and l_{2b} denote the equivalent linear heat diffusion distances from the contacting surfaces to the heat sink (holding clamp).

The actual physical lengths for the two test geometries are shown as l_1 and l_2 in figure 3.12. These are smaller than the equivalent linear diffusion distances, which depend not only on the physical lengths but also on other parameters such as the thermal contact resistance between the clamp holder and the slider.

Since the real area of contact is always smaller than the nominal contact area, and the heat transfer coefficient across the clamped interface is small, the equivalent length is larger than the physical length. Ashby et. al., (1991) indicated that the thermal contact resistance often makes the effective diffusion length twice the physical diffusion length and this assumption has been used in the calculations in this thesis.

Equation 3.16 can be rearranged to give:

$$T_b - T_o = \frac{\mu FV}{A_n}\left(\frac{1}{\frac{K_1}{l_{1b}} + \frac{K_2}{l_{2b}}}\right) \tag{3.17}$$

Ball on Flat Contact (Ball on Disc)

The ball on disc contact is shown in figure 3.12 (b). By assuming that the heat flow is conducted linearly from the contacting surfaces, the heat transfer by conduction q_1 into the ball is given by:

$$q_1 = \frac{K_1}{l_{1b}}(T_b - T_0) \tag{3.18}$$

Where, K_1 and l_{1b} are the thermal conductivity of the ball and the equivalent linear heat diffusion distance, respectively. Bass (1982) given an expression for the equivalent linear diffusion distance for a circular heat source which has a contact radius 'a' from the surface of a semi-infinite solid as:

$$l_{1b} = \frac{\pi^{\frac{1}{2}} a}{2} \tag{3.19}$$

Unlike the flat on flat contact geometry, in the ball on disc contact, l_{1b} is defined by the radius of the contact instead of the physical length of the ball. Since the ball is held by a holding clamp, the thermal contact resistance between the ball and the clamp can make l_{1b} larger, and, following Ashby, it has again been assumed that the effective diffusion length is twice the actual contact radius.

The effective heat diffusion length of the disc l_{2b} is shorter than the physical length l_2 as the heat is more easily conducted in to the disc. Ashby, et. al., (1990) derived the effective heat diffusion distance l_{2b} from the solution given by Bass (1982) for a maximum temperature caused by a circular Gaussian source injecting heat into a solid for a time interval t, giving

$$l_{2b} = \frac{a}{\pi^{\frac{1}{2}}} tan^{-1}\left[\left(\frac{2\pi\,\alpha_2}{aV}\right)^{\frac{1}{2}}\right] \tag{3.20}$$

Where, α_2 is the thermal diffusivity of the disc material and a and V, the contact radius and sliding velocity of the contact.

Therefore the equation for bulk temperature, considering the effective heat diffusion length becomes:

$$T_b - T_o = \frac{\mu F V}{A_n}\left(\frac{1}{\frac{K_1}{l_{1b}} + \frac{K_2}{l_{2b}}}\right) \tag{3.21}$$

Where, T_b is the nominal or bulk temperature (ºC), T_o is the temperature of the remote sink to which heat flows (ºC). K_1, K_2 are the thermal conductivities of the surface materials (W/m.K) and the effective diffusion length are given be equations 3.19 and 3.20.

(b) The Flash Temperature Equations

The flash temperatures produced at the asperities from the real area of contact are much higher than those derived for the nominal contact area; they can reach several hundreds of degrees above the nominal or bulk temperature depending on the velocity and load conditions. Considering both contact geometries in figure 3.12, the heat input per unit area q' at the real area of contact A_r, is written as:

$$q' = \frac{\mu F V}{A_r} \tag{3.22}$$

Equation 3.22 is similar to equation 3.15 except that A_r is replaced by A_n. Following the same procedure as outlined above, the equations for average flash temperature for both contact types in figure 3.12 are summarized below.

The equivalent diffusion distances for asperity contacts in thrust washer and ball on disc contact are obtained by substituting l_f for l_b and a_r for a in equation 3.20, giving,

$$l_{if} = \frac{a_r}{\pi^{\frac{1}{2}}} tan^{-1}\left[\left(\frac{4t\,\alpha_i}{a_r^{\,2}}\right)^{\frac{1}{2}}\right] \tag{3.23}$$

Where, a_r is the contact radius for the real area of contact, i correspond to the relevant contacting body (i.e i is 1 for counterface and 2 for substrate).

Barber (1969) indicated that the average life time of an asperity contact is larger than the transit time. If the average life time of an asperity contact is n times larger than the transit time, then the time for heat to inject to an asperity is given by:

$$t = n\frac{\pi a_r}{2V}$$

Substituting this t into equation 3.23, gives

$$l_{if} = \frac{a_r}{\pi^{\frac{1}{2}}} tan^{-1}\left[\left(\frac{n2\pi\,\alpha_i}{V a_r}\right)^{\frac{1}{2}}\right] \tag{3.24}$$

At low velocities, $$tan^{-1}\left[\left(\frac{n2\pi\alpha_i}{Va_r}\right)^{\frac{1}{2}}\right] \approx \frac{\pi}{2}$$

and the effective diffusion distance for flash heating is independent of material properties and applicable to asperity junction of both surfaces.

Therefore, effective diffusion length in both contacting surfaces is obtained as:

$$l_{if} = \frac{\pi^{\frac{1}{2}} a_r}{2} \tag{3.25}$$

Since the contact is continuous, the flash temperature generated at the contact is equal for both surfaces.

Ashby, et. al., (1990) suggested that a reasonable estimate of the average contact radius is given by:

$$a_r = \frac{0.1\times10^6}{H} \tag{3.26}$$

Where H is hardness of the softer material (Pa), and this value can be substituted into equation 3.25 to give an estimate of the effective diffusion length.

Then the flash temperature component is given by:

$$T_f - T_b^{'} = \frac{\mu F V}{A_r}\left(\frac{1}{\frac{K_1}{l_{1f}} + \frac{K_2}{l_{2f}}}\right) \tag{3.27}$$

Where, T'_b is the sink (holding clamp) temperature for the heat flow from an asperity, which is approximately similar to the bulk temperature described earlier.

(Note: Equation 3.27 is similar to equation 3.21, with, A_n replaced with A_r, T_b by T_f and T_0 by T'_b)

3.5.2 The Effect of Surface Films

The influence of a surface film on the substrate could be important when predicting the contact temperatures. For example, the formation of oxide layers with low thermal conductivity will raise the surface temperature (Jaeger, 1942). However, for this effect to be important, the oxide surface film, which has low conductivity, must be thick compared to the molecular dimension (Archard, 1958/59; Jaeger, 1942). In the case of the coatings studied in this project, the films

are thin and conducting. Therefore, they will not restrict heat flow to the substrate, but as they cause a high friction coefficient they will also increase the heat near the contact. As the friction coefficient is used in the temperature calculations, this effect is taken into account in the model presented by the author.

Summary

In this chapter, tribological test equipment was briefly discussed. Specific wear rate calculations using the gravimetric method and profilometer methods were also reviewed. Hertzian and nominal contact pressure calculations for circular contact geometry were also briefly explained. Frictional heating analysis and equations to predict flash temperatures using Ashby's method were summarized. In the next chapter, the test methods used in this study is explained in detail. This description includes the functions of various components in test equipment.

CHAPTER 4

DESCRIPTION OF TEST APPARATUS USED

4.0 Introduction – Test Apparatus

In this project, two types of test apparatus were used to measure friction and wear data on leaded bronze substrates and lead/indium coatings. These were thrust washer test apparatus (TWT 1) already in established use in the laboratory, and a conventional pin on disc apparatus. The thrust washer test replicated the real contact situation in the gear pumps quite well, whereas the pin on disc, representing an accelerated test apparatus, facilitated the application of a high contact pressure over a small area. The same test materials were used on both of these test apparatus, but in different operating conditions due to the different contact geometry and limitations from the test apparatus. An attempt was made to compare the trends of friction and wear data obtained from these two test apparatus to identify the tribological properties of the test materials and to determine the similarity/differences in results from the two types of test. In addition to these test two apparatus, a newly adopted thrust washer test apparatus 2 (TWT 2) was used to examine lead free Toughmet substrate materials. Tests on Graphit-ic and Chromium Graphit-ic coatings were also conducted using TWT 2 apparatus to compare trends of friction and wear data in dry and marginal lubricated test conditions.

4.1 Thrust washer test apparatus 1

The thrust washer test apparatus 1 in the Jost institute of Tribotechnology is based on the conventional ASTM D3702 (Anonymous, 2007) test described in Chapter 3.1.2. This test machine was initially a four ball test apparatus, later modified to be a thrust washer tester. The test geometry consists of a steel washer (counterface), in the shape of a rim with inside diameter of 23 mm and outside diameter of 33 mm in contact with a disc-shaped test specimen (substrate) which is held tightly in a specimen holder. The wear track is defined by the area between the inside and outside diameters of the steel washer in contact with the test specimen. The load applied to the test specimen and the rotational speeds are defined by the desired contact pressure and interfacial sliding speed. A transducer amplifier connected to a load cell on to the stationary specimen holder is used to measure the friction force. This analogue voltage from the load cell is converted to a digital signal by a Pico logger, which allows signals to be displayed on a

computer. The coefficient of friction is obtained from the relationship between the frictional force and load applied. The test apparatus is shown schematically in figure 4.1 and the real test machine used in this project is shown in figure 4.2.

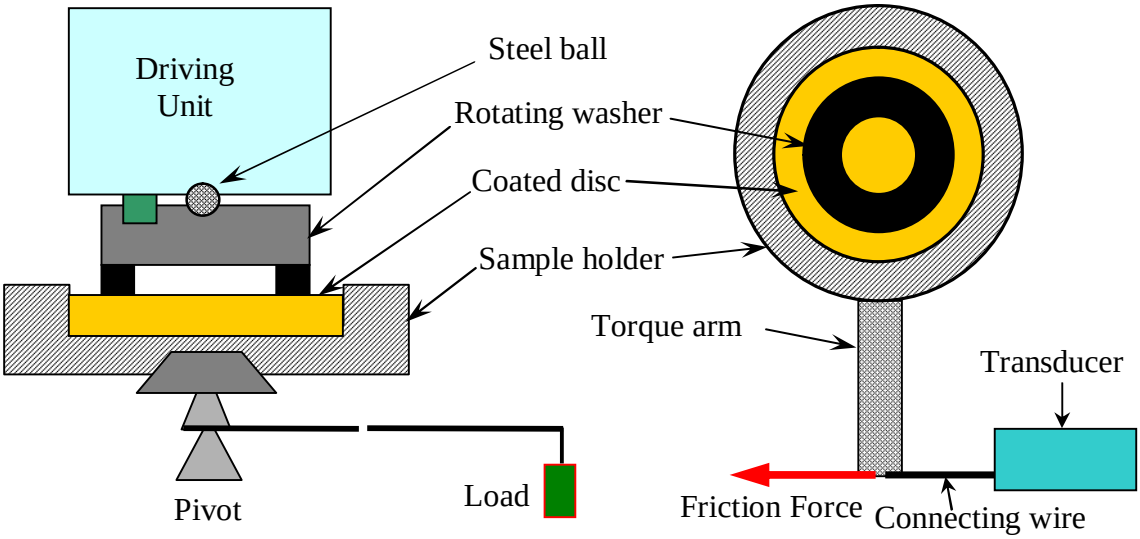

(a) Front View (b) Top View

Figure 4.1 Schematic of thrust washer test apparatus 1.

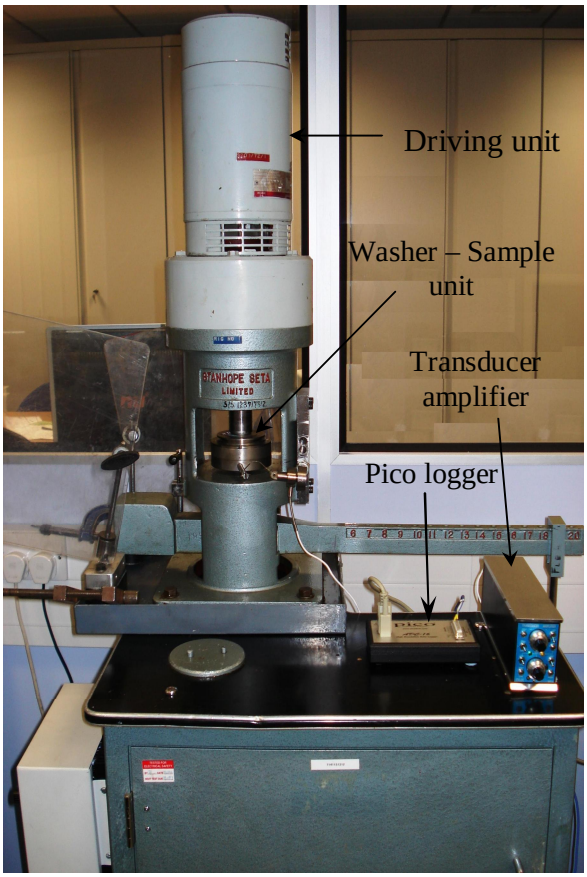

(a) Total unit

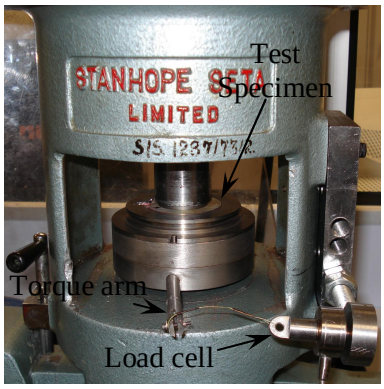

(b) Close view

(c) Loading arm

Figure 4.2 Real thrust washer test apparatus 1.

Detailed descriptions of the various elements of the machine are given below.

(a) Sample Holder

The sample holder platform retains the stationary specimen holder, using a pin to prevent rotation of the specimen holder (figure 4.3 (a)). Rotation of the specimen within the holder is prevented by a wedge and a screw (figure 4.3 (b)).

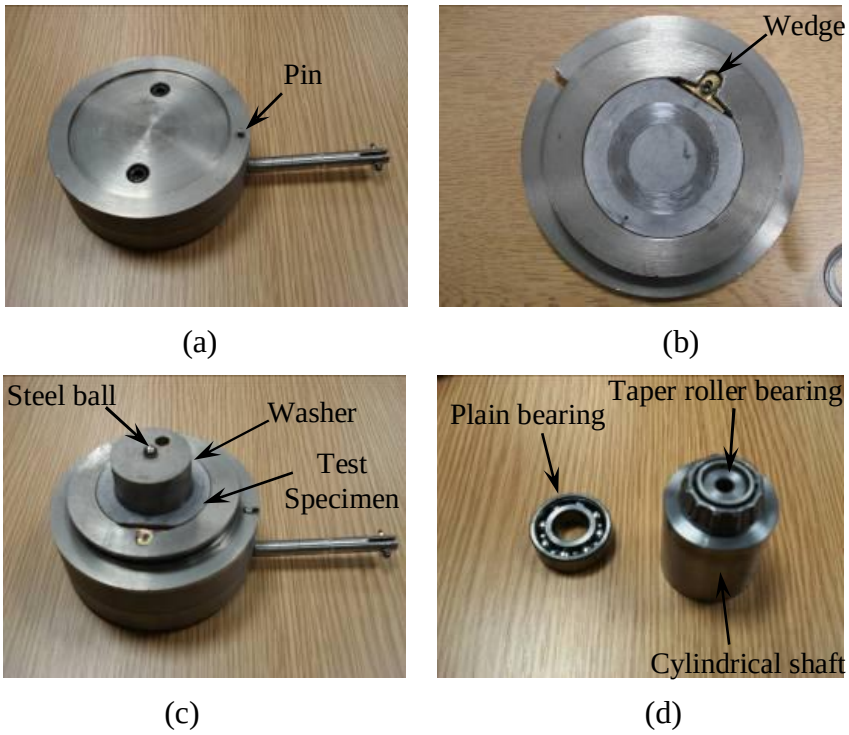

Figure 4.3 Views of various elements in thrust washer tester (a) Sample holder platform (b) Sample holder (c) Washer-sample unit (d) Bearings.

(b) Upper Counterface Specimen

The upper counterface specimen, shown in figure 4.3 (c), has a steel ball located in a conical recess, and the upper part of the ball locates in a similar recess in the end of the drive shaft. This allows self-alignment of the two specimens during rotation. The upper specimen is driven by an eccentric peg on the end of the drive shaft, which locates in the off-centre hole.

(c) Cylindrical Shaft and Taper Roller Bearing

A taper roller bearing is attached to the top of a cylindrical shaft (figure 4.3 (d)) and this whole setup carries the sample holder platform. The load on the test specimen is applied through this arrangement with the cylindrical shaft sliding in a fixed bushing as the load is applied. The main function of the taper roller bearing is to allow low friction of the assembly rotation which is necessary to

measure the friction torque, while controlling the sidewise movement of the sample holder when the steel washer rotates on the test specimen.

(d) V-block and Loading Arm

A V-block carries the loading arm on V-grooves and transmits the load to the test specimen. The loading arm has various positions numbered from 6 to 20 to indicate the load applied on the washer-specimen contact by weights placed on the arm (1 kg to 2 kg).

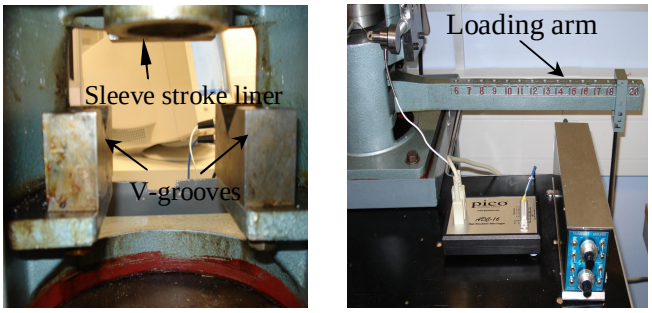

(a) (b)

Figure 4.4 V-block and loading arm (a) V-grooves (b) Loading arm.

(e) Fenner Speed Ranger, Fylde Transducer Amplifier and Pico Logger

Fenner speed ranger (figure 4.5 (a)) is used to control the rotational speed of the steel washer when in contact with the test specimen. The range of speed is from 0 rpm to 3000 rpm. Fylde transducer amplifies the low voltage analogue signals received from the load cell for input to an analogue to digital converter on the Pico logger. The 16 bit Pico logger (figure 4.5 (b)) converts the analogue voltage signal received from the amplifier to a digital signal and sends it to a computer which stores the data and simultaneously displays it on a monitor during acquisition.

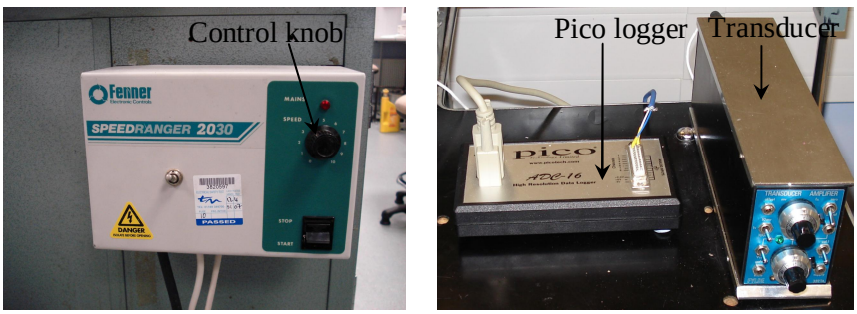

(a) (b)

Figure 4.5 Fenner speed ranger controller (a) Speed ranger (b) Transducer amplifier.

4.2 Experimental Details

4.2.1 Test Procedure

- Before conducting the test, the tribocouple (test specimen and steel washer) is thoroughly cleaned with alcohol and dried in air.
- In a lubricated test condition, the tribocouple is smeared with a small amount of lubricant supplied by GAEC (2009) and a dry tissue is used to remove most of the oil film leaving only a residual lubricant film on the surface.
- The test specimen is secured in the sample holder (figure 4.3 (b)) and this whole unit is placed in the sample holder platform (figure 4.3 (a)).
- The steel washer is positioned on top of the test specimen and held in place by a driving peg at the end of the shaft located in the offset hole (figure 4.3 (c)).
- The sample holder platform is connected to the load cell by the connecting wire.
- The rotational speed and the applied load are set to the desired test conditions.
- The test is stopped after 10 minutes of sliding in both unlubricated and marginally lubricated test conditions.
- The wear loss of the test specimen is assessed using Talysurf profilometer and analysed in WLI.
- The wear loss of the test specimen can also be done using gravimetric method during the unavailability of Talysurf profilometer.

4.2.2 Flow Chart of Thrust Washer Test Apparatus 1 (TWT 1)

The flow chart shown in figure 4.6 describes the set of test materials and test conditions used in the TWT apparatus 1. This process is also common to other test equipments used in this thesis except that the test conditions and test materials may differ.

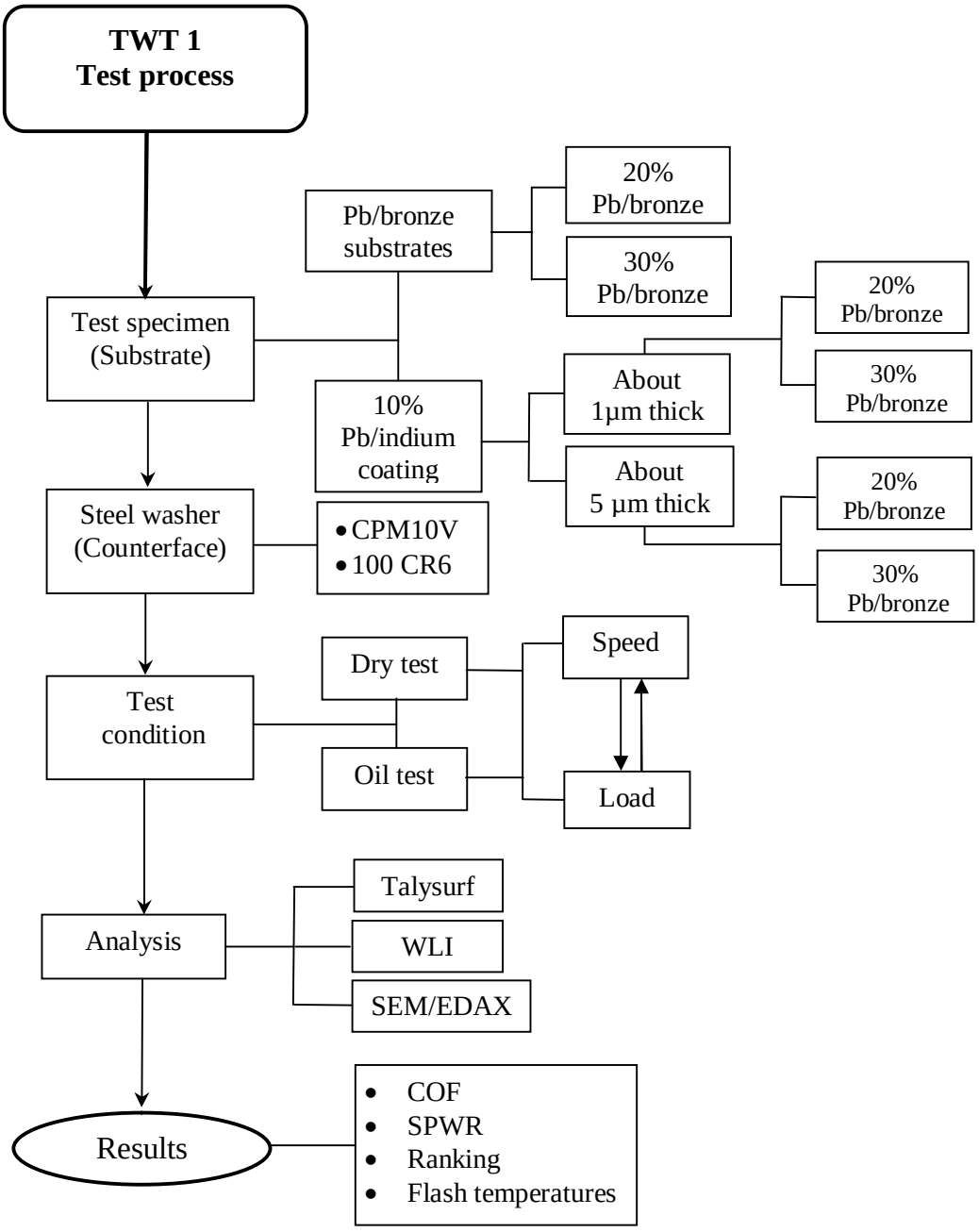

Figure 4.6 Flow chart of TWT

* WLI - White Light Interferometers, SEM/EDAX - Scanning Electron Microscope/Energy dispersion spectroscopy, Pb/bronze - Leaded bronze, COF- coefficient of friction, SPWR- Specific wear rate.

4.2.3 Calibration of Input and Output Devices

(a) Test Machine

Before running the experiments, it was necessary to check that the specimen holder was properly balanced. After placing the sample holder platform on the top

of the bearing holder setup (i.e. along with the loading arm), the whole unit was balanced on the V-groove without adding any load on the loading arm. This ensured that the initial load on the test specimen was zero.

(b) Load Cell

By adding the weights to the load cell used to measure friction by means of a weight carrier and a string pulley arrangement (figure 4.2 (b)) and recording the corresponding output voltage from the transducer amplifier, a relationship between voltage and load applied was then obtained. One example of this process is shown in table 4.1, with the calibration graph shown in figure 4.7. The calibration of load cell was usually conducted once in a week.

Table 4.1 Voltage readings from transducer amplifier.

Weight (N)	Voltage Recorded (Volt)
0	3.97
0.2	4.85
0.3	5.19
0.4	5.77
0.5	6.10
0.6	6.41
0.7	6.71
0.8	7.29
0.9	7.63
1.0	8.00

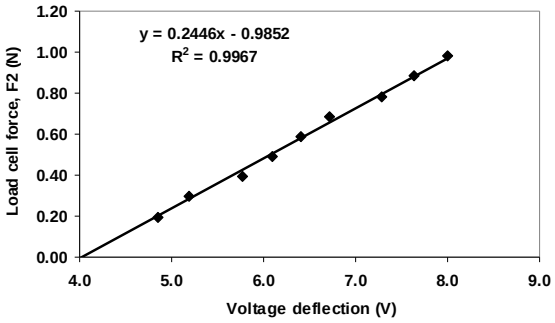

Figure 4.7 Calibration of transducer

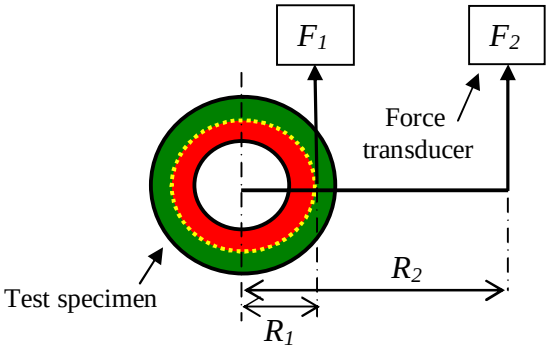

Figure 4.8 Schematic of forces acting on washer-disc contact.

From figure 4.8, the friction force F, at the interface is given from,

$$F_1 \times R_1 = F_2 \times R_2 \text{ or } F_1 = F_2 \times \left(R_2 / R_1 \right) \quad (4.1)$$

Therefore, Coefficient of friction, $\mu = \frac{F_1}{W}$ (4.2)

Where F_1 = Frictional force, F_2 = Load cell force, R_1 = 14 mm, R_2 = 112.8 mm.

4.3 Materials

4.3.1 Steel Washer (Counterface)

The steel washer (figure 4.9) supplied by GAEC (2009) is a chromium tool steel (CPM 10V) with inside and outside diameters of 23 mm and 33 mm. The thermal and mechanical properties, and nominal chemical compositions of CPM 10V are given in table 4.3 and 4.4 respectively.

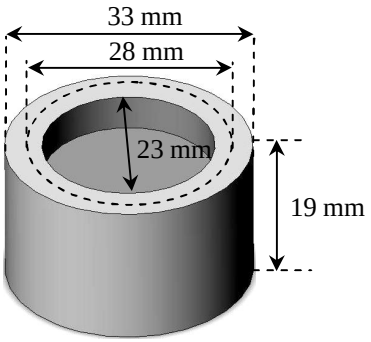

Figure 4.9 Specifications of steel washer.

Mean diameter of the annular face, $D = \frac{D_1 + D_2}{2} = \frac{33 + 23}{2} = 28\ mm$

Area of annular face of washer, $A_w = \frac{\pi\left(D_1^2 - D_2^2\right)}{4} = \frac{\pi\left(33^2 - 23^2\right)}{4} = 439.8\ mm^2$

4.3.2 Test Materials (Substrates)

The test specimens used in this project consist of 20% leaded bronze and 30% leaded bronze substrates and 10 % lead/indium coated leaded bronze substrates supplied by GAEC (2009), Birmingham. Some of the test specimens were coated with a 10% lead/indium films nominally 1 μm and 5 μm thick. All samples were tested dry and marginally lubricated with kerosene. Kerosene was selected as the main fuel in the gear fuel pump thrust bearings. The loads and speeds were selected to replicate the real contacting conditions of the gear pump. The detailed chemical, mechanical and thermal properties of test specimens supplied by GAEC (2009) are shown in table 4.2 to table 4.4. The roughness data of all the test specimens measured from Talysurf profilometer were tabulated in table 4.5.

Table 4.2 Nominal chemical composition of test materials (GAEC, 2009).

Test material	Typical analysis, Wt %								
	Pb	Sn	Ni	Zn	Fe	Sb	P	Cu	In
20% Pb/bronze	18-23	4-5.5	0.8	1	0.2	0.2	0.05	Remainder	-
30% Pb/bronze	27-37	1.5-2.5	0.25-0.75	0.5	0.05	0.50	-	Remainder	-
10% Pb/indium	90-92	-	-	-	-	-	-	-	8-10

* Wt % - Weight percent.

Table 4.3 Nominal chemical compositions (by Wt %) of counterface materials (GAEC, 2009).

Material	C	Cr	Mn	Si	P	Fe	Mo	V	S
CPM 10V	2.45	5.25	-	-	-	81.25	1.3	9.75	-
100 CR6	0.95-1.10	1.30-1.60	0.35	0.230	0.025	97	-	-	0.025

Table 4.4 Mechanical and thermal properties of test materials (GAEC, 2009).

Mat	Properties							*E* (GPa)	*HV*
	ρ (kg/m³)	*C* (J/kg)	*K* (w/mK)			α (m²/s) X 10^{-5}	ν		
			20 ºC	100 ºC	200 ºC				
20% Pb/bronze	8770.22	333.4	56.17	67.63	77.46	1.92	0.36	91.2	40
30% Pb/bronze	9025.89	307.6	81.20	94.9	105.88	2.92	0.37	81.8	30
10% Pb/indium	10747.49	137.3	10	-	-	0.67	0.42	15.5	4
CPM 10V	7418	460	20.2	21.4	23.2	0.59	0.29	203.4	800
100 CR6	7865	460	61	55	52	1.68	0.22	213	720
Toughmet	8941	-	38	-	-	-	0.3	128	300

* Mat – Materials, ρ – Density, *C* – Specific heat capacity, *K* – Thermal conductivity, α – Thermal diffusivity, ν – Poisson's ratio, *E* – Modulus of elasticity, *HV* – Vickers hardness.

Table 4.5 Surface roughness data of test materials measured from Talysurf profilometer.

Material		Thickness µm	R_{a1}	R_{a2}	R_{a3}	R_{avg}
20% Pb/bronze		uncoated	0.2	0.3	0.3	0.26
30% Pb/bronze		uncoated	0.4	0.5	0.4	0.45
10% Pb/indium	20% Pb/bronze	1µm	0.3	0.3	0.3	0.30
	30% Pb/bronze		0.6	0.6	0.5	0.56
10% Pb/indium	20% Pb/bronze	5µm	0.4	0.4	0.5	0.43
	30% Pb/bronze		0.6	0.6	0.7	0.63
CPM 10 V		uncoated	0.04	0.06	0.05	0.05
100CR6		uncoated	0.06	0.07	0.05	0.06

* R_{a1}, R_{a2}, R_{a3} – Roughness data measured at areas 1, 2 and 3 respectively (µm).
R_{avg} – Average roughness (µm).

4.4 Examples of Friction and Wear Measurements

4.4.1 Coefficient of Friction (COF)

One example of the experimental process and calculation of the coefficient of friction is shown below.

Table 4.6 Example COF calculations on a 1 µm lead/indium coated 30% leaded bronze substrate in marginally lubricated test conditions.

Test	Thickness (µm)	Speed (rpm)	Load (N)	Set time (sec)	Finish time (sec)	Initial voltage (mV)	Final voltage (mV)	Mean COF
51	0.52	2000	98.1	1800	925	-6.81	-10.16	0.23

* Negative voltage indicates the direction of load applied

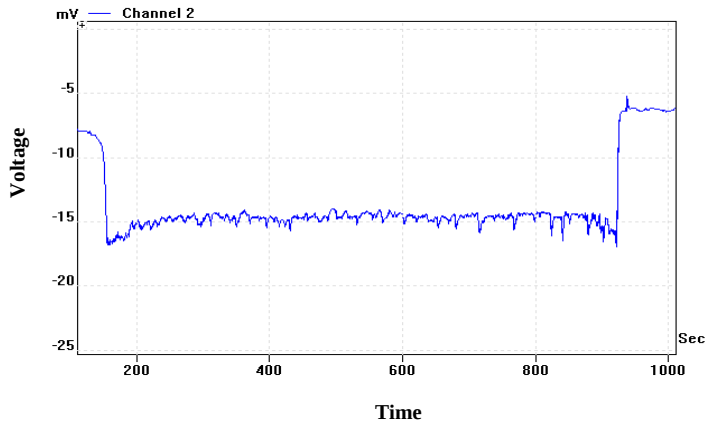

Figure 4.10 Instrument amplitude output (negative voltage indicates the direction of load applied).

From equation 4.1, $F_1 = F_2 \times \left(R_2 / R_1 \right)$

Also from load cell calibration (figure 4.8 (a)),

$$y = -244.57x - 0.9852 \tag{4.3}$$

Where, 'x' is the voltage recorded and 'y' is the load cell force which is 'F_2' in equation 4.1.

$$F_1 = (-244.57x - 0.9852) \times \left(R_2 / R_1 \right) \tag{4.4}$$

By using equation 4.2, the coefficient of friction is calculated. Figure 4.11 shows the coefficient of friction against time graph after converting the voltage values into friction force.

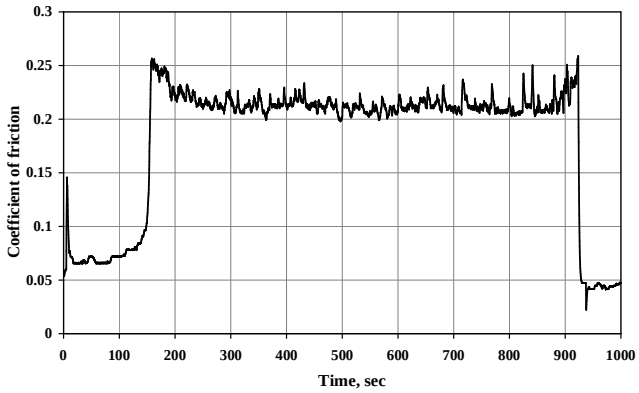

Figure 4.11 An example of a coefficient of friction against time graph.

4.4.2 An Example of Various Characteristics of Friction Vs. Time

To observe the coefficient of friction at various time periods, a graph was plotted for friction coefficient against time, as shown in figure 4.12. The mean coefficient of friction obtained from this test was 0.13 over a time period of 60 minutes. This test was conducted on a 1 µm thick 10% lead/indium coated 30% leaded bronze substrate in a marginal lubricated test condition. The applied load and rotational speed were 98.1 N, 2000 rpm respectively. Various observations recorded during the test are given below.

Real Time Observations from Friction Coefficient Vs. Time Graph

- The test started very smoothly, without any noise from the specimen-washer interface.

- A continuous loud noise was observed from 80 sec until 160 sec. This was associated with the coefficient of friction increasing marked with a dotted circle, in figure 4.12.
- Noise from the sliding contact was always associated with fluctuation of the friction force.
- A continuous, low-level noise was observed from 800 sec to 1600 sec during which time the friction decreased slightly.
- From 1600 sec shaking of the sample holder platform was observed, associated with a rapid increase in friction.
- The experiment was stopped at 1800 sec because strong shaking of the sample holder platform was observed and also to avoid damage to the specimen surface.
- The contact area in the specimen surface was worn unevenly around its circumference (figure 4.14). This test was conducted in lubricated condition, and the oil film was observed to be decomposed into a black layer on the wear surface.

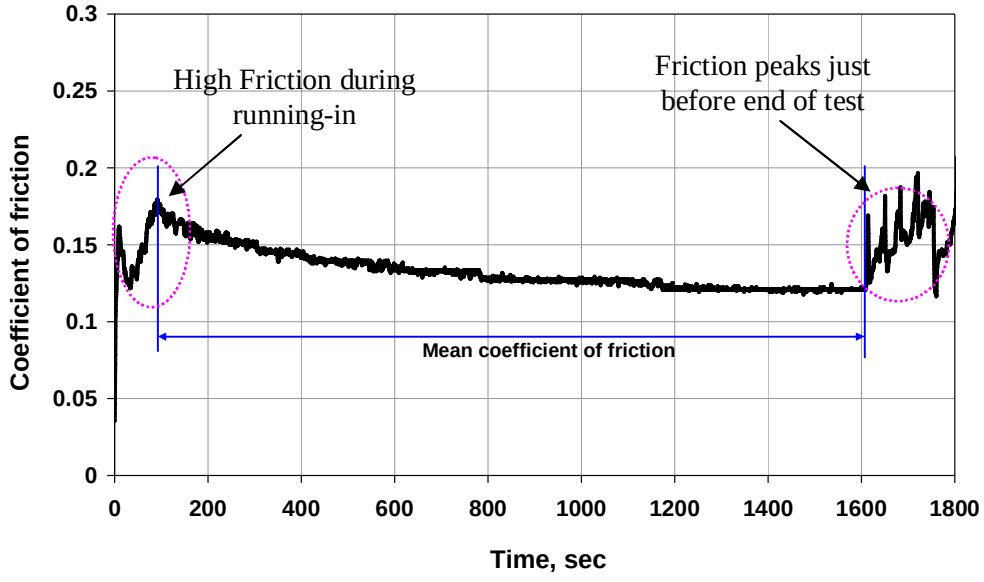

Figure 4.12 Example of a coefficient of friction Vs. time graph showing various characteristics of friction.

In figure 4.12, the mean coefficient of friction represents the average coefficient of friction from the start to the end of the test neglecting the initial running-in

period. Since the running-in period (Suh and Sin, 1981) is associated with the fluctuation of the friction coefficient values, averaging the friction coefficient values in this period will not give the accurate friction coefficient. The mean coefficient of friction was used as the reference parameter when comparing different test material in various loading conditions in this thesis work.

4.4.3 Explaining "Mean Coefficient of Friction"

It can be seen in figure 4.12 that the friction curve fluctuated initially in the running-in period but stabilized later on without any big fluctuation until just before the end of test where high friction peaks were observed. The high friction peaks were due to no lubrication at the contact interface between washer-disk contact which becomes dry contact conditions. It was identified in most of the tests with TWT apparatus 1 that the selection of the mean coefficient of friction against time graph is arbitrary and varies from test to test. Especially in lead/indium coated tests in dry test condition, it was identified that in the initial running-in period, the friction fluctuated severely for a considerable time period and mean coefficient of friction was measured carefully by not considering this running-in period for each individual tests. But in lubricated tests, the friction curve fluctuated after a period of sliding. Some of the typical examples variable friction against times graphs observed in TWT apparatus 1 are shown in figure 4.13. In most of all graphs, the mean coefficient of friction was measured by averaging all the friction values from start of the test to the end of the test neglecting any running-in period observed. But in some cases (see for example 4.13 (f)) especially in lubricated tests where the friction coefficients recorded at the start of the test, up to a small period of sliding was not considered since the amount of lubricant presented varied from test to test (This was due to the smearing of lubricant manually in each test). With lead/indium coated leaded bronze tests, the initial running-in period was higher and friction curve stabilized after this period. Where as, the same coated specimens in lubricated tests, the initial running-in period was not observed.

The test conditions and mean coefficient of friction regions used on few of the examples of friction-time graphs shown below are indicated on the graphs.

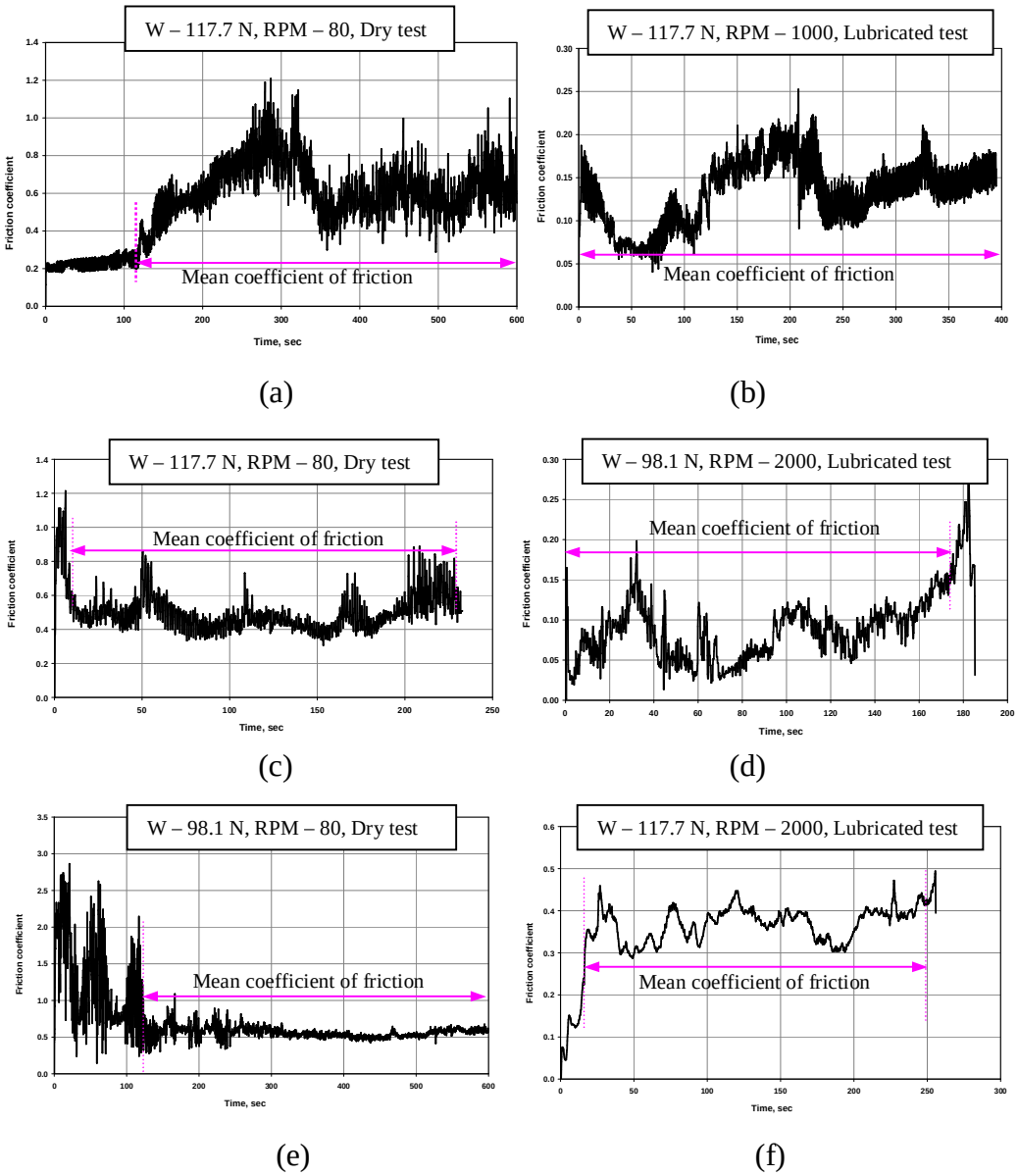

Figure 4.13 Typical examples of coefficient of friction against time graphs from TWT apparatus 1 (a) Uncoated 30% lead/bronze substrate in dry test conditions (b) Uncoated 20% leaded bronze substrate in lubricated test conditions (c) 1µm lead/indium coated 20% leaded bronze substrate in dry test conditions (d) 1.12 µm lead/indium coated 20% leaded bronze substrate in lubricated test conditions (e) 4.93 µm lead/indium coated 20% leaded bronze substrate in dry test conditions (f) 5 µm lead/indium coated 30% leaded bronze substrate in lubricated test conditions. (Note: W – Normal load, RPM – Revolutions per minute or rotational speed).

4.4.4 Specific Wear Rate (SPWR)

The specific wear rate (SPWR) on the worn test specimens was calculated from volume of the material lost using Talysurf profilometer as described in chapter 3.3. One example of specific wear calculations on leaded bronze substrates and lead/indium coatings is given below. The volume loss of leaded bronze substrates was measured by a gravimetric method due to the unavailability of Talysurf profilometer for some period of time and the volume loss of lead/indium coatings was measured by Talysurf profilometer. The gravimetric method was not used on lead/indium coated samples since the weight loss of the coating was too small and additionally could be misleading as it would not be possible to distinguish coating and substrate wear after the coating had worn through.

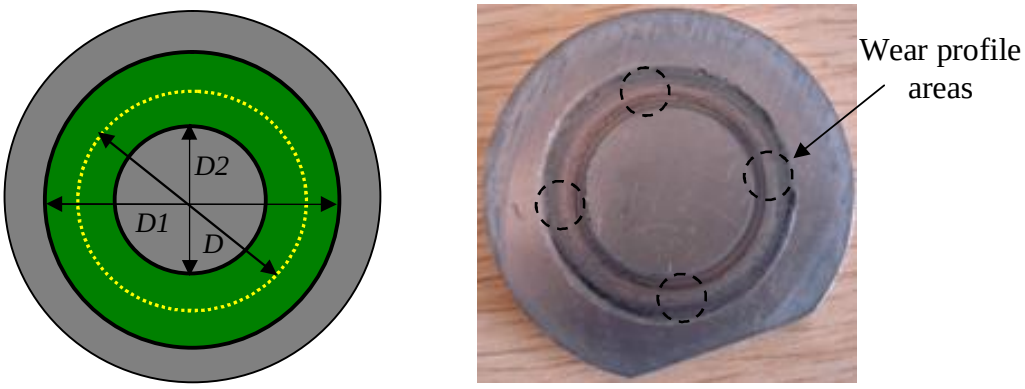

(a) (b)

Figure 4.14 Wear track on a test specimen (a) Schematic of sample (b) Real test sample showing wear areas.

(a) Gravimetric Method

This method is based on the weight loss of the test material i.e. difference in weight of material before the test and after the wear test. As the density of the test material was known the volume loss of material could be obtained by taking the ratio between weight loss of the material and the density of material. Then the SPWR was calculated using equation 3.6 described in chapter 3.3.1. One example on SPWR of 30% leaded bronze tested in lubricated condition was calculated by considering the test conditions as shown in table 4.7.

Table 4.7 Example SPWR calculations on 30% leaded bronze substrate by gravimetric method.

Test	Load (N)	Speed (rpm)	Sliding time (min)	Wt. of specimen BT, (g)	Wt. of specimen AT, (g)	Total Wt. loss, (g)	Density (ρ) (kg/m^3)
UN20	117.72	1000	5	81.0608	81.0596	0.0012	9025.8

* BT- Before test, AT-After test, Wt-Weight, Min-Minutes, Vol. loss – Volume loss.

Example Calculations

In figure 4.14, the mean diameter of washer is obtained as,

$$Mean\ diamter, D = \frac{(D_1 + D_2)}{2} = \frac{(33+23)}{2} = 28\ mm$$

Circumference of the circle = $\pi \times D = \pi \times 28 = 87.96\ mm$

Total sliding distance, L = (Circumference of circle) × (Number of revolutions)

$$L = 87.96 \times RPM \times Time$$

$$= 87.96 \times 1000 \times 5 = 8.8 \times 10^5\ mm = 440\ m$$

Let us assume actual weight loss of test material is 'W' in kg.

Therefore, Volume loss of material, $V = \frac{W}{\rho} = \frac{1.2 \times 10^{-3} \times 10^{-3}}{9025.8 \times 10^{-9}} = 0.13\ mm^3$

The SPWR obtained as,

$$SPWR = \frac{V}{F \times L} = \frac{0.13}{117.72 \times 440} = 2.56 \times 10^{-6}\ mm^3/N.m$$

Where, 'F' is the applied load in Newtons.

The volume loss for the above test specimen UN20 from table 4.7 was also measured by Talysurf profilometer to identify if both gravimetric and Talysurf profilometer methods show similar values. It was identified that both of these methods showed similar volume loss values (UN20 in table 4.7 and table 4.8).

(b) Area of the Wear Track from Talysurf Profilometer

The SPWR of lead/indium coatings were calculated by measuring the area of the wear track from Talysurf profilometer i.e. by taking successive wear profiles (figure 4.14 (b)) across the worn surface by Talysurf profilometer. This process was also used for leaded bronze substrates. One example of SPWR calculations on 1 μm 10% lead/indium coated leaded bronze substrates (test: 27 and 62A in

table 4.8) tested in unlubricated condition is shown below. The operating conditions on 10% lead/indium coatings are given in table 4.8.

Table 4.8 Example SPWR calculations on test specimens using Talysurf profilometer.

Test	Load (N)	Speed (rpm)	Slid time (min)	A_1 (μm^2)	A_2 (μm^2)	A_3 (μm^2)	A_4 (μm^2)	A_{avg} (μm^2)	Vol. loss (mm^3)
27	58.86	80	10	2181	2310	2195	2217	2220	0.19
62A	117.72	80	10	2320	3011	2287	1287	2539	0.22
UN20	117.72	1000	5	1538	1497	1546	1527	1542	0.135

* A_1, A_2, A_3, A_4 – Area of groove at 4 different areas; A_{avg}- Average area, Vol. loss – Volume loss of the materials, Slid time – Sliding time.

In table 4.8, the non-uniform wear loss across the circumference of the wear track areas in test 62A was appeared to be due to the non-flatness of the substrate and problems associated with mis-alignments of the sample-washer contact in the thrust washer test. This was a surprising result since it is expected that the wear loss should be uniform throughout the circumference of the wear track (for example test 27 in table 4.8 and figure 4.15 (a)). Whenever this type of unexpected result observed, as shown in figure 4.15 (b), areas with closely matched wear areas were considered and averaged. The un-matched area was neglected. For example, in the figure 4.15 (b), area A_4 is out of range (i.e. has not been uniformly worn with respect to other areas) compared to other areas and this areas will not be considered when averaging all the void areas. However, this was the only wear test observed with non-uniform wear loss out of all the wear tests conducted.

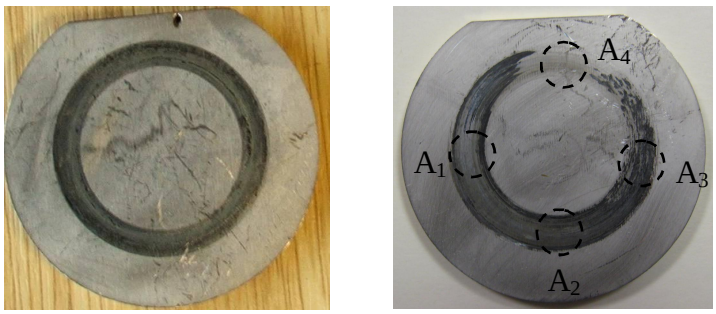

(a) (b)

Figure 4.15 Measured wear areas from Talysurf profilometer (a) Uniform wear loss (b) Non-uniform wear loss.

Example SPWR Calculations

The average area obtained from Talysurf profilometer, $A_{avg} = 2.22 \text{ X } 10^{-3} \text{ mm}^2$

$$\text{Volume loss, } V = \text{Area} \times \text{Circumference of circle} = 2.22 \times 10^{-3} \times \pi \times 28 = 0.195 \text{ mm}^3$$

The SPWR obtained as,

$$SPWR = \frac{V}{F \times L} = \frac{0.195}{58.86 \times 70} = 0.0000473 = 4.73 \times 10^{-5} \text{ mm}^3 / \text{N.m}$$

4.4.5 Correlations of Results

To determine if the wear rate of the coatings were proportional to the product of contact pressure and sliding speed (i.e. the PV factor) supplied by GAEC (2009), combinations of loads and speed were taken that replicate the "start up condition" of the gear pump thrust bearings. Since the GAEC (2009) believes that the bearing behaves hydrodynamic at the running-in speed, so wear will only occur before take off conditions. The slower speeds are therefore relevant to the regime where wear is occurring. Therefore, only the "start up condition" was replicated.

Real Test Operating Conditions on Gear Pump Thrust Bearings

The operating conditions for the thrust bearing of the gear pump supplied by GAEC (2009) are given below.

"Start up condition": P = 0.1 N/mm^2, V = 3.4 m/s; PV= 0.34, RPM = 2020

"Take off condition": P = 0.25 N/mm^2, V = 22 m/s; PV = 5.5, RPM = 13000

Operating Conditions Used on TWT Apparatus

The test conditions used on test specimens in dry and lubricated test conditions to replicate the "start up condition" very closely are shown in table 4.9 and table 4.10.

- **Lubricated test condition**

The maximum rotational speed for the thrust washer test apparatus was 2000 rpm and a maximum applied load of 157 N was used in this project to meet the "start up condition" of the gear pump thrust bearings described earlier.

Table 4.9 Combination of speeds and loads for marginally lubricated test conditions.

Speed (rpm)	Load (N)	P (N/mm2)	V (m/s)	PV (N/mm^2.m/s)
2000	58.86	0.106	2.94	0.31
2000	78.48	0.18	2.94	0.53
1000	117.72	0.212	1.47	0.31
1000	156.96	0.36	1.47	0.53

Table 4.9 shows the combination of speeds and loads that were applied to test specimens in lubricated conditions.

Combination of loads and speeds which give the same PV values were taken from table 4.9 and experiments were conducted in lubricated test conditions. From table 4.9, it can be seen that a load of 58.86 N and sliding speed of 2000 rpm gives the PV value which is equal to the product of PV obtained at a load of 117.72 N and sliding speed of 1000 rpm. These two conditions were compared for the wear rate of the test materials to understand the correlation between PV and wear rate.

- **Unlubricated tests**

In unlubricated tests, the combinations of maximum load and maximum sliding speed that can be applied on the test specimen were 98.1 N, 80 rpm, respectively. It was observed that the tests with sliding speed more than 80 rpm and applied loads more than 98.1 N showed fluctuations of the sample holder in thrust washer test apparatus 1. Therefore, the operating test conditions were limited to these values only. The combinations of load and speed used in unlubricated test conditions are shown in table 4.10.

Table 4.10 Combination of speeds and loads for unlubricated test conditions.

Speed (rpm)	Load (N)	P (N/mm2)	V (m/s)	PV (N/mm^2.m/s)
80	58.86	0.13	0.12	0.016
80	78.48	0.18	0.12	0.021
80	98.1	0.22	0.12	0.026

It can be seen from the table 4.10 that, the maximum PV attained in the dry test is lower than the PV in the "start up condition" of the gear pump. However, the contact pressures are very similar to the "start up condition" of the gear pump and these PV ratios were used to identify the running-in for the lead/indium coatings on leaded bronze substrates and the self lubricating properties of the leaded bronze substrates in dry test conditions.

4.5 Problems with the Thrust Washer Test Apparatus 1

Several problems were encountered in the initial phase of experimental work. The principal technical problems were:

- Vibration and fluctuation problems from the sample holder setup.
- Specimen movement in the specimen holder during the test.

Vibrations from the sample holder set up were identified as the major problem in preliminary experiments in dry test conditions only at high sliding speeds. This was believed to be the loose fit of the sleeve stroke liner inside the main casting (figure 4.4 (a)) and misalignment of the specimen-washer contact due to non-flatness of the supplied test specimens. The initial misalignment of the washer on test specimens resulted in severe scratching on the outer and inner diameters of the test specimen as the outer diameter of the washer had very sharp edges which resulted in severe damage to the test specimen as soon as the test started. These problems were not observed in the lubricated test conditions. To rectify these problems some modifications were made to the test apparatus as described below.

4.5.1 Modifications

Some important modifications were made to TWT apparatus 1 to overcome the fluctuations and vibration problems described above. TWT apparatus 1 was much improved after these modifications and a more uniform wear rate was observed on the test sample.

To summarise, some of the main modifications on TWT 1 were,

- A sleeved stroke liner was placed inside the main casting to improve circularity of the bore (figure 4.16 (a)).

- A tapered roller bearing was changed to a ball bearing (figure 4.16 (b)) to control the sideway's movement of the sample holder unit.
- A clamping system for holding the steel washer at the time of counterface assembly was used (figure 4.16 (c)).
- A polymer coating was applied to the bearing shaft to reduce frictional damage at the sleeve-bearing shaft contact (figure 4.16 (d)).
- The sharp outer edges of the washers were ground at the start of a new test.

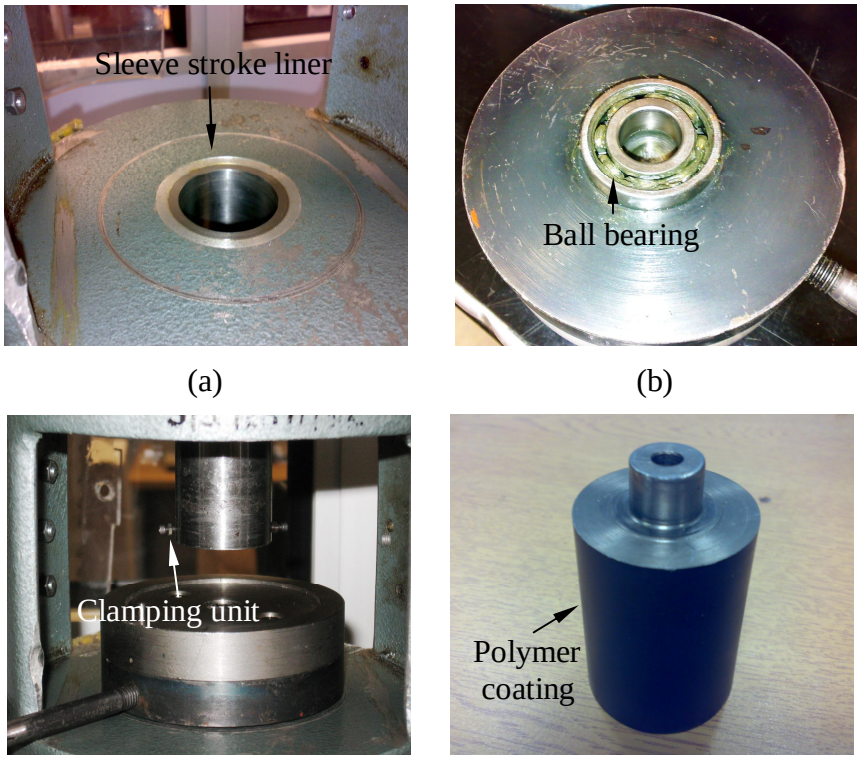

Figure 4.16 Modifications on TWT 1 apparatus (a) Sleeve on bore (b) Plain bearing fitting (c) Washer holding pins (d) Polymer coatings on shaft.

4.6 Thrust Washer Test Apparatus 2 (TWT 2)

Prior to modification of thrust washer test apparatus 1, vibration problems made the sample holder platform unstable, resulting in immediate stoppage of a test at certain loads and speeds. So, to improve the reliability of data, testing of new candidate materials such as Graphit-ic and Chromium Graphit-ic coatings on

Toughmet substrates was carried on the thrust washer test apparatus 2 (figure 4.17). The main difference between the TWT 1 and TWT 2 is that, in the former test apparatus, the steel washer rotated against a stationary test sample and in the later, the test sample rotated against the stationary washer.

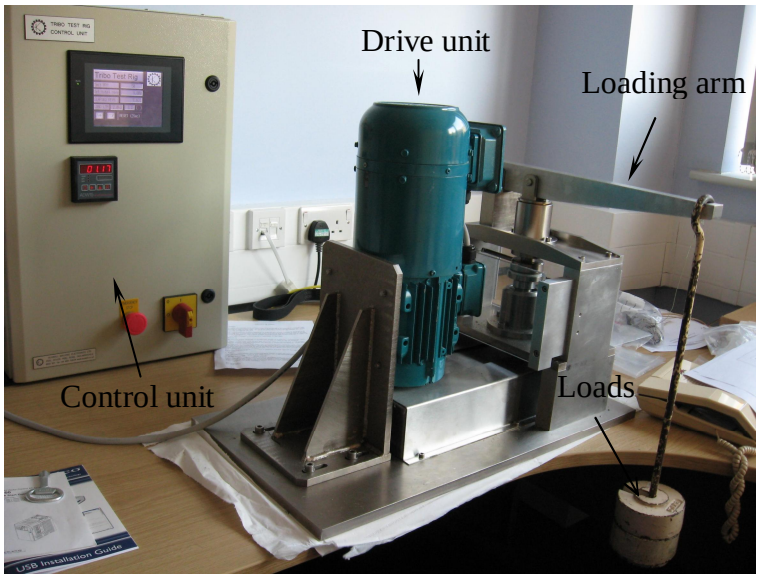

(a)

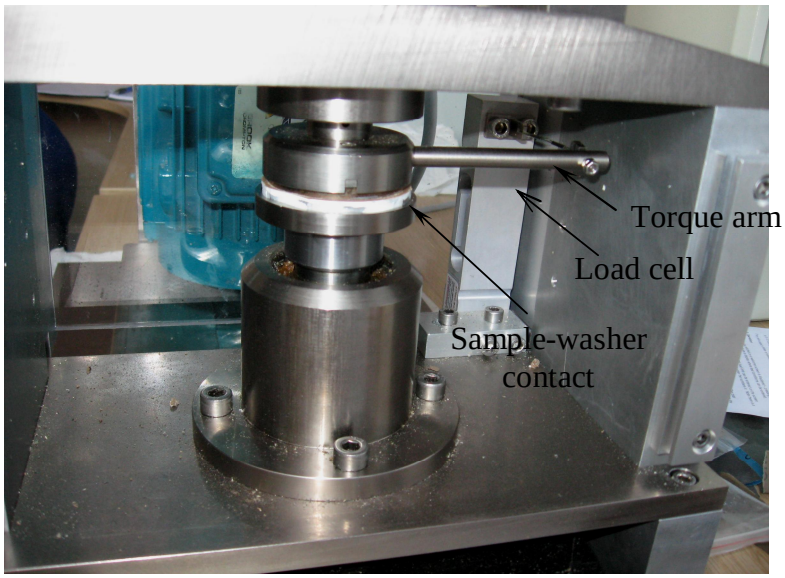

(b)

Figure 4.17 Thrust washer test apparatus 2 (a) Main test apparatus (b) Sample-Washer contact.

In general, TWT 2 consists of a test specimen sliding against a stationary washer in the shape of a rim. The required loads were applied on the washer-sample contact through a loading arm and a driving unit performed the sliding operation

at the speed set by the control unit. Using the control unit, the desired speed, the number of sliding revolutions and friction force limit could be set so that the experiment stopped automatically whenever the friction force limit was exceeded or when a preset number of revolutions were completed.

The ADC pico logger, sent the voltage signals to a display unit which stored the data and simultaneously displayed it on a monitor during acquisition. The computer showed the response of voltage recorded against time from which coefficient of friction was identified. The maximum speed attained with TWT 2 was 3000 rpm and wider ranges of contact loads could be applied. The equations described in sections 4.4 and sections 3.3 were used to identify the coefficient of friction and specific wear rate respectively.

4.6.1 Materials and Test Conditions

Test Materials (substrates)

Two types of Toughmet substrates, AT-110 and CX- 105 were tested with TWT 2 in dry test conditions. Two types of candidate coatings namely, Graphit-ic and Chromium Graphit-ic, both about 2.5 μm thick, were applied to the Toughmet substrates supplied by Teer coatings Ltd (2009). Only few friction and wear tests on these new materials were conducted. The main intention of testing these new candidate coatings in dry test conditions was to obtain an initial assessment of their friction and wear resistance behaviour. These new materials are much harder than lead based materials. A more through investigation and analysis of friction and wear resistance of these candidate materials are planned for the future work.

Steel Washer (Counterface)

The steel washer (figure 4.18) in the shape of a flat ring used in TWT apparatus 2 was slightly different in dimensions, but with same type of material (i.e. similar in terms of chemical and mechanical properties) as the counterface used in thrust washer test apparatus 1. Three different dimensions of flat ring type counterface were available, and depending on the requirements of sliding speed, and contact pressures, the rings were selected. In this thesis work, a medium ring type steel washer was used as the counterface for Toughmet substrates and candidate coatings. The dimensions of steel washers are shown in table 4.11.

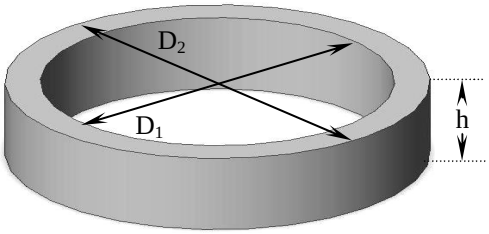

Figure 4.18 Steel washer (counterface).

Table 4.11 Steel washer dimensions for TWT apparatus 2.

Ring type	D_1 (mm)	D_2 (mm)	D_m (mm)	h (mm)	A (mm^2)
Small	25.85	20.3	23.07	8	201.1
Medium	35.85	30.3	33.07	8	288.3
Big	49.85	40.3	45.07	8	676.1

D_1 – Inside diameter, D_2 – Outside diameter, D_m – Mean diameter, h – Height of washer, A – Area of the annulus.

Operating Test Conditions

Table 4.12 shows the combination of loads and sliding speeds used for Toughmet substrates in dry test conditions. A total of 4 tests on each type of Toughmet substrates were taken and each test was conducted for a duration of 10 minutes (i.e. a sliding distance of 100 m). The rotational speed was kept constant at 100 rpm and the contact pressure varied to get a range of PV conditions for comparing test results among similar test specimens. The contact pressure used at the "start up condition" of the gear pump was replicated on these Toughmet substrates.

Table 4.12 Test conditions for Toughmet substrates

Load (N)	Speed (rpm)	$P_{(2)}$ (N/mm^2)	V (m/s)	PV (N/mm^2.m/s)
49.05	100	0.17	0.17	0.03
98.1	100	0.34	0.17	0.06

*$P_{(2)}$ –Contact pressure for "Medium" ring.

Table 4.13 shows the combination of loads and speeds used for the candidate coatings in dry test conditions. One test specimen of each type of coating was

taken and the contact pressure was kept constant at 0.17 N/mm^2 whereas the rotational speed was incremented by 50 rpm for every 15 minutes of the test. A total of five tests on each type of coating was conducted and at the end of each 15 minute increment of each test, the wear track was observed on a while light interferometer for wear loss observations.

Table 4.13 Test conditions for candidate coatings

Load (N)	Speed (rpm)	$P_{(2)}$ (N/mm^2)	V (m/s)	PV (N/mm^2.m/s)
49.05	50	0.17	0.09	0.01
49.05	100	0.17	0.17	0.03
49.05	150	0.17	0.26	0.04
49.05	200	0.17	0.35	0.06
49.05	250	0.17	0.43	0.07

4.6.2 Advantages of Thrust Washer Test Apparatus 2

There were several advantages of TWT 2 over TWT 1. They are,

- A wider range of loads and speeds (up to 3000 rpm) could be selected.
- The wear rate on the test specimen was more uniform.
- The test was smooth in terms of noise and there were no vibration problems as the sample holding unit was balanced using a bearing system.
- There was a friction cut off limit facility so that test would stop when friction exceeded the friction limit.
- A digital control unit allowed wider ranges of rotational speeds and the number of revolutions could be controlled automatically.

4.7 Pin on Disk Test Apparatus

The pin on disc test apparatus used in this project as shown in figure 4.19 conformed to the conventional ASTM G99-95 (Anonymous, 2002). In this test configuration, instead of a steel pin, a 100CR6 steel ball (6mm diameter) was used in contact with a rotating test specimen. The load was applied through the loading arm where equal amounts of load on either side of the arm would be

attached at the beginning of the test. The test apparatus could apply loads from 1 N to 12 N in dry test conditions and up to 60 N in lubricated conditions. The test specimen was placed in a sample holding chuck that could take a wide range of test specimen diameters from 10 to 60 mm. The load in each test was fixed and depending on the sliding length or sliding time, the sliding speed was calculated (and vice versa). The coefficient of friction and frictional force were displayed as a function of time. After measuring the wear loss on the test specimen using Talysurf profilometer, the specific wear rate was calculated using the method described in section 3.3.

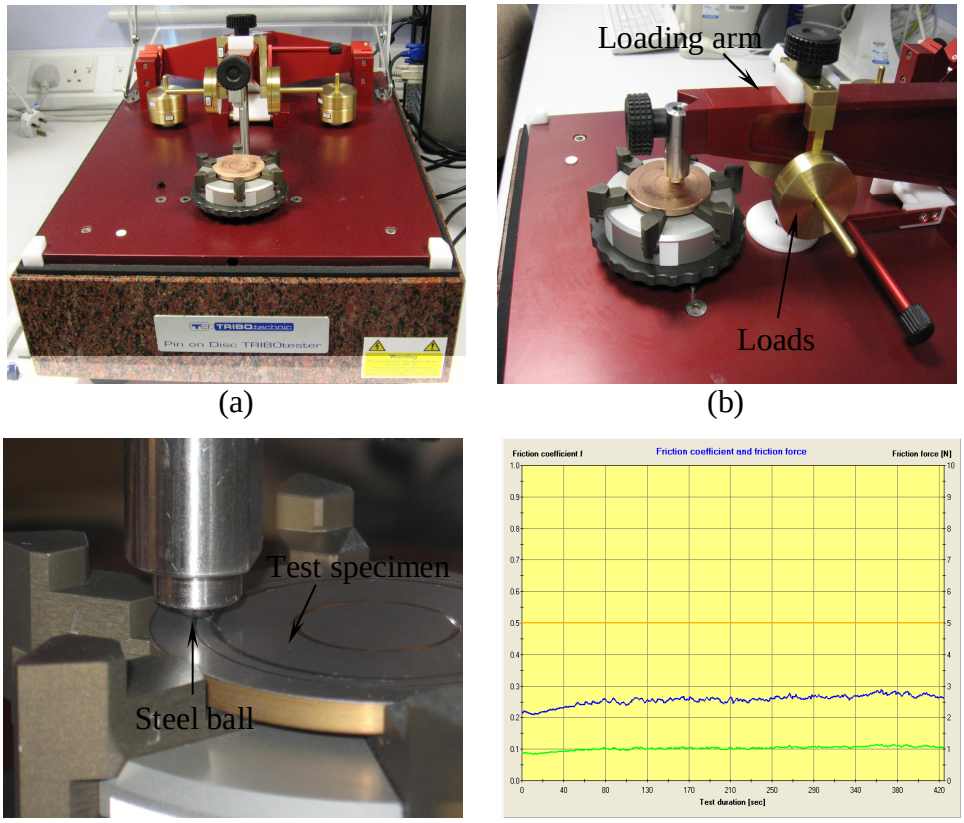

(a) (b)

(c) (d)

Figure 4.19 Pin on disc test apparatus (a) Main unit (b) Side view (c) Close contact (d) Real time friction coefficient-time graph.

Detailed Test Procedure

- Calibration of test apparatus was necessary at each phase of the testing process (or once in a month).
- The test specimens and the steel ball were cleaned completely with a cleaning agent (lotoxine) and dried in air before use.

- In lubricated test conditions, the test specimen was smeared with a few drops of kerosene before it was placed in the chuck.
- The steel ball was placed inside the ball holder and the whole unit was fitted on the loading arm.
- The test parameters such as load, speed, friction coefficient cut off limit and length of test time were set in the software.
- The steel ball was placed on the test specimen and lid was closed to perform the test.
- When the friction coefficient exceeded the cut off limit value, the test was automatically stopped; otherwise the test was run until the desired sliding distance.

4.7.1 Test Materials and Test Conditions

The test materials described in section 4.3.2 were used in the pin on disc apparatus in dry and lubricated conditions to identify friction and wear data. In addition to the lead-based materials, a Graphitic coating type, about 2.5 μm thick on a Toughmet substrate was tested in dry test conditions. The counterface material used in this test apparatus was a 100CR6 steel ball 6 mm in diameter. The mechanical and thermal properties of 100CR6 steel ball are given in table 4.4 and chemical composition is shown in table 4.3. Due to the change in contact pressure at each point of ball sliding on disc, this test does not result in a uniform contact pressure. Therefore, it is strictly not possible to replicate the same PV ratio indicated for the "start up condition" of the gear pump throughout the test. So a contact load velocity product (LV) was taken as the main parameter when comparing the friction and wear results of all test materials. The combinations of loads and speeds used in dry and lubricated test conditions for lead-based and candidate coatings are described below.

Test Conditions Used on Lead Based Materials

Various combinations of loads and sliding velocities were initially tested on a few lead based materials to understand their friction and wear behaviour. Two track radii on the same test specimen were chosen and each track radius had a unique sliding velocity. This was obtained from the dedicated software provided with the POD by keeping the rotation speed constant so that two friction and wear tests on

the same test specimen could be obtained in a short time. The idea of using two track radii and two sliding velocities was to get the same LV value for both track radii so that friction and wear results from both track radii could be averaged. If the sliding velocities at both track radii were equal then the time where the ball completed one revolution in both track radii would be different and friction and wear data could not be compared. Additionally, to identify the influence of different sliding velocities in both track radii on friction and wear, test results for different sliding velocities, even though same LV, were separated and compared among the test materials. For lead-based materials in dry test conditions, the rotational speed and sliding length were kept constant at 250 rpm and 100 m. The table 4.14 and table 4.15 show the combination of loads and speeds taken to get the same LV ratio in two different track radii in dry and marginal lubricated test conditions for lead based materials. The choice of track radius depended on the availability of the test areas in the test specimens.

Table 4.14 Test conditions for lead based material in dry test conditions.

Load (N)	Speed (rpm)	Track radius (mm)	P_I (N/mm²)	P_F (N/mm²)	V (m/s)	LV Nm/s
1	250	18	318.96	49.74	0.47	0.47
2	250	18	401.87	44.21	0.47	0.94
2	250	9	401.87	44.21	0.24	0.47
4	250	9	506.32	39.30	0.24	0.94

*P_I – Initial pressure (based on the contact dimension), P_F – Final pressure (based on the contact dimension)

Table 4.15 Test conditions for lead based materials in marginally lubricated test conditions.

Load (N)	Speed (rpm)	Track Radius (mm)	P_I (N/mm²)	P_F (N/mm²)	V (m/s)	LV Nm/s
1	125	20	318.96	127.32	0.26	0.26
2	125	20	401.87	176.84	0.26	0.52
2	250	5	401.87	176.84	0.13	0.26
4	250	5	506.32	198.94	0.13	0.52

Test Conditions Used on Candidate Coatings

The friction and wear tests on Graphit-ic coatings were conducted at a constant rotational speed of 250 rpm and increasing the load from 1 N to 12 N for every 15 minutes of test on the same test specimen at the same track radius. This was an accelerated test to identify the performance of the coating in a short time. Since the hardness of steel ball (800 HV) was much less than that of the Graphit-ic coating (2000 HV), a fresh steel ball was used for each increment of load. At the end of each test, the material loss on the test specimen was weighed and wear track was observed in WLI. Table 4.16 shown below indicates the test conditions used on Graphit-ic coated Toughmet substrates in dry test conditions.

Table 4.16 Test conditions for Graphit-ic coatings on POD apparatus.

Test condition	Load (N)	Speed (rpm)	V (m/s)
Dry	1 to 12	250	0.32

Validity of POD Compared With Real Test Condition in Gear Pumps

As discussed earlier, the use of the POD apparatus in this project work was to facilitate high contact pressures and to conduct accelerated tests even though the POD did not replicated the real flat on flat contact situation of the gear pump thrust bearings. The test conditions used in POD not only met the “start up condition” of the gear pump, but also able to replicate the “take off condition” of the gear pump. The initial idea was to select two track radii on the same test specimen so that two friction and wear results of two track radii at the same LV conditions would be obtained. But it was identified with the POD apparatus that the sliding velocity for two track radii could not be kept constant since the sliding length and rotations per minute were kept constant. This meant that the ball at small track radii took twice the time to complete the same sliding distance as that at the bigger track radius if the sliding velocity was twice than that at bigger track radius. In these conditions, the same point where the ball meets in every revolution in both track radii was reasonably similar.

Table 4.17 Number of rotations and total test time in different velocities in POD apparatus.

Distance slid (m)	Speed (rpm)	Track Radius (mm)	Track length (mm)	V (m/s)	Number of rotations	Test time (sec)
100	250	18	113	0.47	887	213
100	250	9	56.5	0.24	1770	425
100	125	20	125.6	0.26	797	383
100	250	5	31.4	0.13	3183	764

Table 4.17 describes the number of rotations and total test time taken by the ball for a particular track radius and for a particular sliding velocity when the sliding distance was kept constant.

4.7.2 Coefficient of Friction and Specific Wear Rate Measurements

The coefficient of friction was calculated by taking a ratio between friction force and the normal load (discussed in chapter 3.3). The POD apparatus used in this thesis displays the friction coefficient against time graphs during the test process. Later on, friction coefficient was separated for the running-in period and steady state period (figure 4.18). The friction coefficient during the “running-in” period is associated with the ploughing component of friction whereas the steady state friction represents the constantly moving friction coefficient (or with a small variations in friction coefficient) over the time period considered. The wear rate of all the test materials was determined using the Talysurf profilometer described in chapter 3.3. However, it was believed that in lead/indium coated leaded bronze substrates, the volume loss of coating could not be measured at the end of the test since most of the lead/indium coating was worn away during the running-in period and wear rate obtained would be the wear rate of whole system (i.e. combined wear rate of coating and substrate) not just the coating itself. Therefore the SPWR of each coating was calculated by considering the volume loss of the coating during the running-in period, knowing the nominal coating thickness and identifying the approximate end time of ploughing from the friction-time graph in each test. Figure 4.20 shows an example of SPWR calculations from friction

coefficient against time for a lead/indium coated 20% leaded bronze substrate in dry test conditions.

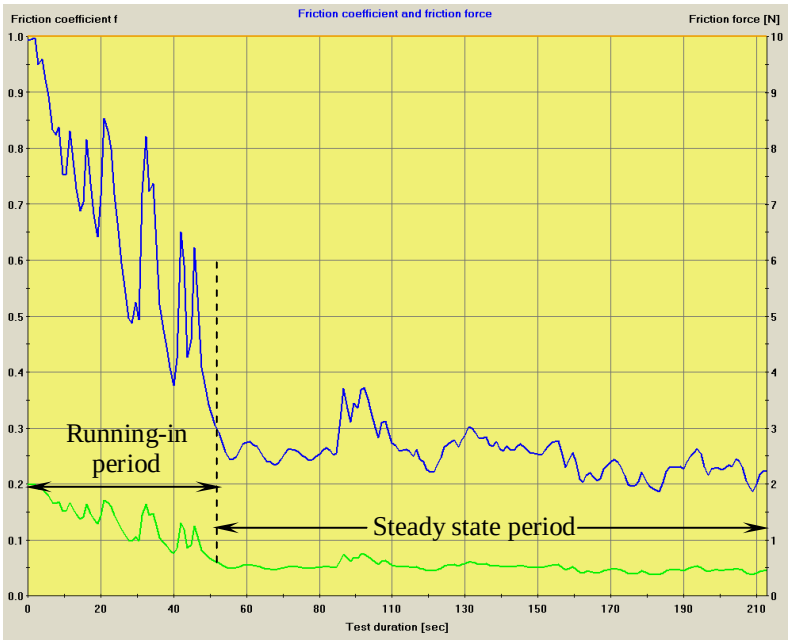

Figure 4.20 Example of Running-in and steady state period for a coated surface.

The run-period indicated in the figure 4.20 is associated with the high ploughing and deformation components of the contact where most of the lead/indium coating was removed. The steady state period represents the constantly moving coefficient of friction where the ball is sliding on the substrate material containing a very thin layer of lead/indium coating. Table 4.18 shows an example calculation for friction coefficient during running-in period and steady state period. The SPWR of the system includes both wear loss of the coating and wear loss of the substrate over the time period considered.

Table 4.18 An example calculations of COF and SPWR during running-in and steady state for lead/indium coated 20% leaded bronze substrates.

Mat	Thick (µm)	Load (N)	V (m/s)	Dist. slid (m)		COF		SPWR coating (mm^3/N.m)	SPWR system (mm^3/N.m)
				R	Sys	R	Steady state		
20%	1.17	2	0.47	25.45	100	0.62	0.24	2.09E-04	2.84E-04

* Mat – Material, Thick – Thickness, Dist. slid – Distance slide, COF – Friction coefficient, R – Running-in period, Sys – System, SPWR – Specific wear rate.

The area of the ploughing component can be calculated by using the equation 2.8 described in chapter 2.5.1 of ploughing theories of friction. In the equation 2.8, the half contact width *(r)* was calculated by using the equation 2.7, where *d* represents the thickness of the coating (since, it was assumed that most of the coating was lost during the running in period).

The volume loss of the coating is calculated as:

Volume loss by the coating, $V = (A_p)$. (Circumference of wear track)

$$V = A_p \,.\, (2\pi\, r_t) \tag{4.5}$$

Where, r_t – is the track radius.

The SPWR is then obtained by dividing the volume lost of the coating with the product of load and sliding distance, as described in chapter 3.3.

Summary

This chapter has covered the complete description and operating procedures of two types of thrust washer test apparatus and a pin on disc test apparatus for measuring friction and wear data. Various components of TWT apparatus 1 and their major roles were described in detail and actual pictures were shown. The test materials used in this project and their mechanical/thermal properties were given in table format. One example each of coefficient of friction and specific wear rate calculation on leaded bronze substrates and lead/indium coatings were described. Several problems identified with the TWT apparatus 1 during preliminary tests and their modifications were discussed. A newly acquired TWT apparatus 2 to perform additional tests on lead free materials was also described. Calculation of coefficient of friction and SPWR of the coated surface for the ploughing and steady state components were described. In the next chapter, all the friction and wear data collected from both TWT apparatus and POD apparatus are shown. The estimated flash and bulk temperatures from Ashby's method on uncoated and lead/indium coated leaded bronze substrates in dry test conditions are tabulated and test results are plotted against PV for TWT apparatus and LV for POD apparatus, respectively.

CHAPTER 5

EXPERIMENTAL RESULTS

5.0 Overview

In this chapter, the friction and wear results obtained from TWT apparatus and POD apparatus are given. This project comprises a substantial number of friction and wear tests on both uncoated leaded bronze substrates and similar substrates coated with various thicknesses of 10% lead/indium alloy. The test results for the different types of test materials are shown as a function of the various test parameters, such as load and speed, against COF and SPWR. Initially, when developing the TWT apparatus 1, many friction and wear tests were conducted, but some of the tests were unsuccessful in dry test conditions due to mis-alignment problems encountered in the test apparatus, as discussed in section 4.5.1. Those unsuccessful test results were not considered and were not reported elsewhere in this thesis. The tests after the modification of TWT apparatus 1 were only considered and reported in this thesis. For efficient use of the available specimens, POD tests were also conducted on the unworn areas of the test specimens used in TWT apparatus 1. The relationships between the apparent pressure-velocity product (PV), SPWR and COF were taken as the main basis to compare the test specimens in TWT apparatus 1. However, the POD test results were considered by investigating how COF and SPWR change as a function of load. An attempt has also been made to compare friction and wear results obtained from TWT and POD even though the test contact conditions were very different.

Friction and wear data from candidate alternative coatings such as Graphit-ic obtained from a second thrust washer test apparatus (TWT apparatus 2) are reported separately in section 5.4 and an attempt has been made to compare these results with those from the TWT apparatus 1 and POD tests outlined above. Theoretical flash and bulk temperatures calculated on lead/indium coated leaded bronze substrates in dry test conditions using Ashby's method for both flat on flat and ball on flat test configurations are also reported in this chapter.

5.1 Thrust Washer Test Results

The friction and wear results obtained from the TWT apparatus 1 are detailed in this section. These are separated according to the type of test conditions (i.e. dry and marginally lubricated tests) and type of test materials used. Since frictional power input is normally considered to be related to bearing wear (Lancaster,

1973; Suh, 1986), the normal load and sliding speed were changed from test to test and PV has been taken as the experimental parameter to compare the performance of the test materials. To get close to the PV values in the real operating conditions, the test conditions were altered in such a way that two tests on a similar type of substrate/coated specimen had the same PV but different values of P and V for comparison purposes. Due to sliding speed limitations of TWT apparatus 1 in dry operating conditions, it was difficult to compare the dry and marginally lubricated test results between different compositions of the leaded bronze substrates and lead/indium coatings, but an attempt has been made to do so. The operating test conditions for TWT apparatus 1 were detailed in chapter 4.4.5. All the test results in this section are discussed in chapter 6 by comparing the test materials according to the operating conditions implemented.

5.1.1 Uncoated 20% and 30% Leaded Bronze Substrates

Dry Test Conditions

The COF and SPWR results of 20% leaded bronze and 30% leaded bronze substrates tested in dry condition are summarized in table 5.1 and the results are compared for pressure against mean COF and SPWR in figure 5.1 and figure 5.2, respectively. The mean COF and mean SPWR obtained at different sliding velocities are summarized in table 5.2.

Some of the important terms such as pressure (P), mean COF and SPWR indicated in table 5.1 have already been discussed in earlier chapters. These terms will be used in discussion of all the test results from the TWT apparatus 1.

The contact pressure (P) between the washer-disk contact was obtained by taking the ratio between the normal load applied (W) and the circumferential contact area (A). It was assumed that the contact pressure remained constant throughout the test. The mean COF for uncoated leaded bronze substrates represents the average COF values recorded from the start to the end of the friction against time graph. The volume loss of the test material was calculated using the gravimetric method described in chapter 4.4.4 and the SPWR represented the wear rate for the total duration of the test.

Table 5.1 Mean COF and SPWR results of uncoated leaded bronze substrates in dry test conditions.

Test	Mat	Load N	Speed rpm	P N/mm^2	V m/s	PV $N/mm^2.m/s$	Mean COF	Vol mm^3	SPWR mm^3/Nm
31A	20%	58.86	80	0.13	0.12	0.016	0.36	0.12	2.85E-05
35A	20%	78.48	80	0.18	0.12	0.021	0.35	0.18	3.24E-05
33A	20%	98.1	80	0.22	0.12	0.026	0.34	0.22	3.20E-05
32A	20%	117.72	40	0.27	0.06	0.016	0.35	0.15	3.63E-05
36A	20%	156.96	40	0.36	0.06	0.021	0.37	0.22	3.20E-05
34A	20%	196.2	40	0.45	0.06	0.026	0.40	0.24	3.40E-05
15	30%	58.86	80	0.13	0.12	0.016	0.35	0.14	3.44E-05
14	30%	78.48	80	0.18	0.12	0.021	0.34	0.21	3.81E-05
12	30%	98.1	80	0.22	0.12	0.026	0.33	0.26	3.69E-05
13	30%	117.72	40	0.27	0.06	0.016	0.33	0.17	4.20E-05
16	30%	156.96	40	0.36	0.06	0.021	0.36	0.23	4.22E-05
11	30%	196.2	40	0.45	0.06	0.026	0.36	0.28	4.10E-05

* Mat – Material, P – Pressure, V – Velocity, PV – Pressure X Velocity, COF – Coefficient of friction, Vol – Volume loss of material, SPWR – Specific Wear Rate.

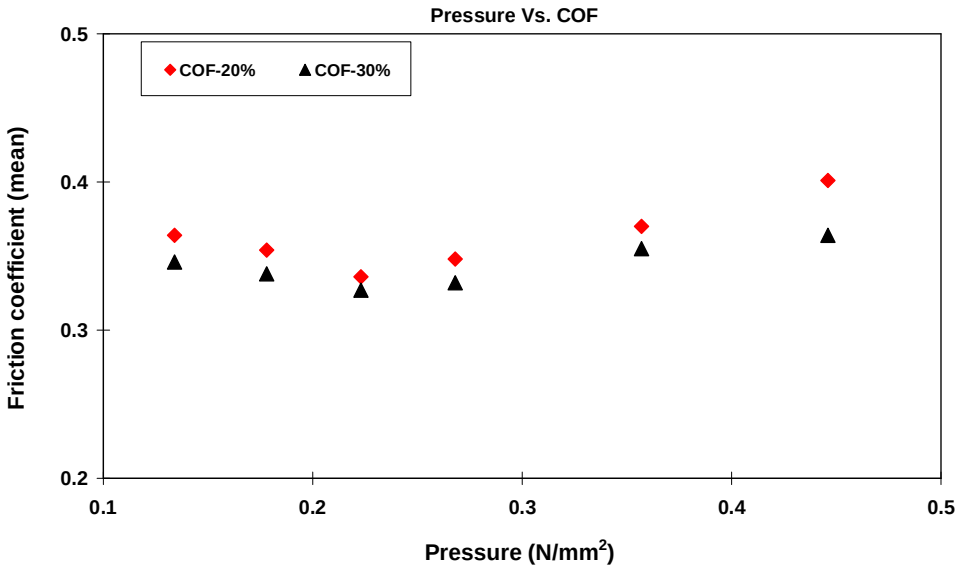

Figure 5.1 Mean COF against contact pressure in uncoated leaded bronze substrates in dry test conditions.

In table 5.1, the contact pressure and sliding velocity in every test was varied to get the same PV ratio and the test results at different sliding velocities were separated to identify the effect of velocity (if any) on friction and wear results. These results are summarized in table 5.2.

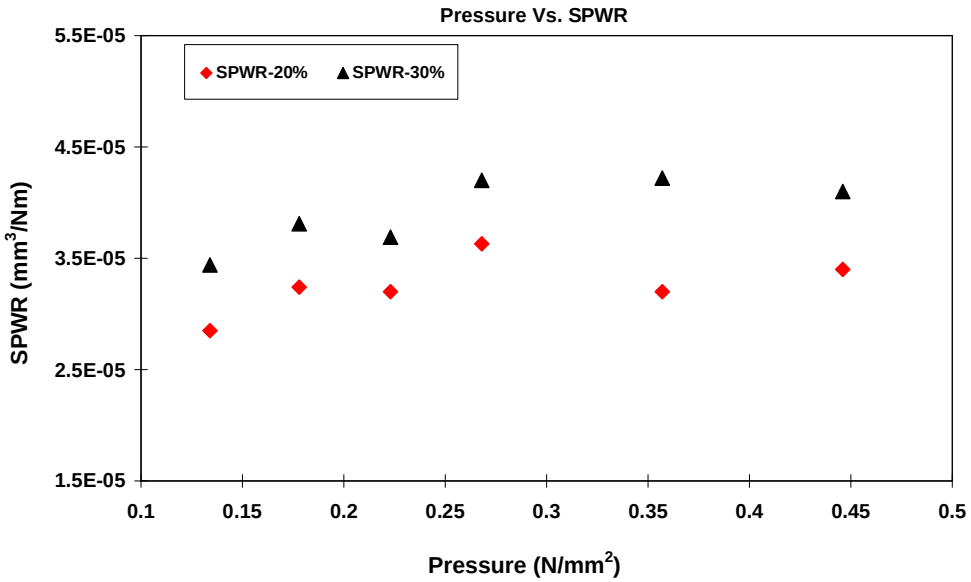

Figure 5.2 SPWR against contact pressure in uncoated leaded bronze substrates in dry test conditions.

It can be seen from table 5.1 that the mean COF and SPWR results at different sliding velocities are approximately constant with increase in PV. Therefore, the mean COF and SPWR at the same sliding velocities among different compositions of leaded bronze were averaged and are tabulated in table 5.2.

Table 5.2 Mean COF and mean SPWR of uncoated leaded bronze substrates at different sliding velocities in dry test conditions.

Mat	Mean COF as a function of velocity (S.D)			Mean SPWR as a function of velocity (S.D)		
	0.12 m/s	0.06 m/s	Average m/s	0.12 m/s	0.06 m/s	Average m/s
20%	0.35 (0.01)	0.37 (0.02)	0.36 (0.01)	3.10E-05 (2.15E-06)	3.41E-05 (2.15E-06)	3.25E-05 (4.39E-09)
30%	0.34 (0.01)	0.35 (0.02)	0.34 (0.01)	3.65E-05 (1.89E-06)	4.17E-05 (6.43E-07)	3.91E-05 (8.80E-07)

*S.D – Standard deviation, Average – Average values from both sliding velocities.

Table 5.3 shown below details the combined mean COF and combined mean SPWR of leaded bronze substrates at the same PV ratio taken from table 5.1 and results are plotted for mean COF and mean SPWR against PV in figure 5.3

Table 5.3 Mean COF and mean SPWR of uncoated leaded bronze substrates at different PV values in dry test conditions.

Mat	Mean COF at increase in PV			Mean SPWR at increase in PV		
	0.016 $N/mm^2.m/s$	0.021 $N/mm^2.m/s$	0.026 $N/mm^2.m/s$	0.016 $N/mm^2.m/s$	0.021 $N/mm^2.m/s$	0.026 $N/mm^2.m/s$
20%	0.36	0.36	0.37	3.24E-05	3.22E-05	3.30E-05
30%	0.34	0.35	0.35	3.82E-05	4.02E-05	3.90E-05

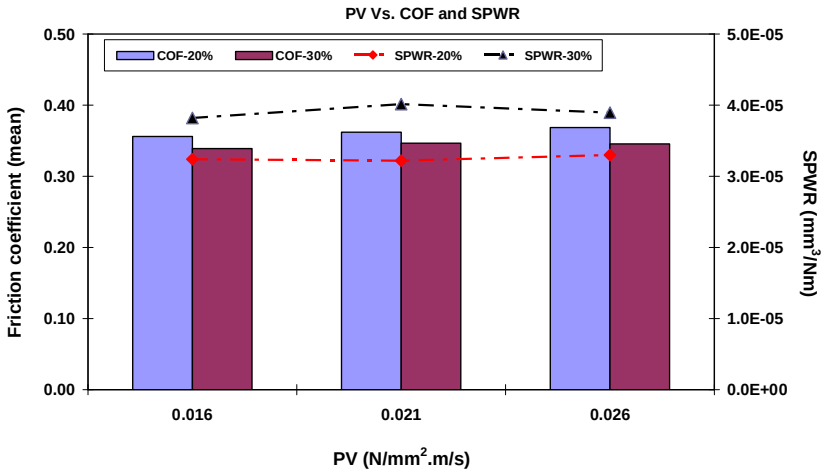

Figure 5.3 Mean COF and mean SPWR against PV of uncoated leaded bronze substrates in dry test conditions.

Figure 5.1 shows that the COF of 20% leaded bronze is higher than that of 30% leaded bronze at each contact pressure. The standard deviation results from table 5.2 confirm that the mean COF and SPWR of both leaded bronze substrates are approximately constant even when the sliding velocity was changed. Therefore, by averaging the mean COF for the same type of substrates at all contact pressures (or sliding velocities), it can be seen from table 5.2 that 20% leaded bronze has a combined average COF of 0.36 compared to the 30% leaded bronze average COF of 0.34. The mean SPWR of 20% leaded bronze is 3.25E-05 compared to the mean SPWR of 3.91E-05 for 30% leaded bronze.

Lubricated Test Conditions

The test results of uncoated leaded bronze substrates in marginally lubricated conditions are summarized in table 5.4 and are schematically shown in figure 5.4 and figure 5.5, respectively. The operating conditions were altered to obtain the same PV ratio.

Table 5.4 Mean COF and SPWR of uncoated leaded bronze substrates in marginally lubricated test conditions.

Test	Mat	Load N	Speed rpm	P N/mm^2	V m/s	PV $N/mm^2.m/s$	Mean COF	Vol mm^3	SPWR mm^3/Nm
UN9	20%	58.86	2000	0.13	2.94	0.39	0.13	0.08	3.12E-06
UN10	20%	78.48	2000	0.18	2.94	0.52	0.13	0.13	2.87E-06
UN4	20%	98.1	2000	0.22	2.94	0.66	0.11	0.09	3.01E-06
UN7	20%	117.72	1000	0.27	1.47	0.39	0.09	0.08	3.23E-06
UN8	20%	156.96	1000	0.36	1.47	0.52	0.09	0.09	3.51E-06
UN22	30%	58.86	2000	0.13	2.94	0.39	0.09	0.18	4.11E-06
UN27	30%	78.48	2000	0.18	2.94	0.52	0.11	0.21	4.68E-06
UN25	30%	98.1	2000	0.22	2.94	0.66	0.09	0.16	4.20E-06
UN21	30%	117.72	1000	0.27	1.47	0.39	0.08	0.17	5.03E-06
UN23	30%	156.96	1000	0.36	1.47	0.52	0.07	0.20	4.35E-06

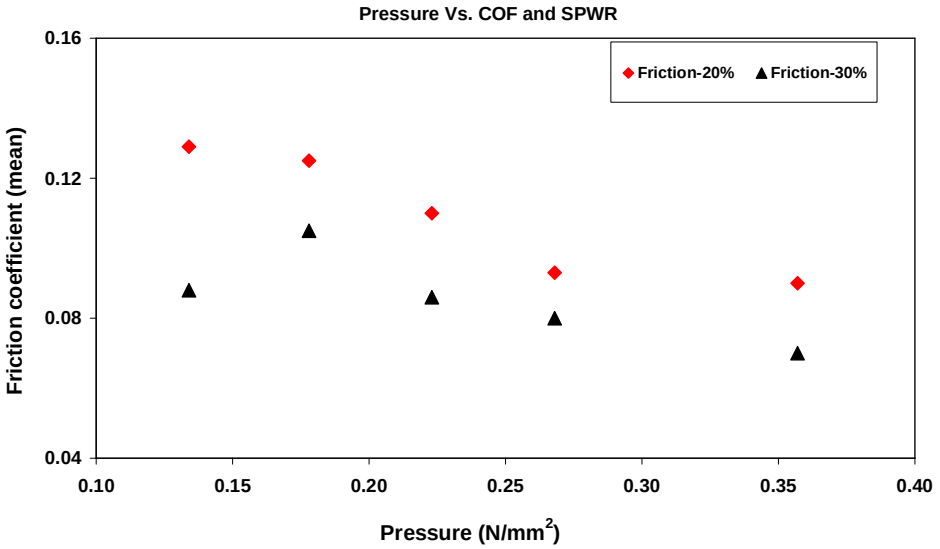

Figure 5.4 Mean COF against contact pressure in uncoated leaded bronze substrates in marginally lubricated test conditions.

The mean COF and SPWR of uncoated leaded bronze substrate in marginally lubricated test conditions were measured in the same way as described for the dry test conditions. Table 5.5 shows the mean COF and mean SPWR and their standard deviation (in brackets) of uncoated leaded bronze substrates (the mean COF and mean SPWR were the average values at all contact loads separating the sliding velocities). It can be seen from the test results that the sliding velocity has no influence on the friction and wear. Therefore the combined average values of all the friction and wear data at all the sliding velocities were taken. These average values are indicated in the "Average" column in table 5.5.

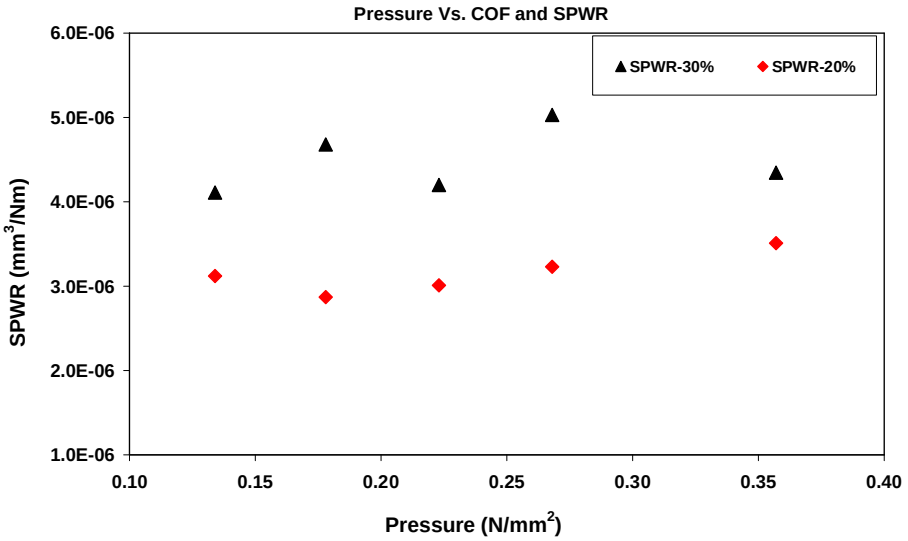

Figure 5.5 SPWR against contact pressure in uncoated leaded bronze substrates in marginally lubricated test conditions.

Table 5.5 Mean COF and mean SPWR and their standard deviation for uncoated leaded bronze substrates at different sliding velocities in dry test conditions.

Mat	Mean COF at change in velocity (S.D)			Mean SPWR at change in velocity (SD)		
	2.94 m/s	1.47 m/s	Average m/s	2.94 m/s	1.47 m/s	Average m/s
20%	0.12 (0.01)	0.09 (0.01)	0.11 (0.01)	3.0E-06 (1.25E-07)	3.37E-06 (1.98E-07)	3.19E-06 (5.14E-08)
30%	0.09 (0.01)	0.07 (0.01)	0.08 (0.01)	4.33E-06 (3.06E-07)	4.69E-06 (4.84E-07)	4.15E-06 (1.25E-07)

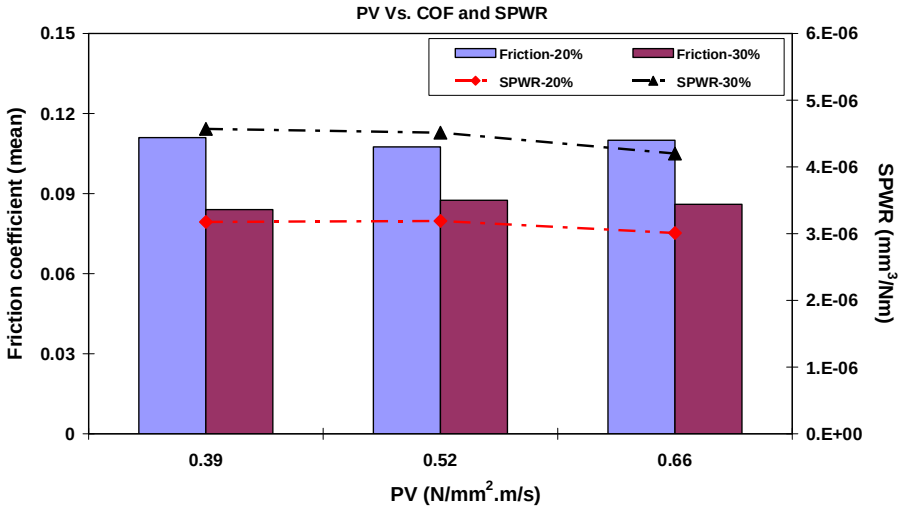

Figure 5.6 Mean COF and mean SPWR against PV of uncoated leaded bronze substrates in marginally lubricated test conditions.

Table 5.6 shown below details the combined mean COF and combined mean SPWR of leaded bronze substrates at similar PV ratios taken from table 5.4 and results are plotted for mean COF and mean SPWR against PV in figure 5.6

Table 5.6 Mean COF and mean SPWR of uncoated leaded bronze substrates at different PV values in marginally lubricated test conditions.

Mat	Mean COF at increase in PV			Mean SPWR at increase in PV		
	0.39 N/mm².m/s	0.52 N/mm².m/s	0.66 N/mm².m/s	0.39 N/mm².m/s	0.52 N/mm².m/s	0.66 N/mm².m/s
20%	0.11	0.11	0.11	3.18E-06	3.19E-06	3.01E-06
30%	0.08	0.09	0.09	4.57E-06	4.51E-06	4.20E-06

From the test results in marginally lubricated test conditions, the mean COF for 20% leaded bronze is higher than that for 30% leaded bronze. From table 5.5, 20% leaded bronze has an average mean COF of 0.11 compared to 0.08 for 30% leaded bronze. Similarly, the average SPWR of 30% leaded bronze is 4.51E-06 compared to the 20% leaded bronze average SPWR of 3.19E-06.

The standard deviation in table 5.5 shows approximately constant friction and SPWR results among the test materials. Table 5.6 shows that the mean COF and mean SPWR when changes in PV were approximately constant in both leaded bronze substrates. However, the mean SPWR of 30% leaded bronze was higher than that of 20% leaded bronze.

5.1.2 1 µm Lead/Indium Coated 20% and 30% Leaded Bronze Substrates

Dry test conditions

The COF and SPWR results for the above test materials in dry test conditions are summarized in table 5.7 and test results are plotted against contact pressure in figure 5.7 and figure 5.8. In this dry test condition, the sliding speed was kept constant at 80 rpm, but the contact pressure was altered to get the same PV ratio among the different substrate materials. Unlike the uncoated leaded bronze substrates where SPWR was evaluated over the time period considered, the SPWR for lead/indium coated leaded bronze substrates here was divided into two

parts: SPWR of coating and SPWR of the system. The SPWR of coating represents the wear rate during the running-in period and SPWR of system corresponds to the wear rate for the total time period considered. An example of these two types was explained in chapter 4.7.2. In table 5.7, the mean ploughing COF corresponds to the COF during the running-in period and the mean COF indicates for the mean steady state COF.

Table 5.7 COF, SPWR of 1 µm lead/indium coated leaded bronze substrates in dry test condition at a sliding velocity of 0.12 m/s.

Mat	Thick µm	Load N	P N/mm²	PV N/mm².m/s	Mean Plough COF	Mean COF	SPWR (R) mm³/Nm	SPWR (System) mm³/Nm
20%	1.17	58.86	0.13	0.016	0.71	0.38	2.49E-03	4.41E-04
20%	1.19	78.48	0.18	0.021	0.66	0.35	2.59E-03	3.50E-04
20%	0.5	98.1	0.22	0.026	0.57	0.36	1.28E-03	4.74E-04
20%	1.32	117.72	0.27	0.031	0.60	0.35	3.51E-03	3.98E-04
30%	1.16	58.86	0.13	0.016	0.70	0.28	2.47E-03	4.69E-04
30%	0.81	78.48	0.18	0.021	0.60	0.29	1.94E-03	3.87E-04
30%	1.3	98.1	0.22	0.026	0.45	0.26	2.49E-03	4.97E-04
30%	0.56	117.72	0.27	0.031	0.42	0.30	1.79E-03	3.84E-04

* Thick – Thickness of lead/indium coating, R – Running-in period, System – total time duration.

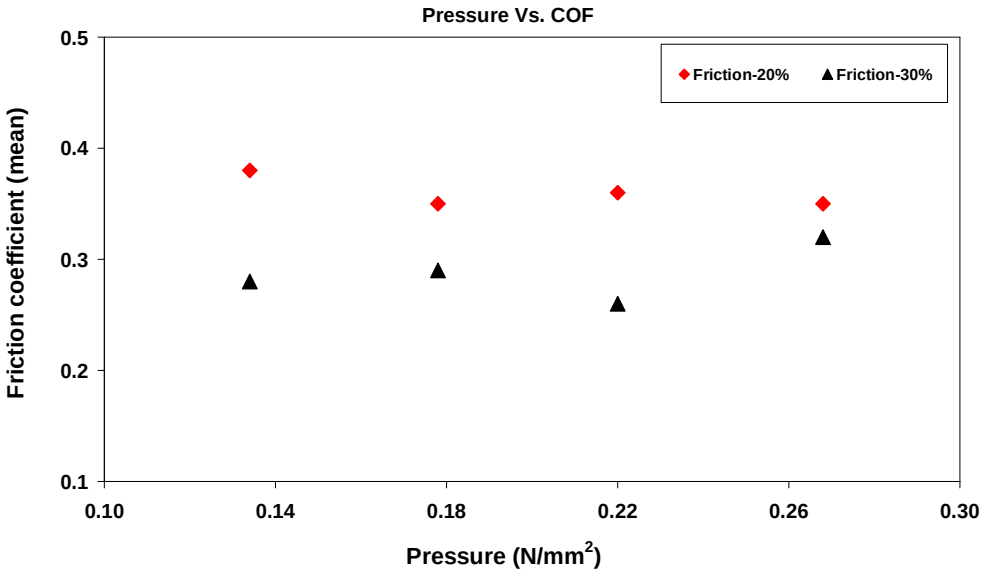

Figure 5.7 Mean COF against contact pressure of 1 µm lead/indium coated substrates in dry test conditions.

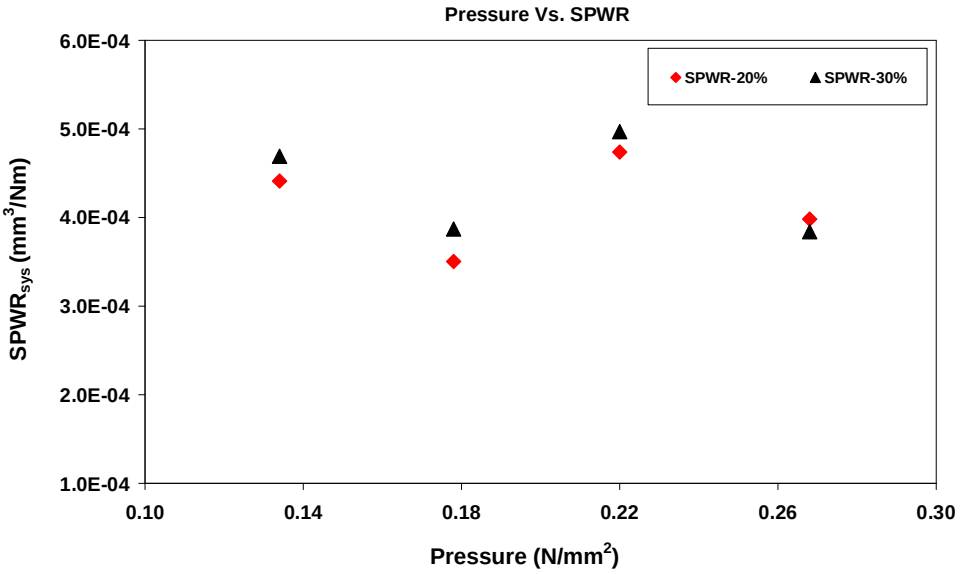

Figure 5.8 System SPWR against contact pressure of 1 µm lead/indium coated substrates in dry test conditions.

From figure 5.7, it can be seen that the mean COF of 1 µm 20% leaded bronze substrates is higher at every contact pressure than that of 1 µm 30% leaded bronze substrates. Figure 5.8 shows that the system SPWR of both 1 µm coated leaded bronze substrates were approximately similar.

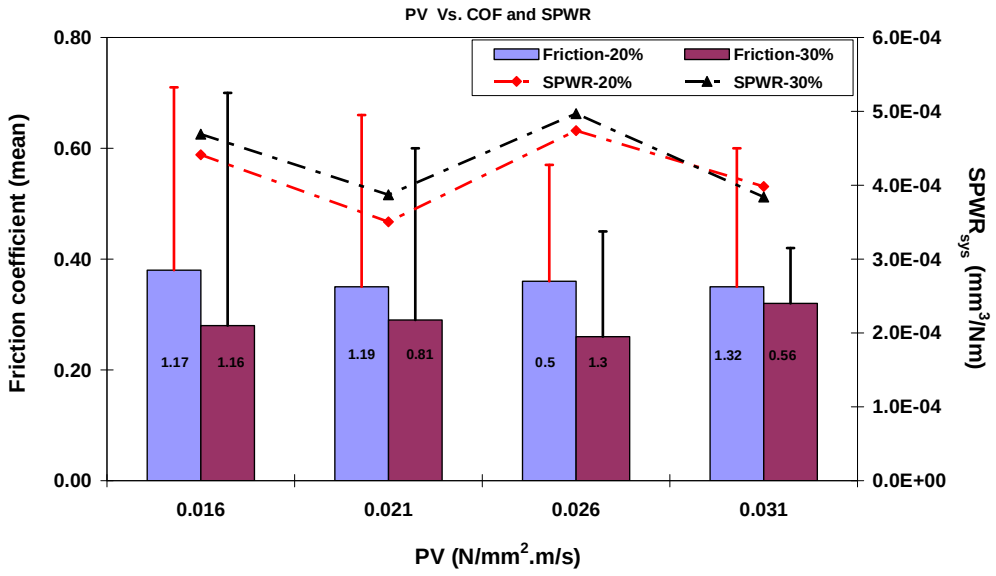

Figure 5.9 Mean COF and system SPWR against PV of 1 µm lead/indium coated substrates in dry test conditions (bar elements show the maximum ploughing COF recorded and the actual coating thickness (in µm) was indicated on the friction bars).

Table 5.8 and 5.9 present the mean COF and mean SPWR at increasing PV taken from the table 5.7. The test results suggest that both mean COF and system SPWR were approximately constant when PV changed. Therefore these test results all PV conditions were averaged among different substrate materials.

From table 5.7, the mean ploughing COF and SPWR over the running-in period for 1 µm 20% leaded bronze are higher than those for 1 µm 30% leaded bronze substrates. From table 5.8, the 1 µm 20% leaded bronze substrates have higher average COF (0.36) than 1 µm 30% leaded bronze substrates (0.28) in dry test conditions.

The average system SPWR of 1 µm 30% leaded bronze appeared to be slightly higher than that of the 1 µm 20% leaded bronze substrate. However, considering the standard deviations of these results from table 5.9, this difference may not be significant.

Table 5.8 Mean COF of 1 µm lead/indium coated substrates as a function of PV in dry test conditions.

Mat	Mean COF at increase in PV values					SD
	0.016 N/mm².m/s	0.021 N/mm².m/s	0.026 N/mm².m/s	0.031 N/mm².m/s	Average N/mm².m/s	
20%	0.38	0.35	0.36	0.35	0.36	0.01
30%	0.28	0.29	0.26	0.30	0.28	0.02

*S.D – Standard deviation from all PV values.

Table 5.9 System SPWR of 1 µm lead/indium coated substrates as a function of PV in dry test conditions.

Mat	SPWR at different PV values					SD
	0.016 N/mm².m/s	0.021 N/mm².m/s	0.026 N/mm².m/s	0.031 N/mm².m/s	Average N/mm².m/s	
20%	4.41E-04	3.50E-04	4.74E-04	3.98E-04	4.16E-04	5.35E-05
30%	4.69E-04	3.87E-04	4.97E-04	3.84E-04	4.34E-04	5.74E-05

Lubricated Test Conditions

The test results for 1 µm lead/indium coated leaded bronze substrates in marginally lubricated test conditions are summarized in table 5.10 and the results are plotted against contact pressures in figure 5.10 and figure 5.11. In this test

condition, the sliding speed was kept constant at 2000 rpm and the initial contact pressure was altered to get the same PV among the different test materials.

Test results were plotted for mean COF and system SPWR against PV in figure 5.12. Since in lubricated test conditions, the initial running-in did not occurred, therefore, only mean COF and system SPWR over the time period considered was reported here.

Table 5.10 Mean COF and SPWR of 1 µm lead/indium coated substrates in marginally lubricated test condition at a constant sliding velocity of 2.93 m/s.

Mat	Thick µm	Load N	P N/mm²	PV N/mm².m/s	Mean COF	SPWR (system) mm³/Nm
20%	1.24	58.86	0.13	0.39	0.16	2.29E-06
20%	1.41	78.48	0.18	0.52	0.15	2.63E-06
20%	1.12	98.1	0.22	0.66	0.13	1.87E-06
20%	1.57	117.72	0.27	0.79	0.12	1.96E-06
30%	0.8	58.86	0.13	0.39	0.12	3.60E-06
30%	1.22	78.48	0.18	0.52	0.11	3.77E-06
30%	0.52	98.1	0.22	0.66	0.12	2.85E-06
30%	0.7	117.72	0.27	0.79	0.11	2.97E-06

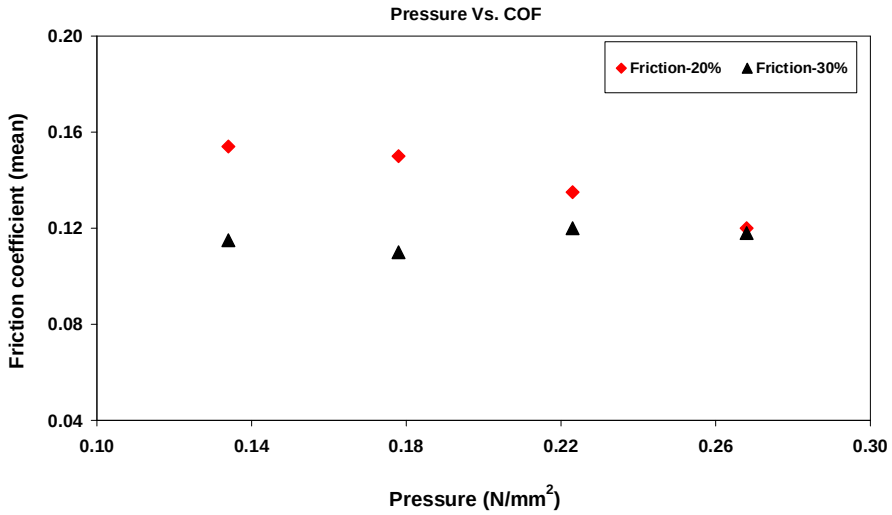

Figure 5.10 Mean COF against contact pressure of 1 µm lead/indium coated substrates in marginally lubricated test conditions.

From figure 5.10 it can be seen that 1 µm coated 20% leaded bronze substrates have a higher mean COF than that for 1 µm coated 30% leaded bronze substrates at every contact pressure. Since the mean and SPWR at change in PV were approximately constant in both test materials, the test results were averaged for

each type of substrate material and these results are shown in table 5.11 and table 5.12. From this table 5.11, the mean COF of 1 µm coated 20% leaded bronze at an average PV is 0.14 compared to 1 µm coated 30% leaded bronze mean COF of 0.11.

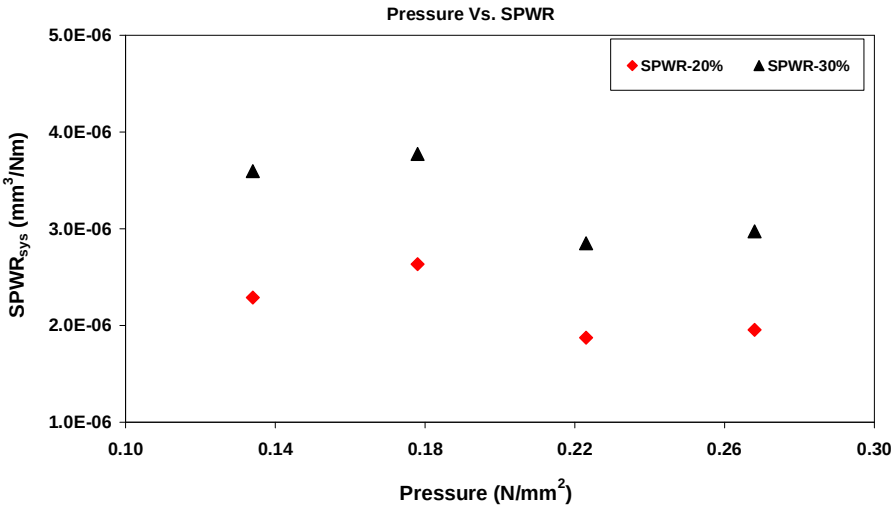

Figure 5.11 System SPWR against contact pressure of 1 µm lead/indium coated substrates in marginally lubricated test conditions.

Figure 5.11 shows that the system SPWR of 1 µm 30% leaded bronze is higher than that of 1 µm 20% leaded bronze at each contact pressure. Table 5.12 shows that the system SPWR of 1 µm 30% leaded bronze was 3.30E-06 compared to 1 µm 20% leaded bronze system SPWR of 2.19E-06.

Table 5.11 Mean COF of 1 µm lead/indium coated substrates at increase in PV in marginally lubricated test conditions.

Mat	Mean COF at different PV values					SD
	0.394 N/mm².m/s	0.523 N/mm².m/s	0.656 N/mm².m/s	0.785 N/mm².m/s	Average N/mm².m/s	
20%	0.15	0.15	0.14	0.12	0.14	0.02
30%	0.12	0.11	0.12	0.11	0.11	0.01

Table 5.12 System SPWR of 1 µm lead/indium coated substrates at increase in PV in marginally lubricated test conditions.

Mat	System SPWR at different PV values					SD
	0.39 N/mm².m/s	0.52 N/mm².m/s	0.65 N/mm².m/s	0.78 N/mm².m/s	Average N/mm².m/s	
20%	2.29E-06	2.63E-06	1.87E-06	1.96E-06	2.19E-06	3.47E-07
30%	3.60E-06	3.77E-06	2.85E-06	2.97E-06	3.30E-06	4.55E-07

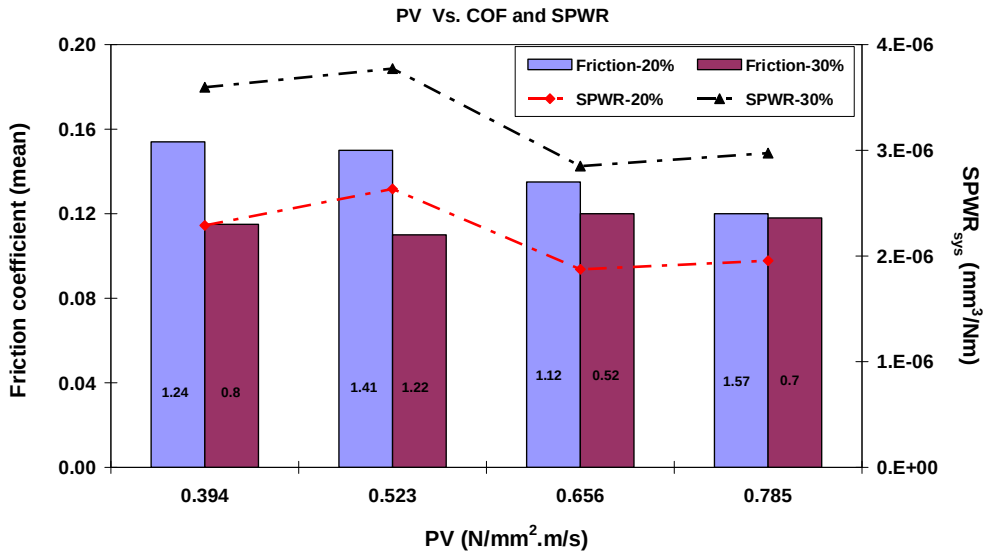

Figure 5.12 Mean COF and system SPWR against PV of 1 µm lead/indium coated substrates in marginally lubricated test conditions.

5.1.3 5 µm coated Lead/Indium Coated 20% and 30% Leaded Bronze Substrates

Dry Test Conditions

The test results for the test materials in dry conditions are detailed in table 5.13 and the test results were plotted against contact pressures in figure 5.13 and 5.14. The COF and SPWR in this test condition are also shown for running-in period and total time period, respectively. The rotational speed was kept constant at 80 rpm and contact pressure was altered to get the same PV among the different test materials.

Table 5.13 Test results of 5 µm lead/indium coated substrates in dry test conditions at a sliding velocity of 0.12 m/s.

Mat	Thick µm	Load N	P N/mm²	PV N/mm².m/s	Mean Plough COF	Mean COF	SPWR (R) mm³/Nm	SPWR (system) mm³/Nm
20%	4.85	58.86	0.13	0.016	0.76	0.42	1.40E-03	1.40E-03
20%	4.94	78.48	0.18	0.021	0.80	0.43	1.18E-03	1.18E-03
20%	4.93	98.1	0.22	0.026	0.87	0.45	1.26E-03	1.28E-03
20%	3.89	117.72	0.26	0.031	0.84	0.45	1.13E-03	1.41E-03
30%	3.77	58.86	0.13	0.016	0.64	0.45	1.20E-03	1.85E-03
30%	5.5	78.48	0.18	0.021	0.61	0.42	1.20E-03	1.82E-03
30%	5.75	98.1	0.22	0.026	0.60	0.42	1.52E-03	2.05E-03
30%	4.37	117.72	0.26	0.031	0.80	0.46	1.16E-03	1.89E-03

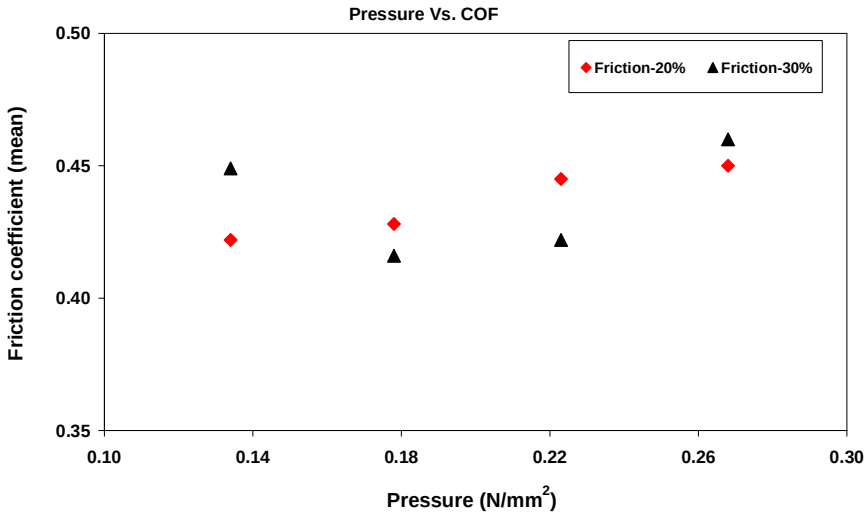

Figure 5.13 Mean COF against contact pressure of 5 µm lead/indium coated substrates in dry test conditions.

Figure 5.13 shows that mean COF of both 5 µm coated leaded bronze substrates are approximately similar. The system SPWR (figure 5.14) of 5 µm coated 30% leaded bronze is higher than that of 5 µm coated 20% leaded bronze substrates at every contact pressure. Considering the standard deviation of mean COF and system SPWR among the same type of substrate materials, it can be seen that the COF and SPWR are approximately constant when contact pressure changed.

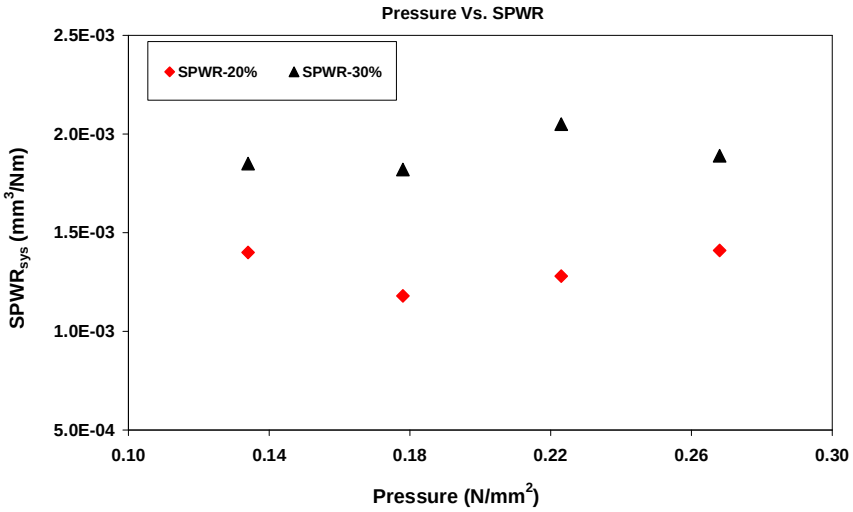

Figure 5.14 System SPWR against contact pressure of 5 µm lead/indium coated substrates in dry test conditions.

Table 5.14 and table 5.15 detail the mean COF and mean SPWR of 5 µm lead/indium coated leaded bronze substrates at different PV taken from table 5.13 for both test materials. The "Average" column denotes the average values of COF and SPWR from all the PV values.

Table 5.14 Mean COF of 5 µm lead/indium coated substrates in dry test conditions at different PV values.

Mat	Mean COF at different PV					SD
	0.016 N/mm².m/s	0.021 N/mm².m/s	0.026 N/mm².m/s	0.031 N/mm².m/s	Average N/mm².m/s	
20%	0.42	0.43	0.44	0.45	0.44	0.01
30%	0.45	0.42	0.42	0.46	0.44	0.02

Table 5.15 System SPWR of 5 µm lead/indium coated substrates in dry test condition at different PV values.

Mat	System SPWR at different PV values					SD
	0.016 N/mm².m/s	0.021 N/mm².m/s	0.026 N/mm².m/s	0.031 N/mm².m/s	Average N/mm².m/s	
20%	1.40E-03	1.18E-03	1.28E-03	1.41E-03	1.32E-03	1.09E-04
30%	1.85E-03	1.82E-03	2.05E-03	1.89E-03	1.90E-03	1.02E-04

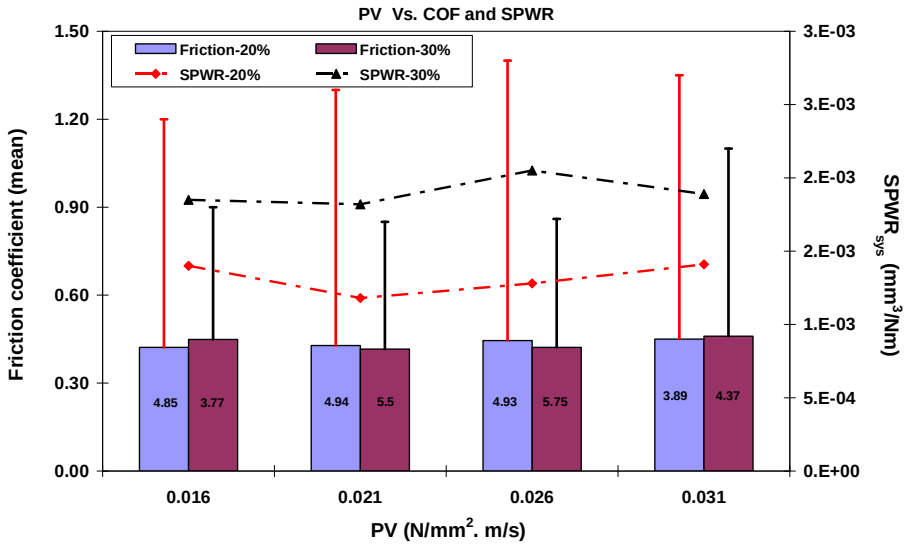

Figure 5.15 Mean COF and mean SPWR against PV of 5 µm lead/indium coated substrates in dry test conditions.

Figure 5.15 shows that mean COF of both 5 µm coated leaded bronze substrates have similar average COF of 0.44. The bar chart elements in figure 5.15 indicated the mean ploughing COF recorded during the test and it can be seen that the mean ploughing COF of 5 µm coated 20% leaded bronze is much higher than that of 5 µm coated 30% leaded bronze. The 5 µm coated 30% leaded bronze has an average SPWR of 1.90E-03 compared to 5 µm coated 20% leaded bronze average SPWR of 1.32E-03.

Lubricated Test Conditions

The COF and SPWR for the above test conditions are detailed in table 5.16 and the results are schematically shown in figure 5.16 and figure 5.17. As described table 4.9 of chapter 4.4.5, two operating speeds were used: 2000 rpm and 1000 rpm on two tests of same substrate material with varying contact pressures so that same PV condition would be attained. The mean COF and system SPWR at an increase in PV are indicated in table 5.17 and 5.18, and these results are schematically shown in figure 5.18.

Table 5.16 Mean COF and SPWR of 5 µm lead/indium coated leaded bronze substrates in marginally lubricated test conditions.

Mat	Thick µm	Load N	P N/mm²	V m/s	PV N/mm².m/s	Mean COF	SPWR (system) mm³/Nm
20%	4.24	78.48	0.18	2.93	0.523	0.14	5.54E-05
20%	4.07	98.1	0.22	2.93	0.654	0.14	5.65E-05
20%	5.57	117.72	0.27	1.47	0.392	0.18	6.20E-05
20%	4.35	156.96	0.36	1.47	0.523	0.16	5.14E-05
20%	4.23	196.2	0.45	1.47	0.65	0.12	5.60E-05
30%	5.01	78.48	0.18	2.93	0.523	0.14	6.07E-05
30%	5.45	98.1	0.22	2.93	0.654	0.18	5.80E-05
30%	5.34	117.72	0.27	1.47	0.392	0.16	5.97E-05
30%	5.65	156.96	0.36	1.47	0.523	0.18	5.41E-05
30%	5.54	196.2	0.45	1.47	0.654	0.19	6.27E-05

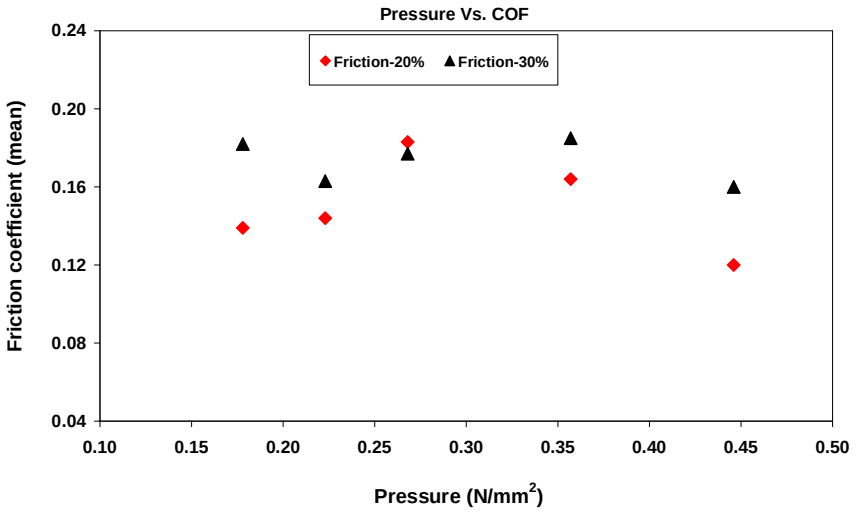

Figure 5.16 Mean COF against contact pressure of 5 µm lead/indium coated substrates in marginally lubricated test conditions at 0.26 m/s.

Table 5.16 shows that test results are approximately constant in both 5 µm coated leaded bronze substrates at change in PV. Therefore, test results at similar PV conditions among different substrates are averaged and shown in table 5.17 and table 5.18. It can be seen that the mean COF of 5 µm coated 30% leaded bronze is slightly higher than that for 5 µm coated 20% leaded bronze in marginally lubricated test conditions. From table 5.17, the average COF of 5 µm 30% leaded bronze is 0.17 compared to 5 µm coated 20% leaded bronze average COF of 0.15. The standard deviation of mean COF of both test materials were constant with increase in contact pressure.

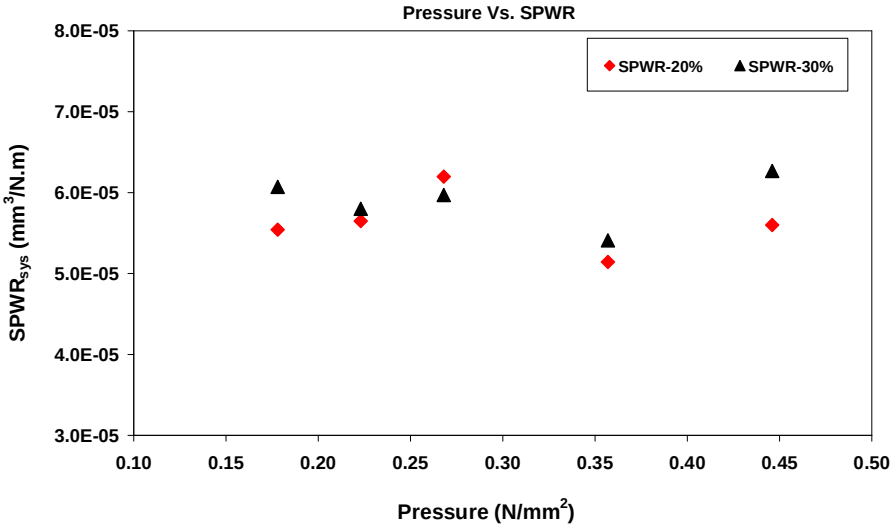

Figure 5.17 System SPWR against contact pressure of 5 µm lead/indium coated substrates in marginally lubricated test conditions.

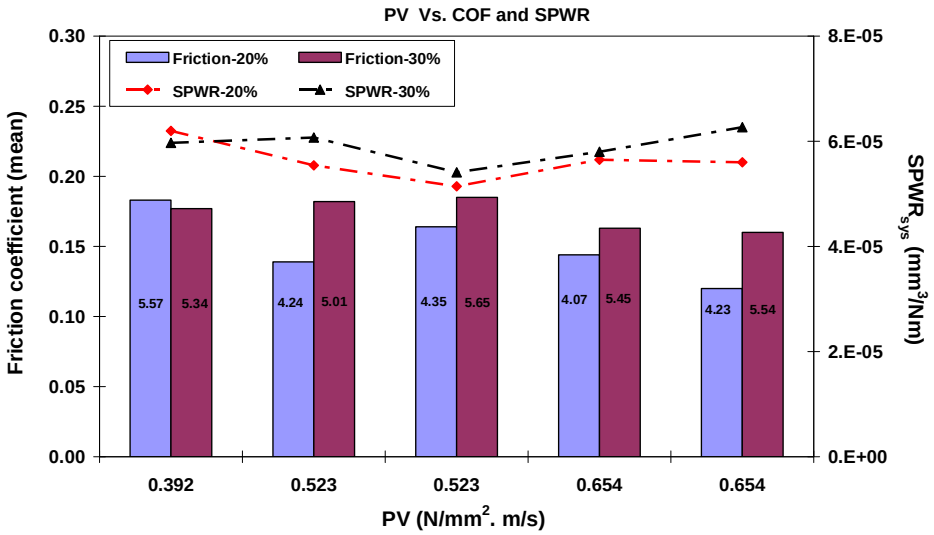

Figure 5.18 Mean COF and system SPWR against contact pressure of 5 µm lead/indium coated substrates in marginally lubricated test conditions.

The average system SPWR of both 5 µm leaded bronze substrates was approximately similar in marginally lubricated test conditions. The average system SPWR of 5 µm coated 20% leaded bronze is 5.83E-05 compared to 5 µm 30% leaded bronze average system SPWR of 5.16E-05.

Table 5.17 Mean COF of 5 µm lead/indium coated substrates at different PV in marginally lubricated test conditions.

Mat	Mean COF at increase in PV				SD
	0.392 N/mm².m/s	0.523 N/mm².m/s	0.654 N/mm².m/s	Average N/mm².m/s	
20%	0.18	0.15	0.13	0.16	0.03
30%	0.16	0.18	0.16	0.17	0.01

Table 5.18 System SPWR of 5 µm lead/indium coated substrates at different PV in marginally lubricated test conditions.

Mat	Mean SPWR at increase in PV				SD
	0.392 N/mm².m/s	0.523 N/mm².m/s	0.654 N/mm².m/s	Average N/mm².m/s	
20%	6.20E-05	5.34E-05	5.96E-05	5.83E-05	4.41E-06
30%	5.97E-05	5.74E-05	5.70E-05	5.16E-05	9.67E-06

5.1.4 Comparing COF and SPWR as a Function of Coating Thickness in TWT Apparatus

The mean COF and system SPWR of uncoated leaded bronze substrates and lead/indium coated leaded bronze substrates are compared for their coating thickness at nominally similar PV conditions, in figure 5.19. The average PV from dry and marginally lubricated test conditions was obtained by averaging all the nominally similar PV values from earlier discussed test results. In table 5.19, the mean COF and mean system SPWR shows the combined average values of these results obtained from nominally similar PV of 0.02 in dry test conditions. Similarly mean COF and mean system SPWR at nominally similar PV from marginally lubricated tests have been considered.

Table 5.19 Comparing COF and SPWR against coating thickness in dry and marginally lubricated test conditions.

Test condition	Mat	Thick µm	PV (avg)	Mean COF	Mean SPWR (system)
Dry	20%	0	0.02	0.37	3.25E-05
		1	0.02	0.36	4.16E-04
		5	0.02	0.44	1.21E-03
	30%	0	0.02	0.34	3.91E-05
		1	0.02	0.28	4.34E-04
		5	0.02	0.44	1.90E-03
Marginal lubrication	20%	0	0.52	0.11	2.27E-06
		1	0.52	0.14	2.19E-06
		5	0.52	0.16	5.83E-05
	30%	0	0.52	0.09	3.41E-06
		1	0.52	0.11	3.20E-06
		5	0.52	0.17	5.16E-05

* Mat – Test material, Thick – Thickness of lead/indium, avg – Average value.

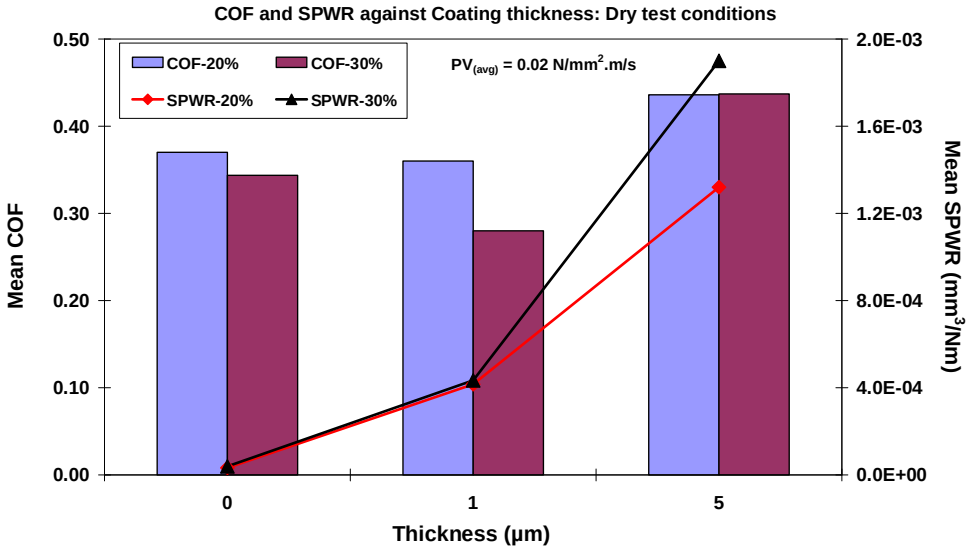

Figure 5.19 Mean COF and mean system SPWR against coating thickness from TWT apparatus 1 in dry test conditions.

Figure 5.19 shows that uncoated leaded bronze substrates have lower SPWR than lead/indium coated leaded bronze substrates, and the 1 µm coating helped in reducing the mean COF for leaded bronze substrates over the time period considered. The mean SPWR was much higher when the substrates were coated with 5 µm thick films but this coating protected the substrates from wear since it

was identified that the 5 µm coating was not completely worn away in all the tests in dry test condition (discussed in chapter 6).

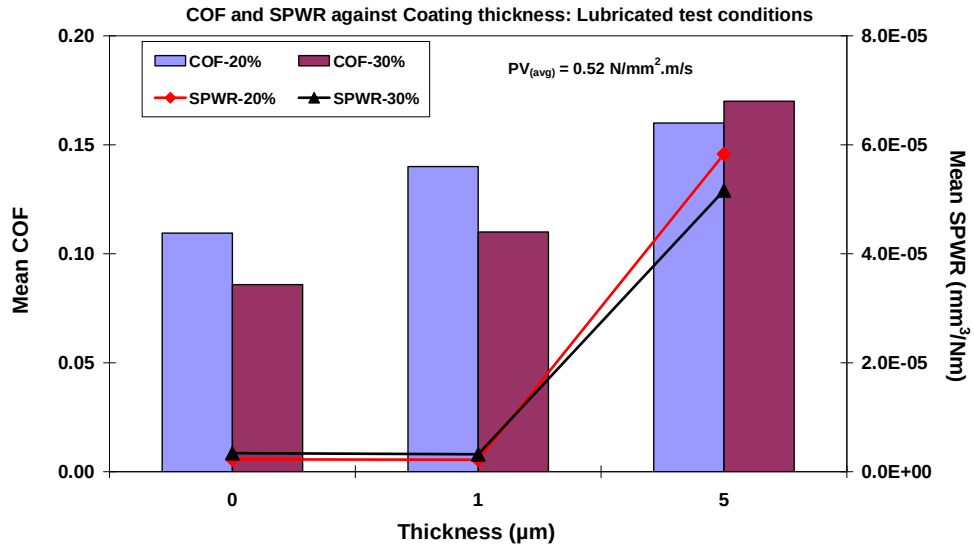

Figure 5.20 Mean COF and mean system SPWR against coating thickness from TWT apparatus 1 in marginally lubricated test conditions.

Figure 5.20 shows that uncoated leaded bronze substrates have lower COF and SPWR than lead/indium coated leaded bronze substrates in marginally lubricated test conditions. The mean COF increases with increase in coating thickness in both substrate materials. The system SPWR of 5 µm lead/indium coating was higher but it protected the substrate surfaces from wear (discussed in chapter 6) as the coating was not removed from the substrate over the time period considered in marginally lubricated test conditions.

5.2 Pin on Disc Test Results

The friction and wear results of all the lead based materials obtained from POD test apparatus are reported in this section. The results are separated according to the type of operating test conditions (i.e. dry and marginally lubricated) and thickness of lead/indium used. Since the POD apparatus used in this project has a non-conformal contact, the ploughing component of friction has a major influence on the wear of coated substrates. For these reasons, the COF was divided into: mean ploughing coefficient of friction and steady state coefficient of friction. The definitions of these terms are exactly same as described earlier for the TWT

apparatus 1. The SPWR over the running-in period was calculated from the area of the ploughing component, described in chapter 4.7.2. The SPWR of the system was calculated from the wear track dimensions, described in chapter 4.4.4. Since the contact pressure in the POD test apparatus was not uniform, normal load (W) was taken as the experimental parameter to compare the performance of the test materials. The operating test conditions used in this apparatus are described in chapter 4.7.1. All the test results in this chapter are discussed in chapter 6.

5.2.1 Uncoated 20% and 30% Leaded Bronze Substrates

Dry Test Conditions

(a) Sliding Velocity: 0.47 m/s, Speed: 250 rpm

The test results for the above test conditions are detailed in table 5.20 and results are compared among substrate materials against load in figure 5.21.

Table 5.20 Mean COF and SPWR of uncoated 20% leaded bronze and 30% leaded bronze substrates in dry test conditions at 0.47 m/s.

Test	Mat	Load N	IP N/mm^2	FP N/mm^2	PV $N/mm^2.m/s$	Mean COF	Vol mm^3	SPWR mm^3/Nm
UN4	20%	1	318.96	49.74	23.44	0.28	0.02	1.62E-04
UN7	20%	2	401.87	44.21	20.84	0.31	0.03	1.42E-04
UN8	20%	3	460.02	48.72	22.96	0.31	0.04	1.42E-04
UN9	20%	4	506.32	44.06	20.76	0.27	0.05	1.22E-04
UN21	30%	1	318.96	22.10	18.75	0.27	0.02	2.27E-04
UN22	30%	2	401.87	24.87	10.42	0.25	0.04	2.21E-04
UN23	30%	3	460.02	23.87	11.72	0.24	0.07	2.17E-04
UN25	30%	4	506.32	24.07	11.25	0.24	0.08	2.11E-04

* Mat – Material, IP – Initial Pressure, FP – Final Pressure, PV – Final pressure X Velocity, Vol – Volume loss of material, SPWR – Specific Wear Rate

In table 5.20, the initial (contact) pressure (IP) was evaluated from the Hertzian contact calculations as described in chapter 3.4. The final (contact) pressure (FP) between the ball and disc was obtained from wear track dimensions by assuming that the contact area developed would be circular. The mean COF was measured by averaging all the COF values from the steady state region of the friction - time graph.

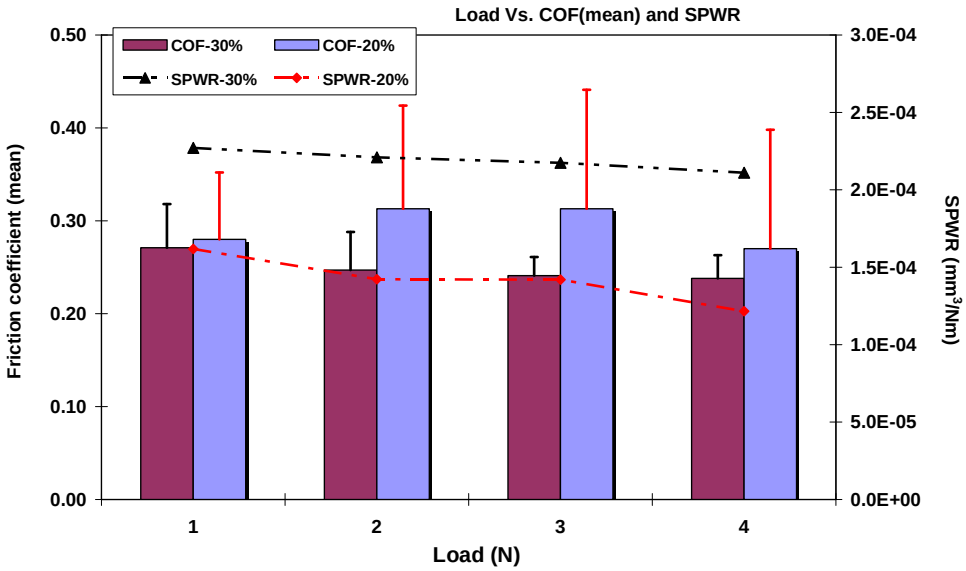

Figure 5.21 Mean COF and SPWR against load in uncoated leaded bronze substrates at 0.47 m/s (Note: bar elements show the maximum COF recorded at the start of the test).

Figure 5.21 shows that mean COF of 20% leaded bronze at each load is higher than that of 30% leaded bronze, but 20% leaded bronze has a lower SPWR than 30% leaded bronze. Since the COF and SPWR of both substrate materials at each contact load is approximately constant with increasing load, the test results at all the contact loads were averaged as shown in table 5.22. From table 5.22, at the sliding velocity of 0.47 m/s, the mean COF of 20% leaded bronze (0.29) is higher than that of 30% leaded bronze (0.25). The maximum COF recorded at each load for 20% leaded bronze was much higher than that for 30% leaded bronze at each load.

The mean SPWR of 30% leaded bronze is 1.42E-04 compared to the mean SPWR of 2.2E-04 for 30% leaded bronze. The final pressure values from 30% leaded bronze confirm the high volume loss of this material compared with 20% leaded bronze.

(b) Sliding Velocity: 0.24 m/s, Speed: 250 rpm

The results for the above condition are detailed in table 5.21 and results are compared against load in figure 5.22. The mean COF and mean SPWR along with their standard deviations at all contact loads are indicated in table 5.22.

Table 5.21 Mean COF and SPWR of uncoated substrates in dry test conditions at 0.24 m/s.

Test	Mat	Load N	IP N/mm²	FP N/mm²	PV N/mm².m/s	Mean COF	Vol mm³	SPWR mm³/Nm
UN4	20%	2	401.87	32.48	7.65	0.33	0.04	1.85E-04
UN7	20%	4	506.32	39.30	9.26	0.34	0.06	1.55E-04
UN8	20%	6	579.59	39.46	9.30	0.30	0.09	1.47E-04
UN9	20%	8	637.92	34.93	8.23	0.30	0.10	1.41E-04
UN21	30%	2	401.87	24.87	5.86	0.27	0.05	2.58E-04
UN22	30%	4	506.32	26.31	6.20	0.26	0.10	2.52E-04
UN23	30%	6	579.59	28.25	6.66	0.25	0.14	2.33E-04
UN25	30%	8	637.92	24.87	5.86	0.24	0.20	2.51E-04

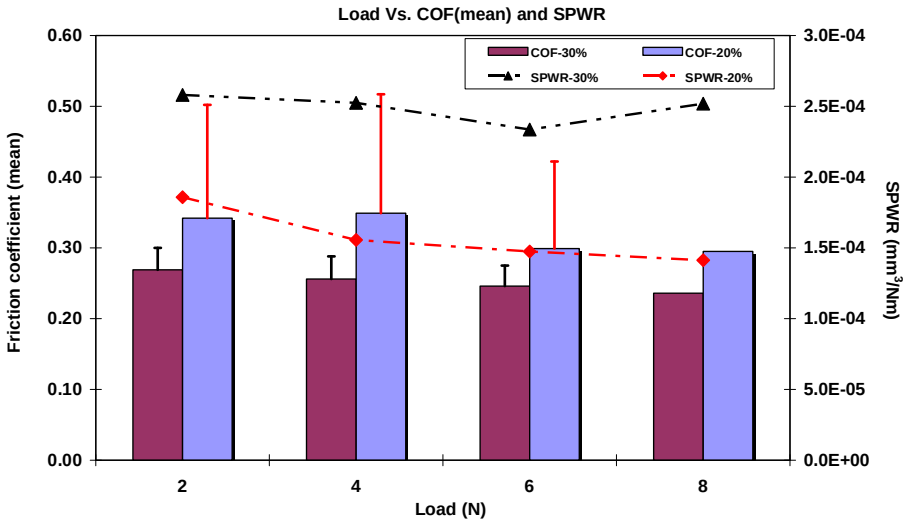

Figure 5.22 Mean COF and SPWR against load for uncoated leaded bronze substrates in dry test conditions at 0.24 m/s. (The bar elements represent the maximum COF recorded at the start of the test).

From figure 5.22, it can be seen that the mean COF of 20% leaded bronze at each contact load is higher than that for 30% leaded bronze. The mean COF of 20% leaded bronze and 30% leaded bronze substrates at all contact loads indicated in table 5.22 are 0.30 and 0.25, respectively. The mean SPWR of 20% leaded bronze is 1.57E-04 compared to the mean SPWR of 2.5E-04 for 30% leaded bronze. The trends of these results are similar to those quoted above for the higher sliding speed. Test results and their standard deviations from both sliding velocities suggest that there is no significant effect of sliding velocity for the uncoated leaded bronze substrates when running dry.

Table 5.22 Mean COF and mean SPWR of uncoated leaded bronze substrates in dry test conditions.

Mat	Mean COF (S.D)		Mean SPWR (S.D)	
	0.47 m/s	0.24 m/s	0.47 m/s	0.24 m/s
20%	0.29 (0.02)	0.30 (0.03)	1.42E-04 (1.64E-05)	1.57E-04 (1.97E-05)
30%	0.25 (0.01)	0.25 (0.01)	2.2E-04 (1.97E-05)	2.5E-04 (1.06E-05)

*S.D – Standard deviation.

Lubricated Test Conditions

(a) Sliding Velocity - 0.26 m/s, Speed - 125 rpm

The test results for the above conditions are summarized in table 5.23 and results are plotted against load in figure 5.23. The mean COF and mean SPWR along with their standard deviations at all contact loads are indicated in table 5.25.

Table 5.23 Mean COF and SPWR of uncoated substrates in marginally lubricated test conditions at 0.26 m/s.

Test	Mat	Load N	I.P N/mm²	F.P N/mm²	PV N/mm².m/s	Mean COF	Vol mm³	SPWR mm³/Nm
UN4	20%	1	318.96	127.32	33.32	0.12	1.5E-03	1.53E-05
UN7	20%	2	401.87	176.84	46.28	0.11	2.1E-03	1.07E-05
UN8	20%	3	460.02	265.26	69.42	0.12	3.5E-03	1.17E-05
UN9	20%	4	506.32	226.35	59.24	0.11	5.0E-03	1.24E-05
UN21	30%	1	318.96	105.23	27.54	0.10	3.1E-03	2.01E-05
UN22	30%	2	401.87	44.21	11.57	0.11	6.3E-03	1.88E-05
UN23	30%	3	460.02	78.92	20.65	0.11	1.0E-02	2.09E-05
UN25	30%	4	506.32	56.59	14.81	0.10	1.4E-02	2.19E-05

Figure 5.23 show that the mean COF of 20% leaded bronze is slightly higher than that of 30% leaded bronze, but is approximately constant with increase in load over the time period considered. From table 5.25, it can be seen that 20% leaded bronze has a mean COF of 0.11 compared to 30% leaded bronze mean COF of 0.10 at all contact loads. The maximum COF recorded (bar elements in figure 5.23) at various contact loads for 20% leaded bronze was higher than that for 30% leaded bronze. The mean SPWR of 30% leaded bronze (2.04E-05) is higher than that of 20% leaded bronze (1.25E-05). The volume loss of both materials from

table 5.23 confirms that 30% leaded bronze wears more than 20% leaded bronze in marginally lubricated test conditions.

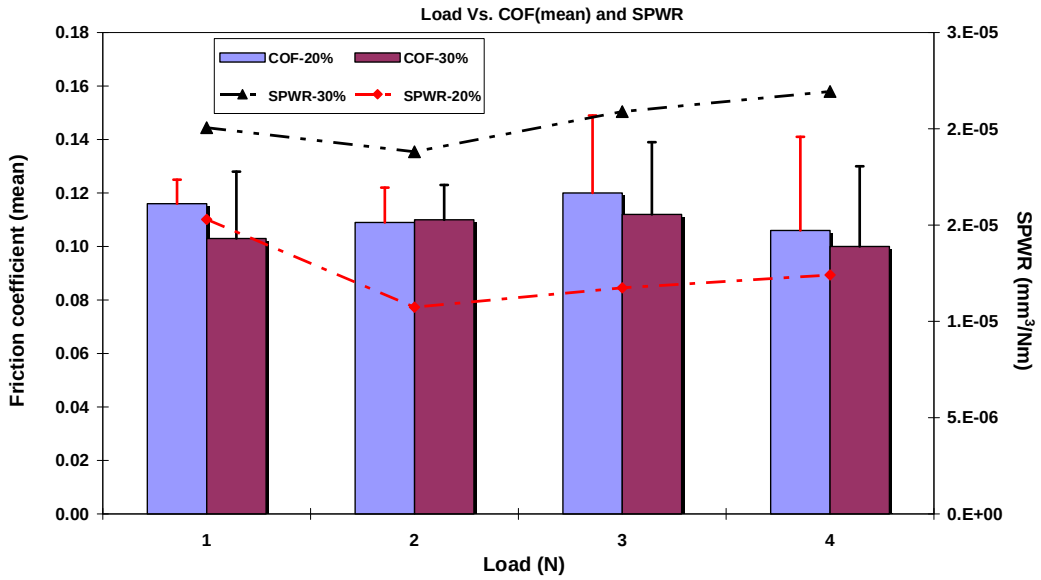

Figure 5.23 Mean COF and SPWR against load for uncoated leaded bronze substrates in marginally lubricated test condition at 0.26 m/s.

(b) Sliding Velocity - 0.13 m/s, Speed - 250 rpm

The test results for the above conditions are detailed in table 5.24 and results are plotted against load in figure 5.24. The mean COF and mean SPWR at all contact loads are indicated in table 5.25.

Table 5.24 Mean COF and SPWR results of uncoated substrates in marginally lubricated test condition at 0.13 m/s.

Test	Mat	Load N	I.P N/mm²	F.P N/mm²	PV N/mm².m/s	Mean COF	Vol mm³	SPWR mm³/Nm
UN4	20%	2	401.87	176.84	23.15	0.11	1.7E-03	8.52E-06
UN7	20%	4	506.32	198.94	26.04	0.12	2.8E-03	7.18E-06
UN8	20%	6	579.59	190.99	25.00	0.14	4.2E-03	7.02E-06
UN9	20%	8	637.92	176.84	23.15	0.15	7.7E-03	9.67E-06
UN21	30%	2	401.87	63.66	8.33	0.10	4.6E-03	1.18E-05
UN22	30%	4	506.32	56.59	7.41	0.12	1.1E-02	1.41E-05
UN23	30%	6	579.59	58.95	7.72	0.13	1.8E-02	1.47E-05
UN25	30%	8	637.92	52.61	6.89	0.15	2.1E-02	1.57E-05

From table 5.25, at sliding velocity of 0.13 m/s, the mean COF of 20% leaded bronze (0.13) is slightly higher than that for 30% leaded bronze (0.12). In general,

the maximum COF recorded for 20% leaded bronze at all contact loads is higher than that for 30% leaded bronze. The mean SPWR of 30% leaded bronze is 1.41E-05 compared to 20% leaded bronze mean SPWR of 8.1E-06.

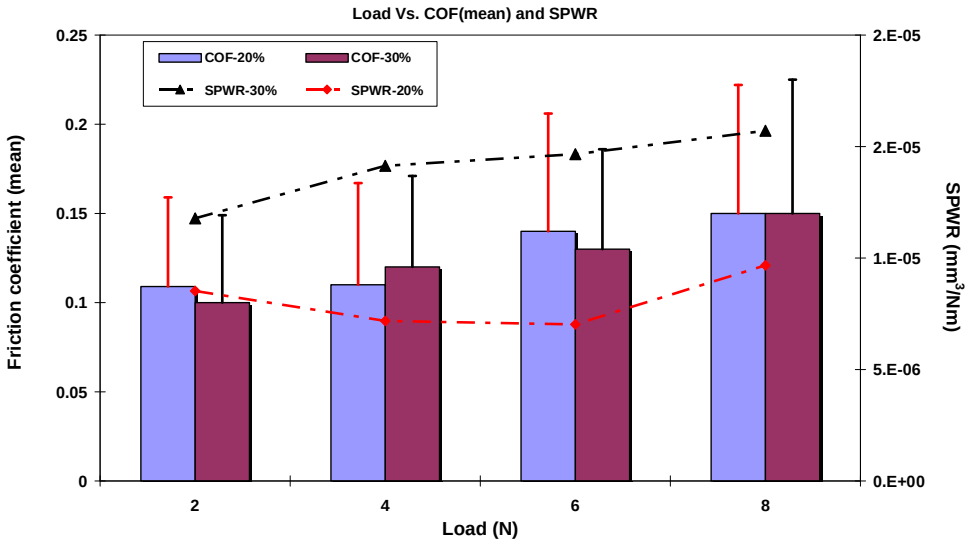

Figure 5.24 Mean COF and SPWR against load for uncoated leaded bronze substrates in marginally lubricated test conditions.

Table 5.25 Mean COF and mean SPWR of uncoated leaded bronze substrates in marginally lubricated test conditions.

Mat	Mean COF (S.D)		Mean SPWR (SD)	
	0.26 m/s	0.13 m/s	0.26 m/s	0.13 m/s
20%	0.11 (0.01)	0.13 (0.02)	1.25E-05 (1.96E-06)	8.1E-06 (1.24E-06)
30%	0.10 (0.01)	0.12 (0.02)	2.1E-05 (1.33E-06)	1.41E-05 (1.66E-06)

5.2.2 1 µm Lead/Indium Coated 20% and 30% Leaded Bronze Substrates

The friction and wear results of the above test materials are presented separately according to the test conditions and sliding velocities used. The COF and SPWR are presented for the running-in period and steady state period. The COF and SPWR over the running-in period are indicated as ploughing COF and running-in SPWR, i.e. SPWR (R) from here on. The steady state COF represents the COF for the total test duration excluding the running-in period. The SPWR for the total test time is indicated as the SPWR of the system.

Dry Test Conditions

(a) Sliding Velocity – 0.47 m/s, Speed – 250

The test results for the above conditions are detailed in table 5.26 and the results are plotted for load against COF and SPWR in figure 5.25 to figure 5.27.

Table 5.26 COF and SPWR of 1 µm lead/indium coated substrates in dry test condition at 0.47 m/s.

Mat	Thick µm	Load N	I.P N/mm²	F.P N/mm²	PV N/mm².m/s	Mean Plough COF	Steady state COF	SPWR (R) mm³/Nm	SPWR (system) mm³/Nm
30%	1	1	88.42	39.30	18.52	0.66	0.32	3.44E-04	3.05E-04
30%	1.13	2	113.18	28.29	13.34	0.54	0.30	3.31E-04	3.27E-04
30%	0.94	3	132.17	26.45	12.47	0.54	0.28	3.01E-04	2.72E-04
30%	0.8	4	141.08	24.07	11.34	0.52	0.28	2.77E-04	2.96E-04
20%	1	1	88.42	49.74	23.44	0.66	0.27	3.10E-04	2.39E-04
20%	1.17	2	113.18	37.67	17.75	0.62	0.24	2.90E-04	2.84E-04
20%	1.19	3	132.17	37.30	17.58	0.62	0.23	2.68E-04	2.48E-04
20%	1.32	4	141.08	28.87	13.61	0.56	0.19	2.68E-04	2.58E-04

* Plough COF – Ploughing COF, R – Running-in time, System – Specific wear rate of the system.

Unlike the uncoated leaded bronze substrates, the initial contact pressure (I.P) for lead/indium coated substrates was measured from the initial contact dimensions using the static loading (i.e. load divided by the contact dimension). The final contact pressure (F.P) was measured from the wear track dimensions using the white light interferometer.

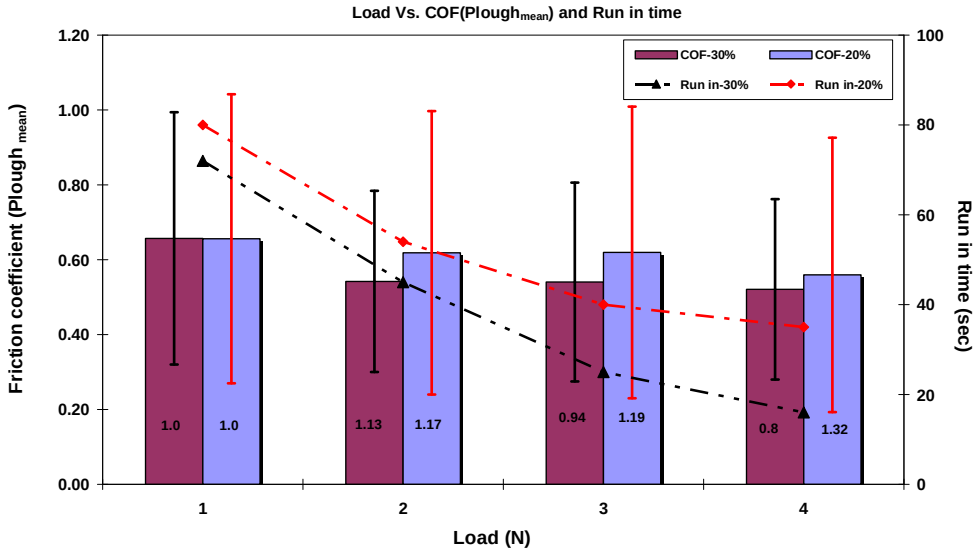

Figure 5.25 Ploughing COF and running-in time against load in 1 µm lead/indium coated substrates in dry test conditions at 0.47 m/s.

Figure 5.25 shows the running-in time recorded from the friction – time graphs at each contact load and actual coating thickness (in µm) on the friction bars. Figure 5.25 also shows the actual coating thickness of each test specimen on the COF bars. The maximum COF and steady state COF are indicated with the bar elements in the above figure at each load condition. It can be seen that the steady state friction is always lower than the mean ploughing COF and the maximum COF represents that highest COF recorded at the start of the test. Figure 5.26 and figure 5.27 presented the COF for the running-in period and steady state period, and SPWR for the running-in period and total time, respectively, in both 1 µm coated leaded bronze substrates.

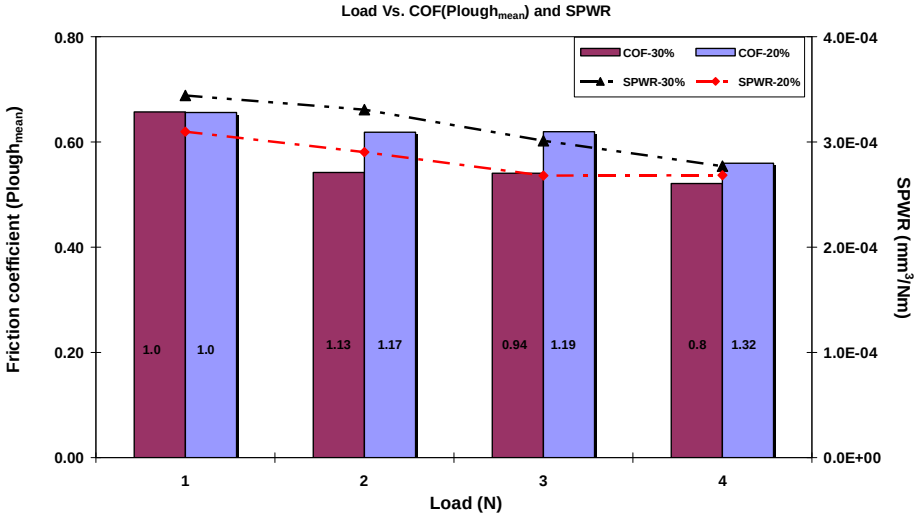

Figure 5.26 Ploughing COF and SPWR (R) against load in 1 µm lead/indium coated substrates in dry test conditions at 0.47 m/s.

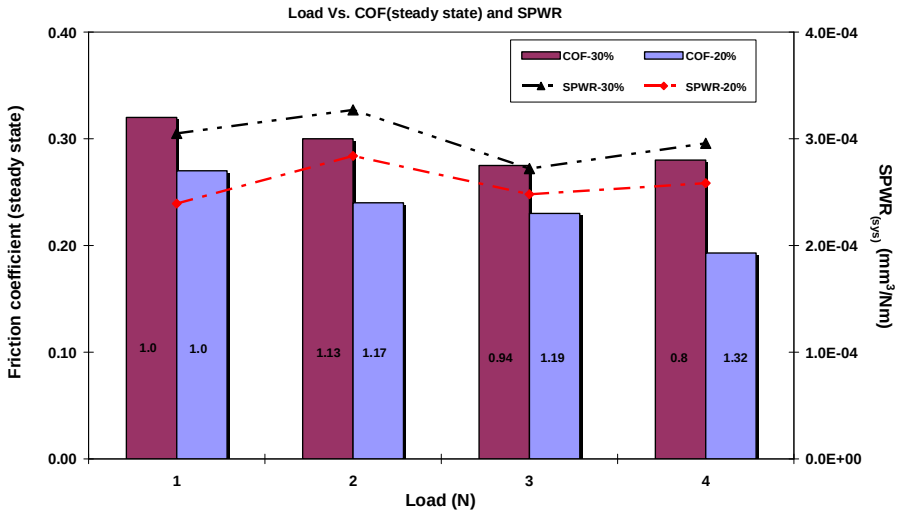

Figure 5.27 Steady state COF and system SPWR against load in 1 µm lead/indium coated substrates in dry test conditions at 0.47 m/s.

It can be seen from the above test results that, 1 µm 20% leaded bronze substrates have slightly higher ploughing COF, but lower steady state COF than 1 µm 30% leaded bronze substrates. The SPWR of 1 µm coated 30% leaded bronze appears to be slightly higher than that of the 1 µm coated 20% leaded bronze. Table 5.28 and table 5.29 summarise the mean COF and mean SPWR of both 1 µm coated leaded bronze substrates at different sliding velocities. The mean values were obtained by averaging COF and SPWR at all contact loads among different leaded bronze substrates.

(b) Sliding Velocity – 0.24 m/s, Speed – 250 rpm

The test results for the above conditions are detailed in table 5.27 and are plotted against load in figure 5.29 and figure 5.30. Figure 5.28 presents the ploughing COF and running-in time data for both 1 µm coated substrates at various contact loads.

Table 5.27 COF and SPWR of 1 µm lead/indium coated substrates in dry test condition at 0.24 m/s.

Mat	Thick µm	Load N	I.P N/mm²	F.P N/mm²	PV N/mm².m/s	Plough COF (mean)	Steady state COF	SPWR (R) mm³/Nm	SPWR (system) mm³/Nm
30%	1.19	2	113.18	24.87	5.86	0.41	0.27	4.47E-04	2.52E-04
30%	1.13	4	141.08	26.31	6.20	0.38	0.26	2.48E-04	2.31E-04
30%	0.94	6	157.84	33.16	7.81	0.32	0.24	1.88E-04	2.36E-04
30%	0.8	8	176.84	37.67	8.88	0.41	0.23	1.48E-04	2.76E-04
20%	1	2	113.18	44.21	10.42	0.42	0.22	3.54E-04	2.12E-04
20%	1.17	4	141.08	39.30	9.26	0.42	0.21	2.45E-04	2.21E-04
20%	1.19	6	157.84	39.46	9.30	0.41	0.20	2.14E-04	2.01E-04
20%	1.32	8	176.84	44.21	10.42	0.42	0.21	2.35E-04	2.41E-04

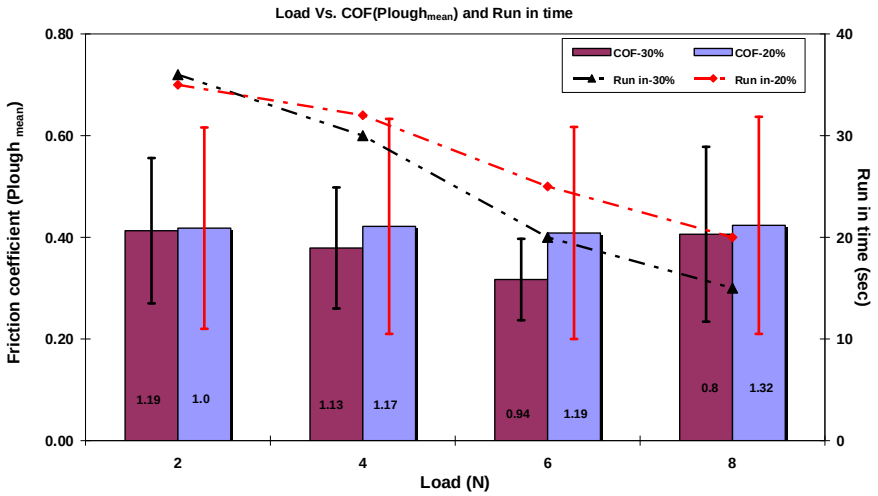

Figure 5.28 Ploughing COF and running-in time against load of 1 µm coated substrates in dry test conditions at 0.24 m/s.

Figure 5.28 shows that the mean ploughing COF of 1 µm coated 20% leaded bronze substrates are slightly higher than those of 1 µm coated 30% leaded bronze substrates. From table 5.28, the mean ploughing COF of 1 µm coated 30% leaded bronze is 0.38 compared to 1 µm coated 20% mean ploughing COF of 0.42 at a sliding velocity of 0.24 m/s. For this sliding velocity, the mean SPWR (R) of 20% is 2.62E-04 compared to 30% mean SPWR (R) of 2.57E-04.

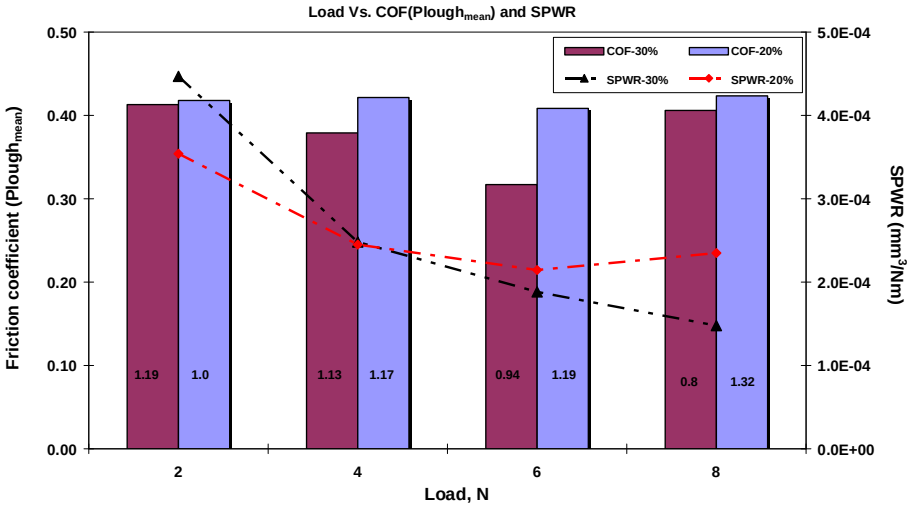

Figure 5.29 Ploughing COF and SPWR (R) against load of 1 µm coated substrates in dry test conditions at 0.24 m/s.

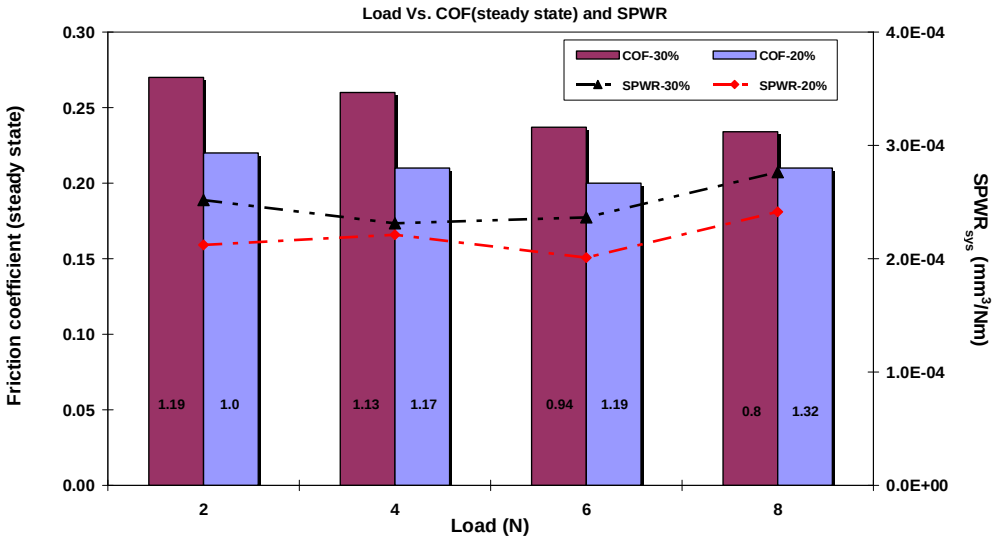

Figure 5.30 Steady state COF and system SPWR of 1 µm coated substrates in dry test condition at 0.24 m/s.

Figure 5.30 shows that 1 μm coated 30% leaded bronze has slightly higher steady state COF and system SPWR than 1 μm coated 20% leaded bronze. It can be seen from table 5.29 that the steady state COF and system SPWR for both 1 μm coated leaded bronze substrates are approximately constant at both sliding velocities. The standard deviation of results for each sliding velocity confirms that there is no significant effect of sliding speed in this range on the tribological properties of these substrates when run dry over the time period considered.

Table 5.28 Mean ploughing COF and mean SPWR of 1 μm lead/indium coated substrates at different sliding velocities in dry test conditions.

Mat	Mean Plough friction (S.D)		Mean SPWR (R) (S.D)	
	0.47 m/s	0.24 m/s	0.47 m/s	0.24 m/s
20%	0.61 (0.04)	0.42 (0.01)	2.84E-04 (2.0E-05)	2.62E-04 (6.26E-05)
30%	0.56 (0.06)	0.38 (0.04)	3.13E-04 (3.01E-05)	2.57E-04 (1.33E-04)

Table 5.29 Steady state COF and system SPWR of 1 μm lead/indium coated substrates at different sliding velocities in dry test conditions.

Mat	Steady state COF (S.D)		System SPWR (S.D)	
	0.47 m/s	0.24 m/s	0.47 m/s	0.24 m/s
20%	0.23 (0.04)	0.21 (0.01)	2.57E-04 (1.94E-05)	2.19E-04 (1.71E-05)
30%	0.29 (0.06)	0.25 (0.01)	3.0E-04 (2.28E-05)	2.49E-04 (2.02E-05)

Lubricated Test Condition

(a) Sliding Velocity - 0.26 m/s, Speed - 125 rpm

The test results for the above conditions are detailed in table 5.30 and results are plotted against load in figure 5.30 to figure 5.32.

Table 5.30 COF and SPWR of 1 µm lead/indium coated substrates in marginally lubricated test condition at 0.26 m/s.

Mat	Thick µm	Load N	I.P N/mm²	F.P N/mm²	PV N/mm².m/s	Plough COF (mean)	Steady state COF	SPWR (R) mm³/Nm	SPWR (system) mm³/Nm
30%	0.94	1	88.42	22.10	5.78	0.31	0.06	5.65E-04	2.71E-04
30%	1.13	2	113.18	32.48	8.50	0.30	0.08	3.72E-04	2.53E-04
30%	1.02	3	132.17	37.30	9.76	0.27	0.05	2.62E-04	2.31E-04
30%	0.8	4	141.08	39.30	10.28	0.28	0.08	1.71E-04	1.94E-04
20%	1	1	88.42	22.10	5.78	0.43	0.13	5.83E-04	2.89E-04
20%	1.17	2	113.18	32.48	8.50	0.40	0.12	3.92E-04	2.76E-04
20%	0.9	3	132.17	42.44	11.11	0.38	0.09	2.28E-04	2.13E-04
20%	1.32	4	141.08	49.74	13.02	0.39	0.10	2.10E-04	2.19E-04

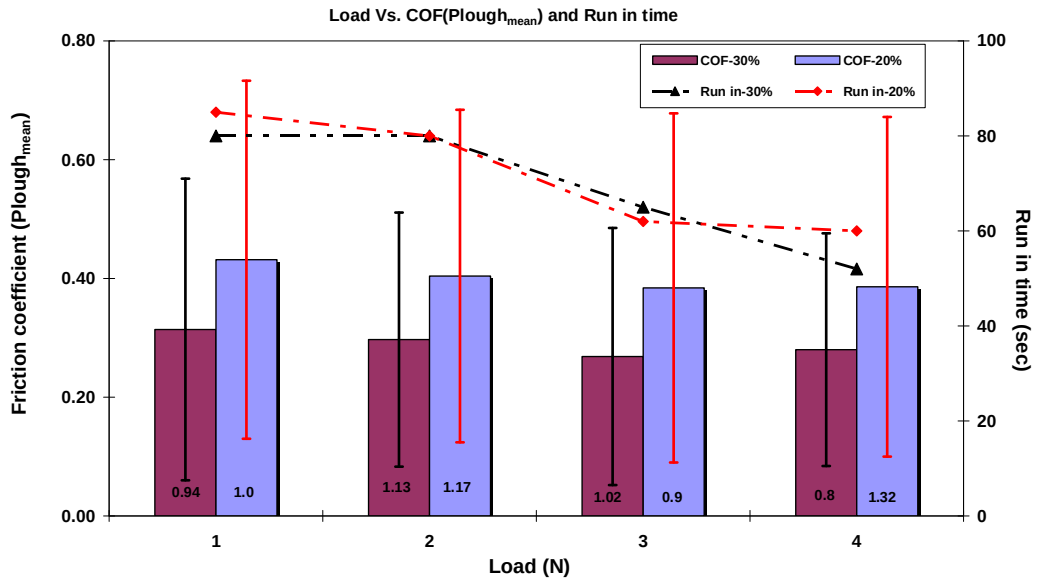

Figure 5.31 Ploughing COF and running-in time against load of 1 µm coated substrates in marginally lubricated test condition at 0.26 m/s.

From the test results detailed in table 5.30 and figure 5.31, it can be seen that the ploughing COF of 1 µm coated 20% leaded bronze is higher than that of 1 µm coated 30% leaded bronze substrates. From table 5.32, the mean ploughing COF of 1 µm coated 20% leaded bronze is 0.40 compared to 1 µm coated 30% leaded bronze mean ploughing COF of 0.29. The running-in time for both materials were similar and, depending on the thickness of coating, the running-in time varied for the same contact loads (actual coating thickness, µm, is shown on the friction bars). The SPWR of 20% leaded bronze is slightly higher than that of 30% leaded bronze. The average SPWR (R) of 1 µm coated 20% leaded bronze is 3.53E-04 compared to 1 µm coated 30% leaded bronze SPWR (R) of 3.42E-04.

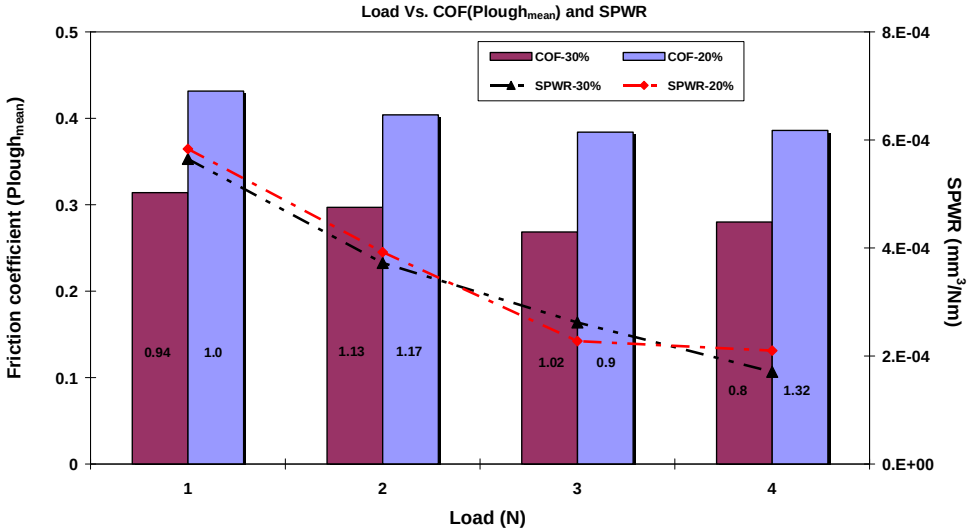

Figure 5.32 Ploughing COF and SPWR (R) against load of 1 µm coated substrates in marginally lubricated test conditions at 0.26 m/s.

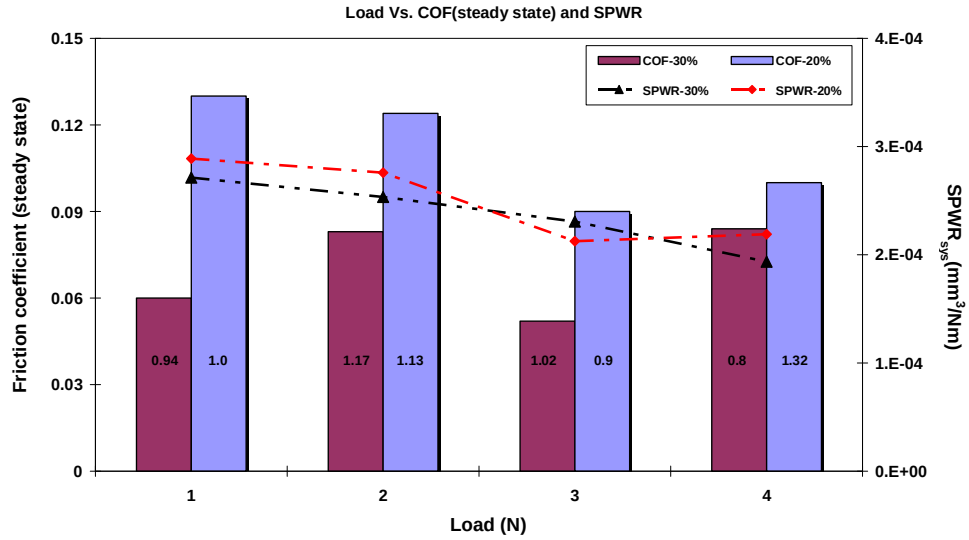

Figure 5.33 Steady state COF and system SPWR of 1 µm coated substrates in marginally lubricated test conditions at 0.26 m/s.

Figure 5.33 and table 5.33 show that 1 µm coated 20% leaded bronze has higher steady state COF and slightly higher system SPWR than that of 1 µm coated 30% leaded bronze substrates in marginally lubricated test conditions. The standard deviation at increase in load show consistent SPWR in both test materials.

(b) Sliding Velocity - 0.13 m/s, Speed - 250 rpm

The test results for the above conditions are detailed in table 5.31 and results are plotted against load in figure 5.34 to figure 5.36.

Table 5.31 COF and SPWR of 1 µm lead/indium coated substrates in marginally lubricated test condition at 0.13 m/s.

Mat	Thick µm	Load N	I.P N/mm²	F.P N/mm²	PV N/mm².m/s	Plough COF (mean)	Steady state COF	SPWR (R) mm³/Nm	SPWR (system) mm³/Nm
30%	0.94	2	113.18	99.47	13.34	0.11	0.09	1.25E-04	2.14E-05
30%	1.13	4	141.08	49.74	6.67	0.12	0.09	9.54E-05	2.80E-05
30%	1.02	6	157.84	58.95	7.90	0.15	0.11	8.18E-05	2.89E-05
30%	0.8	8	176.84	70.54	9.46	0.14	0.10	7.39E-05	2.49E-05
20%	1	2	113.18	78.60	10.54	0.14	0.13	1.24E-04	2.45E-05
20%	1.17	4	141.08	56.59	7.59	0.19	0.12	9.80E-05	2.92E-05
20%	0.9	6	157.84	43.31	5.81	0.18	0.10	8.40E-05	2.36E-05
20%	1.32	8	176.84	44.21	5.93	0.21	0.11	8.19E-05	2.64E-05

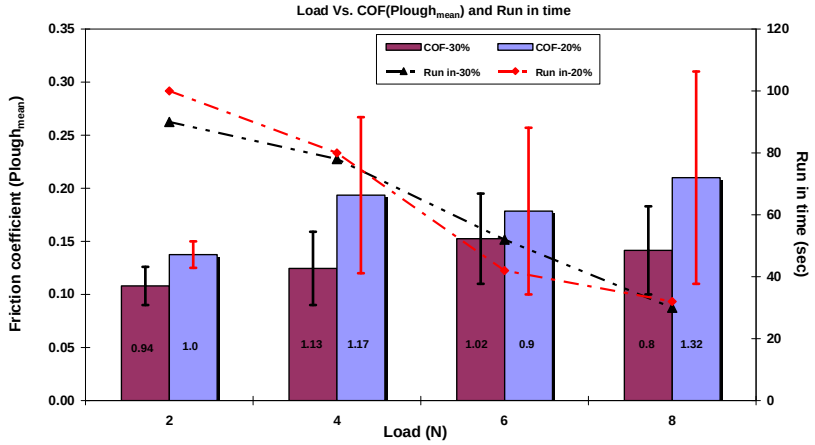

Figure 5.34 Ploughing COF and running-in time against load of 1 µm coated substrates in marginally lubricated test conditions at 0.13 m/s.

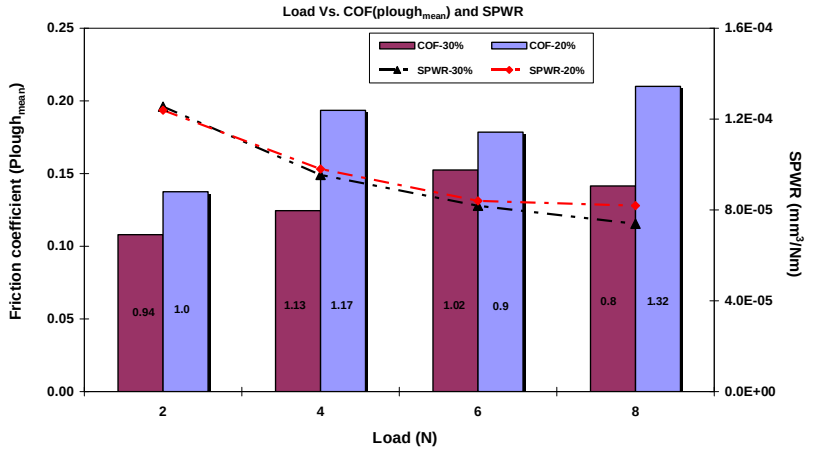

Figure 5.35 Ploughing COF and SPWR (R) against load of 1 µm coated substrates in marginally lubricated test conditions at 0.13 m/s.

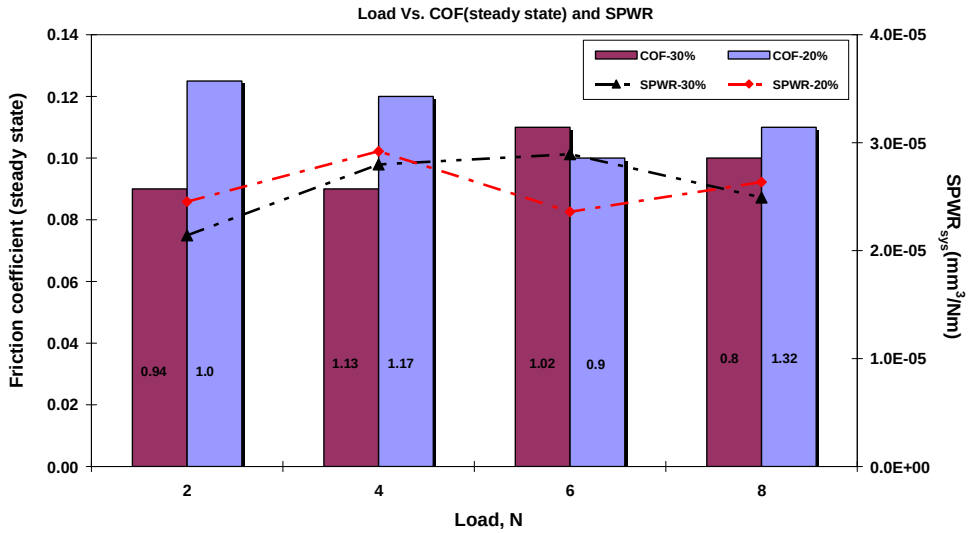

Figure 5.36 Steady state COF and system SPWR of 1 µm coated substrates in marginally lubricated test conditions at 0.13 m/s.

From the test results, the ploughing COF of 1 µm coated 20% leaded bronze is higher than that for 1 µm coated 30% leaded bronze. Table 5.32 shows that the mean ploughing COF of 1 µm coated 20% leaded bronze is 0.18 compared to 1 µm coated 30% leaded bronze mean COF of 0.13. The running-in time for both 1 µm coated leaded bronze is approximately similar. The mean SPWR (R) of 20% leaded bronze is 9.69E-05 compared to 30% leaded bronze mean SPWR of 9.41E-05.

Table 5.33 shows that mean steady state COF and mean SPWR of both test materials are approximately similar.

Table 5.32 Mean Ploughing COF and mean SPWR (R) of 1 µm coated leaded bronze substrates in marginally lubricated test conditions.

Mat	Mean Plough friction (S.D)		Mean SPWR (R) (S.D)	
	0.26 m/s	0.13 m/s	0.26 m/s	0.13 m/s
20%	0.40 (0.02)	0.18 (0.03)	3.53E-04 (1.74E-04)	9.69E-05 (6.49E-05)
30%	0.29 (0.02)	0.13 (0.02)	3.42E-04 (1.70E-04)	9.41E-05 (7.15E-05)

Table 5.33 Mean steady state COF and system SPWR of system for 1 μm coated leaded bronze substrates in marginally lubricated test conditions.

Mat	Mean steady state COF (S.D)		Mean system SPWR (S.D)	
	0.26 m/s	0.13 m/s	0.26 m/s	0.13 m/s
20%	0.11 (0.02)	0.11 (0.01)	2.5E-04 (3.89 E-05)	2.59E-05 (2.47E-06)
30%	0.07 (0.02)	0.10 (0.01)	2.37E-04 (3.35E-05)	2.58E-05 (3.4E-06)

5.2.3 5 μm Lead/Indium Coated 20% and 30% Leaded Bronze Substrates

The friction and wear results of 5 μm coated 20% leaded bronze and 30% leaded bronze substrates were presented in the same way as described for 1 μm coated leaded bronze substrates. The operating conditions used were detailed in chapter 4.7.1. The COF and SPWR for the running-in period and total test time were presented at each contact load for all the test specimens. The test results were plotted against load among the test materials.

Dry Test Conditions

(a) Sliding Velocity - 0.47 m/s, Speed - 250 rpm

The test results for the above conditions are detailed in table 5.34 and are compared for load against COF and SPWR in figure 5.37 to figure 5.39.

Table 5.34 COF and SPWR of 5 μm lead/indium coated substrates in dry test condition at 0.47 m/s.

Mat	Thick μm	Load N	I.P N/mm²	F.P N/mm²	PV N/mm².m/s	Plough COF (mean)	Steady state COF	SPWR (R) mm³/Nm	SPWR (system) mm³/Nm
30%	4.03	2	78.60	3.98	1.88	0.69	0.36	5.89E-04	1.34E-03
30%	5.0	3	105.81	4.72	2.22	0.72	0.36	6.36E-04	1.32E-03
30%	5.0	4	132.57	5.09	2.40	0.70	0.35	5.12E-04	1.45E-03
20%	6.1	2	78.60	3.98	1.88	0.63	0.35	9.09E-04	1.61E-03
20%	6.08	3	105.81	4.93	2.33	0.59	0.28	7.73E-04	1.58E-03
20%	5.6	4	132.57	5.53	2.61	0.53	0.23	5.86E-04	1.35E-03

The initial contact pressure (I.P) and final contact pressure (F.P) for these coated substrate materials was measured in the same way as described for 1 μm coated substrates.

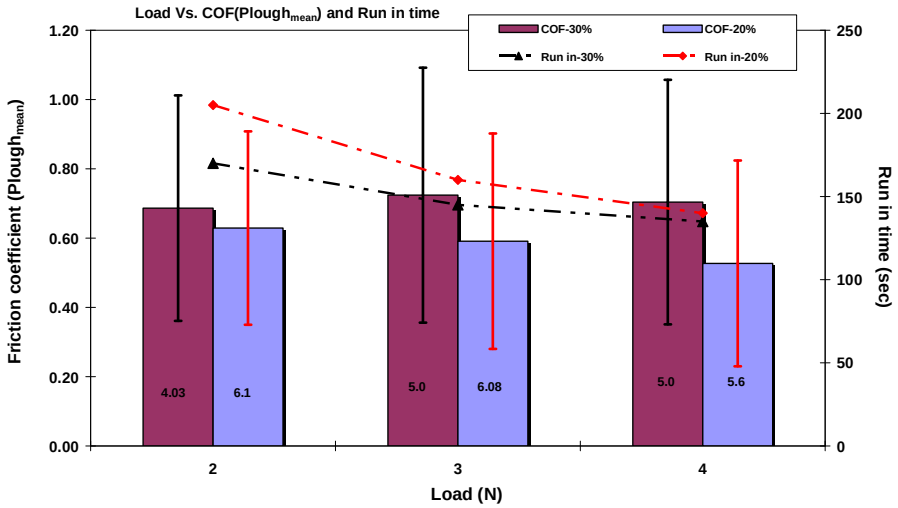

Figure 5.37 Ploughing COF and running-in time against load of 5 µm coated substrates in dry test condition at 0.47 m/s.

Test results detailed in table 5.34 show that 5 µm coated 30% leaded bronze substrates had a higher ploughing COF than the 5 µm coated 20% leaded bronze substrates. In the table 5.36, the average values of mean ploughing COF for 5 µm coated 30% leaded bronze is 0.7 compared to 5 µm coated 20% leaded bronze mean ploughing COF of 0.58. The running-in time for 5 µm coated 20% leaded bronze substrates is higher than for 30% leaded bronze. The SPWR (R) of 5 µm coated 20% leaded bronze is 7.56E-04 compared to 5 µm coated 30% leaded bronze SPWR (R) of 5.79E-04.

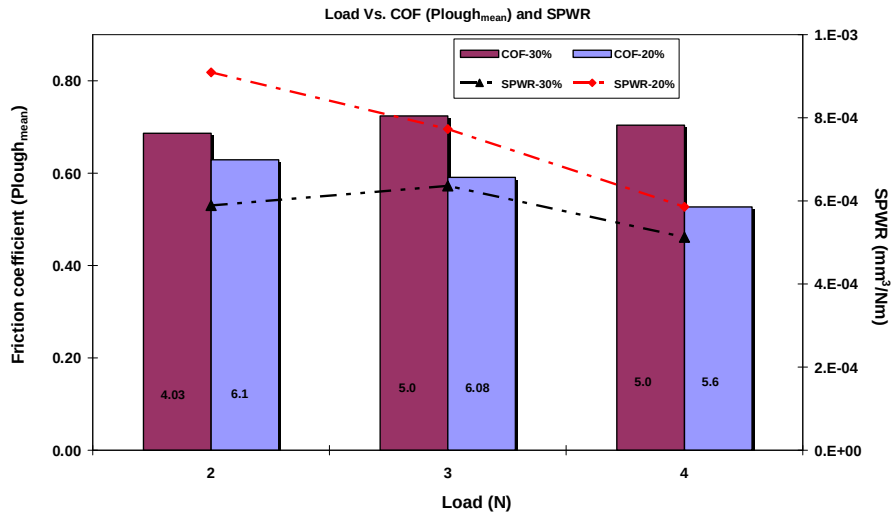

Figure 5.38 Ploughing COF and SPWR (R) against load of 5 µm coated substrates in dry test conditions at 0.47 m/s.

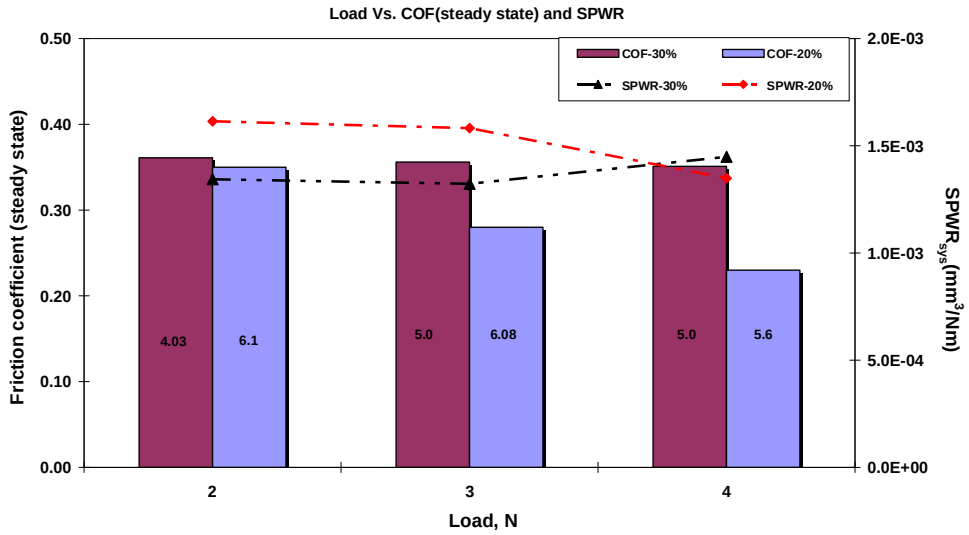

Figure 5.39 Steady state COF and system SPWR of 5 µm coated substrates in dry test conditions at 0.47 m/s.

From figure 5.39 and table 5.37, it can be seen that the 5 µm coated 30% leaded bronze substrates have slightly higher steady state COF, but lower system SPWR than that of 5 µm coated 20% leaded bronze substrates. The standard deviation values of both materials suggest that there is no significant influence of the sliding velocity on wear rate of both materials in dry sliding conditions.

(b) Sliding Velocity - 0.24 m/s, Speed - 250 rpm

The test results for the above conditions are detailed in table 5.35 and results are plotted against load in figure 5.40 to figure 5.42. Table 5.36 and table 5.37 summarize all the average values at different sliding velocities.

Table 5.35 COF and SPWR of 5 µm lead/indium coated substrates in dry test conditions at 0.24 m/s.

Mat	Thick µm	Load N	I.P N/mm²	F.P N/mm²	PV N/mm².m/s	Plough COF (mean)	Steady state COF	SPWR (R) mm³/Nm	SPWR (system) mm³/Nm
30%	4.03	2	78.60	9.42	2.22	0.69	0.29	7.71E-04	4.17E-04
30%	5.00	4	132.57	7.96	1.88	0.64	0.27	6.29E-04	3.23E-04
30%	5.00	6	157.84	9.43	2.22	0.66	0.27	5.77E-04	4.17E-04
30%	5.00	8	176.84	10.19	2.40	0.66	0.26	6.92E-04	3.68E-04
20%	4.24	2	78.60	10.19	2.40	0.67	0.25	7.21E-04	4.85E-04
20%	6.1	4	132.57	10.39	2.45	0.58	0.25	7.17E-04	3.54E-04
20%	4.23	6	157.84	13.58	3.20	0.61	0.24	4.79E-04	3.32E-04
20%	6.08	8	176.84	12.58	2.96	0.56	0.22	7.73E-04	4.57E-04

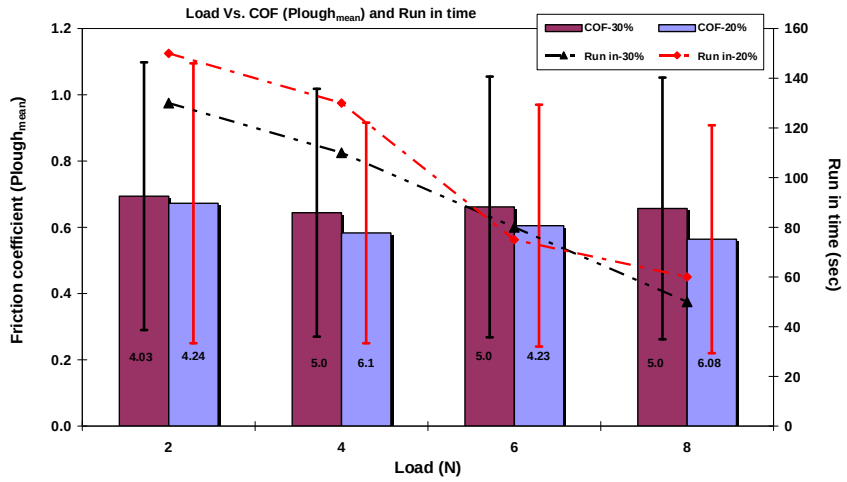

Figure 5.40 Ploughing COF and running-in time against load of 5 µm coated substrates in dry test conditions at 0.24 m/s.

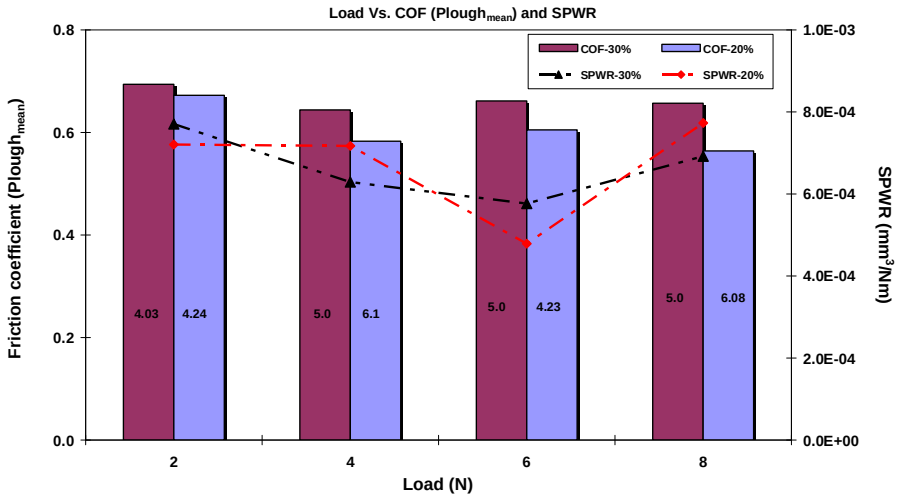

Figure 5.41 Ploughing COF and SPWR (R) against load of 5 µm coated substrates in dry test conditions at 0.24 m/s.

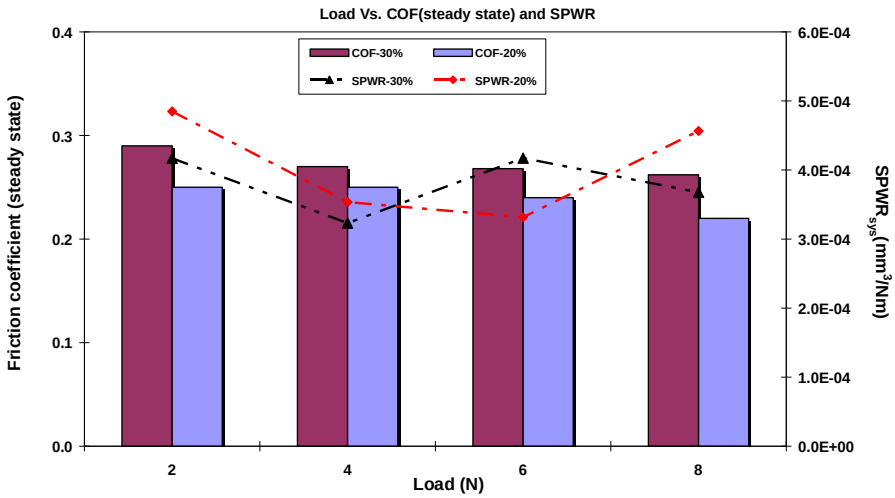

Figure 5.42 Steady state COF and system SPWR of 5 µm coated substrates in dry test conditions at 0.24 m/s.

The test results show that the ploughing COF of 5 μm coated 30% leaded bronze is slightly higher than that for 5 μm coated 20% leaded bronze. From table 5.36, the mean ploughing COF of 5 μm coated 30% leaded bronze at 0.24 m/s is 0.66 compared to 20% mean ploughing COF of 0.61. The running-in time for both materials decreases with increase in load and 5 μm coated 20% leaded bronze has a slightly higher running-in time than that of 5 μm coated 30% leaded bronze, probably due in part to higher coating thickness. The mean SPWR (R) of 5 μm coated 20% leaded bronze is 7.56E-04 compared to 5 μm coated 30% leaded bronze mean SPWR (R) of 5.79E-04. Table 5.37 shows that 5 μm coated 30% leaded bronze substrates had slightly higher steady state COF but lower SPWR than 5 μm coated 20% leaded bronze substrates in dry test conditions.

Table 5.36 Ploughing COF and SPWR (R) of 5 μm lead/indium coated substrates in dry test conditions.

Mat	Mean Plough friction (S.D)		Mean SPWR (S.D)	
	0.47 m/s	0.24 m/s	0.47 m/s	0.24 m/s
20%	0.58 (0.05)	0.61 (0.05)	7.56E-04 (1.62E-04)	6.72E-04 (1.32E-04)
30%	0.70 (0.02)	0.66 (0.02)	5.79E-04 (6.24E-05)	6.67E-04 (8.36E-05)

Table 5.37 Steady state COF and system SPWR of 5 μm lead/indium coated substrates in dry test conditions.

Mat	Mean Steady state COF (S.D)		Mean SPWR (S.D)	
	0.47 m/s	0.24 m/s	0.47 m/s	0.24 m/s
20%	0.28 (0.06)	0.24 (0.01)	1.51E-03 (1.45 E-04)	4.06E-04 (7.45E-05)
30%	0.35 (0.01)	0.27 (0.01)	1.37E-03 (6.74E-05)	3.82E-04 (4.52E-05)

Lubricated Test Conditions

(a) Sliding Velocity - 0.26 m/s, Speed - 125 rpm

The test results for the above conditions are detailed in table 5.38 and are plotted against load in figure 5.43 to figure 5.45

Table 5.38 COF and SPWR of 5 µm lead/indium coated substrates in marginally lubricated test conditions at 0.26 m/s.

Mat	Thick µm	Load N	I.P N/mm²	F.P N/mm²	PV N/mm².m/s	Plough COF (mean)	Steady state COF	SPWR (R) mm³/Nm	SPWR (system) mm³/Nm
30%	4.03	1	49.74	4.71	1.23	0.49	0.13	1.60E-06	4.10E-04
30%	5	2	78.60	7.07	1.85	0.48	0.12	1.38E-06	2.70E-04
30%	5	3	105.81	7.80	2.04	0.47	0.10	9.72E-07	2.01E-04
20%	6.1	1	49.74	6.58	1.72	0.53	0.17	2.76E-06	4.92E-04
20%	6.08	2	78.60	11.05	2.89	0.48	0.14	1.77E-06	2.33E-04
20%	5.6	3	105.81	7.80	2.04	0.44	0.11	1.09E-06	2.04E-04

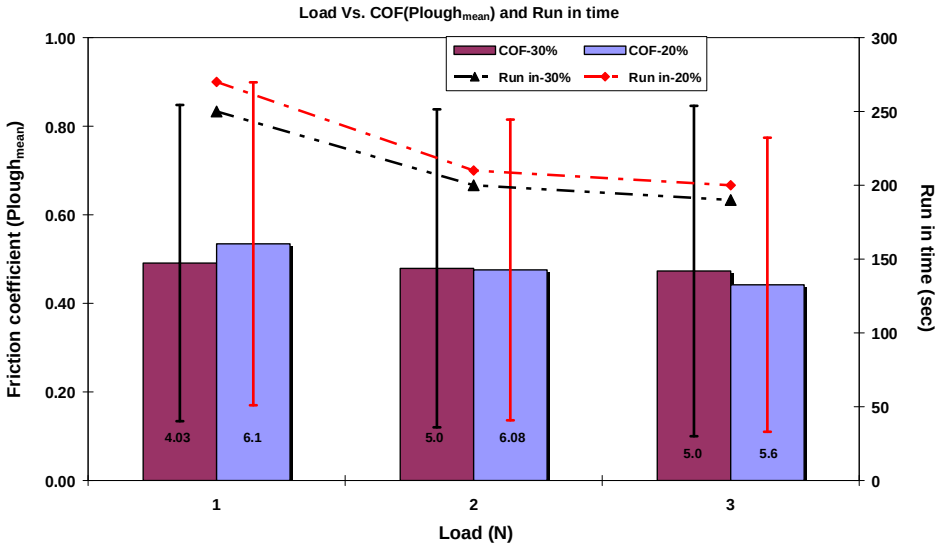

Figure 5.43 Ploughing COF and running-in time against load of 5 µm coated substrates in marginally lubricated test condition at 0.26 m/s.

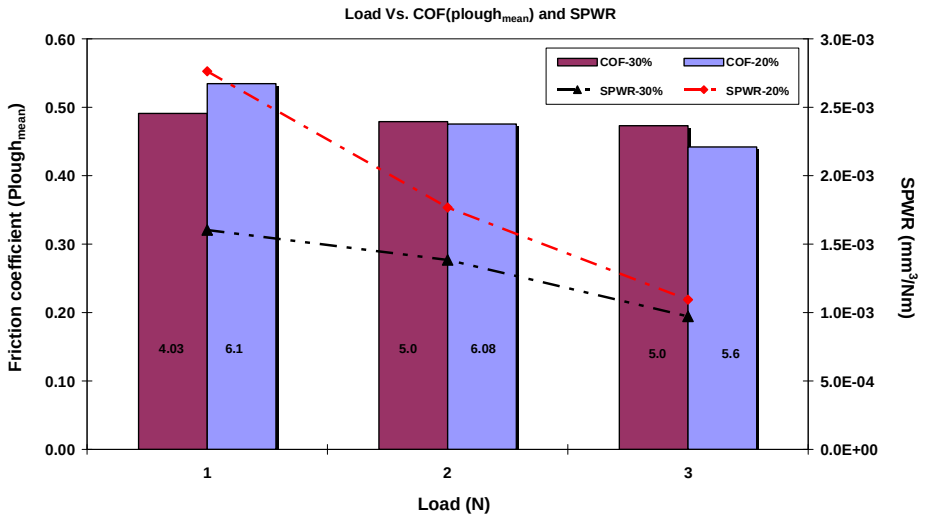

Figure 5.44 Ploughing COF and SPWR(R) against load of 5 µm coated substrates in marginally lubricated test conditions at 0.26 m/s.

From the above test results, the average ploughing COF and running-in time for both 5 µm coated leaded bronze substrates are very similar. Table 5.41 shows that the steady state COF and system SPWR of 5 µm coated 20% leaded bronze is higher than that of 5 µm coated 30% leaded bronze substrates.

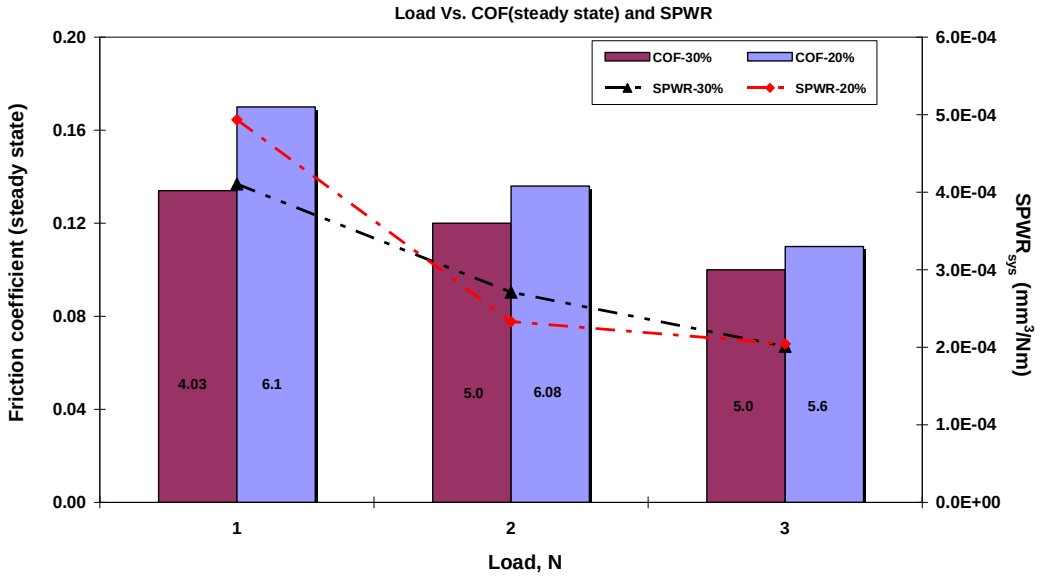

Figure 5.45 Steady state COF and system SPWR of 5 µm coated substrates in marginally lubricated test conditions at 0.24 m/s.

(b) Sliding Velocity - 0.13 m/s, Speed - 250 rpm

The test results for the above conditions are shown in table 5.39 and are plotted against load in figure 5.46 to figure 5.48

Table 5.39 COF and SPWR of 5 µm lead/indium coated substrates in marginally lubricated test conditions at 0.13 m/s.

Mat	Thick µm	Load N	I.P N/mm²	F.P N/mm²	PV N/mm².m/s	Plough COF (mean)	Steady state COF	SPWR (R) mm³/Nm	SPWR (system) mm³/Nm
30%	4.03	2	78.60	8.12	1.09	0.42	0.15	1.67E-03	1.82E-04
30%	5	4	132.57	14.15	1.90	0.40	0.12	1.19E-03	1.45E-04
30%	5	6	157.84	15.59	2.09	0.38	0.14	8.87E-04	1.36E-04
20%	6.1	2	78.60	10.19	1.37	0.44	0.16	2.33E-03	1.96E-04
20%	6.08	4	132.57	17.47	2.34	0.31	0.12	1.43E-03	1.39E-04
20%	5.6	6	157.84	28.25	3.79	0.39	0.12	9.11E-04	1.21E-04

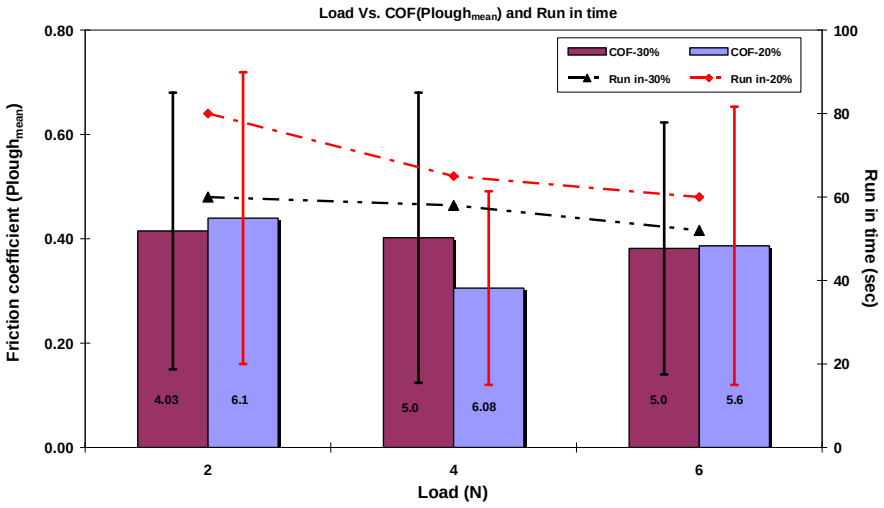

Figure 5.46 Ploughing COF and running-in time against load of 5 µm coated substrates in marginally lubricated test conditions at 0.13 m/s.

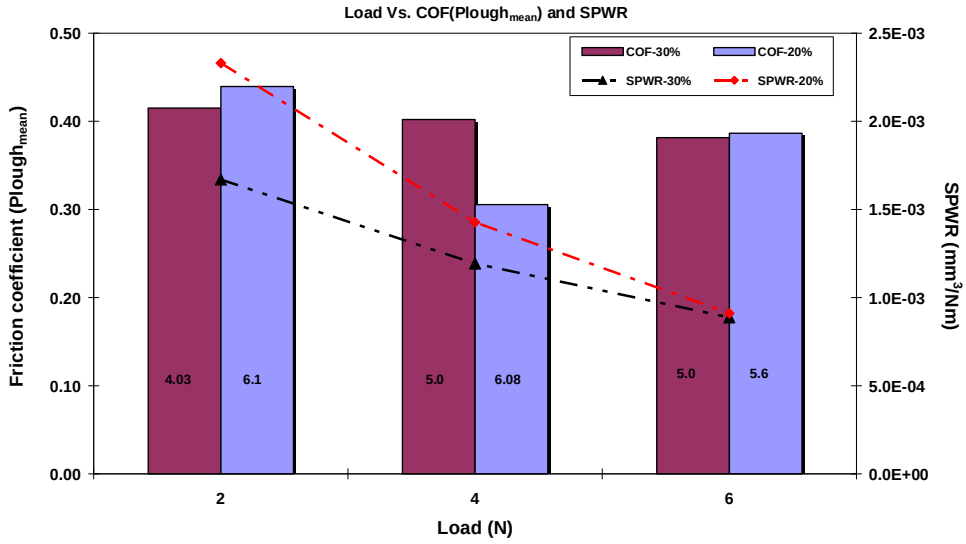

Figure 5.47 Ploughing COF and SPWR (R) against load of 5 µm coated substrates in marginally lubricated test conditions at 0.13 m/s.

Test results for this sliding velocity of 0.13 m/s show that the ploughing COF of both materials have similar values. In table 5.40 and 5.41, the average test results at all loads for the running-in period and steady state period are shown. From these tables it can be seen that the ploughing COF of 5 µm coated 20% leaded bronze is 0.38 compared to 5 µm coated 30% leaded bronze ploughing COF of 0.4. The mean SPWR (R) of 5 µm coated 20% leaded bronze is 1.55E-03 compared to 5 µm coated 30% leaded bronze mean SPWR (R) of 1.25E-03.

Steady state COF and system SPWR from the table 5.41 shows that both 5 µm coated substrates have very similar values.

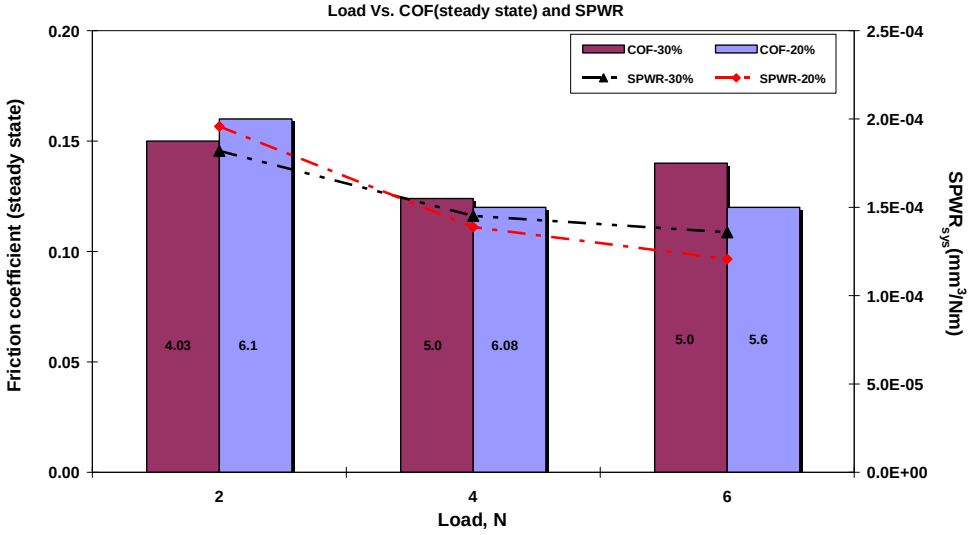

Figure 5.48 Steady state COF and system SPWR of 5 µm coated substrates in marginally lubricated test condition at 0.13 m/s.

Table 5.40 Mean COF and mean SPWR of 5 µm lead/indium coated substrates in marginally lubricated test conditions.

Mat	Mean Plough friction (S.D)		Mean SPWR (S.D)	
	0.26 m/s	0.13 m/s	0.26 m/s	0.13 m/s
20%	0.48 (0.04)	0.38 (0.06)	1.87E-03 (8.4E-04)	1.55E-03 (7.18E-04)
30%	0.48 (0.01)	0.40 (0.01)	1.32E-03 (3.21E-04)	1.25E-03 (3.94E-04)

Table 5.41 Mean COF and mean SPWR of 5 µm lead/indium coated substrates in marginally lubricated test conditions.

Mat	Mean Steady state COF (S.D)		Mean SPWR (S.D)	
	0.26 m/s	0.13 m/s	0.26 m/s	0.13 m/s
20%	0.14 (0.03)	0.13 (0.02)	3.1E-04 (1.59E-04)	1.52E-04 (3.92E-05)
30%	0.12 (0.01)	0.14 (0.01)	2.94E-04 (1.07E-04)	1.54E-04 (2.44E-05)

5.2.4 Comparison of COF and SPWR against Coating Thickness

The steady state COF and system SPWR of all test materials were compared according to their coating thickness at nominally similar contact conditions. Table 5.42 shows the test results of all test materials in dry and marginally lubricated test conditions at similar LV conditions. These test results were compared against the lead/indium coating thicknesses to identify the influence of coating thickness on friction and wear (if any).

Table 5.42 Comparing COF and SPWR against coating thickness in dry and marginally lubricated conditions.

Test condition	Mat	Thick µm	LV m/s	Mean steady state COF	Mean SPWR (system) mm^3/Nm
Dry	20%	0	1.18	0.29	1.50E-04
		1	1.18	0.22	2.38E-04
		5	1.18	0.26	9.61E-04
	30%	0	1.18	0.25	2.34E-04
		1	1.18	0.27	2.74E-04
		5	1.18	0.31	8.76E-04
Marginal lubrication	20%	0	0.65	0.12	1.03E-05
		1	0.65	0.11	1.37E-04
		5	0.65	0.14	1.63E-04
	30%	0	0.65	0.11	1.72E-05
		1	0.65	0.10	1.32E-04
		5	0.65	0.13	1.55E-04

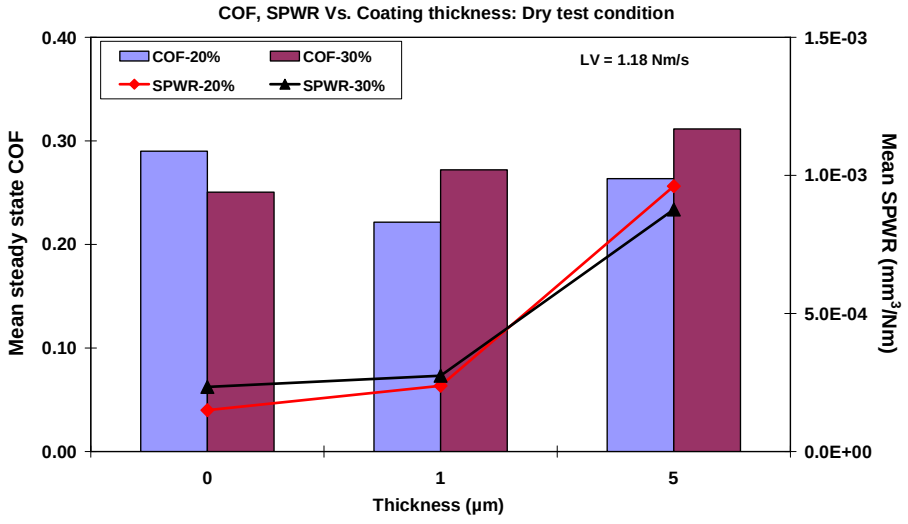

(a) Dry test conditions.

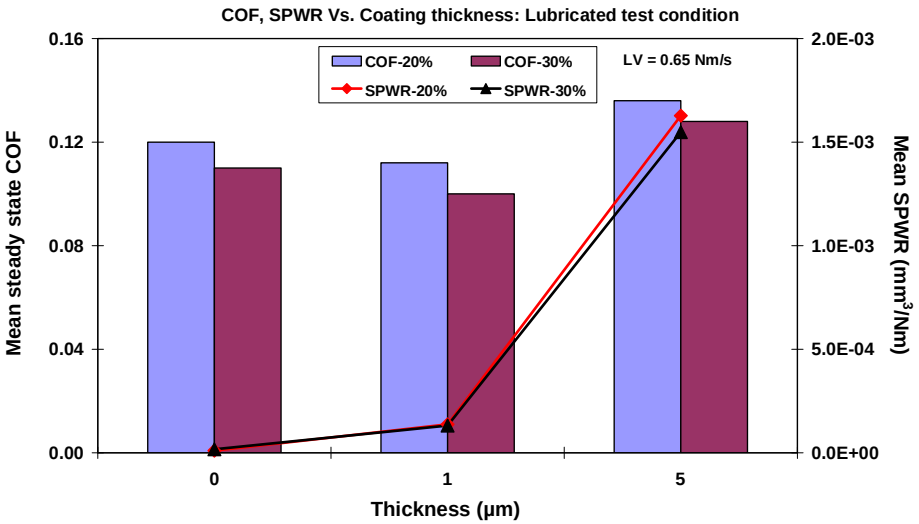

(b) Marginally lubricated test conditions

Figure 5.49 Comparing test results against coating thicknesses.

The test results show that uncoated leaded bronze substrates have better wear characteristics than lead/indium coated leaded bronze substrates in all test conditions. However, lead/indium coating reduced the COF when it was 1 µm thick but not when 5 µm thick. The 5 µm protected the substrate surfaces from wear which is not the case with 1 µm coating. 20% leaded bronze substrate has higher COF but lower wear rate than 30% leaded bronze substrates.

5.2.5 Examples of COF against Time Graph

Examples of COF against time graph recorded during the test process at different thicknesses of lead/indium in dry test conditions are shown below. All tests were conducted at similar contact conditions indicated in table 5.43. These graphs show the initial running-in period and steady state period in both test apparatus.

Table 5.43 Contact conditions used in TWT apparatus and POD apparatus for comparing test materials.

Test apparatus	Load (N)		Velocity (m/s)	
	Dry	Lubricated	Dry	Lubricated
TWT	58.86	58.86	0.12	2.94
POD	2	2	0.47	0.26

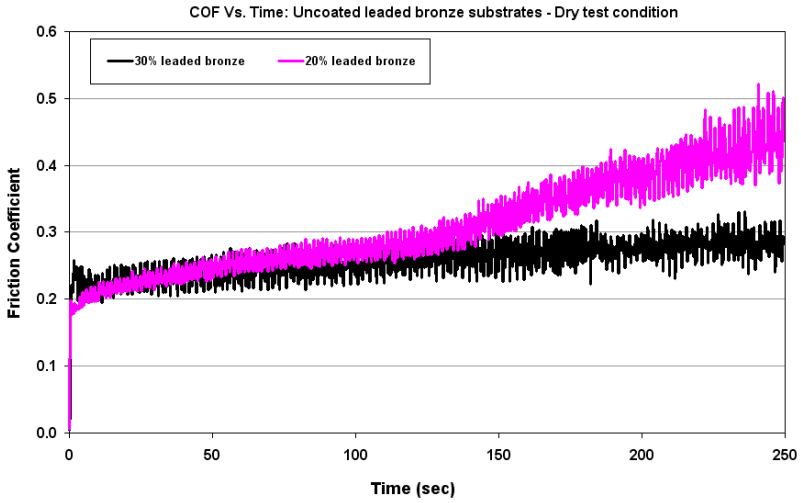

(a) Uncoated leaded bronze substrates.

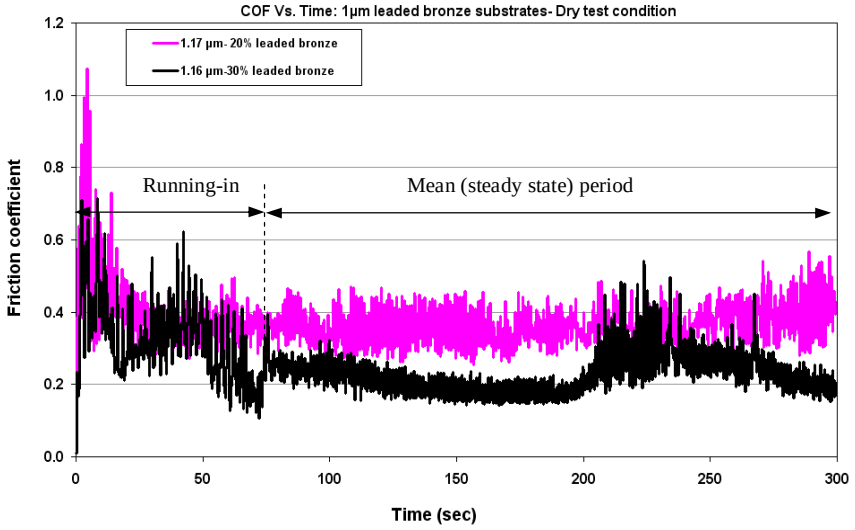

(b) 1 µm leaded bronze substrates.

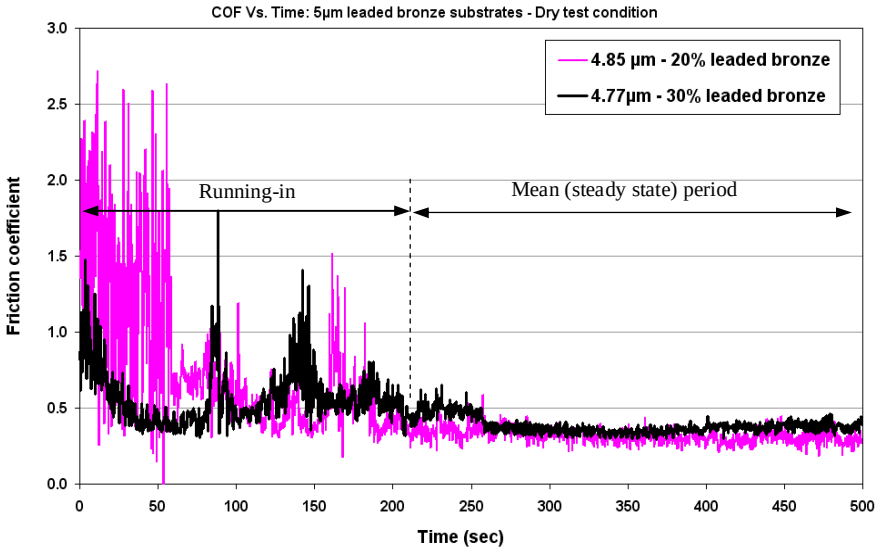

(c) 5 µm leaded bronze substrates.

Figure 5.50 Examples of friction-time graph in TWT apparatus.

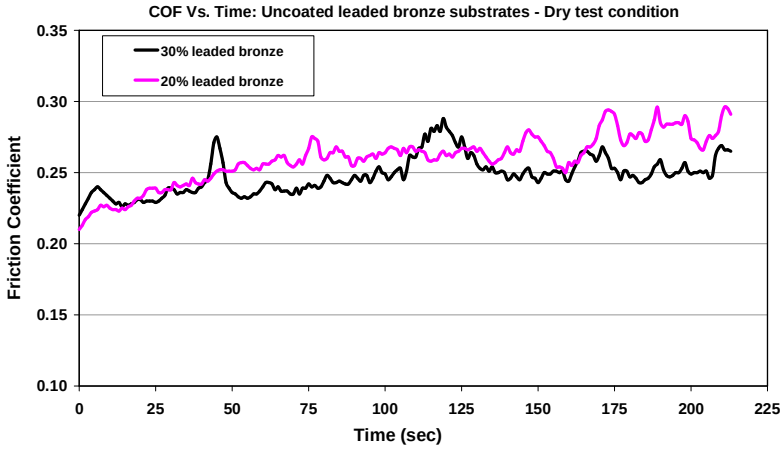

(a) Uncoated leaded bronze substrates.

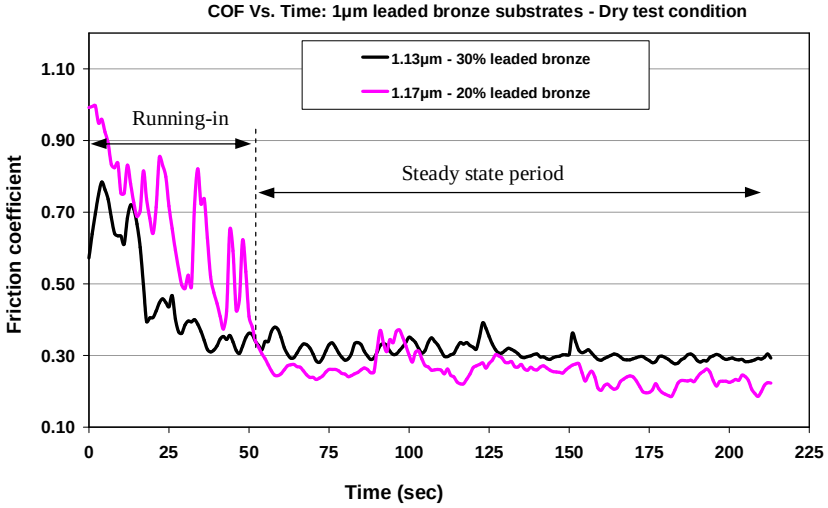

(b) 1 µm coated leaded bronze substrates.

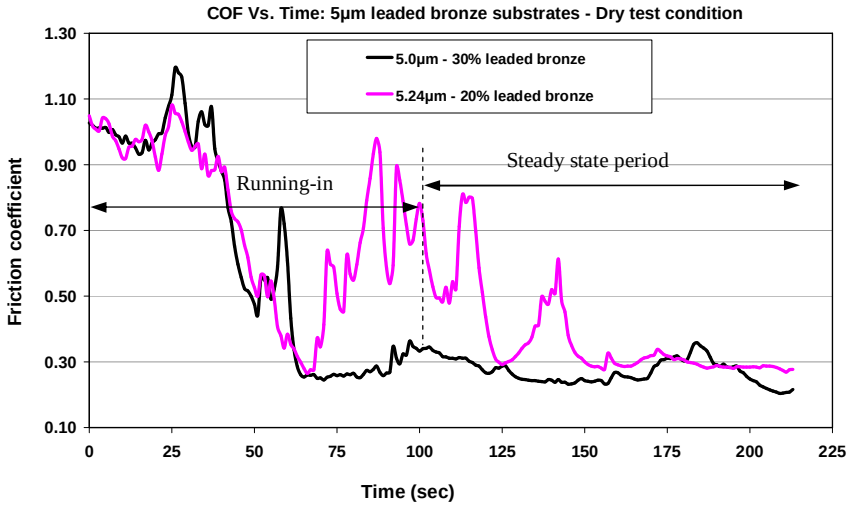

(c) 5 µm coated leaded bronze substrates.

Figure 5.51 Examples of friction-time graph in POD apparatus.

5.3 Frictional Heating Calculations

The flash temperatures and bulk temperatures were calculated from washer-disc contact and ball-disc contact, respectively in dry test conditions using Ashby's method (described in chapter 3.6.1). The main intention was to identify any evidence of melting of lead/indium alloy on leaded bronze substrates at various contact conditions so that effect of temperature on friction and wear could be identified. For temperature calculations on lead/indium coated leaded bronze substrates, all the thermal properties of the lead/indium coating were considered. However, the hardness of the coating was assumed to be equal to the hardness of the substrate. The physical and thermal properties of all test materials were detailed in table 4.4 of chapter 4.

5.3.1 Thrust Washer Test Apparatus

Predicted temperatures from TWT contact geometry are shown in Table 5.44 for various contact conditions. These temperatures were plotted against PV for different thicknesses of lead/indium alloy.

Table 5.44 Temperature measurements from TWT apparatus in dry test conditions at a sliding velocity of 0.12 m/s.

Test	Mat	Thick µm	Load N	PV N/mm².m/s	Mean plough COF[a]	Mean COF[b]	Q_1 watt	Q_2 watt	Flash temp[c] °C	Bulk temp[d] °C
23	20%	1.17	58.86	0.02	0.71	0.39	4.89	2.75	264	24
25	20%	1.19	78.48	0.02	0.66	0.37	6.06	3.40	247	25
27	20%	0.5	98.10	0.03	0.57	0.37	6.54	4.25	216	26
24	20%	1.32	117.72	0.03	0.60	0.35	8.26	4.82	226	27
43	30%	1.16	58.86	0.02	0.70	0.28	4.82	1.93	260	23
60	30%	0.81	78.48	0.02	0.60	0.29	5.51	2.66	226	24
52	30%	1.3	98.10	0.03	0.45	0.26	5.16	2.98	175	25
33	30%	0.56	117.72	0.03	0.42	0.32	5.78	4.41	164	27
47A	20%	4.85	58.86	0.02	0.76	0.32	5.23	2.91	281	24
51A	20%	4.94	78.48	0.02	0.80	0.30	7.35	3.93	295	26
49A	20%	4.93	98.10	0.03	0.87	0.33	9.30	5.11	298	28
48A	20%	3.89	117.72	0.03	0.84	0.33	11.29	6.20	302	29
17	30%	3.77	58.86	0.02	0.64	0.39	4.41	3.09	240	25
18	30%	5.5	78.48	0.02	0.61	0.36	5.60	3.82	255	26
19	30%	5.75	98.10	0.03	0.60	0.34	6.89	4.84	257	27
14	30%	4.37	117.72	0.03	0.80	0.50	11.02	6.34	295	29

* Q_1 – Heat generated from the ploughing COF, Q_2 – Heat generated from the mean COF, Temp – Temperature.

* a – The mean ploughing coefficient was taken as the reference parameter when predicting the flash heating.

b – The mean coefficient of friction was taken as the reference parameter when calculating the bulk heating.

c – The flash temperature was calculated using the effective diffusion lengths of washer and disc described in chapter 3.5.1. The ambient temperature was already added to the given flash temperature values in the table 5.44.

d – The bulk temperature was calculated using equation 3.20 and these bulk temperature values include the ambient temperature.

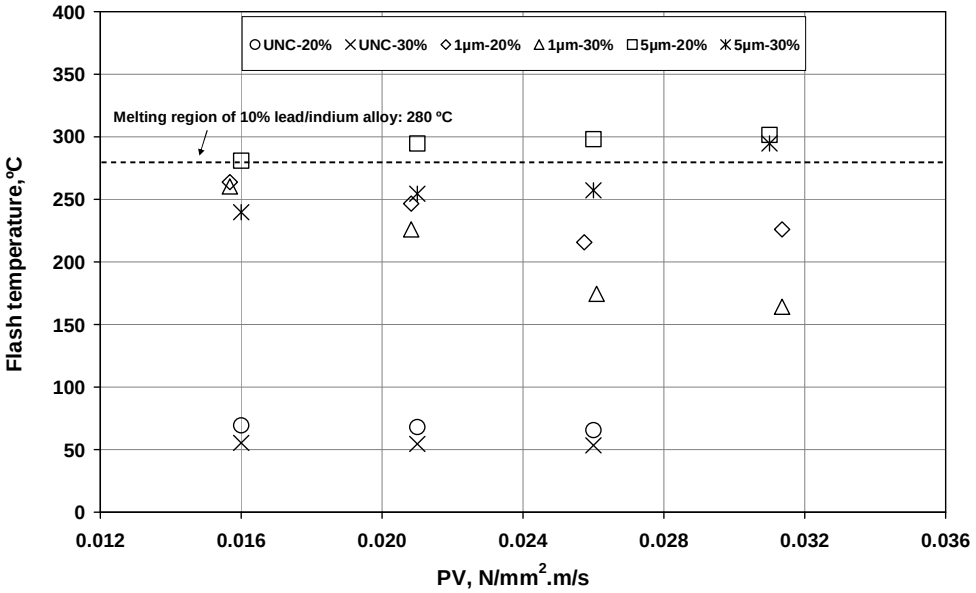

Figure 5.52 Flash temperatures against PV in TWT apparatus.

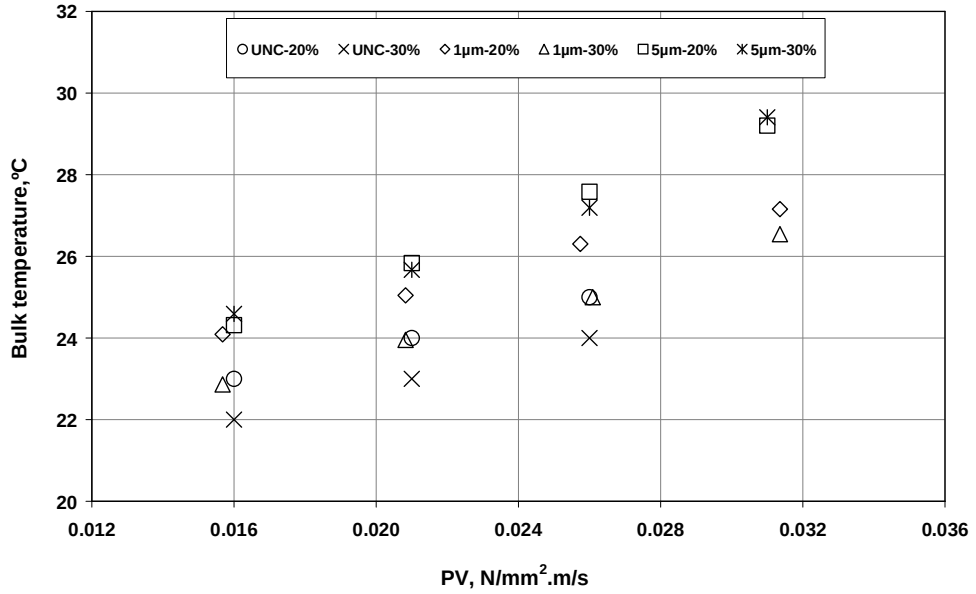

Figure 5.53 Bulk temperatures against PV in TWT apparatus.

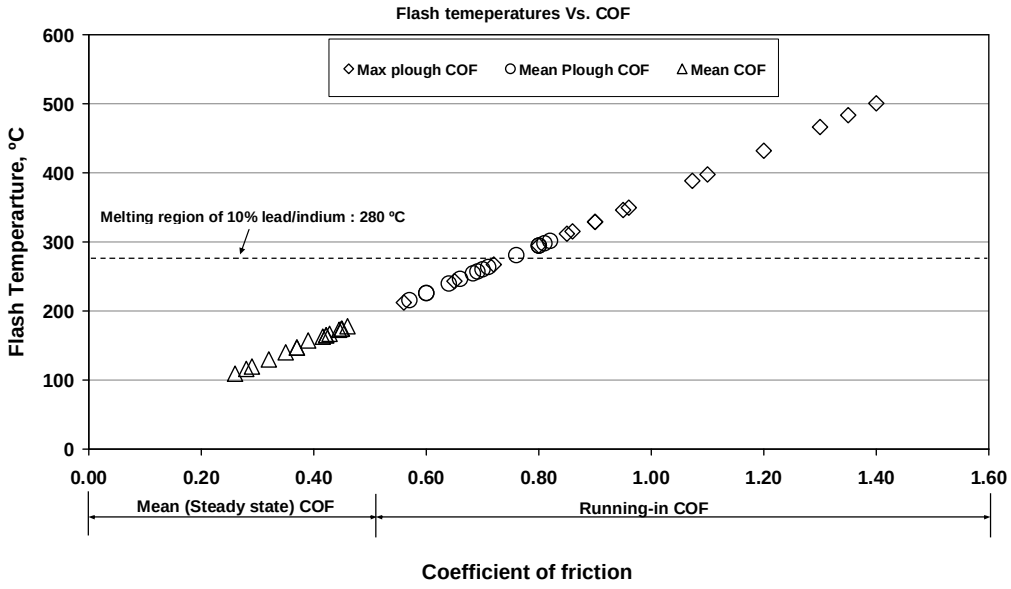

Figure 5.54 Flash temperatures at various stages of coefficient of friction.

Example Calculations from TWT Apparatus

Steps to calculate the flash and bulk temperatures of lead/indium coated leaded bronze substrates shown in table 5.43 are explained by taking an example of test number 23. The test conditions for test number 23 as shown in table 5.44 are: Load: 58.86 N, V: 0.12 m/s, mean ploughing COF: 0.71, mean COF: 0.39

Flash Temperature Calculations

Total heat generated, $Q = \mu FV = 0.71 \times 58.86 \times 0.12 = 4.89\ watt$

Where, μ represents the mean ploughing coefficient of friction.

$$\text{Real area of contact, } A_r = \frac{Load}{Hardness} = \frac{58.86}{0.39 \times 10^9} = 1.5 \times 10^{-7}\, m^2$$

(Note: As indicated in chapter 3.5 of contact pressure calculations that, for thin coatings on harder substrates, the hardness of coating was very close of the hardness of substrate. Therefore, A_r was measured using this assumption. Hardness of substrate was indicated in table 4.4 of chapter 4.3.2)

Heat generated at the real area of contact, q' is,

$$q' = \frac{\mu FV}{A_r} = \frac{4.89}{1.5 \times 10^{-7}} = 3.26 \times 10^7\, Wm^{-2}$$

Using equation 3.25 defined in chapter 3.6.1, at low sliding velocities, the equivalent diffusion lengths of washer and disc can be calculated as:

$$l_{1f} = l_{2f} = \frac{\pi^{\frac{1}{2}} a_r}{2}$$

Where, l_{1f} and l_{2f} are the equivalent diffusion lengths of washer and disc, respectively. a_r is the asperity contact radius calculated using the equation 3.26 defined by Ashby, et. al., (1990b) as:

$$a_r = \frac{0.1 \times 10^6}{H} = \frac{0.1 \times 10^6}{0.39 \times 10^9} = 2.55 \times 10^{-4} m$$

Therefore, $$l_{1f} = l_{2f} = \frac{\pi^{\frac{1}{2}} a_r}{2} = \frac{\pi^{\frac{1}{2}} \times 2.55 \times 10^{-4}}{2} = 2.26 \times 10^{-4} m$$

The flash temperature was calculated using the equation 3.22 as:

$$T_f - T_b^{'} = \frac{\mu F V}{A_r} \left(\frac{1}{\frac{k_1}{l_{1f}} + \frac{k_2}{l_{2f}}} \right) = \frac{3.26 \times 10^7}{\left(\frac{20.2}{2.26 \times 10^{-4}} + \frac{10}{2.26 \times 10^{-4}} \right)} = 244\ ^o C$$

$$T_f = T_b^{'} + 244 = 20 + 244 = 264^o C$$

Where, k_1 and k_2 are the thermal conductivities of washer and coating, respectively (These values were given in table 4.4 of chapter 4.3.2), and T'_b is the sink temperature for the heat flow from an asperity which is the ambient temperature.

Bulk Temperature Calculations

Total heat generated, $Q = \mu FV = 0.39 \times 58.86 \times 0.12 = 2.75\ watt$

Where, μ represents the mean coefficient of friction

Heat generated q, at the contacting interface per unit nominal contact area, A_n, obtained from equation 3.15 of chapter 3.6.1 as:

$$q = \frac{\mu FV}{A_n} = \frac{2.75}{439.8 \times 10^{-6}} = 6.25 \times 10^3 Wm^{-2}$$

Where A_n is the nominal contact area between the washer-disc interface, described in chapter 4.3.1.

The equivalent diffusion lengths of washer (1_{lb}) and disc (1_{2b}) can be calculated by Ashby's assumption, i.e. the thermal contact resistance often makes the effective diffusion length twice the physical diffusion length.

The measured physical lengths of washer and disc were: l_1 = 19 mm, l_2 = 5 mm
Therefore, 1_{lb} = 38 mm, l_{2b} = 10 mm.

The bulk temperature rise was calculated using equation 3.20 as:

$$T_b - T_o = \frac{\mu FV}{A_n}\left(\frac{1}{\frac{k_1}{l_{1b}} + \frac{k_2}{l_{2b}}}\right) = \frac{6.25 \times 10^3}{\left(\frac{20.2}{38 \times 10^{-3}} + \frac{10}{10 \times 10^{-3}}\right)} = 4^o C$$

$$T_b = T_o + 4 = 20 + 4 = 24^o C$$

Where k_1 and k_2 were the thermal conductivities of washer and coating, respectively and T_0 was the ambient temperature.

5.3.2 Pin on Disc Test Apparatus

In pin on disc test apparatus, the estimated flash and bulk temperature were separated according to the sliding velocities used. Table 5.45 and table 5.46 detailed the flash and bulk temperatures for two different sliding velocities and the results were plotted against LV when comparing different test materials in dry test conditions. As indicated earlier, the mean ploughing COF was taken as the reference parameter for the flash heating and steady state (mean) COF for the bulk heating calculations using the Ashby's method. Figure 5.56 schematically shows the flash temperatures against various regimes of coefficient of friction.

Table 5.45 Temperature calculations from lead/indium coated leaded bronze substrates in dry test conditions in POD test apparatus at a sliding velocity of 0.47 m/s.

Test	Mat	Thick µm	Load N	PV N/mm².m/s	Mean Plough COF[a]	Mean COF[b]	Q_1 watt	Q_2 watt	Flash temp[c] ºC	Bulk Temp[d] ºC
26	20%	1	1	23.44	0.66	0.27	0.31	0.13	406	30
23	20%	1.17	2	17.75	0.62	0.24	0.58	0.23	384	30
25	20%	1.19	3	17.58	0.62	0.23	0.88	0.33	384	32
24	20%	1.32	4	13.61	0.56	0.19	1.05	0.36	349	29
20	20%	6.1	2	1.88	0.63	0.35	0.59	0.33	390	24
21	20%	6.08	3	2.32	0.59	0.28	0.84	0.40	368	24
22	20%	5.6	4	2.60	0.53	0.23	0.99	0.43	330	24
6	30%	1	1	18.52	0.66	0.32	0.31	0.15	407	31
8	30%	1.13	2	13.34	0.54	0.30	0.51	0.28	339	31
46	30%	0.94	3	12.47	0.54	0.28	0.76	0.39	338	31
9	30%	0.8	4	11.34	0.52	0.28	0.98	0.53	327	32
13	30%	4.03	2	1.88	0.70	0.39	0.66	0.37	433	24
67	30%	5.00	3	2.22	0.72	0.36	1.02	0.50	446	25
68	30%	5.00	4	2.40	0.70	0.35	1.33	0.66	434	26

Table 5.46 Temperature calculations from lead/indium coated leaded bronze substrates in dry test conditions in POD test apparatus at a constant sliding velocity of 0.24 m/s.

Test	Mat	Thick µm	Load N	PV N/mm².m/s	Mean Plough COF[a]	Mean COF[b]	Q_1 watt	Q_2 watt	Flash Temp[c] ºC	Bulk Temp[d] ºC
26	20%	1	2	10.42	0.42	0.22	0.20	0.10	143	26
23	20%	1.17	4	9.26	0.52	0.21	0.49	0.20	173	27
25	20%	1.19	6	9.30	0.41	0.20	0.58	0.28	140	28
24	20%	1.32	8	10.42	0.42	0.21	0.80	0.40	145	30
56A	20%	4.24	2	2.40	0.67	0.25	0.32	0.12	218	23
20	20%	6.1	4	2.45	0.58	0.25	0.55	0.24	191	24
59A	20%	4.23	6	3.20	0.61	0.24	0.86	0.34	198	25
21	20%	6.08	8	2.96	0.56	0.22	1.06	0.41	186	25
6	30%	1.19	2	5.86	0.41	0.27	0.19	0.13	141	25
8	30%	1.13	4	6.20	0.38	0.26	0.36	0.25	131	27
46	30%	0.94	6	7.81	0.32	0.24	0.45	0.34	113	28
9	30%	0.8	8	8.88	0.41	0.23	0.77	0.44	139	30
13	30%	4.03	2	2.22	0.69	0.29	0.33	0.14	224	23
66	30%	5.00	4	1.87	0.64	0.27	0.61	0.25	209	24
67	30%	5.00	6	2.22	0.66	0.27	0.94	0.38	215	25
68	30%	5.00	8	2.40	0.66	0.26	1.24	0.49	213	25

* Mat – Material, Thick – Coating thickness, P – Final contact pressure, PV – Pressure X Velocity, Plough COF – Ploughing coefficient of friction, Q_1 – Heat generated from the ploughing COF, Q_2 – Heat generated from the mean COF, Temp – Temperature.

* a – The mean ploughing coefficient was taken as the reference parameter when calculating the flash heating.

b – The mean (steady state) coefficient of friction was taken as the reference parameter when calculating the bulk heating.

c – The flash temperature was calculated using the effective diffusion lengths of washer and disc described in chapter 3.6.1.

d – The bulk temperatures were calculated using equation 3.21.

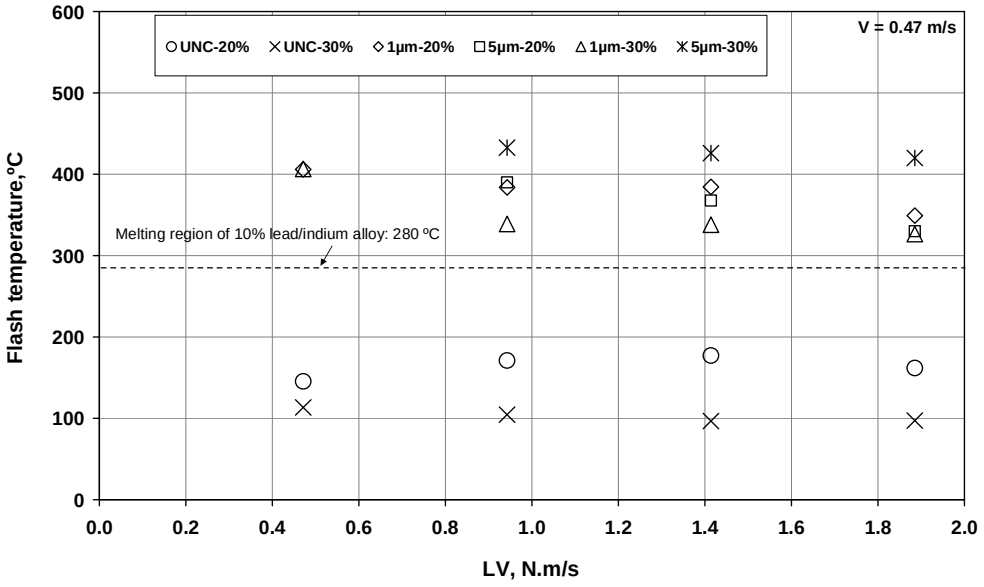

Figure 5.55 Flash temperatures against LV in POD test apparatus at 0.47 m/s.

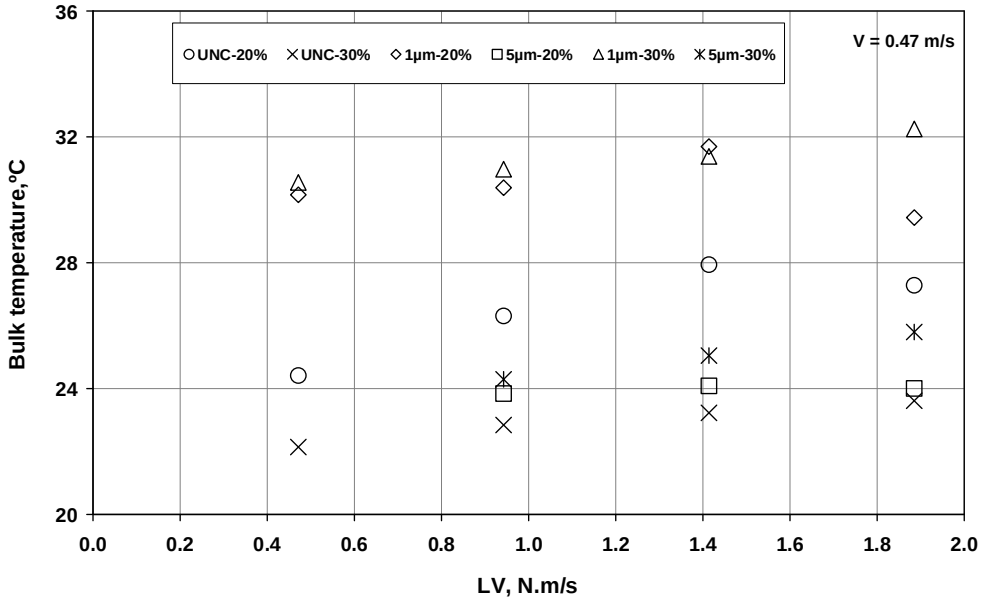

Figure 5.56 Bulk temperatures against LV in POD test apparatus at 0.47 m/s.

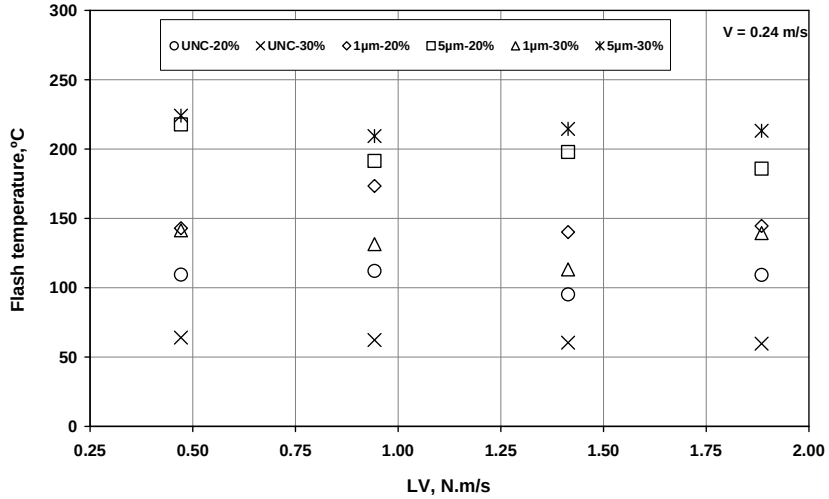

Figure 5.57 Flash temperatures against LV in POD test apparatus at 0.24 m/s.

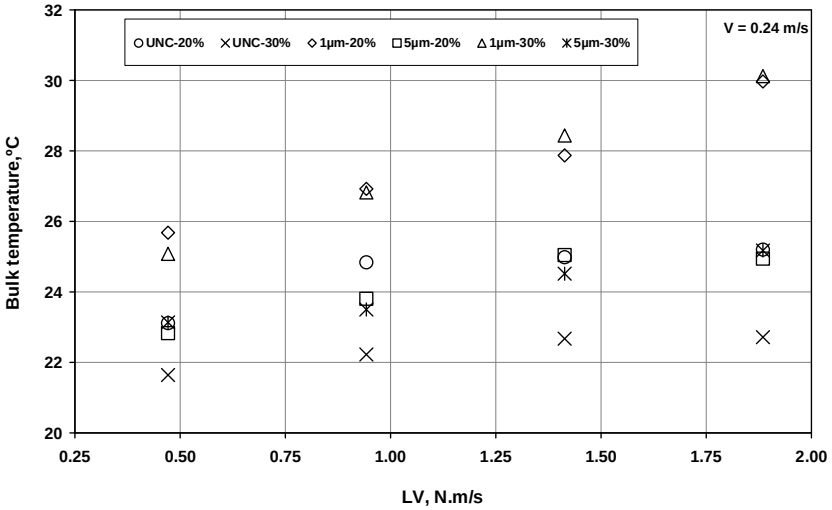

Figure 5.58 Bulk temperatures against LV in POD test apparatus at 0.24 m/s.

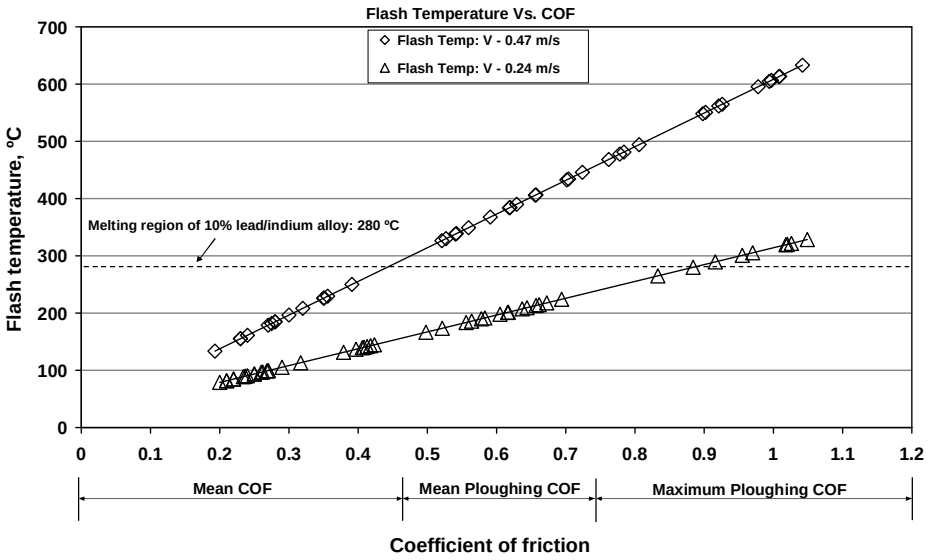

Figure 5.59 Flash temperatures at different sliding velocities in POD apparatus.

Example Calculations from POD apparatus

The frictional heating calculations on ball on disc contact geometry were done in exactly the same way as described for thrust washer test contact. However, the effective diffusion lengths of ball and disc have a considerable difference from washer and disc lengths.

Flash Temperature Calculations

Considering test number: 26 from table 5.45, where, *F*: 1N, *V*: 0.47 m/s, mean ploughing COF: 0.66, mean COF: 0.27.

Heat generated at the real area of contact, q' is,

$$q' = \frac{\mu FV}{A_r} = \frac{0.66 \times 1 \times 0.47}{\left(\frac{1}{0.39 \times 10^9}\right)} = 0.12 \times 10^9 \, Wm^{-2}$$

The real area of contact, A_r was calculated from the load-hardness ratio. As indicated in chapter 3.5 of contact pressure calculations that, for thin coatings on harder substrates, the hardness of coating was very close to the hardness of substrate and this assumption was applied in here also.

Using the equations 3.25, the effective diffusion lengths of ball and disc were calculated as:

$$l_{1f} = l_{2f} = \frac{\pi^{\frac{1}{2}} a_r}{2}$$

Where, l_{1f} and l_{2f} are the equivalent diffusion length of ball and disc, respectively, and a_r is the asperity contact radius calculated using equation 3.26.

$$a_r = \frac{0.1 \times 10^6}{H} = \frac{0.1 \times 10^6}{0.39 \times 10^9} = 2.55 \times 10^{-4} m$$

Therefore, $$l_{1f} = l_{2f} = \frac{\pi^{\frac{1}{2}} a_r}{2} = \frac{\pi^{\frac{1}{2}} \times 2.55 \times 10^{-4}}{2} = 2.26 \times 10^{-4} m$$

The flash temperature was calculated using equation 3.27 as:

$$T_f - T_b^{'} = \frac{\mu F V}{A_r}\left(\frac{1}{\frac{k_1}{l_{1f}} + \frac{k_2}{l_{2f}}}\right) = \frac{0.12 \times 10^9}{\left(\frac{61}{2.26 \times 10^{-4}} + \frac{10}{2.26 \times 10^{-4}}\right)} = 386 \, ^o C$$

$$T_f = T_b^{'} + 382 = 20 + 386 = 406^o C$$

Where, k_1 and k_2 are the thermal conductivities of washer and coating, respectively, and T'_b is the sink temperature for the heat flow from an asperity which is the ambient temperature.

Bulk Temperature Calculations

Heat generated q, at the contacting interface per unit nominal contact area, A_n, obtained from equation 3.17 as:

$$q = \frac{\mu FV}{A_n} = \frac{0.27 \times 1 \times 0.47}{2.01 \times 10^{-8}} = 0.63 \times 10^7 \ Wm^{-2}$$

Where A_n is the nominal contact area between the ball-disc interface measured from the contact dimensions using Talysurf profilometer.

The effective diffusion lengths of ball and disc were calculated using the equations 3.19 and 3.20 described in chapter 3.6.1.

$$l_{1b} = 2a = 2 \times 8 \times 10^{-5} = 16 \times 10^{-5} m$$

Where l_{1b} was the effective diffusion length of the ball and a, the contact radius obtained from the nominal area of contact. Ashby's assumption of effective length of ball, which is the twice contact radius was used here.

$$l_{2b} = \frac{a}{\pi^{\frac{1}{2}}} tan^{-1}\left[\left(\frac{2\pi\alpha_2}{aV}\right)^{\frac{1}{2}}\right] = \frac{8 \times 10^{-5}}{\pi^{\frac{1}{2}}} tan^{-1}\left[\left(\frac{2\pi \times 6.7 \times 10^{-6}}{8 \times 10^{-5} \times 0.47}\right)^{\frac{1}{2}}\right] = 4.14 \times 10^{-5} m$$

Where, l_{2b} was the effective diffusion length of disc and α_2 was the thermal diffusivity of the coating.

The bulk temperature was calculated using the equation 3.21 as:

$$T_b - T_o = \frac{\mu FV}{A_n}\left(\frac{1}{\frac{k_1}{l_{1b}} + \frac{k_2}{l_{2b}}}\right) = \frac{0.63 \times 10^7}{\left(\frac{61}{16 \times 10^{-5}} + \frac{10}{4.14 \times 10^{-5}}\right)} = 10^o C$$

$$T_b = T_o + 6 = 20 + 10 = 30^o C$$

Where k_1 and k_2 were the thermal conductivities of ball and coating, respectively.

5.4 Toughmet Substrates and Graphit-ic Coatings

The earlier test results on leaded bronze substrates show moderate friction but high wear rates, and the use of lead/indium coating does not provide the necessary protection for the substrate materials. Therefore attention has been focussed on a small number of candidate materials that could potentially replace the lead based bearing materials and offer improved friction and wear properties. Also, due to the environmentally damaging nature of the lead-based materials, it is desirable to replace these with a more suitable bearing material. Toughmet substrates, and Graphit-ic and Chromium Graphit-ic coatings were chosen and were supplied by AECS (2009). As described in chapter 4.6.1, a small selection of these materials were tested on POD apparatus and TWT apparatus 2 for their tribological properties using similar test conditions to those used for the lead based materials in dry test conditions. It is planned that these new materials will be investigated in much more detail in further work to establish them finally as potential replacements for lead-based bearing materials. The preliminary results for the newly tested Toughmet and Graphit-ic based materials are described in this section and test results are discussed in chapter 6.

5.4.1 Toughmet Substrates

Toughmet is a copper-nickel-tin based alloy with high strength, corrosion resistance, and wear resistance under high load contact conditions. Toughmet is claimed to have a PV limit twice those of the most conventional bearing materials (Brush Wellman, 2009). Two different types of Toughmet alloys: Toughmet CX-105 and Toughmet AT-110 were tested in dry test conditions. Toughmet AT-110 contains 15% nickel, 8% tin and balance copper whereas Toughmet CX-105 contains 9% nickel, 6% tin and balance copper. The hardness of CX-105 and AT-110 supplied were 280 HV and 300 HV, respectively. The operating test conditions used on Toughmet substrates were detailed in chapter 4.6.1. The test results of Toughmet substrates from TWT apparatus 2 are shown in table 5.47.

Table 5.47 Mean COF and SPWR of Toughmet CX-105 and AT-110 in dry test conditions at 0.17 m/s.

Mat	Load (N)	P N/mm^2	PV (N/mm^2.m/s)	Mean COF	Vol (mm^3)	SPWR (system) (mm^3/Nm)
AT 110-1	49.05	0.17	0.03	0.65	0.45	8.7E-05
AT 110-3	98.1	0.34	0.06	0.66	0.68	6.69E-05
AT 110-5	49.05	0.17	0.03	0.68	0.48	9.44E-05
AT 110-8	98.1	0.34	0.06	0.67	0.74	7.24E-05
CX105-3	49.05	0.17	0.03	0.63	0.55	1.08E-04
CX105-5	98.1	0.34	0.06	0.66	0.89	8.78E-05
CX105-7	49.05	0.17	0.03	0.63	0.57	1.12E-04
CX105-9	98.1	0.34	0.06	0.64	0.87	8.56E-05

* Mat - Material, P – Initial Pressure, V – Velocity, PV – Pressure X Velocity, COF – Coefficient of friction, Vol – Volume loss of test specimen, SPWR – Specific wear rate.

In the table 5.47, the mean COF corresponds to the average COF recorded over the time period considered from the COF against time graph. The system SPWR corresponds to the wear rate over the total time period considered and included both wear rates of substrate and counterface. The contact pressure was calculated by taking the ratio between the normal load applied to the circumferential contact area and the SPWR was evaluated using the gravimetric method described in chapter 4.4.4.

Test results from table 5.47 show that the mean COF and SPWR of both test materials are approximately constant at similar PV conditions. Both Toughmet substrate materials had similar results in terms of COF but Toughmet CX-105 has slightly higher SPWR than AT-110. To compare these test materials schematically, the test results at a nominally similar PV conditions among different types of Toughmet substrates were averaged and results are tabulated in table 5.48. These average test results are plotted against PV in figure 5.60 to compare both Toughmet substrates in dry test conditions.

Table 5.48 Mean COF and SPWR at change in PV of Toughmet substrates.

Mat	PV N/mm².m/s	Mean COF	SPWR (system) mm³/Nm
AT-110	0.03	0.66	9.11E-05
	0.06	0.67	6.97E-05
CX-105	0.03	0.63	1.1E-04
	0.06	0.64	8.67E-05

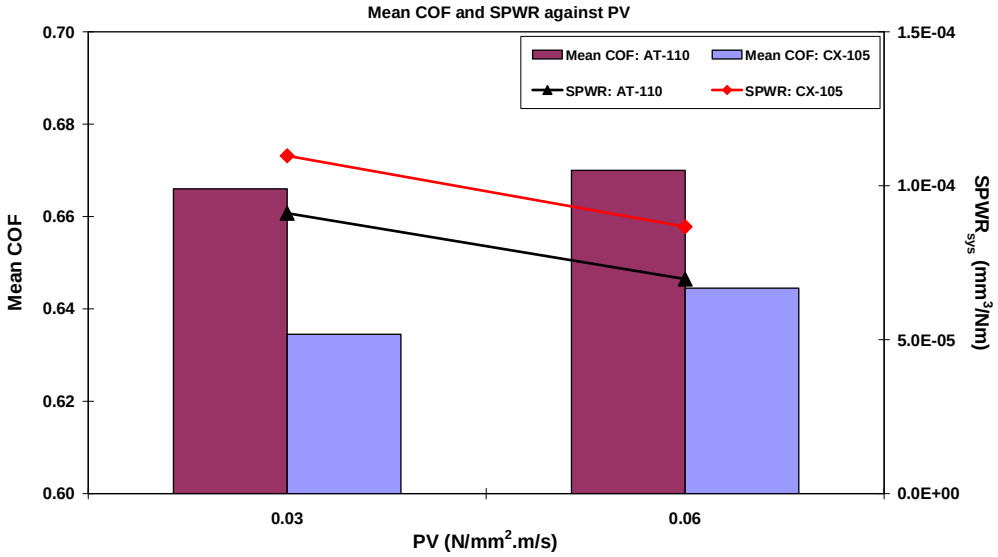

Figure 5.60 Mean COF and SPWR against PV of Toughmet substrates.

It can be seen from figure 5.60 that the mean COF and SPWR of both Toughmet substrates were approximately constant at an increase in PV. In particular, Toughmet AT-110 has slightly higher COF but lower SPWR than Toughmet CX-105. However, by considering the standard deviation of these results, this difference may not be significant.

Example of COF against Time Graph

Examples of COF against time of both Toughmet substrates at similar contact conditions are shown in the figure 5.61. The contact pressure and sliding velocity used were 0.17 N/mm^2 and 0.17 m/s respectively for both materials. Figure 5.61

show that both Toughmet substrates had similar and approximately constant COF in the steady state region.

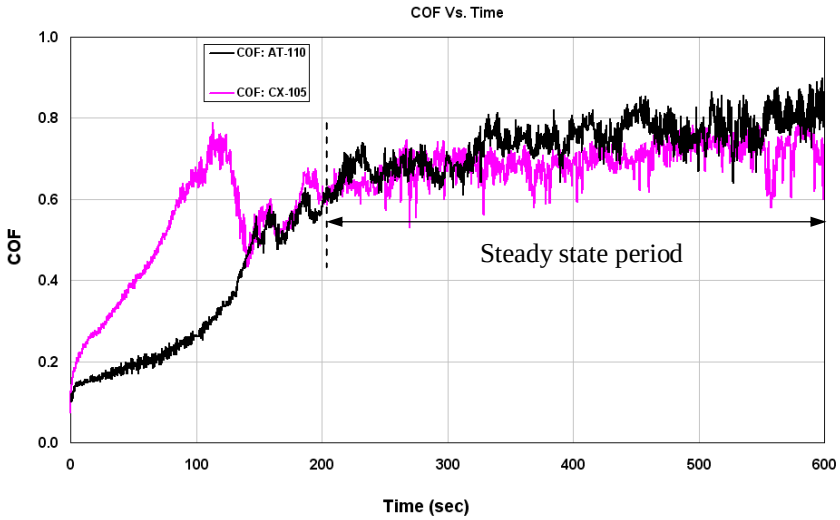

Figure 5.61 An example of COF against time in Toughmet substrates.

Observations Recorded During the Test Process

When conducting the friction and wear tests on Toughmet test specimens, some of the observations recorded from the specimen-washer contacts and friction against time graphs are briefly described below. By considering the friction against time graph of AT-110 as shown in figure 5.61, the main observations recorded were as follows.

- The test process started very smoothly without any high frictional noise from the sample-counterface contact. However, as the test continued, a whistling sound was observed, consistent with the gradual increase of friction coefficient with time.
- The whistling sound stopped around 150 sec and, from then on, a continuous rubbing noise was observed from the specimen-washer contact. This coincided with a substantial increase in friction and fluctuations in the friction curve. During this time there was also considerable wear of the test material.
- The worn material on the test surface was spread throughout its wear track. A typical appearance of a worn specimen is shown in figure 5.62
- It is believed that the worn material in the form of loose debris trapped between the contacting surfaces during the test process and increased the coefficient of friction.

- After wiping out the loose debris on the test specimen, it was identified that the surface of the test specimen on the worn area was polished rather than deeply worn.

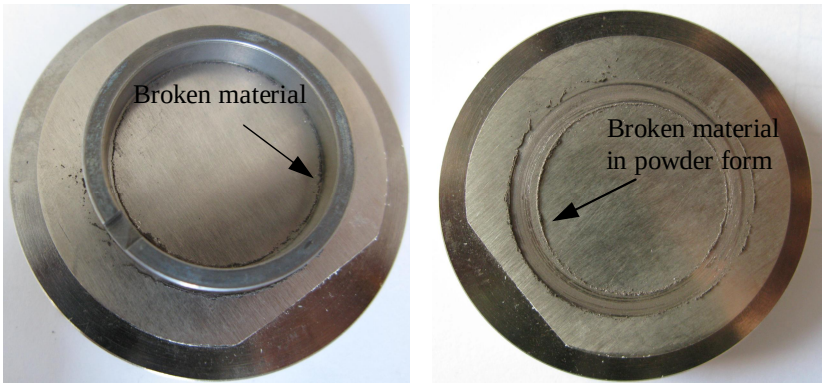

(a) (b)

Figure 5.62 Worn Toughmet specimens after test (a) Metallic powder present at specimen–washer contact (b) Metallic powder spread (in the form of loose debris) after removing the washer from the contact.

5.4.2 Graphit-ic and Chromium Graphit-ic Coatings

As a possible replacement for lead/indium coatings, two type of coatings, Graphit-ic (AT110-20D) and Chromium Graphit-ic (AT110-16D) coatings were tested on TWT apparatus 2 in dry test conditions. Only a small number of tests were conducted keeping the similar test conditions to those used on lead/indium coatings. The main aim was to make a preliminary assessment of their tribological properties compared with those of the lead/indium coatings. These new coatings were deposited on the Toughmet substrates described earlier. The thickness of the Graphit-ic based coatings was about 2.5 µm. The hardness of the Graphit-ic and Chromium Graphit-ic coatings varied from 1700 HV to 2000 HV. In particular, the hardness of Graphit-ic was higher than Chromium Graphit-ic coating. These coating were supplied by AECS (2009) and the actual coatings were deposited by Teer coatings Ltd (2009). Additional information on these coating materials can be obtained from Teer coatings Ltd (2009).

(a) Thrust Washer Test Results

Both Graphit-ic (AT110-20D) and Chromium Graphit-ic (AT110-16D) coatings were tested on TWT apparatus 2 in dry test conditions. The operating test conditions used on Graphit-ic based coatings were detailed in table 4.13 of chapter 4. The mean COF in each test for both test materials was the average COF recorded for the entire duration of the test and the SPWR corresponds to the wear of the total system.

The SPWR was calculated by the gravimetric method since Talysurf profiles were not able to identify wear grooves on the tested coatings as the tips of the coating material were polished rather than worn deeply. The test results from both the test materials are shown in table 5.49 and the test results are compared against the PV in figure 5.63 and 5.64.

Table 5.49 Thrust washer results of Graphit-ic and Chromium Graphit-ic coatings.

Mat	P (N/mm^2)	Speed (rpm)	V (m/s)	Dist (m)	PV ($N/mm^2.m/s$)	Mean COF	SPWR (system) (mm^3/Nm)
AT110-20D	0.17	50	0.09	77.9	0.01	0.24	2.14E-05
	0.17	100	0.17	155.8	0.03	0.27	2.14E-05
	0.17	150	0.26	233.8	0.04	0.29	2.49E-05
	0.17	200	0.35	311.7	0.06	0.26	2.14E-05
	0.17	250	0.43	389.6	0.07	0.30	1.92E-05
AT110-16D	0.17	50	0.06	54.3	0.01	0.28	1.60E-05
	0.17	100	0.12	108.7	0.02	0.25	1.99E-05
	0.17	150	0.18	163.1	0.03	0.32	1.86E-05
	0.17	200	0.24	217.4	0.04	0.27	1.60E-05
	0.17	250	0.30	271.8	0.05	0.31	1.76E-05

* Dist – Distance travelled.

The mean COF and SPWR results from table 5.50 are plotted against PV in figure 5.63 and figure 5.64 as shown below.

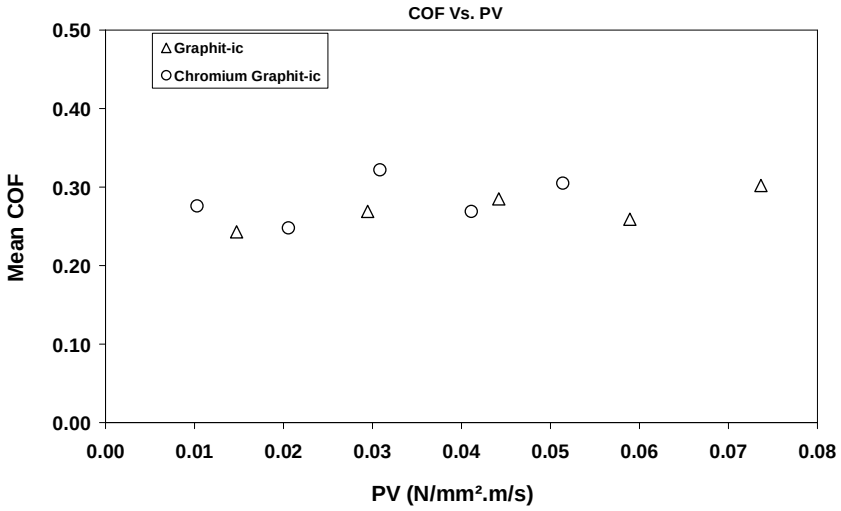

Figure 5.63 Mean COF against PV of Graphit-ic based coatings.

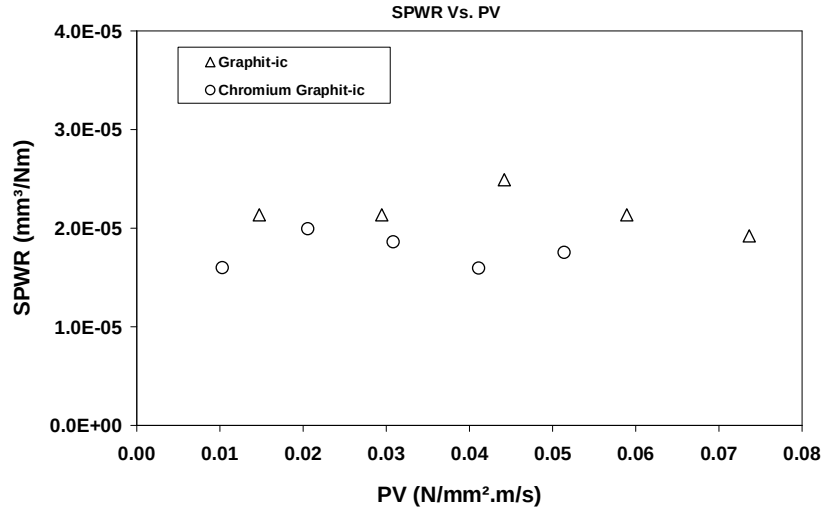

Figure 5.64 System SPWR against PV of Graphit-ic based coatings.

The above test results show that both coatings have similar COF and SPWR when PV increases. In particular, Chromium Graphit-ic coatings have slightly lower wear rates than Graphit-ic coatings at each contact pressure. By averaging all the test results at all PV conditions, the mean COF for Graphitic and Chromium Graphit-ic are 0.27 and 0.29, respectively, whereas the mean SPWR for both coatings are 2.20E-05 and 1.44E-05, respectively.

Observations Recorded During Test Process

Some of the observations recorded during the friction and wear testing of AT110-16D and status of worn test specimen after the end of test are briefly summarized below.

- The coating was not broken completely in any of the tests conducted but a significant amount of wear debris was spread throughout the contacting surfaces as shown in figure 5.65 (a).
- Figure 5.65 (b) shows the wear debris in the form of loose black powder spread throughout after the test but still the coating was not broken (figure 5.65 (c)).
- Also, due to the sharp outer edges from the washer surface, the coating was scratched severely at some areas which led to further removal of wear debris from the coating surface.
- The loose black powder appeared to be smeared and adhered strongly along the circumference of the test specimen as shown in figure 5.65 (d)
- The SEM/EDAX analysis on loose black powder reveal that the counterface material had worn severely and high iron content was present in the black powder as shown in figure 5.65 (e).

(a)

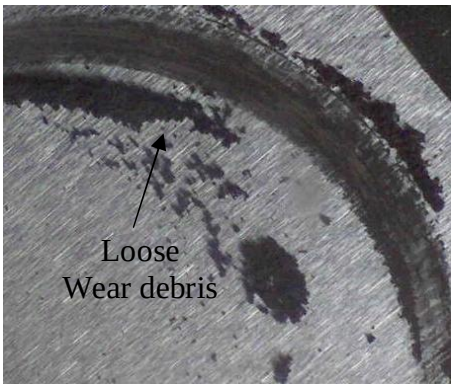

(b)

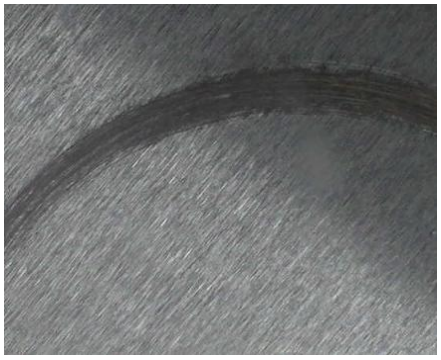

(c)

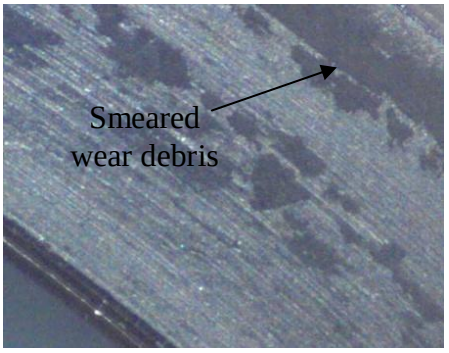

(d)

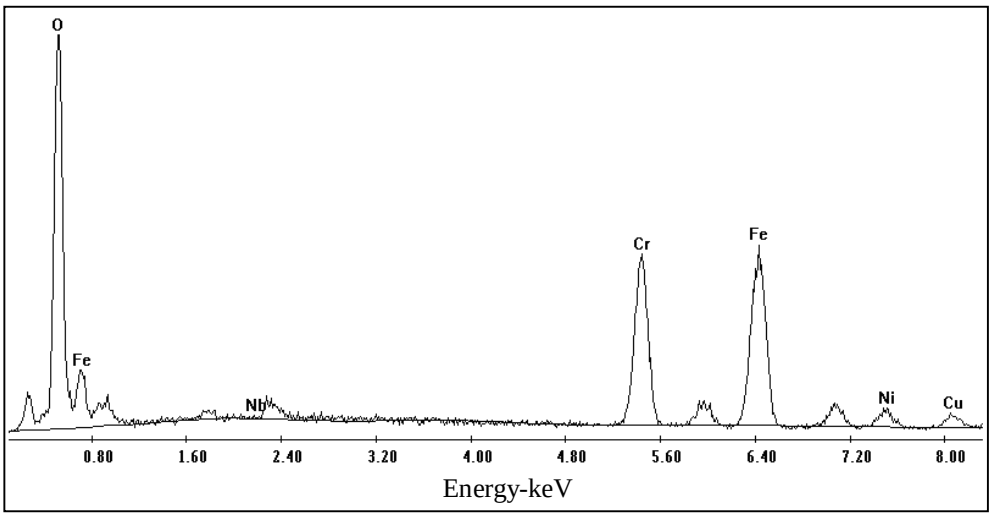

(e)

Figure 5.65 Wear debris on AT 110-16D at P = 0.17 N/mm^2 and speed = 250 rpm test (a) Washer-specimen contact (b) Loose wear debris on the test specimen after test (c) Severe scratched test specimen after removing the wear debris (d) Smeared wear debris on the scratched areas (e) EDAX analysis on loose black powder on worn test specimen.

(b) Pin on Disc Tests on Graphit-ic Coatings

Friction and wear tests were conducted on Graphit-ic coatings using the POD test apparatus in dry test conditions. The operating test conditions used these test specimens were detailed in table 4.16 of chapter 4.7.1. The test results are tabulated in table 5.50.

Table 5.50 POD test results of Graphit-ic coatings in dry test conditions.

Load N	P (N/mm^2)	V (m/s)	PV (N/mm^2.m/s)	Vol mm^3	Mean COF	SPWR (system) (mm^3/Nm)
1	344.43	0.32	108.57	0.04	0.23	1.41E-04
2	433.96	0.32	136.79	0.08	0.27	1.41E-04
3	496.76	0.32	156.59	0.16	0.30	1.88E-04
4	546.75	0.32	172.35	0.12	0.31	1.06E-04
5	588.97	0.32	185.65	0.16	0.32	1.13E-04
6	625.87	0.32	197.29	0.08	0.33	4.69E-05
7	658.87	0.32	207.69	0.08	0.35	4.02E-05
8	688.86	0.32	217.14	0.20	0.38	8.80E-05
9	716.45	0.32	225.84	0.20	0.33	7.82E-05
10	742.06	0.32	233.91	0.29	0.34	9.85E-05
11	766.01	0.32	241.46	0.16	0.33	5.12E-05
12	788.55	0.32	248.57	0.25	0.34	7.04E-05

* P – Initial contact pressure, V – Velocity, PV – Pressure X Velocity, Vol – Volume loss of material, COF – Coefficient of friction, SPWR – Specific wear rate.

The mean COF at each contact represent the average COF recorded over the time period considered. The system SPWR shows the combined wear rate of the ball and the coating. The SPWR was calculated using the gravimetric method since the Talysurf profilometer could not identify any measurable wear grooves on rubbed test specimen.

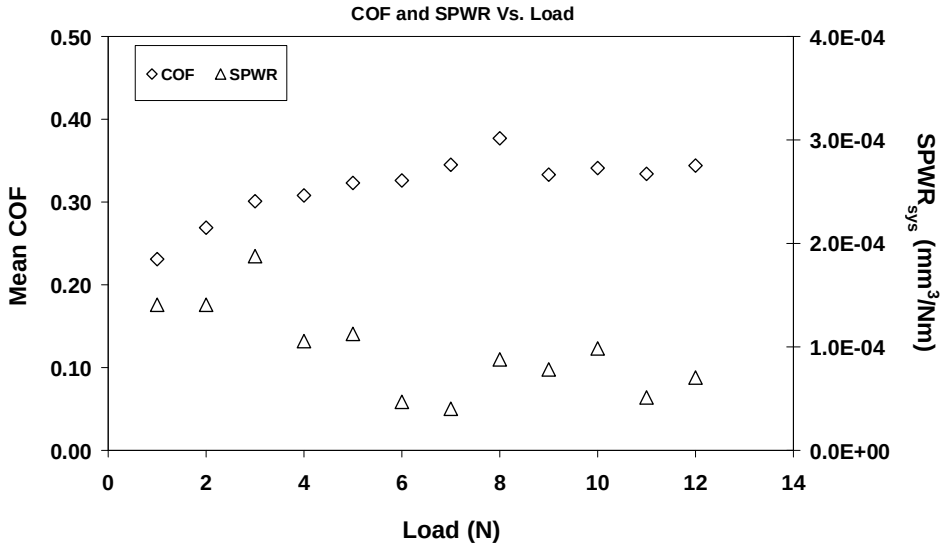

Figure 5.66 Mean COF and system SPWR against load for Graphit-ic coating in dry test conditions.

The mean COF and SPWR results from table 5.51 are compared against the normal load in figure 5.66. Test results show that the mean COF gradually increases with increase in load whereas the SPWR was initially high but then remained constant with increase in load. The coating was not completely broken even at the maximum load of 12 N, but the test surface was severely scratched.

After the end of each test, it was observed from WLI analysis that the ball material had worn much more severely than the coated material as shown in figure 5.67. This is probably due to the higher hardness of coating compared to the substrate (ball) hardness and the ball surface was completely flat whereas the test specimen surface was severely scratched as shown in figure 5.67.

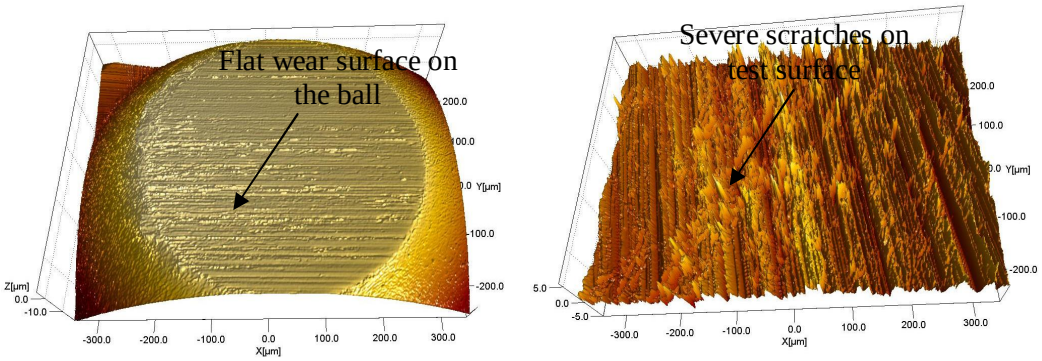

(a) (b)

Figure 5.67 Ball and test specimen after 6 N load, 250 rpm (a) Steel ball (b) Graphit-ic coating.

5.5 Comparison of Toughment with Leaded Bronze and Graphitic with Lead/Indium

The friction and wear test results of Toughmet substrates and leaded bronze substrates from TWT apparatus were compared at nominally similar contact conditions (i.e. at similar PV) in dry test condition as shown in figure 5.68. Similarly, test results of Graphitic and lead/indium coatings from TWT apparatus are compared at nominally similar contact conditions in figure 5.69.

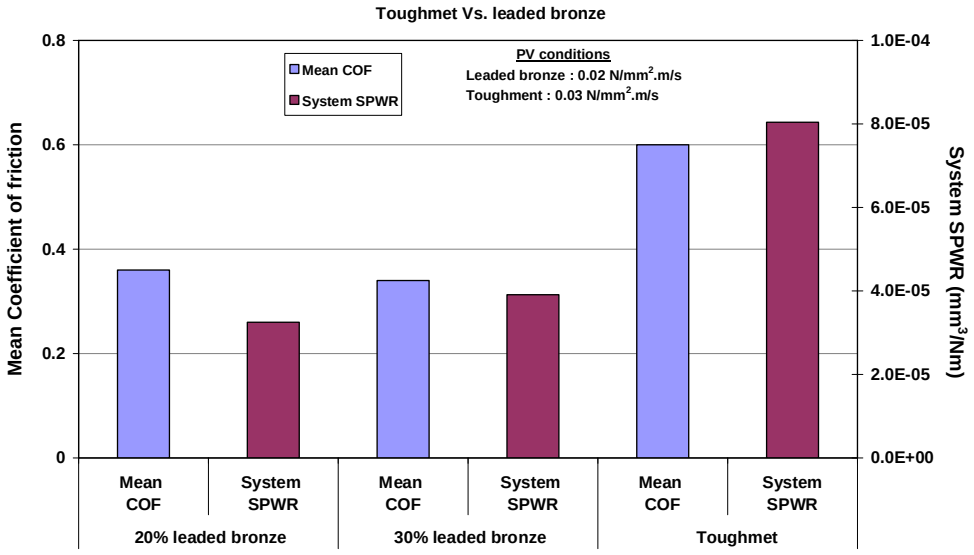

Figure 5.68 Comparing Toughmet substrates with leaded bronze substrates from TWT apparatus in dry test conditions.

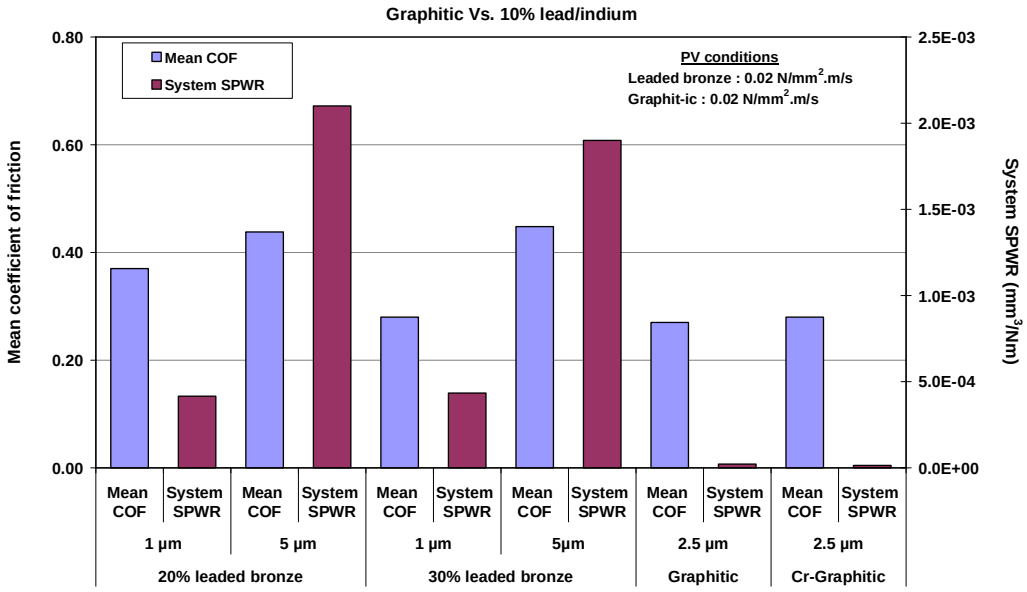

Figure 5.69 Comparing 10% lead/indium coated leaded bronze substrates with lead free coatings from TWT apparatus in dry test conditions (The PV conditions were indicated in the graph).

The dry test results from POD apparatus for different thicknesses of 10% lead/indium coated leaded bronze substrates and Graphitic coatings were compared at nominally similar contact conditions (i.e. LV ratio) in figure 5.70.

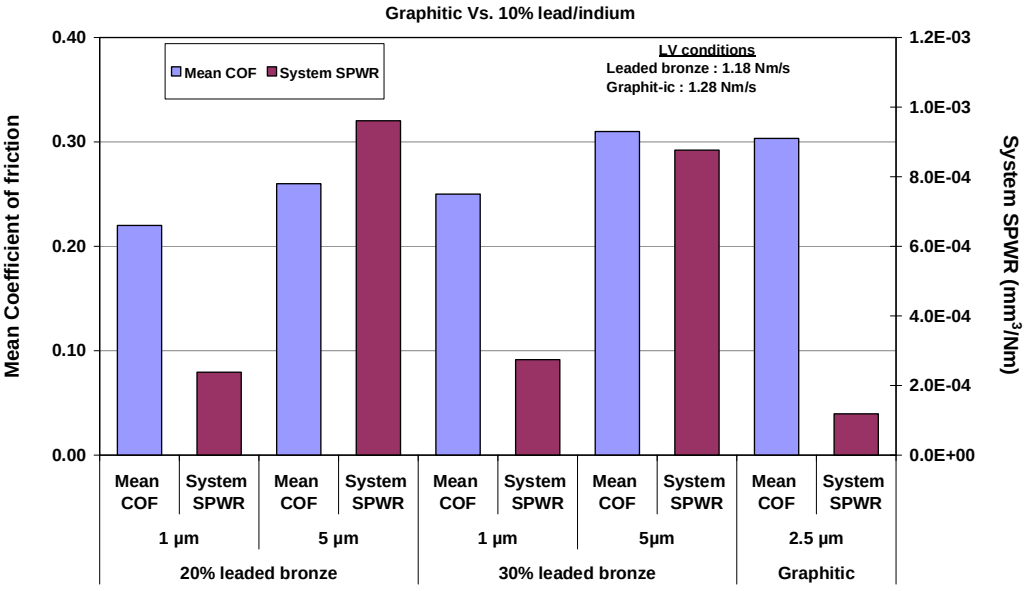

Figure 5.70 Comparison of 10% lead/indium coated leaded bronze substrates and Graphit-ic coated Toughmet substrates from POD apparatus in dry test conditions (LV conditions were indicated in the graph).

5.6 Comparison of TWT Apparatus and POD Apparatus

The trends of friction and wear data obtained from TWT test apparatus and POD test apparatus were compared so that the rankings of test materials can be identified. Since, both test apparatus had different contact geometries and operating conditions implemented on them, it is difficult to compare the friction and wear data. However, an attempt has been made to compare both test apparatus at the best possible way by choosing average LV (i.e. product of load and velocity) used on each of the test apparatus. The average LV values used on both test apparatus in dry test conditions were 8.8 Nms^{-1} and 1.18 Nms^{-1} whereas, in marginally lubricated test conditions, the average LV values were 230 Nms^{-1} and 0.65 Nms^{-1}, respectively. It should be noted that the contact area between the washer-disc contacts in TWT apparatus was bigger than that of ball-disc contact in pin on disc.

Figures 5.71 and 5.72 compare the test results of all lead based materials in dry and marginally lubricated test conditions, respectively. The average LV values used for each test apparatus is indicated on the comparison graphs. The mean COF and system SPWR in the comparison graphs were taken from the summary table of each test apparatus described earlier in the results section.

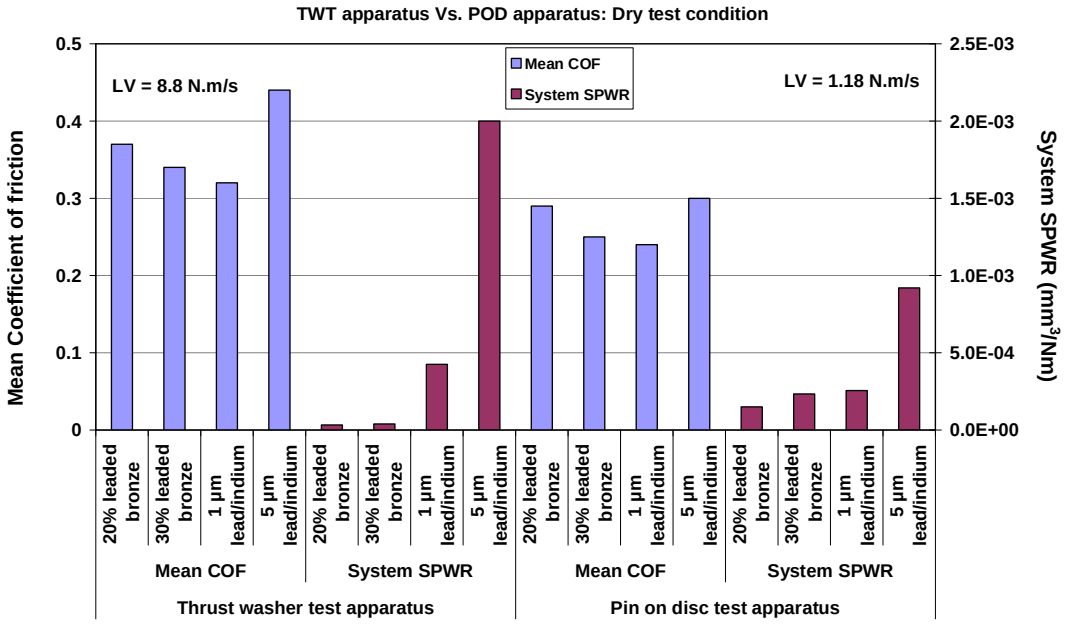

Figure 5.71 Comparison of trends of test results among the test apparatus in dry test conditions.

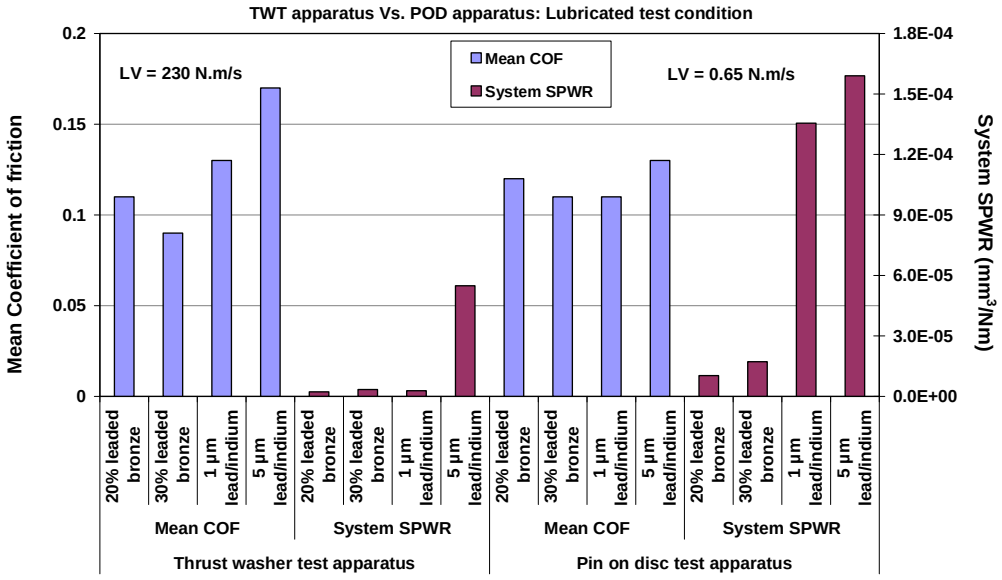

Figure 5.72 Comparison of trends of test results among the test apparatus in marginally lubricated test conditions.

Summary

This chapter has been divided into two parts. In the first part (section 5.0 to 5.3), the COF and SPWR of 20% leaded bronze and 30% leaded bronze substrates and both these substrates coated with 1 µm and 5 µm lead/indium coatings from POD and TWT apparatus 1 were tabulated separately according to the type of test condition and coating thickness. These test results were compared against PV in the case of TWT apparatus 1 and contact load in case of POD test apparatus. A summary containing average values of COF and SPWR against the contact

conditions compared the different coating thicknesses of lead/indium in both test apparatus. The mean COF and mean SPWR were plotted against the coating thickness for both test conditions. In second part (section 5.4), the COF and SPWR of Toughmet substrates, Graphit-ic and Chromium Graphit-ic coatings tested with TWT apparatus 2 were given. The results were plotted for PV against COF and SPWR, and some of the observations recorded during the test process were briefly described. Later, the friction and wear results of Graphit-ic coatings obtained from POD test apparatus were tabulated and results were compared against the contact load. Lead based test materials were compared against lead-free test materials and both test apparatus were compared for the friction and wear trends of lead based bearing materials. In the next chapter, the results obtained from TWT apparatus and POD apparatus in different test contact conditions and their influences are discussed. Various important observations and various effects of test parameters on friction and wear are also considered for discussions.

CHAPTER 6

OBSERVATIONS

&

DISCUSSION

6.0 Overview of The Project

In this project, copper based bearing alloys used in journal bearings and thrust bearings in fuel pumps were investigated. The principal materials tested were uncoated 20% leaded bronze, 30% leaded bronze and both these substrate materials coated with 1 µm and 5 µm 10% lead/indium alloy. Many experiments for this project were conducted using a thrust washer test apparatus that had a flat on flat contact geometry which replicated the contact between the thrust face of the journal bearing and thrust face of the gear shaft on the real application. In addition, accelerated tests on the same test materials were conducted on a pin on disc tribometer to facilitate high contact pressures and high velocities in a rapid test. Wear loss on the test samples was determined using a Talysurf profilometer and gravimetric method. Worn surfaces were also analysed by SEM/EDAX to establish the elemental composition of transferred material from the counterface/substrate surfaces. The COF and SPWR of these test materials were compared by plotting pressure against COF and SPWR in TWT apparatus and load against COF and SPWR in POD apparatus. Preliminary friction and wear tests on Toughmet substrates and Graphit-ic coatings were also conducted using the TWT apparatus 2 and POD to asses their performance as potential replacements for lead based materials.

In this chapter, the friction and wear test results of all the test materials presented in chapter 5 are discussed. The influence of various operating conditions and frictional heating effects on the friction and wear of test materials are also considered.

6.1 Thrust Washer Test Results

The friction and wear data for uncoated leaded bronze substrates and lead/indium coated leaded bronze substrates obtained from TWT apparatus 1 are discussed in this chapter by classifying the test materials according to thickness of the lead/indium coating and by considering dry and marginally lubricated test conditions.

6.1.1 Uncoated 20% and 30% Leaded Bronze Substrates

Dry Test Condition

From the TWT results of dry test conditions given in table 5.1, it was observed that the COF of 20% leaded bronze at every contact pressure was slightly higher than 30% leaded bronze substrate in dry test conditions. One of the reasons for high COF might be the lower lead content. As indicated by many authors lead provides solid lubrication and higher lead content may more readily enable formation of a thin soft layer which limits direct substrate contact reducing the coefficient of friction (Bowden et. al., 1950; Montgomery, 1970; Prasad, 2004). Montgomery (1970) concluded that the high percentage of lead in leaded bronze provided solid lubrication and reduced the coefficient of friction at high sliding speeds. Also a higher lead content may have the ability to embed more wear debris inducing abrasion in sliding (Prasad, 2004). It was also observed from the table 5.2 and figure 5.1 that the sliding velocity has no influence on the friction coefficient. Kayaba (1962) reported that, coefficient of friction is not greatly affected by the sliding velocity unless the sliding velocity is very slow. In the PV against COF graph shown in figure 5.3 when the PV increased the COF of both leaded bronze substrates was approximately constant. It was also observed that both substrates showed slightly higher COF at low sliding speeds/high contact loads compared with high sliding speeds/lower contact loads.

From the SPWR test results in dry test conditions, it can be seen from table 5.1 and figure 5.2 that wear for the 30% leaded bronze substrates at each contact pressure was higher than that for 20% leaded bronze substrates. However, at an increase in PV, it was observed (figure 5.3 and table 5.3) that the SPWR was approximately constant in both test materials. The higher SPWR of 30% leaded bronze was due to high lead content present which makes the substrate softer. As is well known, materials do not produce the same wear rate even when two tests with same test conditions are carried out and the contact conditions, contacting materials and material properties influence the wear loss (Molian, et. al., 1991). It is known that even a slight change in one of these parameters can produce different wear rates. Also, if materials have hardness differences (the hardness of 30 % leaded bronze (294.2 MPa) is lower than that of 20% leaded bronze (392.3

MPa)), the softer the material will have the higher the wear rate as suggested by Archard's wear equation. It was observed that the transfer of material from substrate to counterface was more commonly observed for 30% leaded bronze than that of 20% leaded bronze. The standard deviation of SPWR results for both test materials (table 5.2) suggested that the SPWR at different sliding velocities was approximately constant and sliding velocity has no influence on the wear as indicated by Archard's wear equation.

Lubricated Test Conditions

From the table 5.4 and figure 5.4, it can be concluded that COF of 20% and 30% leaded bronze substrates in marginally lubricated test conditions are much lower than in dry test conditions. The mean COF for 20% leaded bronze was higher than that for 30% leaded bronze and for both these materials, the mean COF decreased with an increase in pressure. It is possible that this arises because increased pressure improves the distribution of lead and its lubricating effectiveness (This was also suggested by Tsuya and Takagi (1964)). In marginally lubricated test conditions, the lubricant initially protected the sliding surfaces from direct metal to metal contact by providing a thin layer of liquid film at the contact. This is clearly one of the reasons for the relatively low COF in comparison with unlubricated test conditions. However, the marginal lubrication protects the surfaces only for a limited period of time and, as the lubricant evaporation started due to the frictional heating between the contacts, the situation became a dry contact. The Stribeck curve described in chapter 2.8.1 shows that the initial boundary lubrication where a thin layer of lubrication protects the surface from direct contact and with increase in load, the lubrication regime changes to mixed lubrication where a mixture of boundary and hydrodynamic lubrication takes place which in turn reduced the COF. This is what exactly happened with the marginal lubrication in leaded bronze substrates. However, considering the increase in PV conditions in table 5.6 and figure 5.6, both test specimens showed constant mean COF.

In marginally lubricated test conditions, the SPWR of 30% leaded bronze was higher than that of 20% leaded bronze and the wear of both these substrate materials was approximately constant with changes in PV as shown by table 5.6

and figure 5.6. The SPWR of both these materials in marginally lubricated test conditions was much lower than in the dry test condition since in marginal lubrication, lubricating film protected the surfaces from wear for a shorter period of time. A black smeared layer was observed on leaded bronze surfaces after the test. SEM/EDAX analysis (figure 6.1) on this black smeared layer suggested that increased temperature at the contact might have caused oxidation of metal components in leaded bronze. It is possible that formation of lead oxide and cuprous oxide at the contact interface protected the sliding surface from high wear as noted by Nojiri, et. al., (1971) and Haseeb, et. al., (2009). Also from the individual test results of both these materials at different contact pressures (table 5.4) suggested that the SPWR slightly increases with increase in pressure. This was due to the rapid depletion of lubricating film at high contact pressures resulting in higher wear compared to the low contact pressures. However, the standard deviation of the SPWR (table 5.5) suggested that sliding velocity has no influence on the wear rate. The higher SPWR of 30% leaded bronze compared to that of 20% leaded bronze was due to the lower hardness. This type of high SPWR was observed more commonly for 30% leaded bronze substrates and less commonly in 20% leaded bronze. After the friction and wear tests, analysis on the worn specimens confirmed transfer of substrate material to the counterface was much higher for 30% leaded bronze than for 20% leaded bronze substrates.

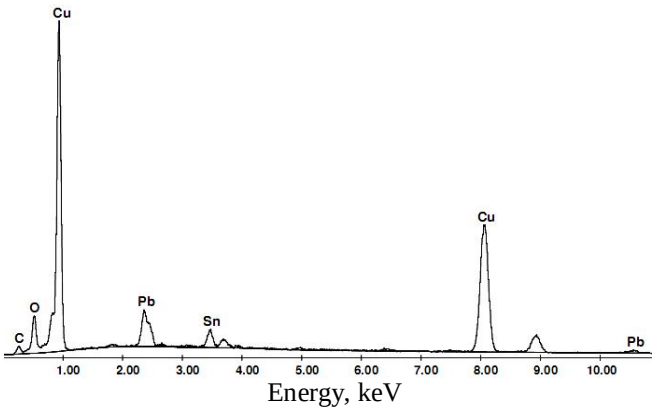

Element	Wt %	At %
C	5.13	20.02
O	7.88	23.07
Sn	5.21	2.06
Cu	71.18	52.46
Pb	10.60	2.40

Figure 6.1 EDAX analysis and elemental composition of the black layer produced in marginally lubricated 20% leaded bronze substrate.

Therefore, it was concluded that 20% leaded bronze had slightly higher COF but lower SPWR than that for 30% leaded bronze in both unlubricated and marginally lubricated test conditions.

6.1.2 1 µm Lead/Indium coated 20% and 30% Leaded Bronze Substrates

Dry Test Conditions

Test results from Table 5.7 and figure 5.7 show that the mean ploughing COF was higher than the mean COF of the system whereas the SPWR for the running-in period was much higher than that of system period in both test materials. It was observed from the friction-time graph from each test specimen that the COF was higher at the start (high COF at the start was shown as bar elements in figure 5.7), fluctuated for a small period of time and decreased slowly until the running-in period where it was observed that most of the coating was polished and its thickness was reduced. The high COF at the start was due to the plastic deformation of the coating (since the hardness of the coating was much lower than initial contact pressure) and increased contact area at the contact interface between the counterface and coating (Bowden and Tabor, 1950; Sherbiney and Halling, 1977; Holmberg, 1992a). During the running-in time, since the COF was very high and reached, in some cases, a friction coefficient close to 1, the flash temperature (by Ashby's method) suggested that the lead/indium reached softening/melting temperatures (table 5.44). Therefore, lead in lead/indium acted as a solid lubricant due to high frictional heating at the contact and the low melting point of lead/indium alloy. From the mean COF and system SPWR data as shown in figure 5.7 and figure 5.8, it can be seen that 1 µm lead/indium coated 20% leaded bronze substrates have a higher mean COF but slightly lower SPWR than that of 1 µm lead/indium coated 30% leaded bronze substrates. This is again due to the hardness differences between both coated leaded bronze substrates indicated earlier. It was observed in both 1 µm coated leaded bronze substrates that, lead/indium coating was worn away in some areas on the test specimen. SEM/EDAX on worn areas (figure 6.2 (a)) showed copper as one the elements from the substrate surface. From figure 5.9, it can be seen that mean COF and system SPWR of both 1 µm lead/indium coated substrates were approximately constant with increase in PV. From table 5.7, the mean ploughing COF and SPWR during the running-in period for 1 µm 20% leaded bronze is higher than 1 µm 30% leaded bronze substrates. This may be due to the slightly higher coating

thickness of lead/indium deposited on 20% leaded bronze compared with 30% leaded bronze. Probably the increase in coating thickness increases the effect of ploughing and contact area with the counterface, resulting high COF (An effect also described by Bowden and Tabor (1950) and Roberts (1990)).

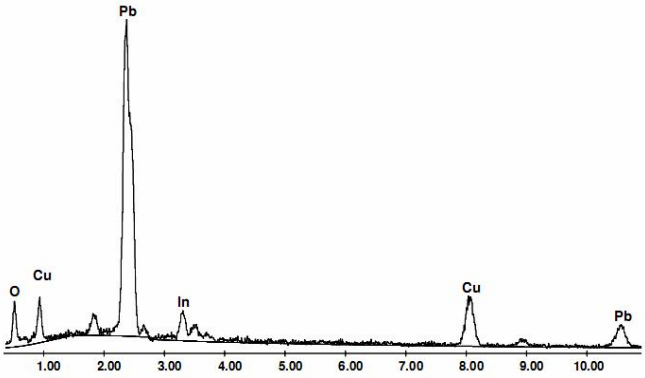

Element	Wt %	At %
O	8.48	45.75
In	6.89	5.18
Cu	14.67	19.93
Pb	69.96	29.14

(a)

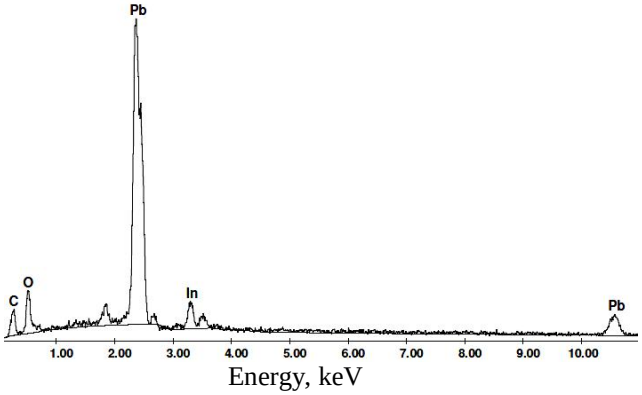

Element	Wt %	At %
C	8.01	36.85
O	11.59	40.03
In	7.80	3.75
Pb	72.61	19.37

(b)

Figure 6.2 EDAX analysis and elemental composition of worn areas of lead/indium coated leaded bronze substrates. (a) Dry test (b) Marginally lubricated test.

Marginally Lubricated Test Conditions

The test results for 1 µm lead/indium coated 20% leaded bronze and 30% leaded bronze substrates in marginally lubricated conditions are given in table 5.10. In these results, the mean ploughing COF of 1 µm lead/indium coated 20% leaded bronze is slightly higher than that of the 30% leaded bronze substrates. This might be due to their slightly higher coating thickness, resulting in higher contact area with the counterface indicated earlier for dry test condition. The friction and wear

values in these test conditions were much smaller than those of the dry test conditions as the marginal lubrication protected the surfaces from direct metal-metal contact until it evaporated. From figure 5.10, it can be seen that both test materials had similar friction values at high pressures, but differed slightly in low pressures. However, 1 µm lead/indium coated 20% leaded bronze substrates have slightly higher mean COF than the 1 µm lead/indium coated 30% leaded bronze substrates. This was due to the hardness difference of both test materials and 20% leaded bronze being harder than 30% leaded bronze. However, considering the standard deviation of test results from table 5.11, these differences may not have any significant influence. When it comes to the running-in SPWR, both types of test specimens had similar values. In case of system SPWR, 1 µm lead/indium coated 30% leaded bronze worn higher than 1 µm lead/indium coated 20% leaded bronze due to its lower hardness. It was observed that at higher load, the lubricant tends to break down much earlier and could not separate the surfaces from metal to metal contact. Once the lubricant broke down, the mechanism was dry contact which obviously depends on the properties of the substrate materials and/or any tribofilm. A thin black smeared layer was observed on the all lead/indium coated leaded bronze substrates after the running-in and EDAX analysis (figure 6.2 (b)) on the smeared black layer revealed that formation of oxide layer from lead and indium (In_2O_3) protected the substrate surface from wear. The oxide layer from lead could be PbO_2, since the formation oxide phases begin with PbO_2 (Lyamkin, 2009). From the table 5.12 and figure 5.12, it can be seen that as the PV increased there was a suggestion of decrease of SPWR in both test materials. Low wear rate is associated with the formation of stable layer from lead/indium on the substrate surface at high PV conditions (Sherbiney and Halling, 1977). However, considering the standard deviation, this difference might not have any significant influence on tribological properties of these materials.

Overall, it was concluded that 1 µm lead/indium coated 20% leaded bronze had slightly higher COF, but lower SPWR than that of 1 µm lead/indium coated 30% leaded bronze in unlubricated and marginally lubricated test conditions.

6.1.3 5 µm Lead/Indium Coated 20% Leaded Bronze and 30% Leaded Bronze Substrates

Dry Test Conditions

1 µm lead/indium coatings were worn away during the running-in period and did not protect the substrate surface directly for long, especially in dry test conditions. In contrast, the 5 µm lead/indium coated leaded bronze substrates provided more protection of the substrate in sliding contacts over the test period considered in this work. Due to the high coating thickness of lead/indium, the coefficient of friction and wear rate were higher than that of 1 µm coatings. The increase in COF with increase in coating thickness is due to the decrease in load carrying capacity from the substrate and high ploughing of the softer coating (Sherbiney and Halling, 1977). The higher ploughing COF was observed in both 5 µm coated 20% leaded bronze and 30% leaded bronze, as shown in table 5.13. The ploughing COF in the running-in period was much higher and observed for considerable period of time (one such example is shown in figure 5.50 (c)). Additionally, flash temperatures reached the melting point of lead/indium (table 5.44) and the steadily reducing COF during running-in may partly arise as the lead in lead/indium becomes molten/better distribution to act as a solid lubricant as well as a result of the reduction in ploughing as wear progresses. From the table 5.14, the mean COF of both 5 µm coated substrates were roughly similar, but the SPWR of 5 µm coated 30% leaded bronze was higher than for the 5 µm coated 20% leaded bronze. This was again thought to be lower hardness of 30% leaded bronze causing this material to be removed more readily than 20% leaded bronze. In 5 µm coated 30% leaded bronze, some of applied the load is carried by the substrate which deforms along with the deformation of coating (An effect also described by Leroy and Villechaise (1990 and Holmberg et. al., (1994)) and wear rate is higher than that of 5 µm coated 20% leaded bronze. It was observed at the end of each test that the lead/indium coating was not completely worn away and this coating protected the substrate surface from wear. Table 5.15 demonstrated that the SPWR of both 5 µm coated test specimens remained constant with PV.

Marginally Lubricated Test Conditions

In marginally lubricated test conditions, table 5.16 shows the mean COF of 5 µm coated 30% leaded bronzes were generally slightly higher than that of the 5 µm coated 20% leaded bronze substrates. However, considering the standard deviation of the COF at changes in PV, as shown in table 5.17, it appears these differences are not significant. The SPWR on both 5 µm coated substrates were approximately constant with PV. However, 5 µm thick coatings wore much more quickly than the 1 µm coated substrates during the running-in period and wear debris, consisting of black powder adhered and smeared on to the substrate surface and was appeared in most of the tests, as shown in figure 6.3 (a). The black powder adhered to the substrate surface and was difficult to remove. EDAX analysis on smeared black layer suggested the formation of oxides probably involving both lead and indium.

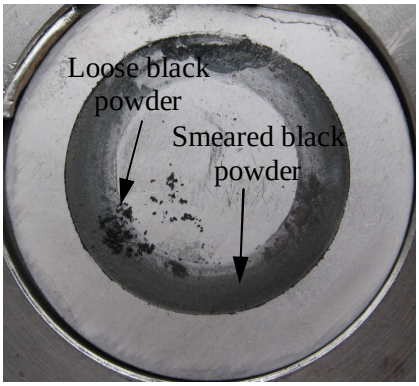

(a)

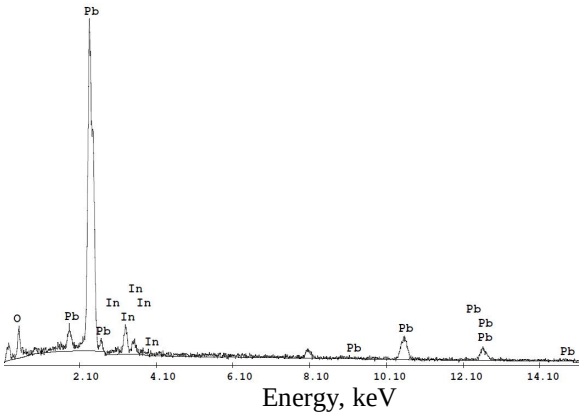

(b)

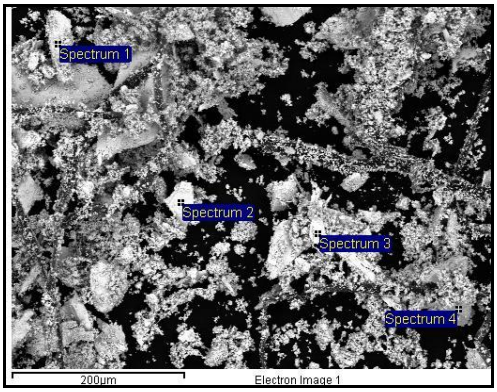

(c)

Spectrum	In Wt %	Pb Wt %	O Wt %	Total Wt %
1	6.97	84.01	9.02	100
2	7.34	83.46	9.20	100
3	7.54	87.43	5.03	100
4	8.34	87.51	4.15	100

(d)

Figure 6.3 5 µm lead/indium coated leaded bronze substrate (a) Black powder on worn specimen (b) EDAX image of worn specimen (c) EDAX on selected wear debris (d) Elemental composition of wear debris

Figure 6.3 (c) illustrates the wear debris which was comprised particles of size between 200 µm and less than 1 µm. The composition of the particles was analysed using SEM/EDAX system and found to be consistent with the 10% lead/indium coating. The absence of copper from the EDAX results indicated that substrate wear debris had not been generated during the test.

It was concluded from test results that both 5 µm coated substrates have approximately similar COF, but 30% leaded bronze had higher SPWR than 20% leaded bronze in unlubricated test conditions.

6.1.4 Comparison of COF and SPWR According to Coating Thickness

Table 5.19 detailed the mean COF and system SPWR of uncoated, 1 µm and 5 µm coated leaded bronze substrates in both dry and marginally lubricated test conditions at nominally similar PV conditions. Figure 5.19 and figure 5.20 compare the influence of lead/indium coating thickness on COF and SPWR of all test materials in dry and marginally lubricated test conditions, respectively, and it was concluded that the uncoated leaded bronze substrates had “better” tribological properties than the lead/indium coated substrates over the time period considered. The lead/indium coatings protected the substrate surface from wear, but the wear rate of the lead/indium coating was higher than that of uncoated leaded bronze substrates. The marginally lubricated test results show lower COF and SPWR than in dry test conditions, but again Pb/indium coatings have higher COF and SPWR than uncoated leaded bronze substrates. The lubricant prevented initial high ploughing COF and protected the coated surfaces for a short period of time which was the main reason for lower substrate wear loss.

6.1.5 Various Observations and Influences of Test Parameters on Friction and Wear Behaviour of Test Materials

There were some important factors that influenced the friction and wear of leaded bronze substrates and lead/indium coatings. These are discussed below.

(a) Test Conditions

The test parameters such as high speed and high load conditions have direct influence on the COF and wear rate (Andrew et. al., 2007). In particular, with high load-low sliding speed and high load-high sliding speed, the COF was very high (more than 1) initially during the running-in period. During the running-in period, it was observed that the most of the lead/indium coating was worn away and the thickness of the coating was reduced. Especially with 5 µm coatings, high PV conditions resulted in high ploughing COF and high coating material loss. Using this high ploughing COF data in Ashby's frictional heating calculations (table 5.44), it was found that the lead/indium coating reached the melting phase during the running-in period, possibly improving its ability to lubricate. For uncoated leaded bronze substrates this was not the case as the surfaces of leaded bronze substrates were much harder than those of the lead/indium coatings and generated a stable COF throughout the test. A continuous loud rubbing sound was observed and small amount of black powder was gathered from the interface in dry test conditions especially with lead/indium coatings suggesting that coating started to wear as soon as the test process started.

(b) Contact Area

It was observed that due to the softness of lead/indium compared to leaded bronze substrates, greater plastic deformation of the contacting surfaces resulted in increased contact area with the counterface for lead/indium coating compared with that of leaded bronze substrates. However, due to its relative softness, a higher material transfer to the harder counterface surface was also observed. Therefore 30% leaded bronze showed high wear rates compared to 20% leaded bronze. Additionally, 30% leaded bronze had a lower COF due to the higher amount of free lead presented in comparison with 20% leaded bronze substrates (The lower COF at increased lead content is also observed by Montgomery (1970) and Prasad (2004)). The thin 1 µm coatings showed low COF and SPWR than thick 5 µm coatings due to lower contact area with the counterface. This is again due to the better load support from substrate in the thin coating compared with that of thick coatings where contribution of ploughing is high (Tsuya and Takagi, 1964). However, lead/indium coatings had higher system wear rates than uncoated

leaded bronze substrates over the considered time period in dry and marginally lubricated test conditions.

(c) Edge Effects

An 'Edge effect' was encountered with the flat on flat test configuration in TWT apparatus 1 where sharp right angled edges from the outer and inner diameters of the washer at the slight uneven loads caused severe local "edge wear" at the start of the test. This was observed in several tests conducted at low load-high speed conditions where wear loss was uneven, as shown in figure 6.4, and the test was stopped to avoid further damage to the test material.

Figure 6.4 Worn-unworn areas on test disc in TWT apparatus 1.

As discussed previously, with high contact loads and sliding speeds, the alignment of the washer on substrate/coated specimen is critical as any small misalignment in the rotation of the washer causes the coating to be heavily worn at these sharp edge areas. So it was necessary to increase the radius of the edge to avoid any initial damage on to the substrate/coating specimens.

(d) Influence of Microstructure on Friction and Wear

It is well known from literature that, lead in leaded bronze acts like a solid lubricant and protects sliding surfaces from direct metal-metal contact. Therefore, the percentage and distribution of lead particles in the alloy has a very important influence on the friction and wear (Molian et. al., 1991; Teruji Nojiri, et. al., 1971; Equey et. al, 2010). Equey, et. al., (2010) described that microstructure plays an important role in the formation of antifriction flat debris which reduce friction and wear. The micrographs of the inter-dendritic lead size distribution for 20% leaded bronze and 30% leaded bronze alloy used in this project are shown in figure 6.5.

In the figure 6.5 (b), the lead phase is finely dispersed and ranges in size up to 75 µm in maximum dimension for the 20% leaded bronze alloy. The 30% leaded bronze (figure 6.5 (a)) on the other hand, has a coarser distribution of inter-dendritic lead phase accompanied by large 'islands' of free lead which can be greater than 1 mm in maximum dimension. It is believed that the fine distribution of lead in 20% leaded bronze, the wear rates obtained were uniform and lower than that of 30% leaded bronze. However, due to slightly higher hardness of 20% leaded bronze, the COF was higher than that of 30% leaded bronze.

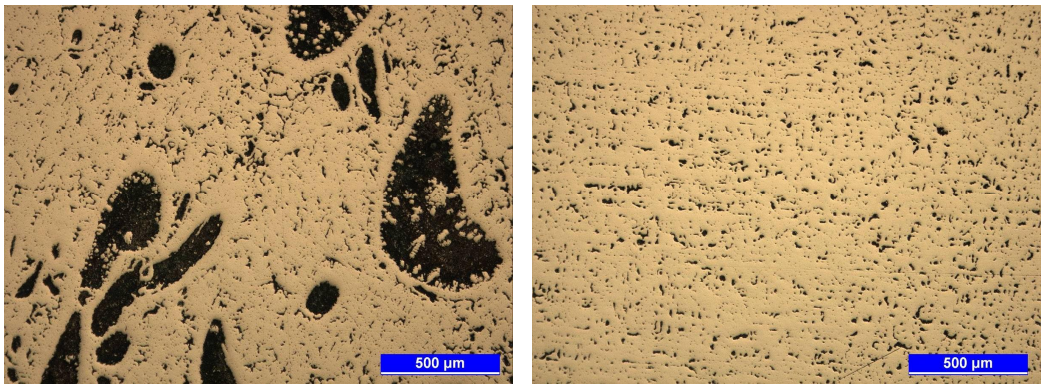

(a) (b)

Figure 6.5 Microstructure of leaded bronze showing dark areas of lead distribution (a) 30% leaded bronze (b) 20% leaded bronze.

(e) Equilibrium Diagram of Lead/Indium Alloy

It was suggested by the frictional heating calculations that, during the running-in period, the lead/indium alloys reached its melting phase (figure 5.52) and this may have given the substrate surface some protection from wear. The lead/indium phase diagram shown in figure 6.6 details the melting phase of indium and lead with temperatures. The melting temperature of 10% indium in lead is around 280 °C to 300 °C. Pure lead melts at 327.5 °C whereas pure indium melts at 156.8 °C. For 10% lead/indium, when the temperature reaches to 280°C, the 10% lead/indium becomes soften and the solid phase changes to liquid until the temperature reaches to 300 °C. After this temperature, the alloy becomes molten and the alloy exists only in the liquid form until the temperature drops less than the melting temperature (Humpston and Jacobson, 2005; ICA, 2010).

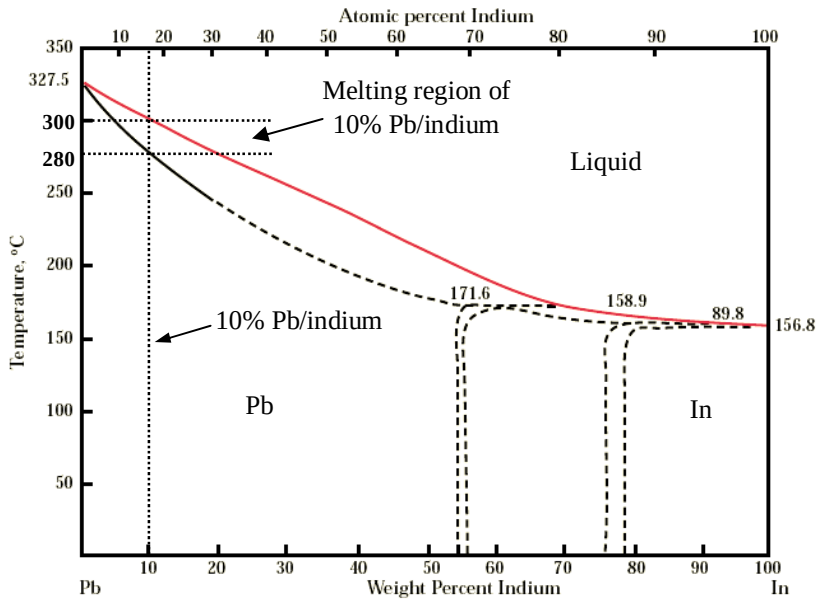

Figure 6.6 Equilibrium diagram of 10% lead/indium (After Humpston and Jacobson (2005)).

From the friction results, when the mean COF was used in the Ashby's method, lead/indium did not reach its melting point (figure 5.54) whereas for the ploughing COF, it does. Therefore, it was believed that the lead/indium might have melted during the running-in, but not after the running-in period.

6.1.6 Ranking of Materials from TWT Apparatus

Since various operating conditions and different coating thicknesses of lead/indium were used, it was difficult to rank the test materials among themselves. However, it was clear from the individual test results that uncoated leaded bronze substrates had better friction and wear properties than lead/indium coatings over the time period considered. To compare the uncoated and lead/indium coated substrates separately, average PV values were taken from each type of specimen and plotted against mean COF and system SPWR as shown in figure 5.19 and figure 5.20 for dry and marginally lubricated test conditions, respectively. From these results, it can be concluded that, for a given PV in dry test conditions, the 1 µm coated 30% leaded bronze substrates have lower mean COF than uncoated and 5 µm coated leaded bronze substrates. Also the COF of 1 µm coated 20% leaded bronze substrates was similar to that of leaded bronze substrates at the same PV. In terms of SPWR, uncoated 20% leaded bronze substrates were better than that of uncoated 30% leaded bronze substrates and

were lower than those of 1 µm and 5 µm coated substrates. The 5 µm coated substrates had higher friction and SPWR than uncoated and 1 µm coated leaded bronze substrates. This suggests that the coatings on leaded bronze substrates were much more worn than those of substrates alone even though the coatings were protected the substrate surface from wear. Of the uncoated substrates, 20% leaded bronze has a lower wear rate than 30% leaded bronze due to its higher hardness discussed earlier. In marginally lubricated test conditions, uncoated leaded bronze substrates have lower COF and SPWR than both coated leaded bronze substrates.

Overall, it was observed that uncoated leaded bronze substrates had better friction and wear properties than 1 µm and 5 µm lead/indium coated substrates.

6.2 POD Test Results of Leaded Bronze Substrates and Lead/Indium Coatings

The pin on disc results showed much more reproducible friction and wear data than TWT apparatus. The test results for the POD test apparatus were separated according to the sliding velocities used. Since two different track radii, each having a unique sliding velocity were used, it was necessary to separate the results to identify the influence of sliding velocity on COF and SPWR (if any). It was observed from friction and wear tests that during initial running-in period, a high COF was recorded with lead/indium coated leaded bronze substrates. The ploughing of the ball on thin coated substrates during the running-in period resulted in high friction and wear rates (an equivalent running-in period was not observed for uncoated leaded bronze substrates). During this running-in period, high frictional heating resulted in melting of lead/indium alloy that acted as a solid lubricant and protected the substrate surfaces from wear. The COF after running-in period was roughly constant until the end of test. It was also observed after the running-in period that the coating thickness was reduced and in some tests at high contact loads, the coating was completely removed. This was the case with 1 µm lead/indium coated leaded bronze substrates in dry test conditions. However, the wear rate obtained was uniform and COF was steady compared to TWT apparatus. The test results of leaded bronze substrates and lead/indium coatings at different contacting conditions were discussed below.

6.2.1 Uncoated 20% and 30% Leaded Bronze Substrates

Dry Test Conditions

From the individual test results of leaded bronze substrates at different sliding velocities shown in table 5.20 and table 5.21, it was observed that the mean COF of 20% leaded bronze was higher than that of 30% leaded bronze. The maximum COF recorded at the start of the test was higher at each contact load compared to the mean COF. One of the main reasons for high COF of 20% leaded bronze was its high hardness compared with 30% leaded bronze as discussed earlier in TWT results. Also the higher lead content in 30% leaded bronze provided better solid lubrication than that of 20% leaded bronze. So these uncoated dry test results resemble the TWT results. However, the wear rates were increased due to the application of greater pressure. Increased contact pressures increased the deformation of the 30 % leaded bronze (due to lower hardness) and the contact area with the counterface increases (Holmberg and Matthews, 1994; Holmberg, et. al., 2000). This was thought to be the reason for the high SPWR of 30% lead bronze compared with 20% leaded bronze. When comparing the test results of same materials at different sliding velocities using table 5.20 and table 5.21, it can be seen that the mean COF and mean SPWR were slightly higher at low sliding speed. The slightly high COF and SPWR at lower sliding velocity were due to the more number of rotations of ball sliding on the disc (chapter 4.7.1 and table 4.17). Table 5.22 shows the mean COF, mean SPWR and their standard deviations for 20% and 30% leaded bronze substrates at both sliding velocities. It can be seen that the mean results indicate a slight increase in COF and SPWR when the sliding velocity is reduced from 0.47 m/s to 0.24 m/s. However, when the standard deviations of the values are considered, it is clear that these slight differences are probably not significant so it is unlikely that sliding speed in this range influences the tribological properties of these uncoated substrates when run dry.

Marginally Lubricated Test Conditions

With marginal lubrication, both materials were protected from metal-metal contact initially, but with repeated sliding on the same surface, the lubricant was lost after a few rotations of ball on the disc. From the test results detailed in table

5.23 and table 5.24 at different sliding velocities, it was concluded that the mean COF of 30% leaded bronze and 20% leaded bronze substrates were approximately similar. However, 30% leaded bronze substrates exhibited higher SPWR than 20% leaded bronze at every contact load. The high SPWR of 30% leaded bronze was due to its higher lead content and lower hardness as described earlier. Due to higher plastic deformation of 30% leaded bronze, the contact area with the ball is higher, resulted in higher wear rates (This was also observed by Molian et. al. (1991)). From the table 5.25, the standard deviations of mean COF and mean SPWR at two different sliding velocities suggested that there was a considerable difference in COF and SPWR when sliding velocity reduced from 0.26 m/s to 0.13 m/s. This was possibly due to the higher number of passes of the disc at lower sliding velocities resulting in earlier lubricant depletion and high wear rates. The standard deviations of the results, shown in table 5.25 confirm that there was a much greater scatter in the COF results for the lower sliding speed, which is consistent with this explanation. The SPWR increases with increase in load for both materials. This is in contrast to the behaviour for the dry test conditions and, again, is probably an effect of more rapid lubrication depletion at the higher loads

6.2.2 1 µm Lead/Indium coated 20% and 30% Leaded Bronze Substrates

Dry Test Conditions

Table 5.26 and table 5.27 show the COF and SPWR of the above mentioned test materials for the running-in period and total test time, respectively, at two different sliding velocities. Test results from these tables confirm that 1 µm coated 20% leaded bronze substrates have higher ploughing COF, but lower SPWR than 1 µm coated 30% leaded bronze substrates for the running-in period. This was due to slightly higher coating thickness of lead/indium on 20% leaded bronze than that of 30% leaded bronze. Additionally from figure 5.25 and figure 5.28, it can be seen that the running-in times for 1 µm lead/indium coated 20% leaded bronze substrates at each contact load were higher than those of 1 µm lead/indium coated 30% leaded bronze substrates. This is possibly due to the variations in the nominal lead/indium coating thickness on the substrates. (Lead/indium coating thicknesses were generally slightly thicker (typically 0.2 µm-0.5µm thicker) for 20% leaded

bronze than that for 30% leaded bronze.) This suggested that a higher coating thickness was retained longer than that the lower coating thickness. However, this effect may also be related to the impact of substrate hardness on stress distributions in the coating. The running-in time decreased with increase in load in both test specimens due to high deformation of the coating with increasing load. The maximum ploughing COF recorded at each contact load for each coated test specimen is indicated as bar elements with higher values in figure 5.25 and figure 5.28, respectively. Figure 5.27 and figure 5.30 show the steady state COF and system SPWR, of both 1 µm coated leaded bronze substrates at two different sliding velocities and it was concluded that 1 µm coated 30% leaded bronze has higher COF and SPWR than 1 µm coated 20% leaded bronze substrate at every contact load.

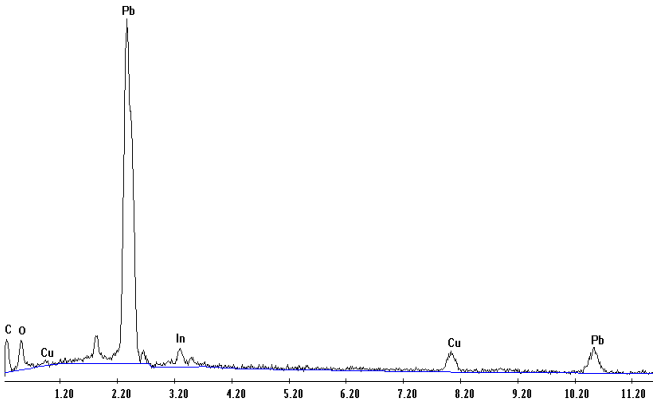

(a)

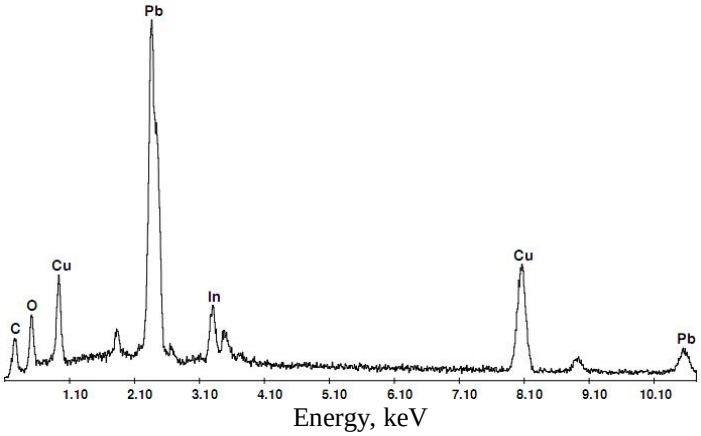

(b)

Figure 6.7 EDAX analysis on worn test specimens (a) 1 µm coated 20% leaded bronze (b) 1 µm coated 30% leaded bronze.

After the running-in period it was observed that the some of lead/indium coating was removed from both the substrate surfaces and substrate hardness influenced the COF and SPWR. EDAX analysis on both worn leaded bronze surfaces (figure 6.7) identified high percentage of substrate (copper) material observed, especially from 1 µm coated 30% leaded bronze, suggesting that lead/indium coating did not protect the substrate material from wear.

Table 5.28 and table 5.29 show the COF and SPWR of both 1 µm coated test specimens along with their standard deviations during the running-in period and total time period, respectively. It can be seen from these test results that the mean ploughing COF and the mean SPWR were higher at high sliding velocities than those at low sliding velocities. In contrast, mean COF and mean SPWR of both coated substrates were approximately constant. The standard deviation suggested that there was no significant effect of sliding velocity on the tribological properties of these coated substrates when running dry.

Marginally Lubricated Test Conditions

In marginally lubricated test conditions, for the first few revolutions, the kerosene protected the ball on disc contact from a high COF. The influence of ploughing of the ball on the disc was lower compared to the dry test conditions. This was due to the protection of the marginal lubricating film against the transfer of coating material to the mating surface. From table 5.30 and table 5.31 presenting test results at two different sliding velocities, it can be seen that 1 µm lead/indium coated 20% leaded bronze substrate had a higher ploughing COF and steady state COF than the 1 µm coated 30% leaded bronze substrates. This was again due to the slightly higher coating thickness and higher hardness of 20% leaded bronze compared with that of 30% leaded bronze as indicated earlier in the TWT results. However, the SPWR of running-in period and system SPWR for both specimens were approximately similar. The running-in time decreased with increase in load in both test materials due to the increased plastic deformation of the coating with increase in load (Holmberg, 1992a). The standard deviation of COF and SPWR for the running-in period and total time, shown in table 5.32 and table 5.33 indicated that there was no influence of sliding velocity on tribological properties

of coated substrates. A thin oxide layer in the form of a thin black layer from lead/indium protected the substrate surfaces from wear.

6.2.3 5 µm Lead/Indium Coated 20% and 30% Leaded Bronze Substrates

Dry Test Conditions

From the test results for 5 µm coated leaded bronze substrates shown in table 5.34 and table 5.35, it can be concluded that 30% leaded bronze substrates had a slightly higher COF than that for 20% leaded bronze substrates in dry test conditions. This was due to the high deformation of substrate surface (due to lower hardness) and high ploughing of the coating in 30% leaded bronze substrate than that of 20% leaded bronze substrate (The mechanism of substrate deformation and ploughing of thick coatings was experimentally demonstrated by: Sherbiney and Halling, 1977; Suh, 1986). However, the SPWR on both these test materials were similar at each contact load since the lead/indium coating protected the substrate surface from wear throughout the test. From table 5.36 and table 5.37, it was observed that there was no influence of sliding speed on the tribological properties of these materials. The running-in time of both these test materials were decreased with increase in load. This was due to the increased ploughing of ball on thick coated disc with increase in load. The running-in time for 5 µm coated 20% leaded bronze were higher than 5 µm coated 30% leaded bronze due to their high coating thickness. From figure 5.37 and 5.40, it was shown that the maximum ploughing COF recorded for 30% leaded bronze at each contact load was slightly higher than that of 20% leaded bronze and this was one of the reasons for the high ploughing COF. The mean steady state COF for 30% leaded bronze was higher than that for 20% leaded bronze due to the lower load carrying capacity of the substrate surface indicated earlier. It was observed that the lead/indium coating was not removed completely after the running-in period and the coating protected the substrate surface from wear. It was also identified that at high sliding velocities, the lead/indium reached its melting point (table 5.45 and figure 5.57) and may have acted as a solid lubricant. A thin black smeared layer on the test surface and a shiny thick transferred layer on steel ball surface were observed after the test. SEM/EDAX analysis on both test material surfaces

indicated that lead/indium was smeared on to the counterface and probably protected the substrate surface from wear.

Marginally Lubricated Test Conditions

In marginally lubricated test conditions, both 5 µm coated 20% leaded bronze and 30% leaded bronze substrates had a similar COF and SPWR at each contact load. The running-in time for both test materials was similar. However depending on the precise thickness of the coating, the running-in time varied. From figure 5.45 and figure 5.48, it can be seen that the steady state COF and SPWR of both 5 µm coated leaded bronze substrates decreased with increase in load. As indicated before, high load-high speed conditions, increased temperature at the contact interface resulted in large concentration of lead oxide and improved lubrication in the contact. It was observed in a few of the tests at lower contact loads that the coating wore away rapidly initially then the wear rate reduced in the remainder of the test. It was observed at high loads that a black thin layer formed on the worn surface that seemed to protect the surfaces from wear and was accompanied by a low COF. This black thin layer seemed to be formed, as shown in figure 6.8, from the wear debris smeared on the wear track. It also protected surfaces from severe scratching. EDAX analysis on the black smeared layer (figure 6.8) revealed that this was entirely lead/indium coating.

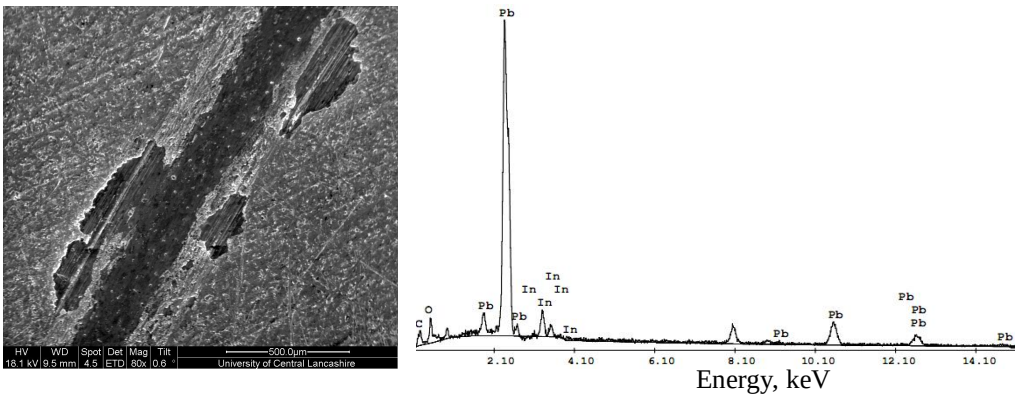

(a) (b)

Figure 6.8 Thin black layer from lead/indium smeared on leaded bronze substrates (a) 5 µm coated 30% leaded bronze at 0.47 m/s (b) EDAX on black layer.

From table 5.41, when the sliding speed was reduced by half, the SPWR decreased by 2 times. The decrease in COF and SPWR is therefore, associated

with the higher number of rotations of the ball on the substrate when it runs at lower sliding speeds. This repetition of sliding creates a thin smeared layer of lead on the substrate surface. By considering the standard deviation of test results, it was concluded that sliding velocity in fact had no effect on the tribological properties of the 5 µm coated leaded bronze substrates.

It was observed from the test results of 5 µm lead/indium coated leaded bronze substrates that leaded bronze substrates cannot be compared for their tribological response since the lead/indium coating was not removed from the substrate and protected the surfaces for the entire duration of the tests. Both 5 µm coated leaded bronze substrates showed roughly similar friction and wear results, and depending on the precise thickness of lead/indium coating, the test results varied.

So overall it was concluded from the pin on disc tests that, as with TWT results, the uncoated leaded bronze substrates have better friction and wear resistance characteristics than 1 µm and 5 µm coated leaded bronze substrates in all test conditions over the time period considered. It should be noted that beyond the time period considered, the performance ranking of the test materials, especially uncoated leaded bronze substrates and 5 µm lead/indium coated substrates may differ. The 5 µm lead/indium coated substrates were better than 1 µm coated substrates in terms of protecting the substrate surface from wear. Among the uncoated substrates, 20% leaded bronze has higher COF and lower wear than 30% leaded bronze substrates. The use of marginal lubrication slightly protected the substrate/coated surfaces for the first few revolutions of the ball sliding and decreased the effect of high COF. However, once the kerosene was removed from the contact interface, the oxide layer from coating controlled the COF further.

6.2.4 Comparing COF and SPWR According to Coating Thickness in POD Apparatus

In the previous discussion, the friction and wear results of leaded bronze substrates and lead/indium coatings were compared among themselves at various contacting conditions. However, to compare COF and SPWR data according to coating thickness, all test results from nominally similar contact conditions were averaged among the different types of leaded bronze substrates and at various

thickness of lead/indium coatings. The mean product of load-velocity (LV) was calculated from all the operating conditions and, mean COF and mean SPWR were compared among different types of substrates/coating thicknesses shown in figure 5.49. From table 5.42 and figure 5.49, it was clear that uncoated substrates have slightly higher COF, but lower SPWR than lead/indium coated substrates in both dry and marginally lubricated test conditions. The lead/indium coating reduced COF when the coating thickness was 1 µm, but not 5 µm. WLI observations suggested that 5 µm lead/indium protected the leaded bronze substrates from wear, but had higher COF and wear rates than others. Therefore, it can be concluded that uncoated leaded bronze substrates have better tribological properties than lead/indium coated leaded bronze substrates in all test conditions.

6.2.5 Various Observations and Influences of Test Parameters on Friction and Wear of Test Materials

(a) Operating Conditions

A high COF was observed with smaller loads in dry test conditions especially with the lead/indium coated substrates. Examples of high COF at low load and low COF at high load in the early stages of the test were shown in figure 6.9. The high friction in the early stage was due to the harder ball sliding on the softer coating where ploughing and plastic deformation is dominant and this stage was more prolonged at lower loads. As the coating became thinner, due to wear, the COF settled down at a lower level. The running-in time for lead/indium coated leaded bronze substrates decreased with increase in load and depending on the thickness of the coating, the running-in time varied. The running-in period was not observed in uncoated leaded bronze substrates and this was one the reasons for lower SPWR than lead/indium coated substrates.

It was observed from POD test results that sliding velocity had no major influence on steady state COF and system SPWR. However, higher COF at the start of test (figure 6.10), especially on thin 1 µm coated leaded bronze substrates was observed at higher sliding velocities compared to the lower sliding velocities. As indicated in chapter 4.7.1, two sliding velocities, 0.47 m/s and 0.24 m/s were used at two different track radius of 18 mm and 9 mm, respectively, in dry test

conditions. Tests conducted at a sliding velocity of 0.47 m/s show high ploughing COF at the start of the test and tests at a sliding velocity of 0.24 m/s show lower ploughing COF, on the same coated test specimen. This was believed to be the rapid depletion of soft coating by the harder steel ball at high sliding velocity than that of low sliding velocity even though, the time required to complete one full rotation of the ball on the disc was equal for both track radii. For the same contact load, but at high sliding velocity, the plastic deformation of the coating is higher and the contact area between the ball and coating increases.

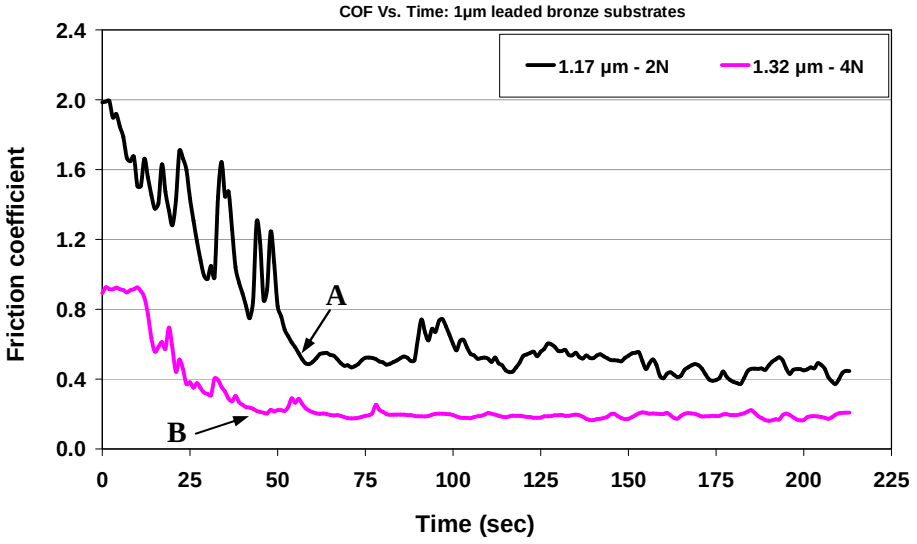

(a)

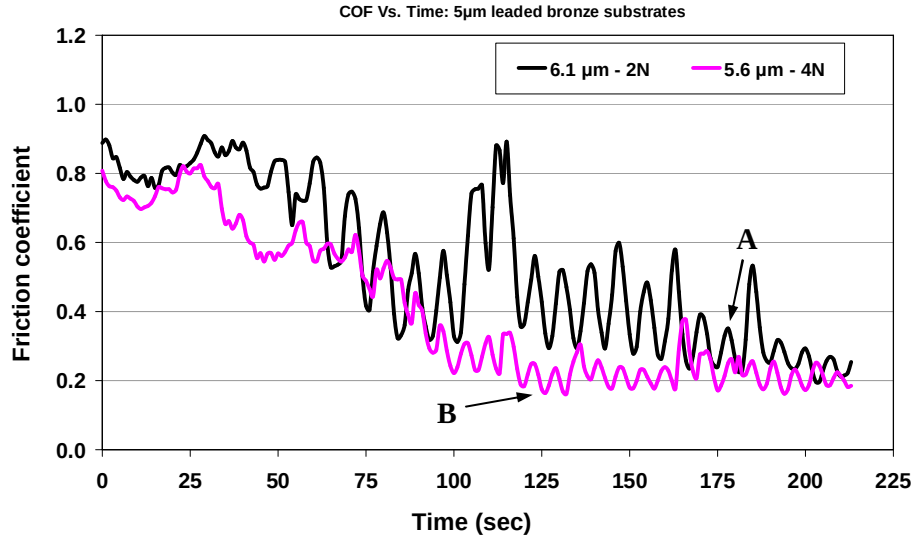

(b)

Figure 6.9 Decrease in running-in time with increase in load (a) 1 µm coated leaded bronze substrates (b) 5 µm coated leaded bronze substrates (A and B denotes running-in time at 2 N and 4 N loads, respectively)

Also due to higher sliding velocities, the heat generated at the contact was higher (table 5.45 & 5.46), this probably resulted in higher material transfer from soft coeting to the harder ball surface and COF fluctuate long, whereas, this effect is smaller for low sliding velocities. In the figure 6.10, it can be seen that for same contact load and rotational speed, the ploughing COF varied for different sliding velocities but the steady state COF is similar.

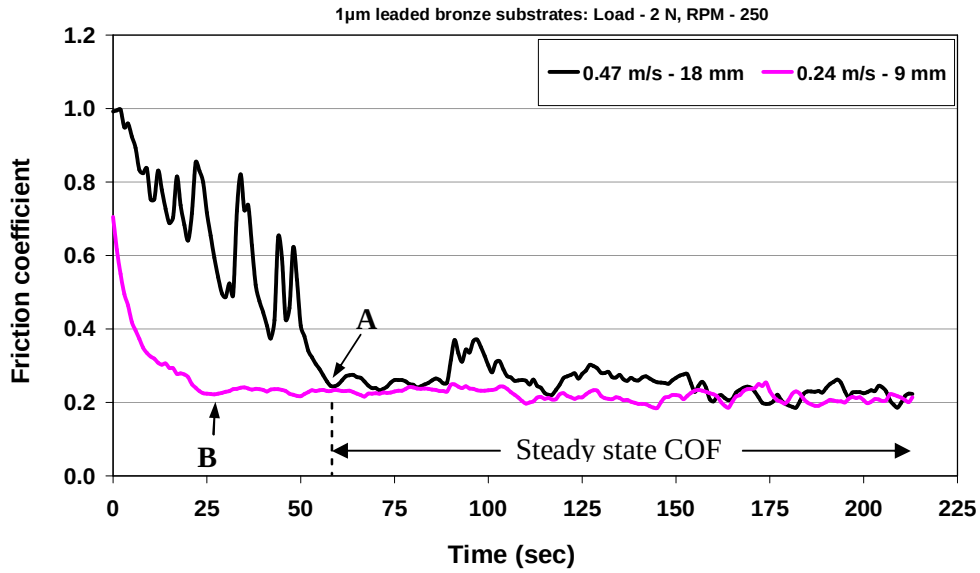

Figure 6.10 Influence of sliding velocity on ploughing COF at different track radii in dry test conditions: Load – 2 N, Speed – 250 rpm. (A and B denotes the running-in time in both sliding velocities)

(b) Material Transfer

It was observed from WLI images of the contacting surfaces that substrate material was transferred to the steel ball surface (figure 6.11). The transferred material from the uncoated leaded bronze substrates was very hard to remove from the ball surface. It formed a highly adherent thick layer on the ball. Among the leaded bronze substrates, the transfer material from 30% leaded bronze substrates to the ball surface was higher in quantity than for 20% leaded bronze substrates. This was probably due to the higher quantity of lead in the 30% leaded bronze and also may be connected with the grater "globularity" of the microstructure (Mohan, et. al., 1990; Molian, 1991; Prasad, 2004).

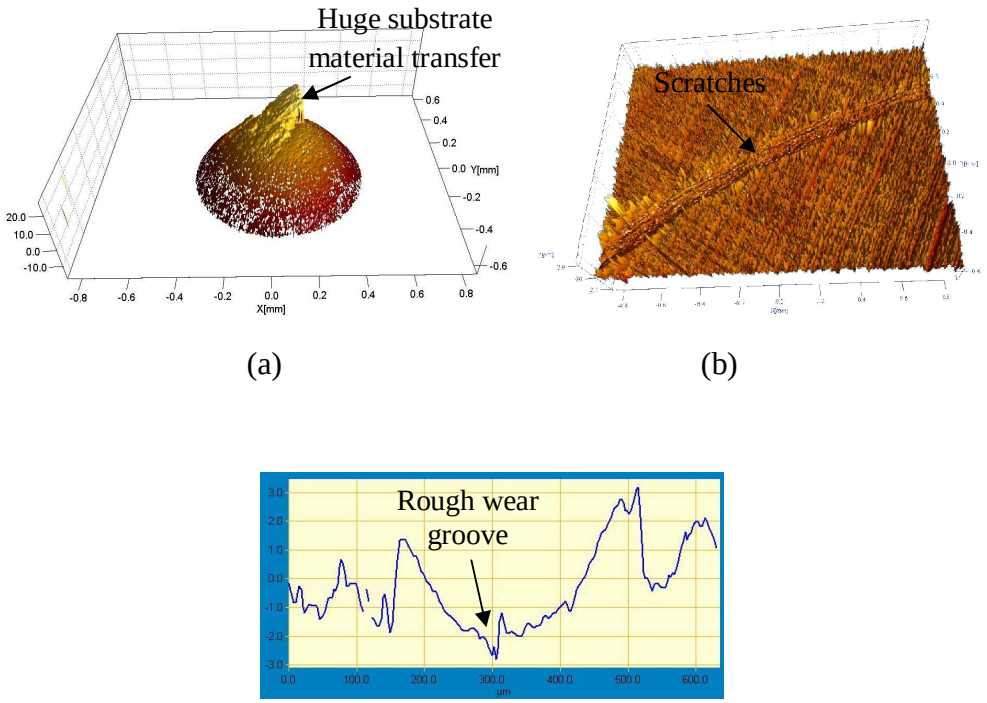

Figure 6.11 Material transfer from leaded bronze substrates to the steel ball surface in dry test conditions (a) Adhesion to the steel ball (b) Scratches on the substrate wear track (c) Rough wear groove observed from Talysurf profilometer.

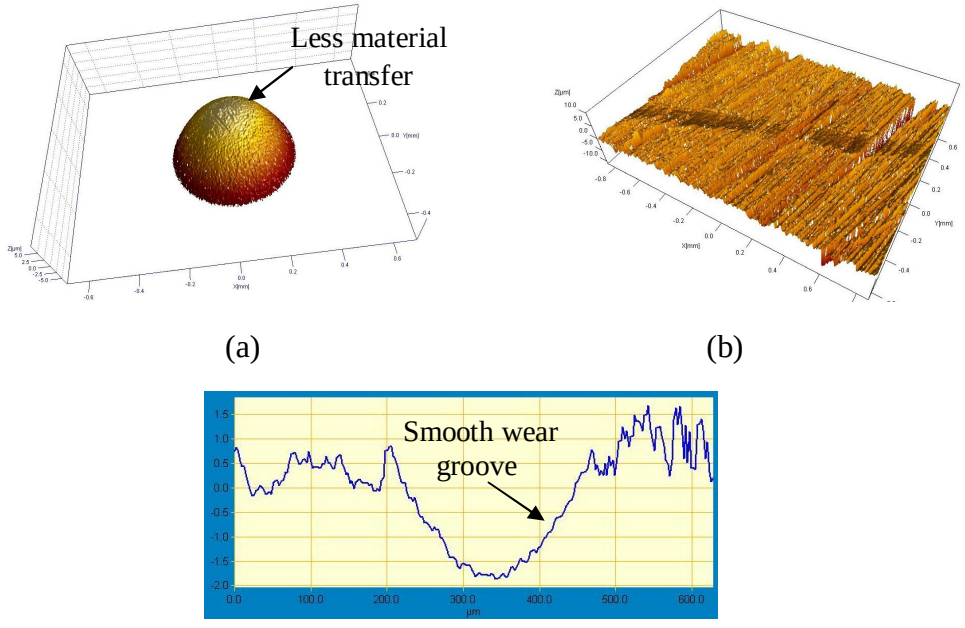

Figure 6.12 Material transfer from leaded bronze substrates to the steel ball surface in lubricated test conditions (a) Limited adhered material to the steel ball (b) Wear track on the substrate (c) Wear groove from Talysurf profilometer.

Material from lead/indium coating was also transferred to the steel ball surface, but this was not difficult to remove. In addition, the surface of the substrate/coating after sliding was found to be very rough. Many scratches were visible after the test in the worn areas. In marginally lubricated test conditions the effect of adhesion was less, compared to the dry test conditions. Figure 6.11 and figure 6.12 indicate the material transfer on to the ball surface from the substrate, scratches on the substrate surface and wear groove in the worn area.

(c) Ploughing and Deformation

Ploughing and deformation was observed on 30% leaded bronze substrates (figure 6.13 (a)) especially in high load-high speed conditions.

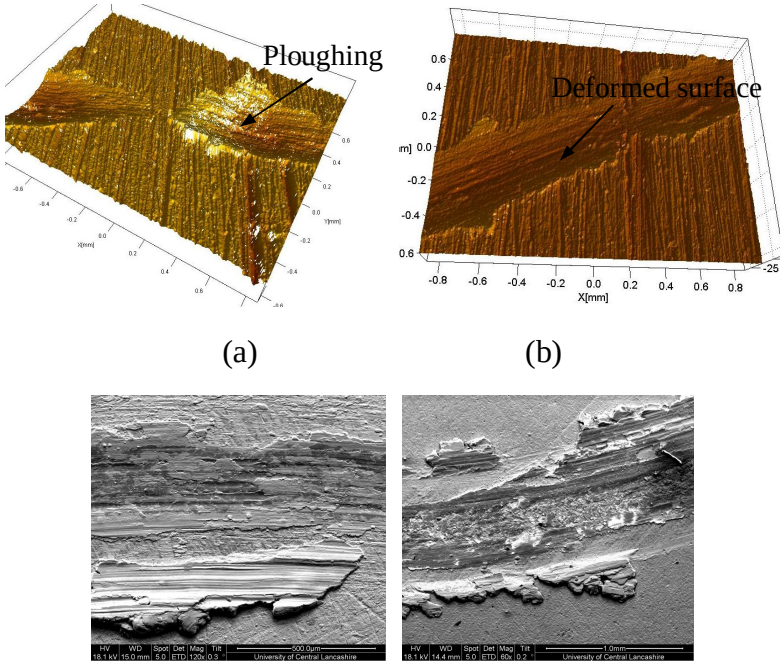

Figure 6.13 Various effects from leaded bronze substrates and lead/indium coatings (a) Ploughing of ball on leaded bronze substrates (b) Deformed surface (c) Deformed 1 µm lead/indium coating (d) Deformed 5 µm lead/indium coating.

A highly deformed substrate surface (figure 6.13 (b)) was also identified when tested with a small radius of rotation of the disc, possibly because the number of passes of the ball sliding on the disc was higher at small track radius than with higher track radius. Due to these effects, the COF and wear rates in dry test conditions were higher.

(d) Smearing of Lead

At high load/high speed conditions, the smearing of lead provided solid lubrication, but the wear rate was much higher. A thin layer of lead/indium coating formed on the substrate surfaces (figure 6.14) and protected the surfaces from high COF during the steady state conditions. Since the ball was repeatedly running on the same coated surface, the loose black powder formed from the wear debris, embedded between the contacting surfaces was probably smeared in a thin layer of oxide. This helped in creating a lubricating effect for the ball-disc contact and COF was low during the steady state period. This phenomenon was most commonly observed with 5 µm lead/indium coatings.

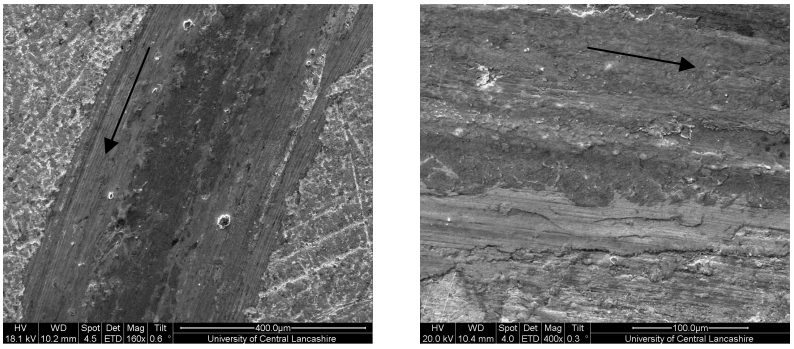

(a) (b)

Figure 6.14 Smeared thin black layer (dark areas) from lead/indium coatings (a) Marginally lubricated test conditions (b) Dry test conditions. (Arrow shows direction of sliding).

(e) Influence of Film Thickness

Coating thickness plays an important role in the outcome of the friction and wear according to Sherbiney and Halling (1976). They have explained that for thin coatings such as lead, on a harder surface such as mild steel, the wear behaviour is influenced greatly by the properties of the substrate, whereas, for large film thickness, the coating properties govern the behaviour. Considering this statement in relation to 1 µm and 5 µm coated leaded bronze substrates, 1 µm coatings have shown a lower wear rate than 5 µm coated leaded bronze substrates. This appears to be due to higher contribution of the substrate hardness for the 1 µm coating than that of 5 µm coatings. An optimal value between 1 and 5 µm might show good anti wear properties that might be optimally influenced by the properties of

both the lead/indium and leaded bronze substrates, and the wear rates attained might be similar to those of the leaded bronze substrates. Halling (1986) also suggested that, for soft films on hard surfaces, as the film thickness increases, the load carrying capacity of the system decreases and COF increases. When comparing lead/indium coatings with leaded bronze substrates, it was identified that the COF of 5 µm lead/indium coatings were higher than those of leaded bronze substrates due to the lower load carrying capacity. The 1 µm coatings did not protect the substrate surface from wear where as the 5 µm coatings did over the time period considered. Figure 6.15 shows the depth of wear track of 1 µm and 5 µm coated 20% leaded bronze substrates at 2 N loads. It can be seen in figure 6.15 (a) that wear depth of 1 µm coated 20% leaded bronze exceeded the actual thickness of coating, suggesting that the substrate material was in contact with the counterface after running-in period. However, the wear depth of 5 µm coated 20% leaded bronze substrate (figure 6.15 (b)) was not exceeded the actual coating thickness, suggesting that substrate surface was protected by the coating.

(a)

(b)

Figure 6.15 Wear depths of test materials after running-in period: Load 2 N (a) 1 µm coated 20% leaded bronze (b) 5 µm coated 20% leaded bronze.

6.2.6 Ranking of Materials from POD Apparatus

Ranking of materials in POD tests was done in the same way as for the TWT apparatus. From the dry test results shown in figure 5.49 (a), it was observed that for nominally same Load-Velocity (LV) conditions over the time period considered, 30% leaded bronze substrates had lower COF and higher SPWR than 20% leaded bronze substrates. 1 µm coated 20% leaded bronze had lower COF and slightly lower wear rate than 1 µm coated 30% leaded bronze substrates and 5 µm coated 30% leaded bronze had higher COF and slightly lower SPWR than 20% leaded bronze substrates.

In marginally lubricated test conditions from figure 5.49 (b), it was concluded that for the same Load-Velocity (LV) conditions, uncoated 30% leaded bronze had lower COF but slightly higher SPWR than that for 20% leaded bronze. The 1 µm lead/indium coated 30% leaded bronze substrates had lower COF and similar SPWR than that for 1 µm lead/indium coated 20% leaded bronze substrates. 5 µm lead/indium coated 20% leaded bronze substrates had high COF but similar wear rates than that for 5 µm lead/indium coated 30% leaded bronze substrates.

Overall it was observed from all the above results that, the uncoated substrates had better tribological properties than the lead/indium coated leaded bronze substrates over the time period used in this thesis. The 5 µm lead/indium coated substrates had the highest COF and SPWR than uncoated and 1 µm coated substrates. The 1 µm coated substrates COF and SPWR lie between those for uncoated and 5 µm coated leaded bronze.

6.3 Comparison of TWT Apparatus and POD Apparatus

One of the objectives of this thesis was to compare trends in friction and wear data obtained from TWT apparatus and POD apparatus to determine if tests on these apparatus showed similar trends/rankings. Friction and wear data were compared in figure 5.71 for dry tests and figure 5.72 for marginally lubricated test conditions at an average LV conditions implemented on each of the test apparatus.

From figure 5.71, it can be concluded that all the lead based test materials showed similar trends in terms of friction and wear in both test apparatus in dry test

conditions. However, the TWT apparatus had higher friction and wear rates than the POD apparatus. The 5 µm lead/indium coated leaded bronze substrates in the TWT apparatus had higher wear rates than in the POD apparatus. This was believed to be due to the higher contact areas in TWT apparatus resulting in higher wear rates and also due to the high contact loads implemented on the test specimens. From figure 5.72 it was observed that POD apparatus showed higher SPWR than the TWT especially on lead/indium coated leaded bronze substrates. This was due to the immediate breakdown of the lubricating film in POD apparatus since the ball repeatedly slid on the same path and the contact area was much smaller compared to TWT apparatus. In TWT apparatus, due to higher contact area, the marginal lubricant protected the contacting surfaces for a considerable period of sliding and wear rates were lower.

Therefore, it can be concluded that the trends of test results and the rankings obtained from both test apparatus are similar.

6.4 Frictional Heating Calculations from Ashby's Method

The frictional heating from washer-disc contact and ball-disc contacts were predicted using Ashby's method described in chapter 3.5.1. In Ashby's method, the friction heating between the flat on flat and ball on flat contacts were predicted using the "equivalent diffusion distances" which quantifies the distance that heat travels to the "heat sink" (In this case the substrate holding clamp) to the sliding surfaces. This distance was evaluated using the Ashby's equations described in chapter 3.5.1. In these calculations, the COF was one of the main parameters that influenced the flash heating predictions. The prediction of flash temperatures from the thin lead/indium coated leaded bronze substrates was very important to identify the melting effect (if any) in dry test conditions. Since, from the test results on lead/indium, it was known that the ploughing COF was higher during the running-in period, and especially in 5 µm coated lead/indium, it was believed that the lead/indium might have melted (at least) during the running-in period and reduced the COF and SPWR for the remainder of the test.

6.4.1 Thrust washer Test Apparatus (Flat on Flat Contact)

The frictional heating calculations obtained at different coating thicknesses of lead/indium from the TWT apparatus are detailed in table 5.44. The flash temperatures were estimated by using the mean ploughing COF and bulk temperature evaluated using the equation 3.27 (chapter 3.5.1). Table 5.44 shows that the flash temperature of 10% lead/indium was reached when thickness of lead/indium was 5 µm, but not when in case of uncoated leaded bronze substrates. However, by considering the maximum COF recorded during the running in period, the flash temperatures obtained were well beyond the melting point of 10% lead/indium. Figure 5.54 shows the flash temperature calculated at various values of friction coefficient and it can be concluded that the melting of lead/indium probably happened when the COF was at its maximum value (i.e maximum ploughing COF). It was observed that the running-in period of 5 µm coated leaded bronze substrates were longer than for 1 µm coated substrates (figure 5.50), and during the running-in period, due to the high frictional heating by the sliding surfaces, melting of lead/indium might have happened during this period (This was also found by Tian et. al., 1994; Jeng-Haur et. al., 2002). The flash temperatures predicted for uncoated leaded bronze substrates were much lower than that for lead/indium coated substrates. This was due to the higher conductivity and lower COF of leaded bronze substrates than that of lead/indium coatings. Since the mean COF in the steady state period was lower than that of running-in period, by using this mean COF in Ashby's method, the melting point of 10% lead/indium was not attained in the steady state period.

The bulk temperatures were calculated using the mean COF, since the duration of the friction tests after the running-in period was longer (figure 5.50) and during this period, the mean COF was approximately constant. The bulk temperatures predicted were only slightly higher than the ambient temperature (Typically 22 ºC to 32 ºC). The hardness of the coating was assumed to be similar to the hardness of the substrate when calculating the frictional heating of the TWT contact. This assumption was based on the work of Arnell, et al., (1991) who described that, for thin soft coating on a hard substrate, the contact area is defined by the hardness of the substrate. The same assumption was also used for the ball on disc contact.

Overall it was concluded that the 10% lead/indium might have melted during the running-in period where maximum COF was observed at the highest contact loads. This melting of lead/indium helped in reducing the COF and wear rates of leaded bronze substrates.

6.4.2 Pin on Disc Test Apparatus (Ball on Flat Contact)

In the pin on disc test apparatus, frictional heating between the ball and thin lead/indium coated disc was calculated in the same way as described for the TWT apparatus using the Ashby's method. However, the heat conduction length for the ball was estimated from the average contact radius (using equation 3.25 in chapter 3.5.1) by considering the hardness of the softer material (i.e. hardness of the substrate) rather than the physical length of the ball. For the disc, Ashby's assumption (i.e. an effective conduction length of disc would be twice its physical length (i.e. thickness) was used.

The flash and bulk temperatures predicted at different sliding velocities are detailed in table 5.45 and table 5.46, respectively. The mean ploughing COF was used for predicting the flash heating whereas the mean COF was used for the bulk heating in ball on disc contact. Unlike in flat on flat contact where the melting temperatures of lead/indium were only attained for maximum ploughing COF, here even at mean ploughing COF, the melting temperatures of 10% lead/indium were attained at high sliding velocities. This was due to the higher contribution of ploughing during the running-in and lower contact area with the mating surface resulting in higher heat generation. Table 5.45 shows that the maximum flash temperatures obtained from ball on disc contact at each contact condition was within the melting phase of 10% lead/indium and these are schematically shown in figure 5.51. Due to the high mean ploughing COF recorded during the running-in period of lead/indium coated substrates, the flash temperatures were exceeded the melting point of 10% lead/indium. However, at higher contact load and low speed conditions, as shown in table 5.46, the predicted flash temperatures did not reach the melting point of 10% lead/indium. This was due to the lower mean ploughing COF recorded at low sliding speed during the running-in period. As described earlier, at high load-low sliding speed conditions, the deformation of coating was higher due to the higher number of sliding passes of ball on disc,

since the track radius for high sliding speed was twice that of low sliding speed. For both sliding speeds, the bulk temperatures obtained were slightly beyond the ambient temperatures.

Figure 5.59 shows the flash temperature calculated at various regions of COF at different sliding speeds. It was concluded from figure 5.59 that melting temperatures of 10% lead/indium were reached when maximum and mean ploughing COF was used rather than mean COF at a sliding speed of 0.47 m/s only. High flash temperatures were obtained for 5 µm coated leaded bronze substrates than 1 µm coated leaded/bronze substrates due to their higher ploughing COF.

Overall it was concluded that frictional heating of the ball on disc contact probably melted lead/indium at the high speed during the running-in period which could have reduced the effect of friction and wear after the running-in period and protected the substrate surfaces.

Microscopic Evidence of Melting of Lead/Indium

Prediction of frictional heating using Ashby's method in flat on flat and ball on flat test configurations had suggested that lead/indium reached its melting point during the running-in period. Additionally smearing of a thin layer of lead at the contact interface had been observed to prevent high COF and substrate wear loss during the steady state period. To identify the microscopic of evidence of melting of lead/indium, SEM analysis on the wear test specimens were made after the running-in period. "Sphere" or Globule shaped metal particle characteristics of melted contacts were observed (Similar evidence also observed by Singh and Tsai (2003)), as shown in figure 6.16, near the edges of the wear track from lead/indium coated leaded bronze substrates in dry test conditions. It is believed that during the sliding of washer or ball on the lead/indium coated leaded bronze, the molten metal from lead/indium slipped away from the contacting surface and adhered to the edges of the track. At the contact interface between the ball and disc, no Spherical shaped particles from lead/indium were found. However, it is likely that any spheroid lead/indium particles that might have generated will have been subsequently "squashed" into the wear track if they had been trapped in the sliding interface.

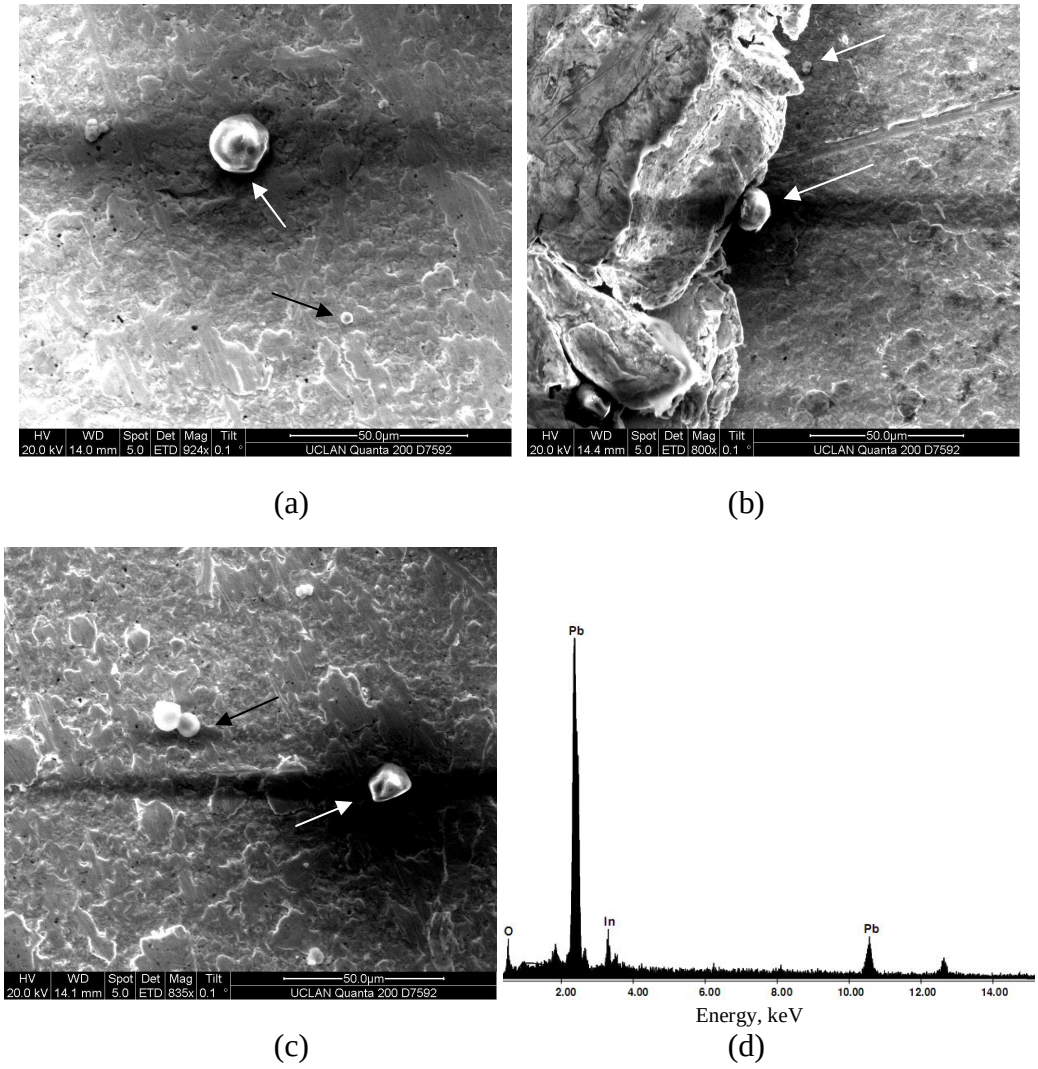

Figure 6.16 Evidence of melting of lead/indium. (a) Sphere shaped lead/indium particles found beside the wear track. (b) Lead/indium attached to the built up edge of the wear track (c) Melted lead/indium particles attached together (d) Elemental composition of Sphere shaped lead/indium particle seen in (b). (Note: The arrow shows the melted lead/indium particles)

6.5 Toughmet Substrates, Graphit-ic and Cr-Graphitic Coatings

Due to the hazardous nature of lead to the environment, lead free materials and other coatings, potentially useful in bearings were, investigated for their tribological behaviour. As described in chapter 5.4, a small number of tests on harder substrates, such as “Toughmet”, and low friction and high wear resistant coatings such as “Graphit-ic” and “Chromium Graphit-ic” coatings were investigated to identify their COF and SPWR using the POD apparatus and TWT apparatus. It was found that these new materials had superior friction and wear

properties (Stallard and Teer, 2009) to those of leaded bronze and lead/indium coatings. However, it is clear that these new materials have to be investigated more thoroughly in the future before recommending them as a potential replacement to the lead based bearings in fuel pumps.

6.5.1 Toughmet Substrates

Table 5.47 detailed the mean COF and system SPWR of two different types of Toughmet substrates tested at low PV and high PV, respectively in dry test conditions. It was observed that, both types of Toughment substrates had a similar COF, but the SPWR of CX-105 was slightly higher than that of AT-110. This might be due to the slightly higher hardness of CX-105 compared with AT-110 (Teer coatings, 2009). When conducting the sliding friction tests, these materials emitted loud noises. After the test, it was found that both substrate and counterface material had been lost. Therefore, the SPWR shown in the table 5.47 is given as the combined SPWR of washer and the substrate.

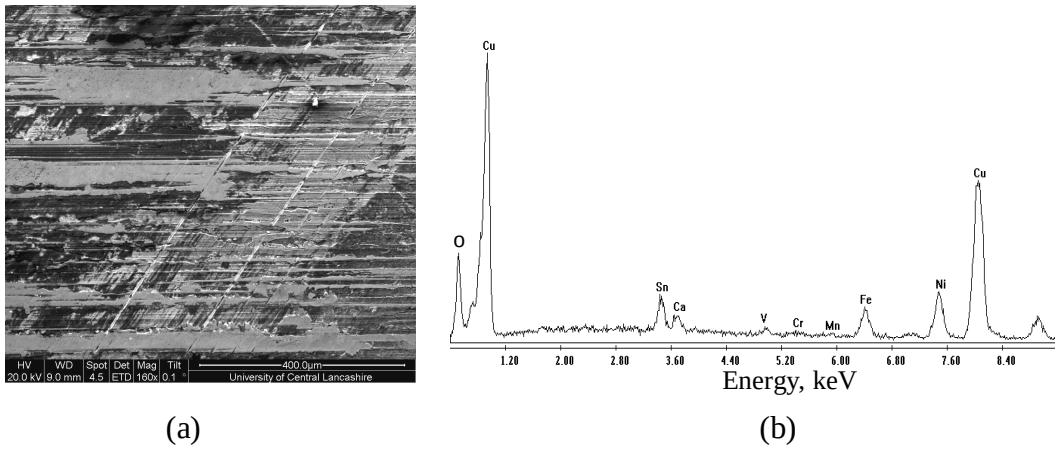

(a) (b)

Figure 6.17 SEM/EADX observations on Toughmet CX-105 (a) Smeared black-silver powder on substrate surface (b) Elemental analysis on substrate surface.

Figure 6.17, indicates that the sharp asperities from the substrate surface were polished and counterface material was transferred to the substrate surface. Loose wear debris, in the form of a black-silver powder, was also collected. Since the surface of the substrate was rougher than the worn counterface, it was believed that the embedded loose black-silver wear debris increased the COF through abrasive phenomena (Increased COF due to the abrasive phenomena is described by Holmberg and Matthews, 1994). Figure 5.60 shows the COF against time

graphs of both type of Toughmet substrates and it was observed that the COF increased steadily for some time and then remained approximately constant after 200 sec in both test specimens. The materials started to form wear debris particles and trapped between the surfaces. SEM/EDAX analysis showed that the smear of black-silver powder was partly from the steel counterface, but mainly from the Toughmet substrate material.

6.5.2 Graphit-ic and Cr-Graphit-ic Coatings

These coatings were selected and supplied by GAEC (2009) as possible replacements for the lead/indium coated leaded bronze bearing materials for the fuel pumps. These coatings are known to have excellent friction and wear properties (Teer coatings Ltd., 2009). Only a few tests were performed on these materials in this project, but it was identified that these coatings were tribologically superior to lead/indium coatings in many respects and would show no sign of wear even at high PV values. To replace the lead/indium coating with these new candidate coatings, a through investigation of how they behave in practical distribution in various test conditions and in real operation needs to be a topic of future work.

(a) Thrust Washer Test Results for Graphit-ic and Chromium Graphit-ic Coatings

Both Graphit-ic and Chromium Graphit-ic coatings showed stable and low COF even at high PV values. In table 5.49, the COF and SPWR of Graphitic (AT110-20D) and Chromium Graphit-ic (AT110-16D) are shown and in figure 5.63, these test results were plotted against PV. It was identified that both coatings had similar COF. With increases in PV, the COF was approximately constant for both coating types. When comparing these coatings, Graphit-ic coatings had a slightly lower COF than Chromium Graphit-ic due to lower hardness. In terms of SPWR, both coatings had excellent wear resistant properties. Surface profilometer measurements identified that the tested samples were only polished rather than worn. Since hardness values of both the coating and the counterface are similar, both materials were worn during the test. Therefore, the wear rate obtained was the combined wear of coating and counterface material. EDAX analysis on the worn test surface (figure 5.65) showed elements of counterface material on the

coating. When comparing the SPWR of these coatings, it appeared that AT110-16D had slightly higher wear resistance than AT110-20D. Additionally on analysing the counterface and worn surfaces it seemed that the effect of material transfer was very small. During the experimental process, a black loose powder was identified (figure 5.65 (b)). It was believed that the loose wear debris embedded between the contacting surfaces had increased the COF.

(b) Pin on Disc Tests on Graphit-ic Coatings

Figure 5.66 shows the test results of Graphit-ic specimen as a function of load and it can be seen when the load increased, the mean COF steadily increased whereas the SPWR decreased (also observed by Field et. al., (2009)). Since the hardness of this coating was much higher than ball, the ball wore much more than the coating. WLI observations on substrate surface (figure 5.67) showed that, only the asperity tips of the coating surface were polished and the coating was not broken even at maximum load. A flat wear surface on the ball was observed at every contact load. There was no obvious ploughing/deformation of the coating since the coating was much harder than ball which would be expected and the friction coefficient was approximately constant throughout the test.

So, overall, it was concluded that the Graphit-ic coating had excellent friction and wear resistant results in dry test conditions.

6.6 Comparison of Toughmet and Leaded Bronze Substrates

Figure 5.68 compared the mean COF and system SPWR of Toughmet substrates and leaded bronze substrates at a nominally similar PV in dry test conditions. It was concluded that the mean COF and system SPWR of Toughmet substrates were much higher than leaded bronze substrates. This was due to the hardness differences of both types of substrates which exceeded those of leaded bronze by a large margin. The hardness of Toughmet was 2.7 GPa compared to the leaded bronze hardness of 0.4 GPa. However, the friction results for Toughmet substrates were much more consistent than for leaded bronze substrates. The SPWR of Toughmet substrates represented the combined wear rates of washer and substrate since both materials were worn during the test. In contrast, leaded bronze substrates are softer than the counterface, so the material lost was higher from

substrates than that from counterface. Additionally, in leaded bronze substrates, the free lead acted as a solid lubricant which was absent in Toughmet substrates.

It was also observed from wear surfaces of Toughmet substrates that the "edge effect" from washer was severe as these substrates were much harder, plastic deformation and conformability/embeddability properties were very poor compared to leaded bronze substrates.

It can be concluded that leaded/bronze substrates do have some better tribological properties, but are inferior in terms of SPWR than Toughmet substrates.

6.7 Comparison of Graphitic and Lead/Indium Coatings

Figure 5.69 compared friction and wear results obtained using TWT apparatus with lead/indium coatings and lead free coatings at nominally similar contact loads. It can be concluded from these results that the lead free coating of Graphit-ic type have some superior tribological properties than lead/indium coatings in dry test conditions.

Figure 5.70 show POD test results of different thickness of lead/indium coated leaded bronze substrates and Graphit-ic coatings at nominally similar contact conditions. It was observed that Graphit-ic coating have some superior tribological properties over lead/indium coatings. Test results from TWT apparatus and POD test apparatus shown similar rankings when comparing the lead based materials against lead/free materials.

6.8 Conclusions from All Test Materials

The lead/indium coated leaded bronze substrates and the candidate coatings investigated in this project had very different friction and wear properties. These specimens differ in their hardness, topography, thickness, deposition process etc. Lead/indium coatings are "classic" coatings for bearing materials and have been used for a long period of time. Because of their low melting point and low shear properties, the coefficient of friction observed was slightly lower than that of uncoated leaded bronze substrates. However, the wear rates for these coatings were much higher than for uncoated leaded bronze substrates during the running-in period.

The friction and wear properties of lead/indium coatings were also influenced by the properties of the substrates used. The 20% leaded bronze substrates have shown lower SPWR, but higher COF than 30% leaded bronze substrates in all test condition. When lead/indium was deposited on these substrates, it was observed that they influenced the COF and the SPWR at high PV values by carrying part of the load. It was also identified that the wear rates increased with increase in lead/indium coating thickness during the running-in period. This indicates that the coating was worn heavily and did not protect the washer-disc or the ball-disc contact when the coating thickness was thinner (i.e. 1 μm). However, thick lead/indium coatings protected the substrate surface from wear at the expense of high COF values over the time period considered. (Beyond this period, the performance of the coating may differ.)

The general bearing alloy properties such as conformability, embeddability, wear resistance etc., discussed in chapter 2 were not relevant performance features for the lead/indium coatings in this thesis as the coating was very thin and was deposited on a softer substrate for other tribological reasons, i.e., to reduce friction and wear. The compatibility of lead/indium when deposited on 20% leaded bronze was better than when lead/indium deposited on 30% leaded bronze in terms protecting the substrate from wear. The main advantage of lead/indium coatings over leaded bronze substrates was low thermal conductivity and low melting temperature leading to distribution during running-in. As a consequence, the lead/indium coating reduced the COF and provided more effective solid lubrication at the contact interface during the steady state period. On the other hand, it was shown that leaded bronze substrates showed better wear resistance than coated systems over the period considered.

One of the major problems identified in gear pumps thrust bearings in fuel pumps is the breakdown of the fluid film during the running-in period due to the failure of fuel supply or frequent start up or shut down. The experimental tests conducted in this thesis, especially those on TWT apparatus, were conducted at PV conditions similar to those in operation. These tests showed that the leaded bronze substrates can resist lubricant failure for a short of time. For lead/indium coatings, marginal lubrication in the experiments protected surface from contact for a very

limited time and wear of the coating was observed as soon as the lubricant evaporated or was wiped away.

The fact that the new candidate coatings have shown superior wear resistance does not mean that they are necessarily the best coatings for the real applications, but they are potential coatings for the bearing material from this thesis. However, these lead free coatings are much harder than lead based coatings, therefore, the low shearing properties needed for bearing applications used in this thesis are missing. A harder coating deposited on harder substrates limits friction and wear by preventing ploughing as well as reducing the contact area with the counterface. However, the important bearing properties such as conformability, embeddability etc., discussed earlier are not observed with lead free coatings due to their high hardness. This may create serious problems in the real applications. These lead free coatings have better wear resistance, even at high PV conditions there was no sign of coating wear. Instead, the counterface (ball) was worn heavily. Even though these coatings showed no sign of wear loss, whether they perform better in the real application is still a question. But, in this thesis, it was shown that these coatings were superior to lead/indium coating in terms of friction and wear and they are less hazardous to nature. However, these and other lead free materials to be identified and tested in the future to attempt to provide all the important requirements needed for the current bearing application in fuel pumps.

CHAPTER 7

CONCLUSIONS AND FURTHER RECOMMONDATIONS

7.0 Conclusions

Various conclusions were drawn from the test results of all test materials in this thesis work. The final test results are summarized below.

1) The friction and wear results from pin on disc and thrust washer tests show similar friction and wear ranking of uncoated leaded bronze substrates and the same materials with 1 µm and 5 µm lead/indium coatings over the time period considered.

2) Uncoated lead/bronze substrates have better tribological properties against tool steel counterfaces than the same substrates coated with lead/indium.

3) 1 µm lead/indium coatings on the leaded bronze substrates have lower COF than uncoated and 5 µm lead/indium coated substrates. However, 5 µm coating protected the substrate surface from wear more effectively.

4) Conclusions 1, 2 and 3 are true both for dry rubbing and with marginal kerosene lubrication.

5) Using Ashby's method for frictional heating calculations, it was identified that the melting temperature of lead/indium was attained during the running-in period. Microscopic evidence of melting of lead/indium was also identified. Melting of the coating probably aids the tribological performance of the system.

6) Graphit-ic and Cr-Graphit-ic coatings on Toughmet substrates have wear properties which are far superior to those of the lead/indium coatings on leaded bronze substrates in this thesis work. However, their use as bearing materials may be restricted because, these materials does not provide conformability, embeddability, solid lubricating properties required for a bearing application, particularly used in gear pump thrust bearings.

7.1 Further Recommendations

Due to the high coefficient of friction and wear rates shown by the leaded bronze substrates and lead/indium coatings, and the superior wear properties from the new candidate coatings, several recommendations are made for further work on the materials for the gear pump thrust bearings. These recommendations have been divided into:

a) New materials and surface engineering
b) Experimental investigations
c) Wear mechanism analysis
d) Data analysis

7.1.1 New Materials and Surface Engineering

It is very important to search for better low friction and high wear resistant materials in the future. Various conventional lead free coatings and substrate materials are currently available which have good tribological properties in sliding contact applications. One example of such type of coatings are the carbon based Graphit-ic coatings which were tested in this thesis. Since these lead free coatings are much harder, surface topography is a very important factor when measuring the friction and wear rates. Therefore, some recommendations on the new test materials and their surface topography are summarized below.

- Preliminary friction and wear tests (chapter 5.4) on new candidate coatings such as Graphit-ic and Chromium Graphit-ic have shown far superior wear resistance properties compared with the bearing materials in current use, therefore, they can be a possible replacements for the thrust bearings in the gear pumps. However, a more detailed study of these coatings on a range of substrate materials, including Toughmet and phosphor bronze, should be carried out in future.
- Literature study on various types of wear resistant coatings for sliding bearing applications suggested that the topography of the coating can have a very important effect on tribological behaviour, particularly on counterface wear (Franklin and Beuger, 2007). As these new coatings faithfully reproduce the topography of the substrate, it is possible to

prepare on the substrate the required topography of the coating. Surface topographies ranging from ground to diamond lapped and very fine turned should be investigated to explore the possibility of generating an optimal topography combining minimal counterface wear and adequate lubricate retention.

- Thrust washer test results in this thesis showed that "edge effect" was severe in case of coated/uncoated substrate materials, where any mis-alignments in the washer-disc contact resulted in heavily worned test surface due to the sharp right angled edges of the washer from the inner/outer diameters. Therefore, in future experiments, it is important to increase the radius on the edges of the washer to avoid any initial damage to the coating/substrate surface.

7.1.2 Experimental Investigations

Friction and wear testing on new material should be carried out using a thrust washer test apparatus to replicate the real contact conditions in the gear pumps and a pin on disc test apparatus for facilitating high contact pressures. The summaries of investigations to be done in future are,

- Friction and wear testing should be carried out in unlubricated, marginally lubricated and fully lubricated test conditions to identify the tribological properties of test material at various PV conditions.
- Design of Experiments techniques should be used to determine how many experimental tests have to be performed for better understanding and data analysis purpose. With the use of 'Design of Experiments' software, the number of test specimens needed and optimum number of tests to be performed can be easily identified.
- Nano hardness measurements should be carried out on the substrate/coated surfaces to identify the influence of hardness to modulus of elasticity ratio on the observed wear behaviour so that the elastic/plastic deformation behaviour of test materials can be identified at various contact pressures. However, this measurement is only important if the test materials used in future are hard metal based.

7.1.3 Wear Mechanism Analysis

Wear loss measurements on the test specimens could be carried out using the Talysurf profilometer method to identify and compare the tribological performance of various test materials at various stages of testing. The summaries of various methods to analyse the wear mechanisms for the further work are,

- Scratch testing should be used to characterise coating adhesion and to identify the coating failure in a more effective way. This method particularly useful when assessing the adhesion strength of hard coatings on hard substrates and to measure the critical failure load of the coating. Since this test is quick and simple, the load conditions needed for the coating can be identified before performing the real test application.
- For comparing the wear rates of uncoated and coated substrate materials in the steady state period, the wear rate of substrates should be evaluated separately rather than the wear rate of the system (since the system wear rate represents the combined wear loss of the coating and the substrate).
- Various models of flash temperature/bulk temperature at the sliding contacts could be identified and the best model that is appropriate for the test geometry and test conditions should be used to identify the melting temperature the coating/substrate (if any) to asses the solid lubricating properties required for the gear pump thrust bearing applications.
- Wear mechanism maps and temperature maps should be prepared to identify the wear and temperature regions as recommended by Lim & Ashby (1987) to identify the wear transitions of the test materials at various PV conditions.

7.1.4 Data Analysis

Friction and wear data collected from the experimental tests should be analysed for better understanding on the behaviour of the test materials at various operating conditions. Therefore, the summaries of the friction and wear data analysis for the further work are,

- Comparison of the tribological properties of the Graphit-ic coatings and Toughmet substrates with those of alternative coatings/substrates for ranking of test materials to choose the appropriate test material for the bearing applications in fuel pumps.
- Ranking of test materials should be done according to their friction and wear behaviour under the same PV conditions as used in fuel pump thrust bearings so that choice of test materials at the best ratings can be identified and recommended to GAEC (2009).

References

Ahsan, Q., Haseeb, A. S. M. A., Haque, E., and Celis, J. P. (2003), "Wear failure of a Leaded Bronze Bearing: Correlation between Plant Experience and Laboratory Wear Test Data", *Journal of Materials Engineering and Performance*, Volume 12, Issue 3, pp. 304-311.

Amontons, G. (1699), "De la résistance cause dans les machines", *Mem. Acad. Roy. Sci.*, pp. 257-282.

An, J., Liu, Y. B., and Lu, Y. (2004), "The influence of Pb on the friction and wear behaviour of Al–Si–Pb alloys", *Materials Science and Engineering*, Vol. 373, Issues 1-2, 25, pp. 294-302.

Andrew E., Karthikeyan, S., Kim, H. J., Rigney, D. A. (2007), "The effect of sliding velocity on the tribological behaviour of copper", Wear, Vol. 263, pp. 614–618.

Anonymous (1990), "Properties and selection: Non-ferrous alloys and special purpose materials", ASM Metals handbook, Vol. 2, 10th edition, *ASM international*, Ohio.

Anonymous (1992), "Friction, lubrication and wear technology", ASM handbook, Vol. 18, 10th edition, *ASM international*, Ohio.

Anonymous (2000), "Mechanical Testing and Evaluation", ASM handbook, Vol. 8, *ASM international*, Ohio.

Anonymous (2002), ASTM standard G 99-95a, "Standard test method for wear testing with a pin-on-disk apparatus", *ASTM International*, West Conshohocken, PA, DOI: 10.1520/G0099-95AR00E01, Available at: www.astm.org (Accessed 10 Sep 2009).

Anonymous (2007), ASTM standard D3702-94, "Standard Test Method for Wear Rate and Coefficient of Friction of Materials in Self-Lubricated Rubbing Contact Using a Thrust Washer Testing Machine", *ASTM International*, West Conshohocken, PA, DOI: 10.1520/D3702-94R09, www.astm.org (Accessed 10 Sep 2007).

Anton Van Beek (2004), "Machine life time performance and reliability", *Tribos*, 1st edition, ISBN 9037002080.

Archard, J. F. (1953), "Contact and rubbing of flat surfaces", *J. Appl. Phys*., Vol. 24, pp. 981-988.

Archard, J. F. (1958/59), "The temperature of rubbing surfaces", *Wear*, Vol. 2, pp. 438-455.

Archard, J. F., and Hirst, W. (1956), "The wear of metals under unlubricated conditions", *Proc. R. Soc. Lond*. A 236, pp. 397-410.

Arnell, R. D. (1990), "The mechanism of Tribology of thin film systems", *Surface and coating technology*, Vol. 43-44, pp. 674-687.

Arnell, R. D., Davies, P. B., Halling, J. and Whomes, T. L. (1991), "Tribology: principles and design applications", *Macmillan education ltd*.

Arnell, R. D., Soliman, F. A. (1978), "The effect of speed, film thickness and substrate surface roughness on the friction and wear of soft metal films in ultra high vacuum", *Elsevier, Thin solid films*, Vol. 53, pp. 333-341.

Ashby, M. F., Abulawi, J., and Kong, H. S. (1990), "On surface temperatures at dry sliding surfaces", *report No. CUED/C-MATS/TR160*, Cambridge University Engineering Dept., Cambridge, UK.

Ashby, M. F., Abulawi, J., and Kong, H. S. (1990), "T-MAPS software user manual", Cambridge University Engineering Dept., Cambridge, UK.

Ashby, M. F., Abulawi, J., and Kong, H. S. (1991), "Temperature maps for frictional heating in dry sliding", *Tribology transactions*, Vol. 34, Series 4, pp. 577-587.

Balić, E. E., and Blanchet, T. A. (2005), "Thrust-washer tribological evaluation of PS304 coatings against Rene 41", *Wear* , Vol. 259, Issues 7-12, pp. 876-881.

Barber, J. R., (1969), "Thermoelastic Instabilities in the Sliding of Conforming Solids", *Proc. Roy. Soc. London*, A 312, pp. 381-394.

Barwell, F. T. (1979), "Bearing systems - Principles and practice", *Oxford University Press*, Oxford, 565 p.

Bass, M., "Physical Processes in Laser-Material Interaction", in NATO Advanced Studies Institute Series R: Physics, M. Bertollotti, (1982) ed., *Plenum Press*, New York, pp. 77-108.

Bekir, S. (2009), "Investigation of tribological and mechanical properties of metal bearings", *Indian Academy of Sciences*, Bull. Mater. Sci., Vol. 32, No. 4, pp. 451-457.

Bhushan, B. (1999), "Principles and applications of Tribology", *John Wiley & Sons*, *Inc*.

Bhushan, B. (2001), "Modern Tribology handbook", Vol. I & II, *CRC press LLC*.

Bhushan, B., Gupta, B. K. (1997), "Handbook of Tribology: Materials, coatings, and surface treatments", *McGraw-Hill*, New York.

Blok, H. (1937), "Theoretical study of temperature rise at surfaces of actual contact under oiliness lubricating conditions", *Proceedings of the General Discussion on Lubrication and Lubricants,* Institute of Mechanical Engineers, London, Vol. 2, pp. 222-235.

Bojan Podgornik, Joze Vizintin (2003), "Tribology of thin films and their use in the field of machine elements", *Pergamon*, Vacuum, Vol. 68, pp. 39–47.

Bowden, F. P., and Tabor, D. (1950), "The friction and lubrication of solids", part 1, *Clarendon press*, Oxford, UK.

Bowden, F. P., and Tabor, D. (1964), "The friction and lubrication of solids", part II, *Clarendon press*, Oxford, UK.

Brush wellman Inc. (2009),"Copper Nickel Tin alloys", [online] (updated 25 July 2009) Available at www.brushwellman.com/Alloy.aspx?id=278&id2=1352 (Accessed 10 April 2010).

Buckley, D. H. (1981), "Surface effects in adhesion, friction, wear and lubrication", *Elsevier*, Amsterdam.

Carignan, Forest J., and Rabinowicz, Ernest. (1980), "Friction and Wear at High Sliding Speeds", *Tribology Transactions*, Vol. 23, Issue 4, pp. 451-459.

CDA (2010), "Copper and copper alloys", [online] (updated 10th July 2010) Available at www.copper.org .

Clauss, F. J., (1972), "Solid Lubricants and Self-Lubricating Solids", *Academic press*, New York.

Davis, F. A., and Eyre, T. S. (1991), "Wear of Plain Bearing Materials with Particular Reference to Soft Phases", *Materials Science and Technology*, Vol. 7, pp. 746-756.

Equey, S., Bosc, P., Mischler, S. (2010), "Effect of microstructure on the wear and frictional mechanisms of copper-based bearing alloys", *Nordtrib 2010*, paper-0147.

ESDU (Engineering Sciences Data Unit) (1988), "Selection of alloys for hydrodynamic bearings", Vol. 88018, pp. 26.

Fein, R. S. (1969), *ASLE Trans*., Vol. 12 53; Discussion in Proc. NASA Sponsored Symp., interdisciplinary Approach to Friction and wear: Ku, P. M., Ed., U.S. Government Printing Office, Washington, 1968, p. 321.

Field, S. K., Yang, S., Teer, D. G., (2009), "The Deposition, Tribological Properties, and Applications of Sputtered Carbon Coatings", *Teer coatings Ltd*., [online] Available at: www.teercoatings.co.uk.

Franklin, S. E., Beuger, J. (2007), "A comparison of the tribological behaviour of several wear-resistant coatings", *Surface and Coatings Technology*, Vol. 54-55, Part 2, pp. 459-465.

Fuller, D. D. (1984), "Theory and Practice of Lubrication for Engineers", 2nd edn. *John Wiley & Sons*, New York.

George Plint (2006), "Guidance Notes on Test Specimens", Available at: www.phoenix-tribology.com/cat/at2/index/test%20specimens.pdf. (Accessed 20th March 2010).

Gerkema, J. (1985), "Lead thin film lubrication", *Wear*, Vol. 102, pp. 241 – 252.

Glaeser, W. A. (1992), "Materials for Tribology", *Tribology series,* Vol. 20, Elsevier.

Goddard, J., and William, M. (1962), "A theory of friction and wear during the abrasion of metals", *Wear*, Vol. 5, pp. 114-135.

Godfrey, D. (1968), "Boundary lubrication: interdisciplinary approach to friction and wear". *NASA SP-181*, pp. 335-1318.

Goodrich Aero Engine Controls (2009), A Rolls-Royce plc and Goodrich Corporation joint venture, [online] Available at: www.aeroenginecontrols.com (Accessed 15 May 2009).

Guermazi, N., Elleuch, K., Ayedi, H. F., Fridrici, V., Kapsa, P. (2009), "Tribological behaviour of pipe coating in dry sliding contact with steel", *Materials and Design*, Vol. 30, pp. 3094–3104.

Halling, J. (1986), "The Tribology of surface coatings, particularly ceramics", *Pro. Instn. Mech. Engrs*., Vol. 200, No. C1, pp. 31-40.

Hamrock, B. J. (1994), "Fundamentals of fluid film lubrication", *McGraw-hill*, New York.

Haseeb, A. S. M. A., Masjuki, H. H., Ann, L. J., Fazal, M. A. (2010), "Corrosion characteristics of copper and leaded bronze in palm biodiesel", *Fuel Processing Technology*, Vol. 91, pp. 329-334.

Hertz H. (1896), **"**Miscellaneous Papers"**,** *Macmillan*, London.

Hokkirigawa, K., and Kato, K. (1988), "An experimental and theoretical investigation of ploughing, cutting and wedge formation during abrasive wear", *Tribology International*, Vol .21, pp. 51-57.

Holmberg, K. (1991b), "A suggestion for the classification of tribological mechanisms in coated surfaces", *Finnish Journal of Tribology*, Vol. 11, pp.1-17.

Holmberg, K. (1992a), "A concept for friction mechanism of coated surfaces", *Surface and coating technology*, Vol. 56, pp. 1-10.

Holmberg, K., Matthews, A. (1994), "Coatings Tribology: Properties, Techniques and Applications in Surface Engineering", Elsevier, *Tribology series*, Vol. 28.

Holmberg, K., Ronkainen, H., Matthew, A. (2000), "Tribology of thin coatings", *Ceramics International*, Vol. 26, pp. 787-795.

Holmberg, K., Ronkainen, H., Matthew, A. (2003), "Thin films in Tribology", Amsterdam, *Elsevier*, pp. 399-407.

Hu Zhongliang, Chen Zhenhua, Xia Jintong, Ding Guoyun. (2008), "Effect of PV factor on the wear of carbon brushes for micro motors", *Wear*, Vol. 265, pp. 336–340.

Humpston, G., Jacobson, D. M. (2005), "Principles of soldering", *ASM international*, Chapter 2, pp. 45-47.

Hutchings, I. M. (1992), "Tribology: friction and wear of engineering materials", *Edward Arnold*, 1st edition, London

Indium Corporation of America (ICA) (2010), "Indium/lead phase diagrams", [online] Available at: www.indium.com. (Accessed 5th June 2010).

Jackson, R. L., Green, I. (2001), "Study of the tribological behaviour of thrust bearings", *Tribology Transactions*, Vol. 44, Series 3, pp. 504-508.

Jaeger, J. C. (1942), "Moving sources of heat and the temperature at sliding contacts", Proc. *Roy. Soc.*, NSW, Vol. 76, pp. 203-224.

Jahanmir, S., Abrahamson E. P., and Suh, N. P. (1976), "Sliding wear resistant of metallic coated surfaces". *Wear*, Vol. 40, pp. 75-84.

Jeng-Haur Horng, Mu-Long Len, Jian-Shing Lee. (2002), "The contact characteristics of rough surfaces in line contact during running-in process", *Wear,* Vol. 253, pp. 899–913.

Johnson, K. L. (1985), "Contact Mechanics", *Cambridge University Press*, Cambridge, pp. 84–118.

Kayaba, T. (1962), "A study of the wear and friction of some bearing materials", *Wear*, Vol. 5, pp. 173-181.

Kazuhisa Miyoshi. (2000), "Fiction and wear properties of selected solid lubricating films, Part 2: Ion-plated lead films", *Glenn research centre*, Ohio.

Kuwano, H. (1990), "Solid lubricant film formation using fast atom beam sputtering", *Japanese J. of Tribology*, Vol. 35, pp. 291-300.

Lancaster, J. K. (1973), "Dry bearings: a survey of materials and factors affecting their performance", *Tribology Int*., Vol. 6, pp. 219-51.

Landown, A. R., Price, A. L. (1996), "Materials to resist wear: a guide to their selection and use", *Oxford: Pergamon cop*.

Leroy, J. M., Floquet, A. & Villechaise, B. (1990), "Thermo mechanical behaviour of multilayered media: Theory", *J. of Trib. Trans.*, ASME, Vol. 111, pp. 538-544.

Lim, S. C., and Ashby, M. F. (1987), "Wear mechanism maps", *Acta. Metall*, Vol. 35, pp. 1-24.

Ludema, K. C. (1996), "Friction, Wear, Lubrication: A textbook in Tribology", *CRC press*, ISBN 0849326850.

Lyamkin, S. A., (2009), "Initial Stages of the Formation of Lead Oxide Phases", *Russian Metallurgy (Metally)*, Pleiades Publishing Ltd., Vol. 3. pp. 197-200.

Mohan, S., Agrawa, V., and Ray, S. (1990), "The Effect of Lead Content on the Wear Characteristics of a Stir-Cast Al-Pb Alloy", *Wear*, 140, pp.83-92.

Molian, P. A., Buchanan, V. E., Sudarshan, T. S., and Akers, A. (1991), "Sliding wear characteristics of non-equilibrium Cu-Pb alloys", *Wear*, 146 257-267.

Montgomery, R. S. (1970), "Friction and wear of some bronzes under lubricated reciprocating sliding", *Wear*, Vol. 15, pp. 373-387.

Moore, D. F. (1972), "The friction and lubrication of Elastomers", *Pergamon*, Oxford, UK.

Neale, M. J. (1996), "Tribology handbook", *Butterworth-Heinemann*, London.

Okamoto, H. (2006),"In-Pb (Indium-Lead)", *Journal of Phase Equilibria and Diffusion,* Vol. 27, pp. 312.

Pathak, J. P. (1993), "Seizure Resistance Characteristics of Cu-Pb Bearing Al-alloys," *Materials Science and Technology*, Vol. 9, pp.403-07

Pathak, J. P., Tiwari, S. N. (1992), "On the mechanical and wear properties of copper-lead bearing alloys", Wear, Vol. 155, Issue 1, pp. 37-47.

Prasad, B. K. (2004), "Sliding wear behaviour of bronzes under varying material composition, microstructure and test conditions", *Wear*, Vol. 257, pp. 110–123.

Prasad, B. K., Patwardhan, A. K., and Yegneswaran, A. H. (1996), "Factors controlling dry sliding wear behaviour of a leaded tin bronze", *Materials Science and Technology*, Vol. 12, pp. 427- 435.

Rabinowicz, E. (1995), "Friction and Wear of Materials", 2nd edition, *Wiley cop*, New York.

Rabonowicz, E., Dunn L. A., and Russell, P. G. (1961), "A study of abrasive wear under three body abrasion", *Wear*, Vol. 4, pp. 345-355.

Ravikiran, A., Lim, S. C. (1999), "A better approach to wear-rate representation in non-conformal contacts", *Wear*, 225–229, pp. 1309–1314.

Ravindran, K. A., Ramasamy, P., Laddha, G. S. (1980), "Frictional behaviour of thin films of soft metals", Thin Solid Films, Vol. 66, pp. 249-254.

Rigney, D. A. (1981), "Fundamentals of friction and wear of materials", *Am. Soc. metals*, Metals Park, Ohio.

Roberts, E. W. (1990), "Thin solid lubricant films in space", *Trib. Int.*, Vol. 23, Issue 2, pp. 95-104.

Roy Chowdhury, S. K., Kaliszer, H., and Rowe, G. W., (2003), "An analysis of changes in surface topography during running-in of plain bearings", Wear, Vol. 57, Issue 2, pp. 331-343.

Ruggeri, O., Sambogna, G., Balboni, C. P., and Volpato, G. A. (1980), "Dry lubrication with soft metals: the tribological behaviour of steel a thin film of cadmium rubbing on carbon", *Wear*, Vol. 59, pp. 433 – 446.

Sedlaček, M., Podgornik, B., Vižintin, J. (2009), "Influence of surface preparation on roughness parameters, friction and wear", *Wear*, Vol. 266, Issue 3-4, pp. 482-487.

Sherbiney, M. A., Halling, J. (1976), "The Hertzian contact of surfaces covered with metallic films", *Wear*, Vol. 40, pp. 325–337.

Sherbiney, M. A., Halling, J. (1977), "Friction and wear of ion-plated soft metal films", *Wear*, Vol. 45, pp. 211-220.

Singh, A., Tsai, A. P., (2003), "Melting behaviour of lead and bismuth nano-particles in quasicrystalline matrix-The role of interfaces", *Sudhana*, Vol. 28, Parts1&2, pp.63-80.

Stachowiak, G. W., Batchelor, A. W. (2005), "Engineering Tribology", 3rd edition, *Elsevier*, Amsterdam, Netherlands, 801 pp.

Stallard, J., and Teer, D. G. (2009), "The friction and wear properties of CrN, Graphit-ic and Dymoni-ic, coatings in air and under oil-lubrication", *Teer coatings Ltd*., [online] Available at: www.teercoatings.co.uk.

Stolarski, T. A. (1990), "Tribology in machine design", *Heinemann Newnes*, ISBN: 0434918261, pp. 80-82.

Suh, N. P. (1986), "Tribo physics", *Prentice-hall*, Englewood Cliffs, New Jersey.

Suh, N. P., Sin, H. C. (1981), "The genesis of friction", *Wear*, Vol. 69, pp.91-114.

Tabor, D. (1945), "The Frictional Properties of Some White Metal Bearing Alloys: The Role of the Matrix and the Hard Particles", *J. Appl. Phys*., Vol. 16, pp. 325-37.

Teer coatings Ltd. (2009), Graphit-ic coatings, [online] (updated 25 May 2009) Available at: http://www.teercoatings.co.uk/index.php?page=40 (Accessed 10 April 2010).

Temel Savas-kan, Osman Bican. (2010),"Dry sliding friction and wear properties of Al–25Zn–3Cu–3Si alloy", *Tribology International*, Vol. 43, Issue 8, pp. 1346-1352.

Teruji Nojiri, Fusavo Hayama, Shigeo Oya. (1971), "The relationship between Lead-bronze and its casting structure", *Trans. JIM*., Vol. 12, pp. 261-267.

Tian, X., Kennedy, F. E. (1994), "Maximum and average flash temperature in sliding contact, *ASME Trans., J. Tribol*., Vol. 116, pp. 167–174.

Tsuya, Y., Takagi, R. (1964), "Lubricating properties of lead films on copper", Wear, Vol. 7, pp. 131-143.

Ugur Ozsarac, Fehim Findik, Mehmet Durman. (2007), "The wear behaviour investigation of sliding bearings with a designed testing machine", *Materials and Design*, Vol. 28, pp. 345–350.

White house, D. J. (1997), "Surface metrology", *Meas. Sci. Technol*., Vol. 8, pp. 955-972.

Williams, J. A. (2005), "Engineering Tribology", Cambridge university press, Newyork, pp. 392-393.

Zeren, A. (2007), "Embeddability behaviour of tin-based bearing material in dry sliding", *Materials and Design*, Vol. 28, Issue 8, pp. 2344-2350.

Zeren, A., Feyzullahoglu, E., Zeren, M. (2007), "A study on tribological behaviour of tin-based bearing material in dry sliding", *Materials and Design*, Vol. 28, pp. 318–323.

Zhang, Y. S., Wang, K., Han Z., Liu, G. (2007), "Dry sliding wear behaviour of copper with nano-scaled twins", *Wear*, 262, pp. 1463–1470.

Appendix

Presentations and Publications

Sarma Volety, (2008). "Tribological evaluation of lead-bronze substrates and lead-indium coatings using thrust washer tester". *Tribology UK V**,** student networking event**,** University of Southampton,* Southampton

Sarma Volety, Sherrington Ian, Arnell Derek., (2008). **"**Tribological evaluation of lead-bronze substrates and lead-indium Coatings". *Mission of Tribology*, *Research 17, December 3, 2008*, The Institute of Mechanical Engineers, Westminster, London

B. S. Volety, R. D. Arnell, I. Sherrington, T. Hirst, (2010). "Dry Sliding Friction and Wear Characteristics of Lead Bronze Bearing Materials", *Nortrib 2010, No. 0098, Storforsen, Sweden.*

B. S. Volety, R. D. Arnell, I. Sherrington, (2010). "Tribological Characteristics of Lead Based Bearing Materials in Dry Sliding Contact Conditions", *Tribology Society of India*.

Dry Sliding Friction and Wear Characteristics of Lead Bronze Bearing Materials

B. S. Volety*, R. D. Arnell*, I. Sherrington*, T. Hirst+

* Jost Institute for Tribotechnology, University of Central Lancashire, Preston, PR1 2HE, Lancashire, UK.
+ Aero Engine Controls – A Rolls-Royce and Goodrich Corporation Joint Venture, Shaftmoor Lane, Hall Green, Birmingham B28 8SW, UK.

Abstract

A pin on disc machine has been used to measure the tribological characteristics of 20% and 30% lead in bronze, generally known as "lead bronze" materials. These materials are commonly used in high performance hydrodynamic bearings. The two types of lead bronze were studied, in uncoated form and with lead 10% indium electroplated coatings. The tribological properties of the hard commercial coating "Graphit-ic" were also studied. Its greater environmental acceptability, outstanding wear resistance and moderately low friction make it a potential replacement for lead containing materials in some applications.

Keywords: Bearing materials, lead indium coatings, environmentally acceptable bearing materials.

1. INTRODUCTION

Bearing materials may be designed to have low friction, high wear resistance, high load carrying capacity and self lubricating properties. They are generally made of copper-tin -lead alloys and may also have coatings containing lead, such as the lead indium system investigated in this paper, to give the bearing properties such as: conformability, embeddability, corrosion resistance etc [1]. These films may also exhibit limited self lubricating properties to enhance performance when insufficient liquid is available for fluid lubrication. Due to the environmentally hazardous nature of lead and the increased availability of wear resistant coatings, bearing manufacturers and users are now looking towards the use of lead-free coatings. To allow benchmark performance details to be obtained, this study has investigated high lead content copper-tin-bronzes. These materials are tested alone and with lead indium coatings as used in commercial bearings. It is planned that the performance of these materials will be compared with lead-free materials with the potential to be used as bearing materials. The early stages of this work are also reported.

2. EXPERIMENTAL DETAILS

Tests to establish friction and wear characteristics were performed in dry sliding, with three test specimens of each type of substrate or substrate coating combination tested using a conventional pin on disc (POD) test apparatus with an ASTM G99-95 configuration [2]. The test equipment is illustrated in figure 1. Each test was conducted under normal loads of 2N, 3N and 4N while keeping the rotational speed constant at 250 rpm. A total sliding length of 100 m was used. The sliding velocity was 0.47 ms^{-1} for all the materials except for 5 μm 30% lead bronze substrates which

were tested at 0.24ms^{-1} (by using a different sliding radius).

Lead bronzes with 20% and 30% lead, CuPb20Sn5 and CuPb30Sn2 respectively, were investigated. They were tested alone and with electroplated coatings of 10% indium in lead alloy, referred to as "lead indium", of 1 μm and 5 μm nominal thicknesses. (In this film the 10% dispersed indium atoms in the lead structure serve to lower the melting point of the lead improving its performance as a tribological aid to sliding.) A 6 mm diameter, 100 Cr6 steel ball was used as the counterface in all the tests. The contact situation in POD was non-conformal and did not replicate the contact geometry in plain bearings. However, the use of this test apparatus allowed high contact pressures to be applied, accelerating testing.

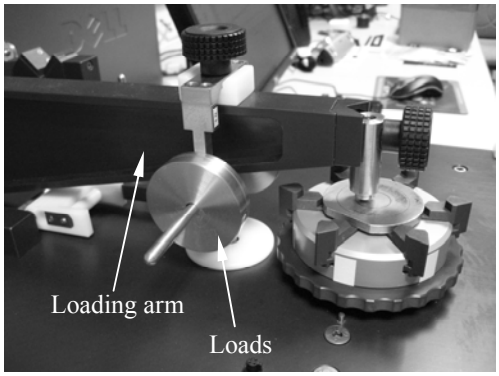

(a) Pin on disc test apparatus

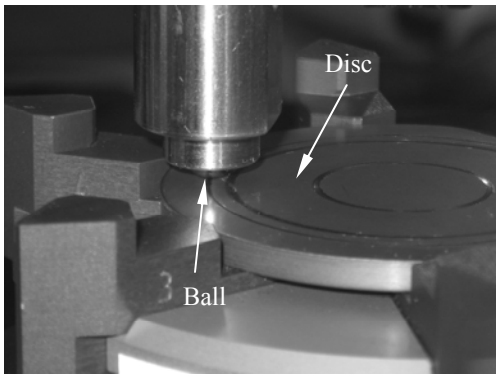

(b) Close view of contact

Figure 1 Conventional pin on disc test configuration

The PC software interfaced to the test equipment allowed the coefficient of friction (COF) and frictional force to be displayed as a function of time. The coefficient of friction, μ, was evaluated straightforwardly as the ratio between the frictional force, measured by a lateral force transducer in the test equipment and the normal load.

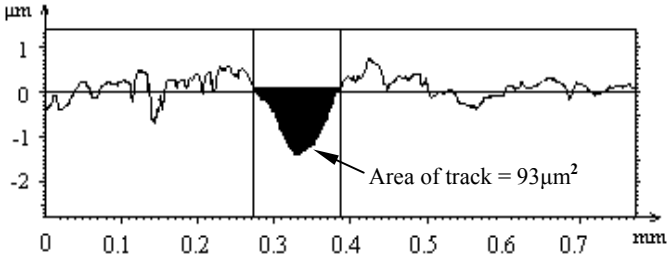

Figure 2 Wear profile from Talysurf profilometer

The instantaneous value of the friction coefficient was found to vary considerably during the tests. It was, therefore, necessary to select the stable phase of the friction history from each test and to average this data to obtain a representative value for the friction.

As only small wear volumes were generated during testing, gravimetric wear assessment was inappropriate and the wear loss on test specimens was evaluated using Talysurf profilometer data. The degree of wear was quantified by the specific wear rate (SPWR), defined as the volume of material lost per unit sliding distance per unit applied load, as given by:

$$SPWR = \frac{Volume\,lost}{Load * Sliding\,distance} = \frac{V}{W * L} \quad in\ (mm^3/N.m)$$

Where:

$$Volume\,of\ material\,lost = Average\,area\,of\ groove\,cross\text{-}section * 2\pi * Mean\,track\,radius$$

The shaded region in the surface profile in figure 2 indicates the material lost in one region of the circular wear track on a test specimen. By taking area measurements at several points and averaging them, the volume of material lost was estimated.

3. RESULTS

3.1 Changes in Friction

Examples of changes in the friction coefficients observed for sliding between the ball and

substrates, and ball and coated substrates at 2N load and 0.47 ms^{-1} are shown in figure 3.

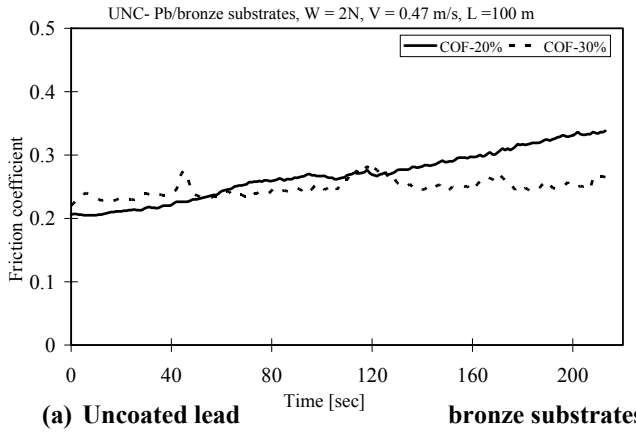

(a) Uncoated lead bronze substrates

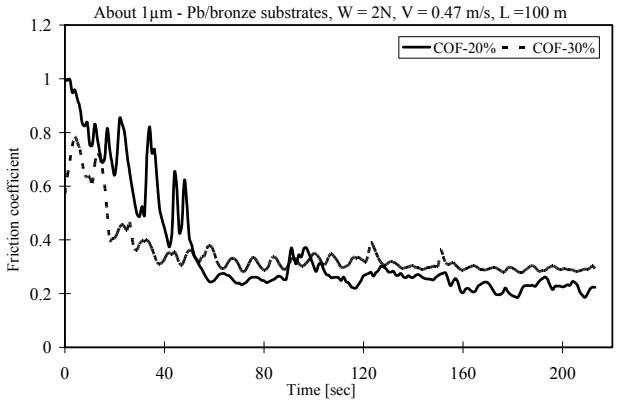

(b) Nominal 1µm thick coating on lead bronze substrates

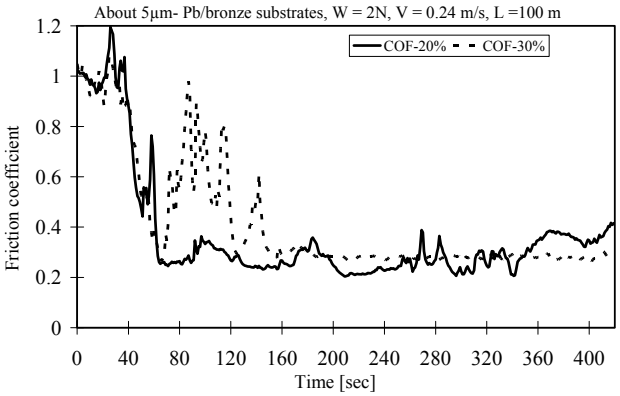

(c) Nominal 5 µm thick coatings on lead bronze substrates

Figure 3 Friction coefficients as a function of sliding time

Figure 3 (a) shows changes in friction coefficient as a function of sliding time for the uncoated substrates. It can be seen that both materials exhibit a gradual increase in friction over the duration of the test, with the friction of the 20% lead bronze increasing more rapidly than that of the 30% lead bronze, which follows an almost constant level.

Figure 3 (b) and 3 (c) illustrate changes in friction coefficient for the same substrate materials coated with nominal 1 µm and 5 µm lead indium films. Ignoring spikes in friction coefficient history, it can be seen that in almost all cases, friction at the start of sliding is high and falls roughly linearly with sliding distance to a fairly stable value. In most cases stable friction coefficients are attained in approximately the same sliding distance, the exception being the case of the 5 µm thick film on the 30% lead bronze substrate.

3.2 Steady state friction and wear

Steady state friction values were calculated as described in section 2 for all test data. In addition specific wear rate was evaluated for the substrate materials.

Figure 4 summarizes friction and wear data obtained from the tests at all loads. Figure 4(a) gives friction and wear data for the 20% and 30% lead bronze substrate materials. It can be seen that friction coefficients and specific wear rates are fairly constant, but significant differences in these values exist for the two types of material.

Figure 4 (b) presents average friction data from the stable phase for the two substrate materials coated with 1 µm thick lead indium films. Again values of friction coefficient differ, with the 30% lead bronze showing higher values and there is a suggestion that the values generally fall slightly with increases in load.

Figure 4 (c) presents average friction data from the stable phase for the two substrate materials coated with 5 µm thick lead indium films. Again, it appears that there is a slight fall in the friction coefficient for the coated 20% lead bronze. The friction coefficient of the coated 30% lead bronze is again generally higher and in this instance it rises with load

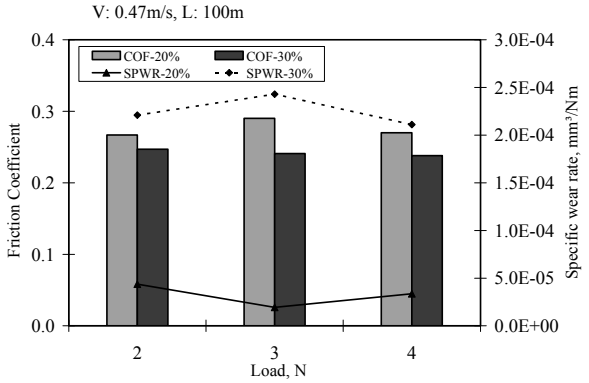

(a) Coefficient of friction and specific wear rate as a function of load for lead bronze substrates

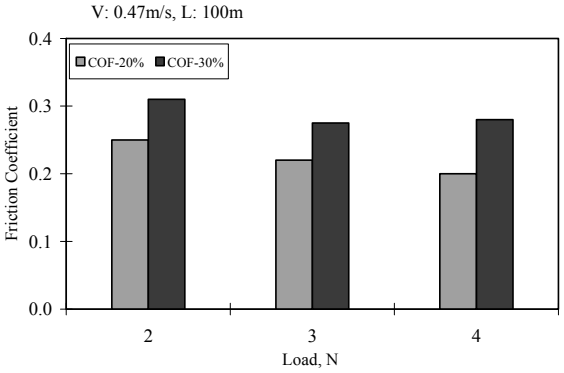

(b) Coefficient of friction as a function of load for lead bronze substrates with a nominal 1µm thick coating

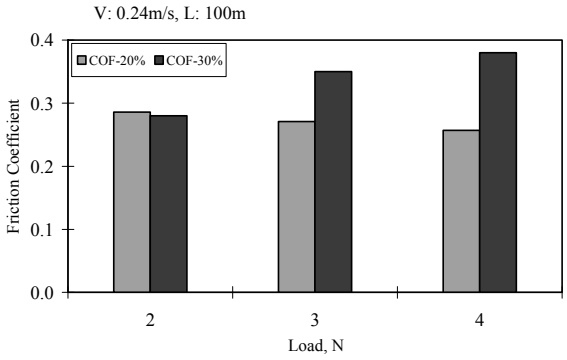

(c) Coefficient of friction as a function of load for lead bronze substrates with a nominal 5 µm thick coating

Figure 4 Steady state friction and wear coefficients as a function of load.

3.3 Contact pressures

The friction coefficient and specific wear rate were plotted against the normal load instead of contact pressure in recognition of the fact that, with the ball on disc arrangement, the contact area between the ball and the counterface changes with track and ball wear during the experiments.

The initial contact pressures between the ball and the counterfaces were evaluated from Hertzian contact calculations. In all cases the maximum contact pressure exceeded the hardness of the substrate and films by a considerable degree, suggesting considerable plastic deformation would occur at contacts. On applying loads to the coated films with the test ball in static tests, this was found to be the case for the coated specimens and the measured area of plastic contact spots are detailed in tables 2 and 3 below. However, somewhat surprisingly, plastic indentation marks were not visible in static contact tests between the ball and substrate test specimens, so Hertzian contact areas and pressure are listed in table 1 as the initial contact areas. Tables 1, 2 and 3 also detail the contact area between the ball and track and the track width at the end of each experiment. Contact pressures were estimated assuming that the ball formed a circular contact spot with the specimen having a diameter equal to the measured final track diameter. Track depth estimates ignore isolated excursions from the track shape.

Table 1. Contact areas and pressures for lead bronze substrates

Load	20% Pb/bronze		30% Pb/bronze	
	I.A (I.P)	F.A (F.P) T.D	I.A (I.P)	F.A (F.P) T.D
2	0.005 (602.8)	0.038 (52.6) 0.5	0.005 (575.5)	0.071 (28.3) 2.0
3	0.006 (690)	0.049 (61.12) 1.2	0.007 (658.8)	0.159 (18.9) 4.5
4	0.008 (759.5)	0.057 (69.86) 1.5	0.008 (725.1)	0.212 (18.8) 5.0

I.P - Initial pressure (Maximum Hertzian pressure),
F.P - Final nominal pressure (Based on Measured area),
I.A - Initial area (Hertzian prediction),
F.A - Final area (Based on track width),
F.P - Final pressure
T.D - Track depth (µm)
(Units: Load - N, pressure - MPa, Area - mm²)

Table 2. Measured contact areas and contact pressures for nominal 1μm thick coated lead bronze substrates

Load	20% Pb/bronze		30% Pb/bronze	
	I.A (I.P)	F.A (F.P) T.D (NSWD)	I.A (I.P)	F.A (F.P) T.D (NSWD)
2	0.012 (163)	0.049 (49.74) 3.0 (2)	0.020 (99.47)	0.075 (26.5) 3.0 (2)
3	0.017 (181.6)	0.080 (37.3) 4.0 (3)	0.025 (117.89)	0.132 (24.07) 4.5 (3.5)
4	0.024 (166.3)	0.132 (30.3) 5.0 (4)	0.028 (141)	0.166 (22.72) 5.5 (4.5)

I.P - Initial pressure (Based on static contact indentation),
F.P - Final nominal pressure (Based on final track width),
I.A - Initial area (Based on static contact indentation),
F.A - Final area (Based on final track width),
NSWD - Nominal substrate wear depth (μm)
(Units: Load -N, pressure - MPa, Area - mm^2)

Table 3. Measured contact areas and contact pressures for nominal 5μm thick coated lead bronze substrates

Load	20% Pb/bronze		30% Pb/bronze	
	I.A (I.P)	F.A (F.P) T.D (NSWD)	I.A (I.P)	F.A (F.P) T.D (NSWD)
2	0.023 (88.1)	0.141 (14.18) 4.0 (0)	0.071 (28.29)	0.636 (3.14) 4.0 (0)
3	0.025 (117.9)	0.203 (14.78) 5.0 (0)	0.080 (37.3)	1.039 (2.89) 8.0 (3)
4	0.031 (127.3)	0.423 (9.46) 5.5 (0)	0.096 (41.57)	1.327 (3.01) 9.0 (4)

I.P - Initial pressure (Based on static contact indentation),
F.P - Final nominal pressure (Based on final track width),
I.A - Initial area (Based on static contact indentation),
F.A - Final area (Based on final track width),
NSWD - Nominal substrate wear depth (μm)

4. DISCUSSION

4.1 Changes in friction

Figure 3(a) shows that friction in the 20% lead bronze increases with sliding distance; in contrast, friction for the 30% lead bronze remains almost constant. The wear tracks for these materials differ significantly. Figure 5 illustrates the typical condition of the ball and track following a test on an uncoated substrate. It can be seen that the condition of the ball and specimen wear track for 20% lead bronze contrasts strongly with those of the 30% lead bronze.

The 30% lead bronze sustained a deep wear groove and, using white light interferometer images of the ball surface, it was also observed that substrate material had transferred to the steel ball surface. This "thick" adhered layer was very hard to remove from the ball surface.

Figures 3(b) and 3(c) show that friction for the coated substrates starts at an elevated value then falls to a steady state. In this phase, rapid wear of the coatings by ploughing at the start of the test is reflected in high, but rapidly reducing friction coefficients as contact area changes and ploughing reduces to be replaced by friction generated by adhesive and abrasive contact between the ball and the substrate / film. At this point it is believed sliding occurs mostly on a thin lead indium film, which moderates the effect of abrasion between the ball and the lead bronze substrates.

4.2 Steady state values

The wear rate for 30% lead bronze was 6.5 times higher than that of 20% lead bronze. The hardness values of these materials differed significantly. The hardness of the 20% lead bronze is 392.3 MPa and the hardness of 30% lead bronze is 294.2 MPa. It is believed that this hardness difference serves to differentiate the impact of ploughing and is at least partly responsible for the difference in wear rates.

Considering the 1μm coated substrates, it can be seen that the coefficient of friction of the coated 30% lead bronze is generally higher than that of the coated 20% lead bronze. Since the lead indium coating is very thin, in the stable regime, probably comprising residual material and wear debris, this difference is again thought to arise partly as a

consequence of the influence of the difference in substrate hardness, with the harder 20% alloy substrate providing a reduced contact area which in turn reduces adhesion.

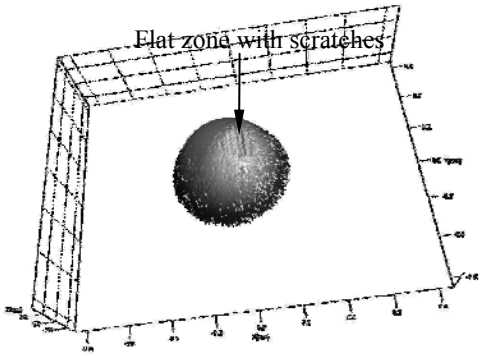

(a) 20% lead bronze: counterface

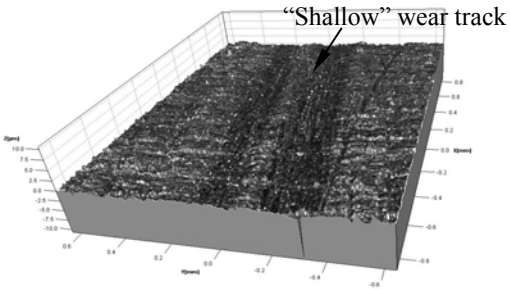

(b) 20% lead bronze: substrate

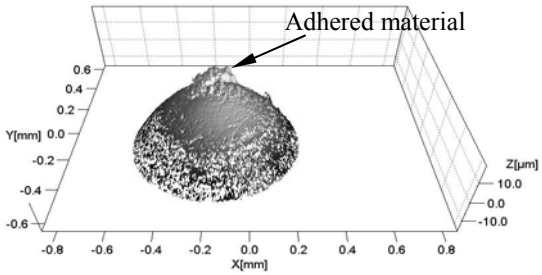

(c) 30% lead bronze: counterface

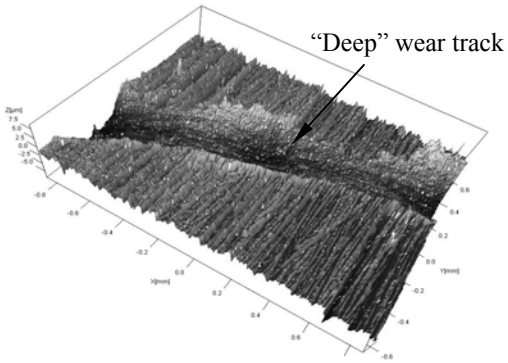

(d) 30% lead bronze: substrate

Figure 5 White light interferometer images of sliding component surfaces

Micrographs of the inter-dendritic lead size distribution for each alloy are shown in figure 6. The lead phase is finely dispersed and ranges in size up to 75µm in maximum dimension for the CuPb20Sn5 (20% lead) alloy. The CuPb30Sn2 (30% lead) alloy has a slightly coarser distribution of inter-dendritic lead phase accompanied by large 'islands' of free lead which can be greater than 1 mm in maximum dimension. The 30% lead bronze has an average friction coefficient of 0.26 compared to 0.28 for 20% lead bronze. It is believed that the greater amount of free lead in the 30% lead bronze microstructure contributes to the significant smearing of lead across the exposed surface of the ball and the greater reduction of adhesion and abrasion between the components.

(a)

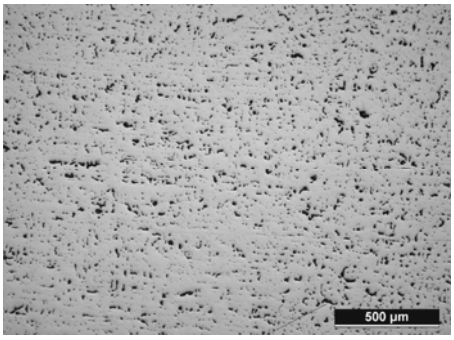

(b)

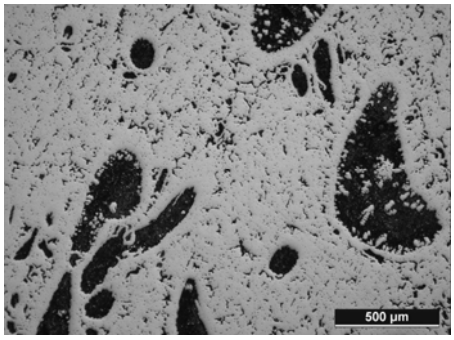

Figure 6 Micrographs showing distribution of inter-dendritic lead (Dark areas).
(a) CuPb20Sn5 (20%) lead alloy
(b) CuPb30Sn2 (30%) lead alloy

When substrates are initially coated with a 5 µm lead indium film, the coefficient of friction is generally higher for the 30% lead bronze substrates after running in. This is again thought to be related to substrate hardness. It can be seen from the wear track data that the harder substrate, 20% lead bronze, has less ploughing and maintains a lower contact area potentially reducing adhesion.

However, it can be seen that the effect of load is entirely different for the run-in film of the 5 μm thick coated 30% lead bronze, the friction coefficient increases with load, rather that reducing as with the 1 μm films.

4.3 Contact pressures

It can be seen from tables 1, 2 and 3 that final contact pressures decrease very substantially as wear progresses during tests. Additionally, for a given test, it can be seen that final track diameters become larger with increasing load, even for the case of the 5 μm thick coated 30% lead bronze in which final friction coefficients are found to increase with load.

As indicated in section 3.3, the contact pressures between the ball and track were calculated assuming that the contact was circular. However, consideration of the contact geometry suggests that it is likely that the contact between the ball and the groove is elliptical rather than circular as assumed, and this would imply that the final contact pressures presented are underestimates.

It is possible to estimate wear of the substrate alone in these experiments by neglecting the wear (ploughing) of the coating. This is achieved by considering the final track depth after subtracting the nominal thickness of the coating, as listed in tables 2 and 3. This data, listed as the "nominal substrate wear depth (NSWD), reveals that the uncoated substrates generally have rather lower wear rates than those coated by the 1 μm lead indium films. This suggests that thinner lead-indium coatings did not protect the lead bronze substrates from wear in dry test conditions, even though friction coefficients of coated surfaces may be lower in some circumstances. However, the thicker 5 μm films did generally serve to reduce wear of the substrate material quite effectively. It is possible in these cases, even after significant sliding, that a substantial portion of the coating remains. Extended ploughing of the thick coating and the softer substrate, may explain why friction coefficients for 30% lead bronze rise with load in contrast to other friction data. Irrespective of the friction behavior, it is likely that a coating of any thickness will provide additional protection from seizure.

Finally, again using the track width and track depth data, it is also possible to confirm the SPWR assessment that 20% Pb/bronze has greater wear resistance than 30% Pb/bronze.

5. CANDIDATE COATINGS

To examine the performance of a lead free material combination, tests were performed on a commercially available micro-crystalline coating with the proprietary name "Graphit-ic" [3] deposited on a hard substrate of copper-nickel-tin alloy known as "Toughmet". The same POD machine was used to measure the coefficient of friction of the combination in dry sliding conditions. In contrast to the other materials tested Graphit-ic is a hard low friction coating which is deposited by a PVD process rather than the electrolytic method used to deposit the metallic materials tested above.

The tests were all conducted on the same test specimen at one sliding speed (250 rpm). During the test the load was increased by 1N after each 15 minute sliding period. The main aim of this test was to make a preliminary assessment of the tribological properties of this material combination to compare with the lead-based materials. The thickness of the Graphit-ic coating was about 2.5 μm. The hardness of the Graphit-ic coatings is known to be in the range 17 GPa to 20 GPa.

The friction history obtained during this test is presented in figure 7. It can be seen that it gradually increased with load, appearing to stabilize at around 0.35 (figure 7(a)).

Wear on the test specimen for this test could not be measured using the Talysurf profilometer as no significant "wear groove" could be detected. In contrast, the 100 CR6 ball exhibited severe wear, as illustrated in figure 7(b) probably arising from abrasion due to its much lower hardness (8 GPa) when compared to the coating material.

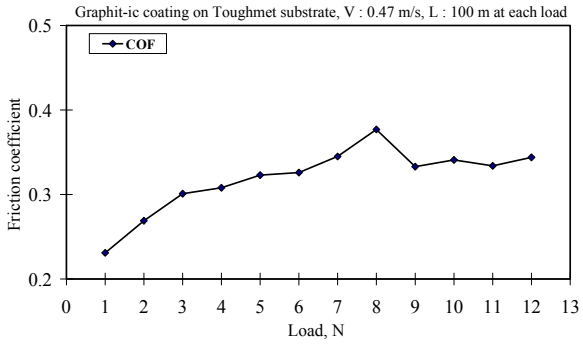

(a) Friction coefficient as a function of load

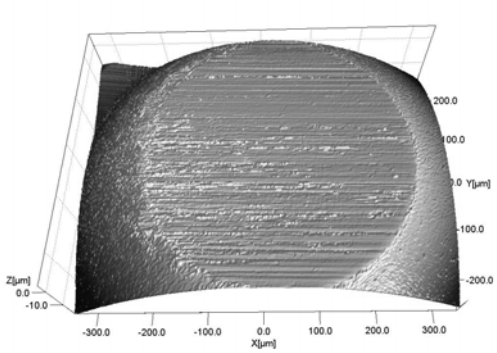

(b) Counterface (ball) surface after 6N load test

Figure 7 Graphit-ic coatings on Toughmet substrate

These results suggest that this coating substrate combination may be a viable, non-lead containing combination for a hydrodynamically lubricated plain bearing. However, if it was to be used in a bearing for such an application, it would probably be sensible to trial it in applications which involved low start up loads and/or infrequent start/stop to prevent unacceptable wear to the counterface.

6. CONCLUSIONS

From the above tests it may be concluded that:

- Uncoated lead bronze substrates have better anti-wear properties than those coated with 1 µm lead indium films, but 5 µm thick coatings appear to reduce substrate wear.
- 20% lead bronze has better wear resistance than 30% lead bronze
- 1 µm thick lead indium coatings on lead bronze appear to offer generally lower friction for run-in surfaces than 5 µm thick coatings. However, the wear rate of the substrate with 1 µm coatings is higher than for 5 µm coatings
- Friction coefficients for coated substrates generally reduce with load, but increase with load for 5 µm thick coatings on 30% lead bronze.
- Graphit-ic coatings on Toughmet substrates have anti-wear properties far superior to those of the lead indium coatings on lead bronze substrates and are potential replacements for bearing materials containing lead in the future. However, issues with counterface wear may arise if frequent contact occurs.

7. FURTHER WORK

The authors have attempted to model the friction history for the coated and uncoated lead bronze. However, this work has not yet yielded an adequately accurate quantitative assessment of observed phenomena. We will continue this work with a view to publishing it, if it is successful, at a future date. We also plan further testing of lead free materials to assess their potential as replacements for lead based bearing materials.

REFERENCES

[1] Holmberg, K., Matthews, A. **Coatings Tribology,** Elsevier Tribology Series, Volume 28. Amsterdam, 1994, pp 335-337. ISBN 978-044888709.

[2] ASTM standard designation G 99-95a (reapproved 2000), **Standard test method for wear testing with a pin-on-disk apparatus, Metal test methods and analytical procedures**. ASTM International, (2002) pp 414-419.

[3] Field, S. K., Jarret, M., Teer, D. G., **Tribological properties of graphite-like and diamond-like carbon coatings,** Trib. Int., 37(11-12) (2004) pp 949-956.